FUNCTIONAL MAGNETIC RESONANCE IMAGING STUDIES OF THE PRIMARY SOMATOSENSORY CORTEX IN RELATION TO COMPLEX REGIONAL PAIN SYNDROME

a thesis submitted to

The University of Exeter

in the subject of physics

for the degree

of doctor of philosophy.

By

Sarah Carr

July 2009

I certify that all material in this thesis which is not my own work has been identified and that no material has previously been submitted and approved for the award of a degree by this or any other University.

(signature) .....

Contents

List of Figures

List of Tables

Abstract

Functional MRI was used to detect brain activations in the primary somatosensory cortex (SI) in response to a vibrotactile stimulus applied to the thumb (D1) and little finger (D5) of the right (R) and left (L) hands. Four studies were carried out with healthy subjects in order to determine the scanning and stimulation protocols that resulted in consistent and robust SI activity. It was found that a strong stimulus, compared to a weak stimulus, led to the SI activity being detected more frequently and at a more statistically significant level. Also, extending the scanning duration per digit further increased the T-scores.

The SI activations for each digit showed multiple foci and were distributed throughout the SI area. However, a clustering occurred in separate centres for stimulation to RD1 and RD5 near the Brodmann area 1/Brodmann area 3 boundary. The Euclidean separations of the cortical digit representations for LD1-D5 and RD1-D5 were calculated on the basis of the 'centre of mass' of the multiple activations. Observed separations ranged between 1.2 mm to 22.8 mm.

A further vibrotactile fMRI study was carried out involving patients with complex regional pain syndrome (CRPS). It has been suggested an altered central processing mechanism is involved in the disease, possibly due to cortical reorganisation in the sensory/motor cortices. The most efficient experimental protocols from the healthy subject studies were used to determine if these cortical differences were present in four patients. Data were acquired over two scanning sessions, approximately four months apart. The study revealed multiple SI foci and overlapping between the digits in both the healthy and CRPS hands, similar to those observed in the first studies. Larger SI activations were detected in one patient,

smaller SI activations were detected in another patient and two patients demonstrated cluster sizes in the normal range. The cluster sizes and the changes in size between the two scans suggest a correlation with the amount of pain experienced by the patients.

A general lack of consistency in the results from all the studies may be attributed to the difficulty of reliably detecting SI activity at a field strength of 1.5 T.

Acknowledgements

Without the assistance of all the study participants this project would not have been possible and I'd like to say a big thank you to everyone, particularly the patients, who kindly gave up their time to take part.

I would also like to thank my supervisor in the department of Physics, Dr Summers for all his help and support over the past three years and, also, my supervisors in the department of Psychology, Dr Williams and Professor Hodgson, for all their assistance and support as well. Thank you to our collaborators Dr Haigh and Mr Peters at the Royal Devon and Exeter Hospital and Dr McCabe at Bath Royal National Hospital for Rheumatic Diseases for all their help, support and input to the project. I would also like to thank DAART for the financial support which allowed this project to be carried out.

Finally, a big thank you to my friends and family, particularly my Mum and Dad, for supporting me through the ups and downs of my PhD and being the understanding and wonderful people they are.

Chapter 1

Introduction

1.1 Introduction

This thesis presents five tactile functional magnetic resonance imaging (fMRI) studies which investigate the somatosensory areas in the brain. Studies 1 - 4 were carried out on healthy control subjects and study 5 was carried out with complex regional pain syndrome (CRPS) patients, together with 'normal' controls. There is evidence to suggest that the somatosensory activity of patients with chronic pain conditions, such as CRPS, is altered in both the location and the size of the activations. The images from patients and controls were compared and contrasted to detect any differences that might exist between their somatosensory cortical areas.

This chapter briefly describes the types of neuroimaging modalities available and discusses the findings of other tactile fRMI studies carried out on healthy subjects. Neuroimaging studies carried out on CRPS patients are also discussed and an overview of the project is given at the end of the chapter.

Chapters 2 to 6 describe the background to the studies and Chapters 7 to 9 detail the methodologies employed, the results of the studies and a discussion of the findings.

In Chapter 2 the nervous system is described including the types of touch receptors in the skin, how touch signals are generated and propagated through

the nerve pathways to the brain, the primary somatosensory cortex where sensory signals are processed and how it is subdivided into Brodmann areas. An overview is also given of the coordinate systems used to describe a point within the brain.

Chapter 3 focuses on CRPS and details the characteristics of the disease including trigger factors, symptoms, diagnostic methods and the peripheral and central nervous system changes that can occur. The central nervous system changes are similar to that described in phantom limb pain and this connection is described in further detail within the chapter. The technique of mirror visual feedback is also described. This therapy is believed to correct central processes by re-establishing congruence between the planned movement and the actual movement through visual feedback of the reflected healthy limb.

The physics of MRI is described in Chapter 4 and parameters such as image encoding, image sequencing and single shot echo planar imaging are discussed. Other topics discussed in this chapter include functional MRI, the BOLD effect, artifacts and noise that can appear in fMR images and a basic description of MRI instrumentation.

Chapter 5 discusses the processing of the raw fRMI data and the software that is used to do this. It includes converting the raw data to 'Analyse' format, applying slice timing correction and realignment, normalising the images to a standard template, and smoothing. The statistical model used to draw the brain activity from the data is also described.

The devices used to deliver the vibratory touch stimulus are described in Chapter 6. The vibration is generated by computer controlled piezoelectric cantilevers which are triggered in synchrony with the acquisition of the images. The timing pattern of the vibration and the frequency with which it is applied are also described.

The experimental procedures are described in detail in Chapter 7. The individual and group analysis results of each study are presented in Chapter 8 and discussed in Chapter 9. Conclusions and suggestions for future work are also described in the latter chapter.

1.2 Perceptual Neuroscience

Perceptual neuroscience is concerned with how a stimulus is perceived and interpreted. It attempts to understand how physiological and cognitive processes influence our perceptions and experiences.

This thesis focuses on the area of tactile perception. When we 'feel' the sensation of touch a myriad of biological processes spring into action, from the senses in the skin to the brain and the highways connecting them. At the same time our emotional and attentional states and previous experiences also contribute to our perception of the stimulus. Therefore the sensation of touch is an experience unique to each of us and is continually changing.

The study of tactile psychophysics attempts to unravel this complex process and often involves experiments where subjects are asked to discriminate between different touch stimuli. The fingertips are often targeted as they are small, easily accessible and very sensitive. (They are usually referred to as D1 - D5 beginning with D1 at the thumb and then counting across the digits to D5, the little finger). When similar experiments are carried out whilst imaging the brain they can reveal valuable insights into the workings of the central nervous system which even in the 21^{st} century still contains many secrets.

There are many neuroimaging techniques available. Electroencephalography (EEG), magnetoencephalography (MEG), positron emission tomography (PET), optical imaging and fMRI are modalities regularly employed in these studies. EEG and MEG measure the changes in the electrical potential and magnetic field surrounding the brain which are induced by neuronal activity. They provide excellent temporal resolution, on the order of milliseconds, but the spatial resolution is limited and small clusters of activity often cannot be resolved. PET requires the injection of a radioactive tracer and indirectly detects neuronal activity by measuring increases in blood flow. It has good spatial resolution but is temporally limited to 10 - 40 seconds. Manufacturing of the tracer also makes this method very expensive. Optical imaging provides good somatosensory data in

animal studies; however, there is poor spatial resolution in human studies due to the thickness of the skull. FMRI indirectly detects neuronal activity in a similar way to PET. It uses the difference in magnetic susceptibility between oxygenated and deoxygenated blood to produce contrast in the image and localise the activity. It does not require a tracer to be injected and so is less expensive and carries less risk to the subject. Image resolution is typically on the order of 2 - 3 mm and is temporally limited to a few seconds. The compromise between cost and resolution make fMRI a popular choice among researchers when imaging brain function.

1.2.1 Previous Studies of Tactile Perception

Many neuroimaging studies have been carried out to investigate different aspects of tactile perception. Several experiments have focused on the arrangement or 'mapping' (somatotopic mapping) of the fingertips on the cerebral cortex in the primary and secondary functional areas, SI and SII [1, 2, 3, 4, 5, 6, 7, 8, 9, 10, 11]. These involve stimulating some or all of the fingertips using various methods of tactile stimulation and recording the resulting activity in the brain. The stimuli range from brushing a monofilament or a tooth brush across the fingertip to engineered devices such as air jets, pneumatically controlled cylinders or air inflated diaphragms. Piezoelectric bimorphs are often used. The latter work well in the MR environment, and produce little or no interference to the MR signal.

In an fMRI study carried out by Francis et al. [1] digits 2 - 5 were stimulated by a piezoelectric bender and the resulting activations were imaged at 3 T. Their results for a representative subject are shown in Figure 1. In most of their eight subjects they found four representations of each digit within the SI area, in concurrence with the cytoarchitectonic map created by Brodmann in the early part of the 20^{th} century and with animal studies on primates (e.g. Kaas et al. [12]). These four areas are called Brodmann areas 1, 2, 3a and 3b.

Vibrations are detected in the fingertip by a group of nerve receptors called the mechanoreceptors. These consist of Pacinian, Meissner and Ruffini corpuscles and

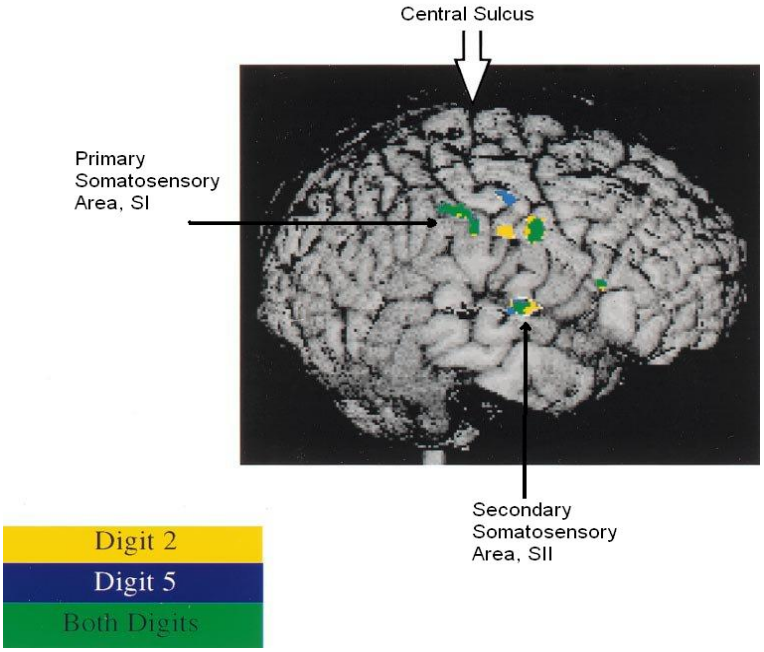

Figure 1: Single subject fMRI data showing the somatosensory D1 and D5 activations from the study by Francis et al. [1].

Merkel's discs and they are most sensitive at different frequencies. For example Meissner corpuscles optimally detect low 'flutter' frequencies (10 - 50 Hz) and Pacinian corpuscles activate most at high 'vibratory' frequencies (50 - 300 Hz) [13]. The different types of flutter and vibratory sensations produce different responses in the brain. Tommerdahl et al. [14] found that flutter sensations produce focused activations in Brodmann areas 1 and 3b and SII. They also found vibratory sensations initially produce a focused activation in the same position in SI as the flutter sensation but this quickly disappeared and was replaced by a large area of deactivation. The SII activations in response to a vibratory stimulus were stronger than the response to flutter sensations and were often bilateral.

Francis et al. and Harrington & Downs [15] also examined the effect of the frequency of the stimulus on the somatosensory activations. Both groups used a piezoelectric bimorph to produce the variable vibration. Francis et al. stimulated at 30 and 80 Hz. Harrington & Downs collected their data on a 1.5 T MR imager

and stimulated D1 - D3 using 35 and 150 Hz. Francis et al. found that as the frequency increased the size of the activated area in SI decreased but the size of the activated SII area increased. Harrington & Downs did not find this but they did find a decrease in the detection rate of SI activity with increasing frequency and an increase in the detection rate of SII activity. The mechanoreceptors are arranged with different densities within the fingertip. Therefore the decrease in SI activation may be reflecting this.

Overduin & Servos [9] imaged digits 1, 2 and 4 at 4 T to investigate the effect of movement over the entire length of the finger. They used a set of air jets positioned along the finger to produce the stimulus which could be fired back and forth. They found the SI activity moved across the surface of the cortex as the stimulus moved along the finger forming multiple discrete bands of activations for each digit. When the stimulus direction was reversed the activations occurred in reverse order. This supports the theory of discrete somatotopic arrangement of the digits on the cortex and the theory of multiple representations for each digit. They also found that the volume of the activity in area 1 was larger compared to area 3b but area 3b contained more bands of activity implying that the two areas are functionally different. Area 3b might be receiving afferent inputs from more than one nerve receptor and therefore processing more than one type of sensation.

Whilst activations of SI are contralateral to the side of stimulation the activations of SII are often bilateral [8, 11]. A study by Ruben et al. [11] focused on the somatotopic organisation of the secondary somatosensory area. They stimulated digits 2 and 5 and the hallux and compared the SII activations. Their results showed there was some localisation present, i.e., a difference in the location of the activity for the fingers and hallux. However, between the digits themselves there was no difference in the location of the activity. This implies that somatotopic mapping in SII is more limited than in SI.

Tactile imaging studies also produce reliable positions for the mapping of the digits and show that the centre of mass of the SI clusters for the little finger is located more medial, more superior and more posterior to the thumb. From

the literature the locations of the activations for each digit in SI and SII can be collated and the data are shown in Tables 1 and 2.

It is also possible to obtain the Euclidean distance on the brain between the mapped digits. Van Westen et al. [6] measured the D1 - D5 separation between the activations of Brodmann area 3b and found it to be 17.2 ± 2 mm. They also calculated the 3b separations between the individual digits, D1 - D2: 10.6 ± 1.5 mm, D2 - D3: 5.5 ± 0.9 mm, D3 - D4: 7.4 ± 1.1 mm and D4 - D5: 6.8 ± 1.2 mm.

Maldjian et al. [7] did a similar analysis using the centre of mass of the clusters of the SI activity instead of area 3b only. Their results are as follows - D1 - D2: 6 mm, D2 - D3: 3 mm, D3 - D4: 3 mm and D4 - D5: 6 mm giving a D1 - D5 separation of 18 mm. Francis et al. also determined the D2 - D5 separation to be 11.2 mm (range 7.2 - 15.1 mm). Gelnar et al. [2] found a D1 - D5 separation of 9.5 mm and Kurth et al. [10] found an area 3b D2 - D5 separation of 6 - 12 mm. Kurth et al. [3] found a mean 3b D1 - D5 separation of 16 mm. The mean of these values gives a D1 - D5 separation of approximately 15 mm. Obviously there is variability between individuals due to the uniqueness of the size and shape of our brains.

Studies have also been carried out to investigate the influence of attentional state on the SI and SII activations [16, 17, 18, 19]. A distractor task is introduced, often counting, to direct the subject's attention away from the touch sensations. Results showed that size and intensity of activation decreases with distraction in both SI and SII. Arthurs et al. [17] carried out the same protocol using both fMRI and EEG. They found the fMRI responses were decreased during distraction but the EEG responses were unchanged indicating that although the neurons fire normally the coupling of the neuronal blood flow is affected by the cognitive state. Hamalainen et al. [18] found a general increase in the amount of activity with attention but found that some of the activated areas were different in the two conditions.

It is also possible to temporarily alter the somatotopic mapping in SI using perceptual illusions. Pleger et al. [20] and Hodzic et al. [21] both used repetitive

Table 1: Coordinates of maximum activation for stimulation of individual digits in SI, given in Talairach coordinates. (Results from four studies, as referenced. Centre of mass is taken using all Brodmann areas detected in SI).

Digit	Brodmann Area	Coordinate	Ref
D1	Not stated,	54 -14 36	[7]
		(Coord group mean)	
	centre of mass	-45 (± 18) -21 (± 11) 42 (± 17)	[9]
	of all BA	(Coord group mean)	
D2	Not stated	50 -18 42	[7]
		(Secondary maxima: 40 -24 48)	
		(coords group mean)	
	BA 1	-48.2 -16.9 43.5	[5, 1]
		-50.8 -18.0 40.3	
		-47.9 -20.6 44.7	
		-51.0 -20.4 44.6	
		-46.9 -23.5 46.3	
		-47.3 -17.2 47.4	
	Centre of mass	-35 (± 18) -32 (± 9) 52 (± 17)	[9]
	of all BA	(Coord group mean)	
D3	Not stated	44 -26 45	[7]
		(Coord group mean)	
D4	Not stated	30 -40 48	[7]
		(coord group mean)	
	Centre of mass	-41 (± 9) -26 (± 8) 54 (± 6)	[9]
	of all BA	(coord group mean)	
D5	Not stated	48 -24 42	[7]
		(Secondary maxima: 36 -36 54)	
		(Coords group mean)	
	BA1	-43.8 -24.9 52.5	[5, 1]
		-42.5 -23.1 52.2	
		-40.7 -25.0 49.8	
		-43.0 -27.6 50.0	
		-38.8 -27.2 43.3	
		-42.1 -25.4 41.9	

Table 2: Coordinates of maximum activation for the stimulation of the individual digits in SII, given in Talairach coordinates. (Results from four studies as referenced).

Digit	Coordinate	Ref
D1	50 -20 19	[5, 4]
	53 -17 17	
	52 -19 17	
	49 -20 20	
D2	-36 -22 12	[11]
	-45 -19 18	
	-45 -22 21	
	-36 -16 12	
	-42 -26 18	
	-42 -22 19	
	-45 -16 15	
	56 -19 10	
	-55 -23 25	[8]
D3	No data	
D4	51 -20 18	[5, 4]
	52 -21 19	
	52 -19 18	
D5	-36 -22 13	[11]
	-44 -19 19	
	-45 -22 22	
	-42 -22 15	
	-43 -25 18	
	-42 -22 18	

passive stimulation from an electrical source covering a large area of a fingertip to produce illusionary changes. After a few hours of stimulation spatial and frequency discrimination were tested and, using fMRI, it was found that SI and SII activations were enlarged. They also noted that spatial discrimination was improved but frequency discrimination had deteriorated.

Schaefer et al. [22] used a very different technique. They created the illusion of an elongated arm by attaching a prosthesis to the hand. The real fingertips were stimulated but visually the subject could only see the prosthetic fingers being stimulated at an extended distance from their body. The fMRI data showed the distance on the brain between digits 1 and 5 decreased and this was correlated with the perceptual experiences of the subjects. Those who felt the prosthesis to be a part of them showed the greatest decrease. It was suggested that this was caused by the arm functional area enlarging and forcing the finger area, located adjacent, to shrink. This was never tested, however.

Although the cortical reorganisation in these studies was temporary and reversed within 24 hours, leaving the subjects with no adverse affects, these results serve to demonstrate the plasticity of the brain. If this level of reorganisation can be achieved easily and within a short space of time then could it not be possible to inadvertently achieve this in everyday life? For example, a fractured limb immobilised with a cast could produce a feeling that the limb is enlarged. What effects would a more prolonged reorganisation have on the body and the brain's perceptions? Could it continue to produce pain or other symptoms even after the injury has healed?

1.3 Chronic Pain Conditions

Functional neuroimaging has many applications as a tool to help us understand the processes occurring in diseases. Numerous studies have been carried out on patients using fMRI, looking at chronic pain conditions such as focal dystonia of the hand (writer's cramp) [23, 24, 25], complex regional pain syndrome

[26, 27, 28, 29, 30], and phantom limb pain [31, 32, 33]. Most concentrate on comparing sensory and motor activations with results from healthy controls and determining how the locations and intensities vary, thus providing an insight into the neurophysiology of the disease.

1.3.1 Complex Regional Pain Syndrome

Complex regional pain syndrome is a painful and debilitating disease that is difficult to diagnose and treat. It is a disease involving the sympathetic and central nervous systems but the underlying mechanisms still remain a mystery. Silas Weir Mitchell first described it in 1864 after a soldier received a gunshot wound in his arm during the American Civil War and went on to develop a burning pain in the limb. The pain was far greater than the wound should have produced and persisted for a number of years. Also stimuli which were not normally painful induced pain in his arm.

Research has led to the identification of two forms of the disease. Type I, also called Reflex Sympathetic Dystrophy, generally occurs after trauma to a region of the body involving little or no nerve damage. The trauma may take the form of a sprain, bruise, skin lesion, fracture, surgical trauma or a cerebrovascular accident. Type 2, also called Causalgia (meaning 'burning pain'), normally occurs after trauma involving damage to the nerves [27, 34, 35].

It has been suggested that cortical reorganisation plays a role in CRPS. However, although there are many researchers around the world working on CRPS few have carried out neuroimaging studies to investigate the extent and role of cortical reorganisation. Two groups stand out, headed by Burkhard Pleger and Christian Maihofner. Below is a summary of their relevant published works.

Pleger et al. [36] used EEG to measure brain activity in patients with CRPS type I of the hand. A non-painful electrical stimulus was used to stimulate the median and ulna nerves. Their results showed differences in the location of the activity between the 'CRPS' and 'non-CRPS' sides of the brain. In the N20 dipole the polar angle was on average 1° smaller. Readings from the healthy hand

produced results comparable to those from control subjects. They also found a strong correlation between the amount of reorganisation and the intensity of the pain experienced by patients. In a different study, Pleger et al. [37] carried out a two point discrimination test on the index finger of patients and controls by applying pairs of needles with varying separations to the fingertip. The subjects had to say if they could feel one or two points. In a separate session, the index finger was electrically stimulated and the brain activity was recorded using fMRI. A reduction in the discrimination threshold correlated with a reduction in the size of the activation in SI and SII. A similar procedure was repeated by Pleger et al. [29] but patients were retested after treatment and subsequent improvement. They observed an increase in the discrimination threshold which became comparable to the control data, and there was increased activity in the somatotopic areas.

Maihofner et al. [38] used MEG to record the activations in response to stimulation to D1, D5 and the lower lip in patients with CRPS type 1 of the hand. They found an increase in the magnetic field strength as well as displacement of the D1 and D5 activations. Compared to 'normal' control data, the fingertip activations were displaced away from the lower lip activation and located closer together. The digit separation was calculated to be 8 mm for the CRPS side of the brain and 13.7 mm for the healthy side, the latter result being similar to the control group measurements. In congruence with the findings of the three Pleger et al. papers they also found a correlation with the degree of reorganisation in SI to the amount of pain experienced by patients. A follow up study was published in 2004 (Maihofner et al. [28]) evaluating the effect of treatment. They discovered that where patients had improved and had a reduction in their pain, the SI reorganisation had reverted to normal. In another study, Maihofner et al. [27] investigated the effect of neuropathic pain on the SI and SII areas using fMRI. Again, they used CRPS patients and induced pinprick hyperalgesia using von-Frey filaments. The stimulus was not painful to the unaffected hand. They found there was increased activity in both somatosensory cortices as well as other associated areas.

Juottonen et al. [26] have also used MEG to investigate CRPS patients. They

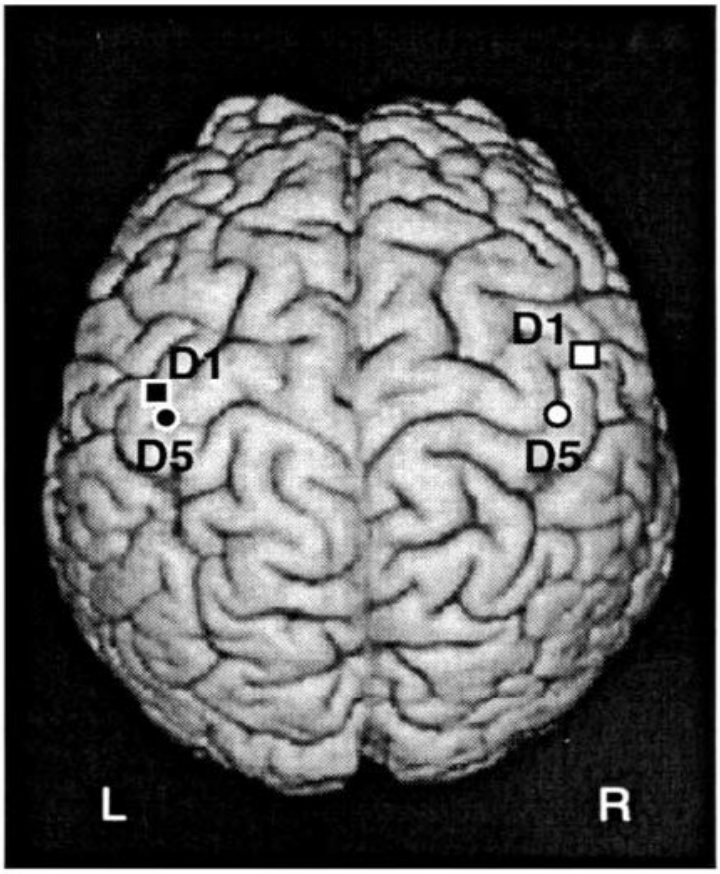

Figure 2: A single subject's results from the MEG study on CRPS patients carried out by Juottonen et al. [26]. SI thumb positions shown with squares, SI little finger position shown with circles. CRPS side of the brain is shown on the left by a black filled circle and square. Control data from the healthy hand is shown on the right with a white filled circle and square.

stimulated D1 and D5 of the healthy and CRPS hands and discovered similar findings of reorganisation correlated with pain as well as a stronger signal for the CRPS hand. Their results are shown in Figure 2. In patients the average separation was 7.0 $\pm$ 1.3 mm, compared to the control group with an average separation of 12.5 $\pm$ 1.5 mm.

From these studies it is clear there are central mechanisms involved in this disease but there have been relatively few neuroimaging studies to investigate these. The main aim of this project is to obtain fMRI data which gives further

information on the nature of cortical reorganisation in CPRS.

1.4 Overview of the Project

This project has two parts. The first relates to sensory fMRI studies on 'normal' subjects to provide baseline data on how touch stimuli are interpreted by the brain. The second applies similar methodologies to investigate how the location and extent of fMRI activations change in patients with CRPS.

In all experiments the same basic methodology was used. Vibrotactile stimulation was applied to one or other of four sites: D1 and D5 fingertips of the left hand, and D1 and D5 fingertips of the right hand. Cortical activation was measured and contrasted between data for the four stimulus locations.

Two comparative studies were carried out initially to determine if the activations were affected by changing the order in which the fingertips were stimulated. The first paradigm involved stimulating D1 and D5 in a randomised alternating sequence within a single scanning session. In the second paradigm the stimulation was separated so that only one digit was stimulated per session. A third study was carried out to determine the effect of increasing the stimulus level by approximately 3 dB and extending the scanning time. A fourth study measured the effects of changing the pattern of the stimulus between a pulsing (0.5 s on, 0.5 s off) 40 Hz vibration and a non-pulsing vibration at the same frequency. As must be expected, it was found that a higher stimulus amplitude and a longer scanning time produced the most robust SI activations at the individual level. Multiple SI activations were detected in response to stimulation to each digit and there was no consistency in the number of foci detected. In some instances one to two activations appeared in the same location for both D1 and D5 of the same hand, but most of the observed activations appeared/disappeared when the stimulus location was changed. Although the digit activations were distributed throughout SI, activity was found to cluster in separate centres for RD1 and RD5 near the BA1/BA3 boundary. The cortical separations between the digit representations,

determined using 'the centre of mass' calculations for the activations relating to each digit, were smaller than expected. This was attributed to the effect of averaging over multiple activations, lying within the same region of SI for RD1 and RD5.

The paradigm which produced the clearest activations was used for measurements on a group of CRPS patients, together with a group of control subjects. Two sets of scans were carried out approximately 4 months apart in order to correlate changes in the patients' symptoms with changes in the scans. It was hypothesised that cortical reorganisation would be present in the patients and that a decreased separation between the D1 and D5 activations would be observed in the CRPS group, compared to the control group, and the areas of activation might be larger or smaller or have higher or lower intensities.

In fact, a consistent pattern of modified activations was not observed in these patients. After 4 months, larger activations were found in one patient and smaller activations were found in another patient. There was also some correlation with changes in the cluster size and the changes in the pain levels experienced by patients between the two scans.

This project was carried out in a collaboration between the School of Physics and the School of Psychology at the University of Exeter, the Royal Devon and Exeter Hospital and Bath National Hospital for Rheumatic Diseases.

Chapter 2

The Nervous System

2.1 Introduction

When an object is placed in our hand it must first be detected by the sensory receptors in the skin which then produce nerve signals via chemical transport and action potentials. Information reaches the brain via a neural chain with several stages. The brain must then interpret the messages and form a coherent picture about the size, shape, texture, temperature and position of the object. It is obvious that this is a complex process involving many systems in the human body. This chapter describes the anatomy and physiology of nerve cells and how specially adapted sensory nerves link with the brain to produce physical sensations.

2.2 Neuron Structure and Generation of Nerve Impulses

Nerve cells (neurons) consist of a cell body (soma), dendrites, axon and axon terminals as shown in Figure 3. The cell body contains the nucleus, cytoplasm, mitochondria and other cell organelles. The dendrites are branch like structures extending from the soma which receive action potentials from the axon terminals of other nerve cells. The axon is a single nerve fibre which also extends from

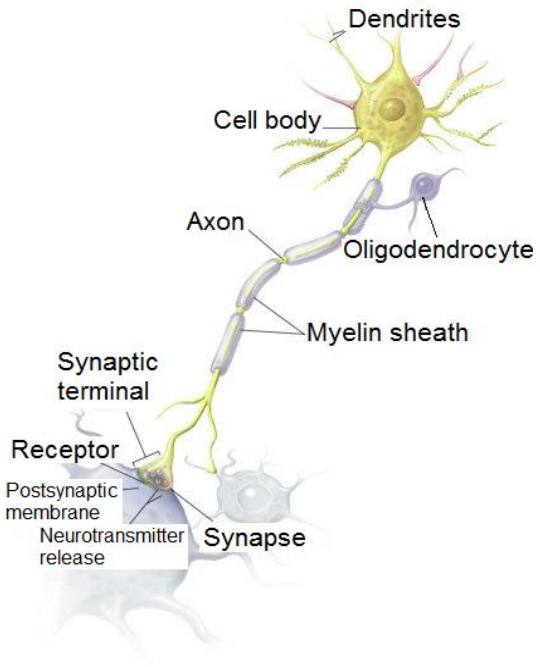

Figure 3: Neuronal structure [39].

the soma. It is typically 1 μm in diameter and can be over a metre long. The electrical impulse is generated by the axon cones at the neck of the axon and is passed along the nerve fibre towards the terminals. In many nerve cells the axon has a fatty myelin sheath which is created by Schwann cells in the peripheries and oligodendrocytes in the brain. There are gaps in the myelin at regular intervals, called the nodes of Ranvier, where there are sodium ion channels. Signals jump from one node to another via electromagnetic effects. Consequently, signals travel faster in myelinated nerves than in unmyelinated ones, (where transport is via ion channels throughout).

The end of the axon branches into terminals which bond with the dendrites of other nerve cells forming a synapse. Neurotransmitter chemicals are released by the terminals in response to the electrical impulse and they travel across the intervening gap to the dendrite neurotransmitter receptors. The amount of neurotransmitters which are released depends on the strength of the impulse which is received. The dendrite then generates an action potential through the transport

of ions across the soma. If the reaction is sufficiently large enough then the axon cones will fire producing another impulse that will pass the information on to the next cell.

2.3 Detecting Touch Sensations

When we touch an object the touch receptors activate ion transport across the cell body which generates electrical impulses that travel along the nerve pathways to the brain where they are interpreted as a certain type of sensation. There are several types of receptors in the skin and they are highly concentrated in the fingertips. They are found at different depths and activate in response to different levels and types of stimulation, e.g., mechanical pressure, temperature and pain.

Touch information is detected by the group of mechanoreceptors which consist of Pacinian, Meissner and Ruffini corpuscles and Merkel's discs (see Figure 4) and together they detect touch, pressure and vibrational sensations. They are arranged in the superficial and subcutaneous tissues in the skin allowing us to sense a broad range of stimuli. These specialised mechanoreceptors are generally associated with large diameter (6 - 12 μm) myelinated Aβ fibres which have a conduction velocity in the range of 35 - 75 m s^{-1} [40].

2.3.1 Pacinian Corpuscles

Pacinian corpuscles were discovered by Filippo Pacini in 1831. They lie in the deep subcutaneous tissue of the skin and activate in response to deep pressure stimulation and high frequency vibrations (50 - 300 Hz) [13]. They are the largest of the mechanoreceptors and are shown in Figure 4. The corpuscles are oval in shape and have a diameter of approximately 1 mm. They have a central fluid filled cavity containing an unmyelinated nerve ending and surrounding this are multiple layers of connective tissue which are formed from modified Schwann cells.

Nerve impulses are generated in the axon in response to the deformation of the cell. A pressure sensitive sodium ion channel is activated producing the impulse

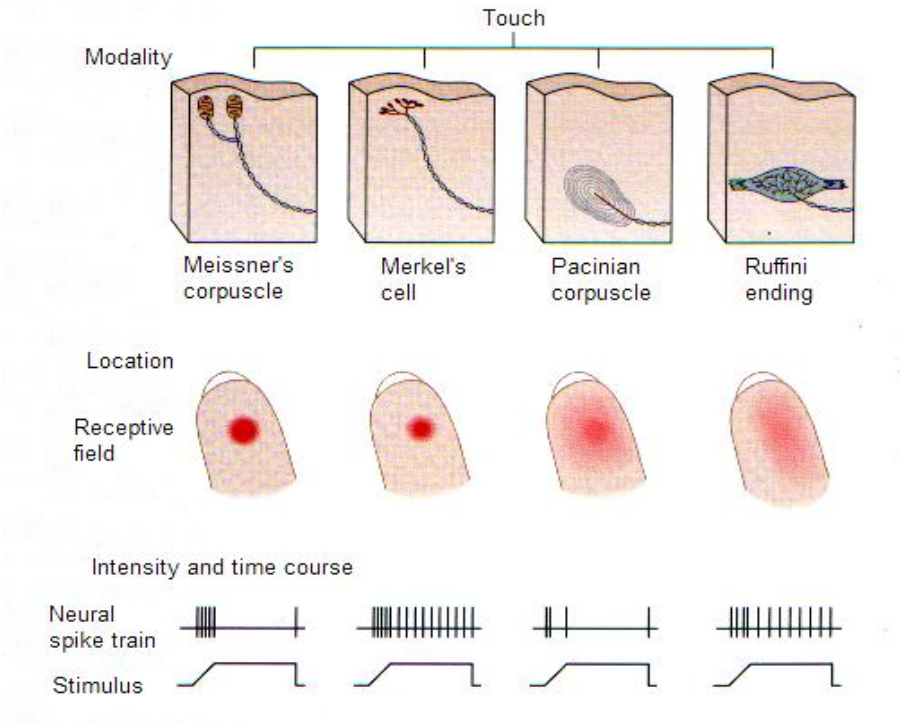

Figure 4: The four mechanoreceptors are shown at the top and the images beneath depict the receptive fields. The section at the bottom shows how the time course of the firing patterns vary for each receptor in response to an applied stimulus [42].

which travels afferently along the axon. The corpuscles adapt rapidly to stimuli and generally fire when they are first deformed then again when the pressure is removed but impulses reduce rapidly while the pressure remains constant. This is demonstrated in the bottom section of Figure 4. They have a large receptive field and are able to detect vibrations from a few centimetres away [42].

2.3.2 Ruffini Corpuscles

Ruffini corpuscles were first described by the Italian histologist Angelo Ruffini in 1892. These receptors are also found in the deeper layers in the skin and are sensitive to stretching sensations. This is useful in gripping objects by detecting any slippage. They also detect mechanical deformations within joints and thus provide

proprioceptive information about position and movement. They also respond to vibrations in the range 15 - 400 Hz [41].

As shown in Figure 4 they have a thin outer cell wall which is long and thin in shape and the nerve ending within it branches profusely. Ruffini corpuscles are slowly adapting receptors and continue to react when a constant pressure is applied. Their receptive field is also large.

2.3.3 Meissner Corpuscles

Meissner corpuscles were discovered by the German anatomist Georg Meissner in 1852. In contrast to the Pacinian and Ruffini corpuscles these lie much closer to the surface of the skin, just beneath the epidermis and therefore respond to lighter touch pressure. The cells are rapidly adapting receptors and the optimum vibrational frequency they detect is between 10 - 50 Hz [13]. They have a small receptive field of only a few millimetres.

The unmyelinated nerve ending meanders through the cell which is surrounded by a layer of connective tissue. The size of the corpuscle is approximately 50 μm by 80 μm. By the age of 50, humans have only a quarter of the number of Meissner corpuscles in their fingertips than they had at the age of 12 [43].

2.3.4 Merkel Discs

Merkel's discs were discovered in 1880 by German anatomist Friedrich Sigmund Merkel. They are found near the surface in both hairy and glabrous skin and in the fingertip they cluster under the ridges of the skin. These cells consist of an unencapsulated nerve ending which is flattened into a disc shape. They are slowly adapting and are sensitive to low frequency vibrations of around 0.3 - 3 Hz [41] as well as deformation of the skin and pressure. Merkel's discs also have a small receptive field in which they can detect a stimulus.

2.3.5 Free Nerve Endings

The skin is also innervated by free nerve endings which do not have a surrounding cell body. They are found at various depths throughout the skin and are unspecialised nerve fibres which can adapt either rapidly, intermediately or slowly to a stimulus. They are able to detect mechanical, chemical and thermal changes and act as nociceptors (detect pain).

Most free nerve endings are formed from two types of nerve fibres:

1) small diameter (1 - 5 μm) myelinated Aδ fibres with a conduction velocity between 3 - 30 m s^{-1}. They are sensitive to increasing temperature and carry pain signals quickly to the brain causing us to experience the initial sharp pain when an insult occurs [40, 42].

2) smaller diameter (0.2 - 1.5 μm) unmyelinated C fibres with a conduction velocity of 0.5 - 2 m s^{-1}. They are sensitive to decreasing temperature and carry pain signals more slowly producing the familiar dull pain which lingers after a noxious event [40, 42].

2.4 Touch Nerve Pathways

The mechanoreceptors and free nerve endings encode sensory information as electrical impulses and send them along their axon to the first relay station which consists of the dorsal root ganglion neuron, a highly specialised cell found in the spinal column. The impulses enter via the posterior horn of the spinal cord ipsilateral to the sensation. Here the information is filtered and sent either through the anterolateral system or the dorsal column medial lemniscal system (DCMLS), shown in Figure 5.

The DCMLS relays information about vibration, pressure and proprioception through the ipsilateral posterior column of nerve fibres to the cuneate nucleus in the medulla in the brain stem. Here the signal is relayed medially in the medulla to the medial lemniscus and is carried through the brain stem to synapse with

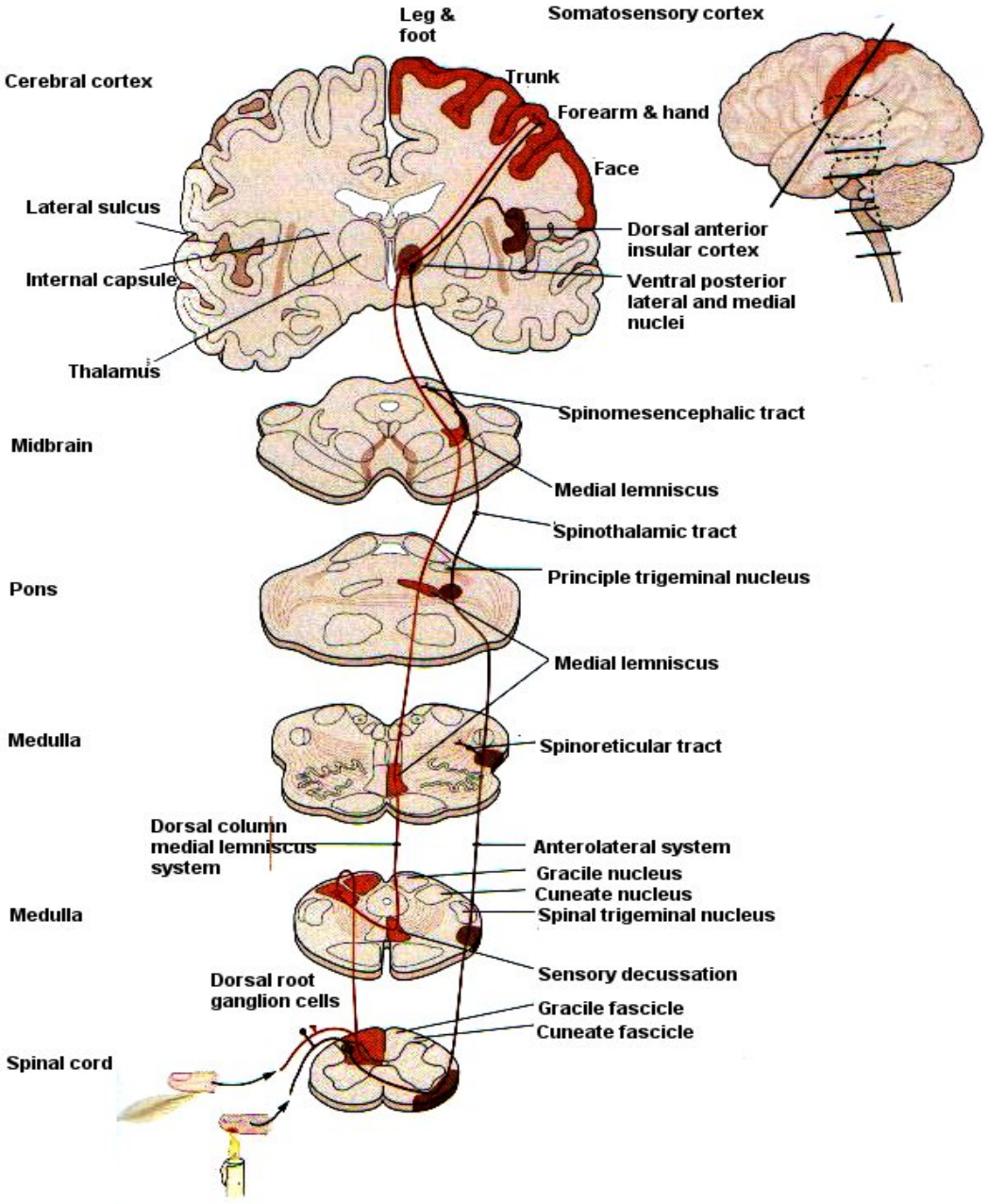

Figure 5: The somatosensory nerve pathways. Sensations of touch, pain and temperature are carried through the anterolateral system and vibration, pressure and proprioception information are carried through the dorsal column medial lemniscal system [42].

the contralateral ventral posterior lateral nucleus in the thalamus. The signal is then sent to the primary somatosensory cortex (SI) located in the postcentral gyrus and the nerve cells here relay it to the secondary somatosensory cortex (SII) located in the lateral sulcus.

When nerve signals are divided in the dorsal root ganglion, nerve fibres carrying information about touch, pain and temperature are sent along the anterolateral system. These nerve fibres cross in the dorsal root ganglion to the anterior contralateral column and ascend to the brain stem. As the nerve signals pass through the spinal cord the fibres cross again to the dorsal horn and eventually join the fibres of the DCMLS in the midbrain. They go on to synapse in the same cells in the thalamus which relay the signals to the SI area. Pain and temperature signals are also relayed to the dorsal anterior insular cortex and the anterior cingulate gyrus.

2.5 Primary Somatosensory Cortex

The cerebral cortex is the outer layer of the brain and consists of neuronal cell bodies. It is made up of a number of lobes, shown in Figure 6. The body and its senses can be mapped across the cortex and functions are localised to specific regions, for example, areas concerned with vision are located in the occipital lobe and language in the temporal lobe. There can be more than one region concerned with the same function, these are often termed the primary, secondary and even tertiary functional areas. Advances in technologies such as magnetic resonance imaging (MRI) and magnetoencephalography (MEG) have enhanced our understanding of how these areas interact and function to produce the sensations and experiences we often take for granted in everyday life.

The body can be mapped across the somatosensory area in the postcentral gyrus by the homunculus shown in Figure 7 and across the motor area in the precentral gyrus in a similar way. The homunculus, meaning ‘little man’, is the image of the human body drawn in proportion to how much surface of the cortex is

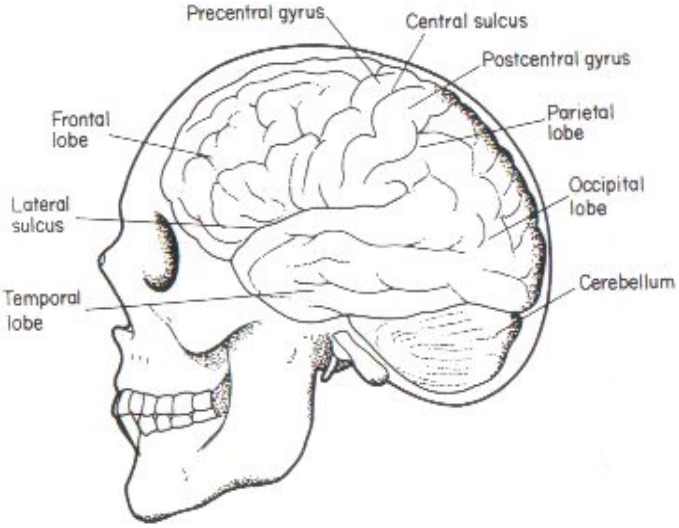

Figure 6: The lobes and most prominent structures of the human brain [44].

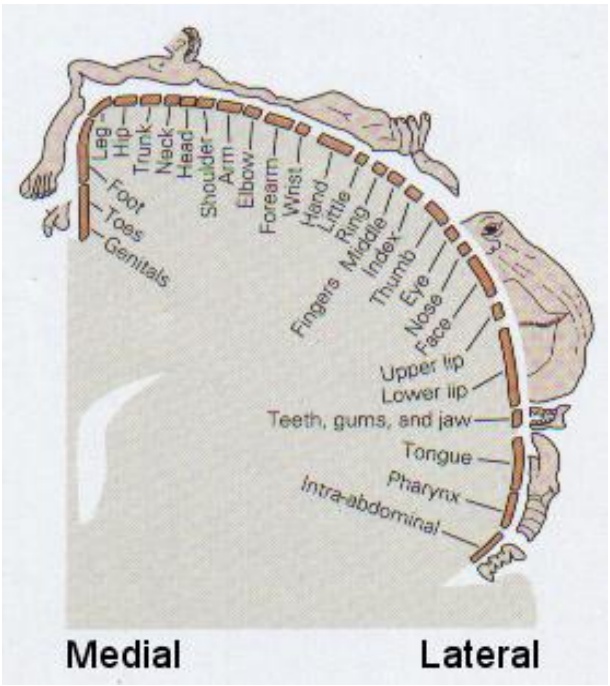

Figure 7: The homunculus mapped across the primary somatosensory cortex [42].

dedicated to the body part. In the somatosensory area, SI, this corresponds to the number of nerve endings in that particular area of skin. For example, human lips are very sensitive as they contain a large number of nerve endings therefore they also have a large area dedicated to them. The homunculus can be traced across the cortex in the sensory and motor areas in both hemispheres. The 'maps' on the right hemisphere correspond to the left side of the body and vice versa due to the crossing of the nerve pathways in the neck. The foot and genital representations are located at the top of the brain in the fissure separating the two hemispheres and the rest of the body extends across and down towards the temporal lobe as shown in Figure 7.

2.6 Brodmann Areas

In the early part of the twentieth century a German anatomist, Korbinian Brodmann, used the cytoarchitecture of the brain to distinguish different areas. This involved looking at the arrangement of the nerve cells within the brain and labelling the areas according to their patterns. He found 52 distinct areas which largely reflect the grouping of functions and they are now referred to as Brodmann areas. As studies into the brain cytoarchitecture continue Brodmann's original maps are being updated.

The SI area covers Brodmann areas 1, 2, 3a and 3b, they are shown in Figure 8. Brodmann area 3a lies at the fundus of the central sulcus and extends up the anterior wall of the postcentral gyrus where it meets area 3b. At the top of the gyrus is area 1 and area 2 lies on the posterior wall and ends at the postcentral sulcus. The cytoarchitecture shows that each area contains its own complete representation of the body and they each receive inputs from different receptors [40, 42, 45, 46]. Areas 1 and 3b receive the nerve signals from the skin receptors and areas 2 and 3a receive nerve signals from the deeper receptors in the muscles and joints. Therefore areas 1 and 3b activate in response to light touch information and areas 2 and 3a respond to deeper vibrational and proprioceptive inputs.

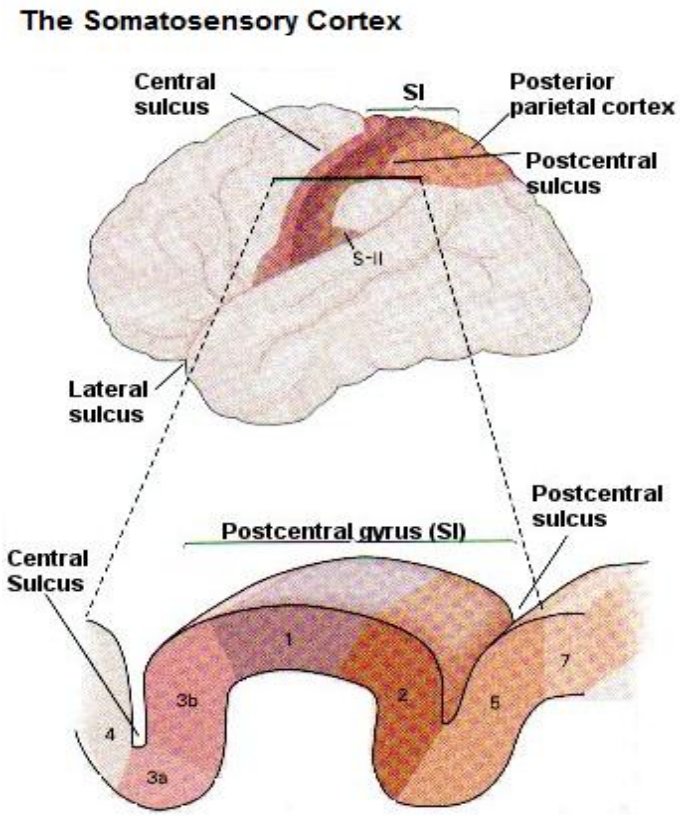

Figure 8: The four Brodmann areas within the somatosensory area. Each area contains it own complete representation of the body [42].

As described in Section 2.4 signals are relayed from the ventral posterior lateral nucleus in the thalamus to the SI areas. Signals are passed predominantly to areas 3a and 3b with only a small amount being projected directly to 1 and 2. Areas 1 and 2 also receive secondary projections from 3a and 3b. All four areas then project signals to the secondary somatosensory area and to Brodmann areas 5 and 7 in the posterior parietal cortex which integrate the touch and proprioceptive inputs. They also integrate bilateral inputs and visual information to form a complete picture of the sensory experience. Some information is also passed to the amygdala and the hypothalamus which are associated with memory and learning.

2.7 Coordinate Systems of the Brain

Functional activations in MRI images can be located according to a coordinate system based on the individual brain. However, if we wish to compare the data of different people it is necessary to use a standard coordinate system and even normalise the images to a standard template. The Talairach system has now been adopted by many groups around the world and was developed by Talairach and Tournoux in 1988 [47] when they performed a post mortem examination of a single female brain and photographed and labelled all the structures. They set their origin reference point to the anterior commissure (AC), a small but easily identifiable structure near the centre of the brain. It is a bundle of white fibres that connects the two hemispheres and lies in front of the fornix. There is also a posterior commissure (PC) which is much harder to discern on an MR image and lies in front of the superior colliculi. The z axis in the Talairach coordinate system is vertical and bisects the two hemispheres along the interhemispheric fissure and intercepts the AC, as shown in Figure 9. This is also called the saggital plane. The horizontal plane, y axis, lies along the plane that is formed by drawing a line through the AC and PC points, (the axial plane). The x axis, coronal plane, lies orthogonal to the y and z axes and intercepts the AC.

It is important to be clear what is meant when coordinates are described using the Talairach system. In some instances MR images are squashed and normalised to a Talairach template that has been formed from the atlas. In others, the images are described as being in Talairach space as the origin is set to the AC and the y axis lies in the plane of the AC/PC line but the images may have been normalised to another template or the person's own structural data.

As the Talairach brain was examined post mortem there will be obvious deformations to any template taken from it. Although many people do use the Talariach template, in this project all images are normalised to the template developed by the Montreal Neurological Institute (MNI) [49] that is supplied with

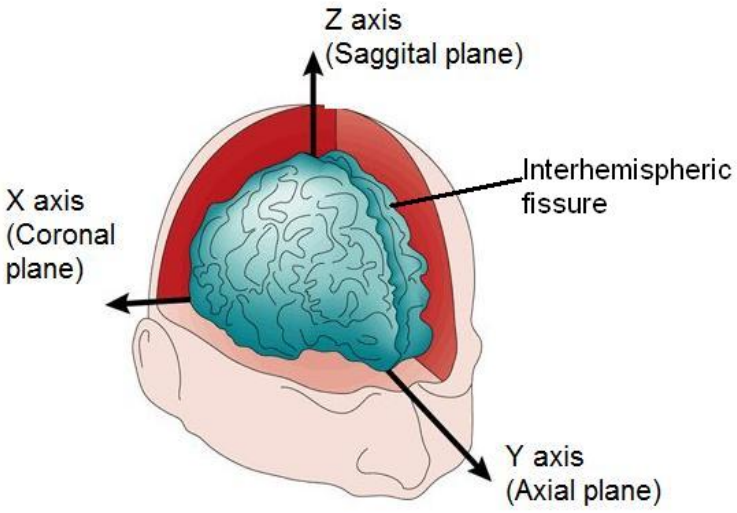

Figure 9: The Talairach coordinate system based on the anterior and posterior commissure line [48].

the SPM processing software. The MNI took 250 structural T_2-weighted MR images of healthy volunteers and identified a set of markers in each scan and then scaled these to the Talairach brain to produce an averaged template that was more representative of the general population. This template has been improved over the years and the current template has had a further 200 images normalised to it and it conforms to the International Consortium for Brain Mapping (ICBM) NIH P-20 project [50]. The origin is placed at the AC and the AC/PC line is used to define the axial plane.

When comparing the MNI brain to the Talairach atlas the MNI template is slightly larger than the Talairach brain and this is most noticeable at the edges of the image where a 10 mm difference can be observed. To locate the Brodmann areas within each template, there is an atlas for the Talairach brain but none exists for the MNI template. MNI coordinates must be corrected to Talairach coordinates before the Talairach atlas can be used. The two conversion methods that exist only provide an estimate as there are many variabilities introduced, eg. the Talairach brain is slightly misshapened due to the post mortem examination, the MNI brain is an average and the subject's own does not normalise to it exactly.

The first method is an affine transformation which applies a scale factor to each x, y and z coordinate:

$$X' = 0.88X - 0.8 \tag{1}$$

$$Y' = 0.97Y - 3.32 \tag{2}$$

$$Z' = 0.05Y + 0.88Z - 0.44 \tag{3}$$

It was developed in 1998 by Andreas Meyer-Lindenberg of the National Institute of Mental Health and the method assumes a linear relationship in all directions. As an example, using an MNI coordinate of, say, (-50 -20 50) would give a Talairach coordinate of (-43.2 -16.1 44.6).

The second method is a non-linear transformation which was developed by Matthew Brett at the MRC Cognition and Brain Sciences Unit (CBU) [49]. It involves applying a different correction to the areas above and below the AC/PC line. The transform above the AC:

$$X' = 0.9900X \tag{4}$$

$$Y' = 0.9688Y + 0.0460Z \tag{5}$$

$$Z' = -0.0485Y + 0.9189Z \tag{6}$$

and below the AC:

$$X' = 0.9900X \tag{7}$$

$$Y' = 0.9688Y + 0.0420Z \tag{8}$$

$$Z' = -0.0485Y + 0.8390Z \tag{9}$$

Using the same example of (-50 -20 50) would return a Talairach coordinate of (-49.5 -21.7 46.9). There is a clear difference between the two methods but the non-linear method attempts a better fit between the two templates therefore where coordinates have been quoted in the Talairach brain in this thesis the second transformation has been used.

The physiological processes involved in the perception of touch have been described in this chapter. The next chapter uses this information to describe the processes involved in CRPS.

Chapter 3

Complex Regional Pain Syndrome

3.1 Introduction

Complex regional pain syndrome is a chronic pain condition characterised (often) by excessive pain, swelling and trophic changes. Although various clinical, imaging and animal model studies have furthered our understanding there is still much left to be investigated and unravelled. Functional MRI is just one tool that is being used in this journey of discovery. This chapter describes the aetiology of the disease and the arguments for cortical reorganisation.

3.2 Onset of the Disease

CRPS can arise after a (sometimes very minor) insult but it can also occur spontaneously where no precipitating injury is identified. It affects both males and females alike and strikes at any age. Symptoms develop up to 6 months after the noxious event [51]. Some studies have suggested a higher incidence of CRPS in women over 50 [52] but this may be explained by the fact that this group is more likely to suffer fractures due to osteoporosis and muscle wasting.

Type I CRPS develops most frequently after wrist and ankle fractures and

it has been estimated that up to 25 % of patients with distal radius fractures develop the disease [53]. Other factors have been found to contribute to the risk of developing the disease. There is a link between certain drugs and the incidence of CRPS, these include phenobarbitone, phenytoin, isoniazid, cyclosporine, tacrolimus and rapamycin. Medical conditions can also make patients susceptible to CRPS, such as diabetes mellitus and hyperthyroidism [51]. Genetic factors have also been linked. Those with CRPS have a high frequency of the gene HLA-DQ1. Genetic patterns also show that patients with CRPS who progress towards generalised dystonia have an association with the gene HLA-DR13 [35, 54].

Although no evidence has been found of psychological factors having a role in the development of the disease [52], chronic pain often results in anxiety, depression and social difficulties as well as financial strain [55].

3.3 Symptoms

When an area of the body develops CRPS it undergoes a number of changes producing a range of symptoms. The changes that occur can be divided into three broad groups - sensory processes, motor responses and the functioning of the sympathetic nervous system [27, 28, 34, 35, 52, 54].

Sensory changes cause the affected area to become hypersensitive, and stimuli that are not normally painful evoke pain (allodynia). The pain is often described as ‘burning’ and is out of proportion to the insult. Pain can also arise spontaneously. Although hypersensitivity is often associated with CRPS, in some patients the converse can be true and they experience sensory loss or numbness.

Motor changes that take place include decreased mobility in the affected limb, weakness, muscle dystonia, tremors and jerking movements (myoclonia). In severe cases there is contracture of the tendons causing the associated joints to become stiff and fixed (ankylosed).

The sympathetic nervous system regulates blood flow and other autonomic functions. This regulation is disturbed in cases in CRPS. Figure 10 shows a

Figure 10: Patient with CRPS in the left hand and forearm [57].

patient with CRPS of the left hand and forearm. It can be seen that redness and swelling are present over the entire area.

It has been identified that there are three stages which the disease may progress through [51, 52]. The disease begins with the *acute* or *hyperaemic* stage and is characterised by vasodilatation (the area becomes warmer) and plasma protein extravasation (oedema). In the next stage, *dystrophic* or *ischaemic*, vasodilatation reverses to vasoconstriction (the area becomes cooler) but swelling can become more extensive. In the final stage, *atrophic*, muscular changes become apparent and the effects of the disease become irreversible. The stages are described in more detail in Table 3. The duration of each stage can vary from weeks to years but generally lasts 3 - 6 months.

The skin undergoes trophic (nutritional) changes in CRPS and may appear dry or moist demonstrating hyper- or hypo- hidrosis. In the early stage patchy bone demineralisation starts (within 3 weeks) and becomes more diffuse as the disease progresses causing permanent damage [51, 56]. It should be noted that patients do not always display all the symptoms or progress through the three stages. It is possible for the disease to present itself in the second stage with the

Table 3: Progression of CRPS [51, 52].

Stage 1 - Acute or hyperaemic
Vasodilatation occurs Skin appears red and feels warm to the touch Oedema may be present
Stage 2 - Dystrophic or ischaemic
Vasoconstriction Skin becomes moist, pale, cold or cyanosed Temperature can fluctuate between hot and cold Oedema can spread Increasing stiffness in associated joints Muscular atrophy begins Hair can become coarse Nails can become brittle and show ridges
Stage 3 - Atrophic
Ongoing cold sensation Trophic changes continue to muscles, tendons and skin becoming irreversible Extreme weakness is exhibited Limited mobility in joints which eventually become ankylosed

affected area appearing cool and cyanosed. It is also possible for CRPS to start in one small area of a limb and spread the entire length of it and eventually develop in the opposite extremity. Also, the disease can spontaneously resolve itself at any point. This variance between patients adds to the difficulty of diagnosis and the understanding of the aetiology of CRPS.

3.4 Diagnosis

The International Association for the Study of Pain (IASP) set out criteria for the diagnosis of CRPS [27, 58]. It listed four points and 2, 3 and 4 should be met to indicate the disease. They are:

1) Symptoms develop after an initiating noxious event.

2) Spontaneous pain or allodynia/hyperalgesia is present and is not limited to the territory of a single peripheral nerve and is disproportionate to the inciting event.

3) There is or has been evidence of oedema, skin blood flow abnormality, or abnormal sudomotor activity in the region of the pain since the inciting event.

4) The diagnosis is excluded by the existence of conditions that would otherwise account for the degree of pain and dysfunction.

CRPS can often be mistaken for other diseases and yet there is a tendency to over diagnose [54]. Diagnosis of CRPS relies on the exclusion of other diseases as there is no known biological marker. Haematology and biochemistry tests usually show no abnormalities [59].

Laser Doppler flowmetry is a procedure that is often used [54] to investigate vascular changes. It measures blood flow using the Doppler effect. Information about vascular function can also be gained from three-phase bone scanning [51]. This procedure involves injecting a radioactive compound into the patient. In the first phase information is detected about vascular function as the compound perfuses into the affected area. During the second phase the compound may 'pool' in the extracellular material indicating hyperaemia (excess of blood). In the final stage the bones are scanned to assess their uptake of the compound. If inflammation is present in soft tissue only then abnormal perfusion will be detected. If the inflammation is more extensive hyperaemia is seen in the second stage. Changes to the bones, such as demineralisation, are detected in the third phase.

In the later stages of CRPS the bone demineralisation causes significant changes which can easily be seen on a standard x-ray image [54]. Magnetic resonance imaging is more sensitive to tissues than bone and can be used to detect changes in joints and soft tissues [54].

Doctors are increasingly using infrared thermography as a means of diagnosis. This shows temperature changes across the body. In CRPS diagnosis, the affected area is measured as $\geq 2.2\ ^0$C warmer than the rest of the body [60].

Hargreaves and von Frey testing are used to assess the level of hyperalgesia and allodynia. This involves applying fine wires or strips to the area and observing the patient's level of pain. The McGill pain scale or a visual analogue scale is commonly used to do this. In the latter, the patient is shown a line drawn on a piece of paper with a 0 at one end and 10 at the other. They are told that zero represents no pain and that ten is the worst pain imaginable. The patient is then asked to mark where they feel their pain is on the scale. The distance from the zero to the mark is then taken as a quantitative measure of the pain [61].

3.5 Changes Associated with CRPS

Over the years scientists and clinicians have investigated different theories as to the cause and aetiology of CRPS. Theories put forward include overactivity of the sympathetic nervous system, a peripheral disease with dysfunctioning primary synapses or a changed response to neurotransmitters, and a central disease involving the substantia nigra [51, 53, 59]. None of these ideas can fully account for the development and progression of the disease or the symptoms that are observed.

3.5.1 Peripheral Changes

The normal sequence of events when the body detects a noxious stimulus starts with the pain receptors in the skin (nociceptors). The small diameter myelinated nerve fibres, Aδ, quickly carry the generated signal to the brain. This produces 'fast' pain which is characterised as a sharp and localised sensation. If tissue damage has occurred then a number of chemicals are released including prostaglandin and bradykinin.

Prostaglandins are formed from essential fatty acids and a number of different types exist with different functions, these include dilation/constriction of blood vessels, raising the temperature of the body, producing inflammation, and influencing the function of platelets. They also sensitise the nociceptors to bradykinin.

Bradykinin is a peptide that attracts leucocytes, increases the permeability of

capillaries and causes vasodilatation. It also stimulates the unmyelinated C fibres. These fibres carry signals much more slowly than the Aδ fibres and produce 'slow' pain, characterised by a dull and diffuse sensation.

Together, prostaglandin and bradykinin have the effect of causing plasma protein extravasation, inflammation and increased blood flow in the injured region.

In CRPS vasodilatation is most prominent during the first two - four months while the disease is still in the acute phase and reverses to vasoconstriction in the later stages as the disease changes to a chronic condition [34]. Weber et al. [62] stimulated nerve fibres in CRPS patients and a control group using transcutaneous electrical stimulation and measured the response of blood flow and protein extravasation. In the CRPS patients blood flow increased significantly and protein extravasation was detected. In the control group blood flow increased only marginally and protein extravasation was not detected. This indicates that neurogenic inflammation in the peripheral nerves is a part of the pathology of the disease.

The body's normal response to inflammation, healing wounds and fractures includes the release of the neuropeptide substance P and calcitonin gene related peptide (CGRP). Substance P regulates activity in the nerves and CGRP regulates the calcium level in the extracellular matrix. The study by Weber et al. [62] also showed that CRPS patients have an increased concentration of these neuropeptides in their blood further indicating an inflammatory response. This is further supported by Guo et al. [56] who carried out a study on rats to investigate the time course of vascular, nociceptive and bony changes after hindpaw immobilisation and fractures. In half the group Guo et al. fractured the hindpaw and placed a cast over it for four weeks. In the other half they left the hind paw intact and simply placed a cast over it for the same amount of time. When the cast was removed both groups showed symptoms of oedema, allodynia and increased warmth in the limb, similar to the symptoms observed in CRPS. They proceeded to treat some of the rats from both groups with a substance P receptor (NK_1) antagonist and noted that spontaneous extravasation, hindpaw warmth

and oedema were all reduced. The neurogenic inflammation may be occurring via an increased release of neuropeptides, impairment of their inactivation or by the receptors becoming over-sensitive [34, 62].

There is increasing evidence that prolonged peripheral tissue ischaemia may also be a factor in the cause of the disease [63]. Although a high arterial flow has been measured in CRPS patients there is low oxygen consumption and an increase in skin lactate. Cold CRPS limbs have reduced blood nutrition supply causing the trophic changes observed. Coderre et al. [63] carried out an ischaemic reperfusion study on rats where circulation to the hindpaw was occluded for three hours. In the four weeks following reperfusion the rats displayed similar symptoms to CRPS patients including hyperalgesia and allodynia. Similar symptoms were also detected in the contralateral hind paw. Symptoms not displayed by the rats were severe muscle weakness and contractures.

There is clear evidence for peripheral changes in CRPS but changes in the cerebral cortex have also been found.

3.5.2 Cortical Changes

Clinical observations of CRPS and other chronic pain conditions converged with advances in scientific imaging to develop our understanding and formulate the idea that CRPS might be caused by reorganisation of sensory-motor pathways in the cerebral cortex. The belief is that neuronal pathways are somehow altered and the homunculus becomes distorted with some functional areas shrinking and others enlarging and overlapping with other functional areas. A number of experimental studies have been carried out to investigate this and are discussed in Chapter 1.3.1. To summarise, the functional imaging data showed that the intensity of the SI activity was greater in some patients and decreased in others. They also showed that the functional area had moved and that the digit representations were closer together on the brain.

In parallel to these studies, other imaging studies of graphic dystonia (writer's cramp) have been carried out. Butterworth et al. [23] used fMRI to investigate

Figure 11: Typical setup of a mirror visual feedback session [64].

cortical reorganisation. The fingertips of patients and a healthy control group were stimulated and the brain activity recorded. They found in the patients that there was a smaller separation between the representations of the index finger and the little finger, 4.1 mm compared to 9.6 mm for controls. Sanger et al. [24] carried out a similar study and also found a degree of reorganisation and abnormal function.

This suggests that reorganisation may be common to many chronic pain conditions and it has been proposed that such reorganisation might be caused by incongruence between sensory input and motor output. A study by McCabe et al. [64] investigated the idea of incongruence causing pain by using mirror visual feedback (MVF) to treat patients with CRPS. This involves placing a mirror between the affected limb and the unaffected limb in such a way as the patient can only see the 'healthy' limb and its reflection, as shown in Figure 11. The patient then attempts to move both limbs in a similar manner, producing an awareness of similar motor commands to the two limbs but (because of the mirror) unawareness of possible differences in movement achieved. The visual input to the brain is that the affected limb is moving correctly and this 'fools' the brain into believing that no pain or stiffness should be felt.

McCabe et al. found this treatment to be very effective at relieving pain and stiffness in patients who had had the disease for less than one year. Patients

with long term CRPS, more than two years, reported no relief of pain or stiffness. This could possibly be due to the firmer establishment of neural pathways or the establishment of long term contractures and trophic changes. When patients carried out the task without the reflection then the pain stayed the same or became worse. These results support the idea that movement is centrally processed in the brain and that congruence is needed between visual input and motor intention for the body to function in a normal way.

This is also supported by another study involving MVF carried out by Moseley [65] using a motor imagery program. This involved three stages each lasting two weeks - the recognition of hand laterality, imagined hand movements and MVF. Patients were shown a series of right and left hands in a number of positions and were asked to recognise whether the hand was the right or the left. Patients took longer to recognise the hand that corresponded to their affected side. For the second part, the patients were asked to imagine moving their own hand to the same position as the pictured hand and finally patients were asked to use MVF and adopt the same position as the pictured hand. After six weeks of treatment pain levels had lowered, finger circumference had reduced and patient response times were quicker. A control group was used for comparison. They were treated with conventional methods and after the six week trial showed no change to the initial measurements.

CRPS and Phantom Limb Pain

An area of medical research that overlaps with CRPS is phantom limb pain. When a limb has been amputated patients can often feel that the limb is still present and, in some cases, they even feel they are able to control its movements [66].

Patients often experience pain as the phantom limb ‘stiffens’. Some patients with upper limb amputation have reported pain which is similar to nails digging into the palm of the hand as if the hand was clenched and that they are unable to unclench it to gain relief [67].

It is estimated that around 78 % of amputees develop phantom limb pain [68]

with some patients able to feel the phantom limb less than twenty-four hours after surgery. This rapid onset is too quick for cortical reorganisation to take place and is probably due to activation of latent neural pathways. Eventually axonal sprouting occurs and new neuronal pathways form resulting in reorganisation [69].

Functional imaging studies have shown that the sensory areas in the cortex on either side of the missing limb enlarge and spread into the missing limb area [31, 32, 33]. The brain's impression of the missing limb is not entirely removed so an overlapping occurs. Considering patients with upper limb amputation, on the cortex the hand is situated between the face and the upper arm. This can lead to a touch on the face being felt in the missing hand [69].

Haigh et al. [70] investigated phantom limb pain and rheumatoid arthritis (RA). They studied patients who, prior to the amputation, had bilateral RA in their lower limbs. The patients were instructed to exercise their intact limb and then imagine exercising their phantom limb which still felt as though the RA was present. The task had the result of relieving the pain in both limbs. Haigh et al. proposed that when a motor command is issued the brain also creates a template of the expected sensory feedback of the movement which is compared with the actual sensory information obtained from proprioception. When there is a continual incongruence between the two signals dysfunction occurs in the central processing resulting in peripheral pain, stiffness and other symptoms.

Ramachandran and Rogers-Ramachandran [67] used MVF to treat upper limb amputees with phantom limb pain. The patients placed a mirror between their limbs as shown in Figure 12. They were asked to move their hand whilst imagining the movement of their phantom hand. The visual feedback informed the brain the phantom hand was present, healthy and moving. Patients reported alleviation of their pain and for one patient, repeated use over a period of two weeks resulted in the complete disappearance of the phantom limb.

Following the suggestion that similar mechanisms are involved in CRPS and phantom limb pain: after fractures, the limb is immobilised and cannot move normally. As in the case of amputees, this incongruence between intention and

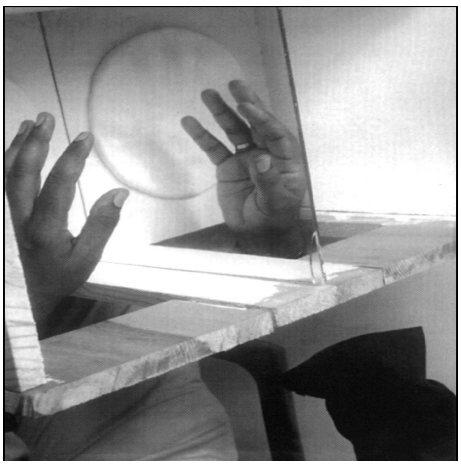

Figure 12: Mirror visual feedback treatment in phantom limb pain [67].

sensory feedback could then lead to dysfunction; this may provide an explanation for the occurrence of CRPS after fracture.

3.6 Summary

There is much evidence to support both a peripheral involvement and a central processing system but it still remains unclear as to what mechanisms are involved in the development of the disease. When the disease can occur spontaneously as well as after a broad range of traumas it is difficult to find one set of rules that fits all the observations. Moseley and Gandevia [71] questioned whether cortical reorganisation caused the pain in CRPS or if the reorganisation was the consequence of the pain (which is caused by another mechanism). Research has yet to resolve this point.

In this chapter the peripheral and cortical characteristics of the disease have been discussed. The next three chapters relate to the equipment used to obtain the experimental data using patients and healthy subjects and the processing of the fMRI data.

Chapter 4

Magnetic Resonance Imaging

4.1 Introduction

The phenomenon of nuclear magnetic resonance (NMR), also known as magnetic resonance (MR), was discovered by both Felix Bloch and Edward Purcell working independently in 1946. The technique was developed for various molecular and medical applications over the coming decades including magnetic resonance imaging (MRI). In 1977 Sir Peter Mansfield demonstrated the echo-planar imaging (EPI) technique [72] which was later developed into functional magnetic resonance imaging (fMRI) by two groups (Ogawa et al. [73, 74, 75, 76] and Belliveau et al. [77, 78]).

FMRI of the brain indirectly detects neuronal activity by detecting the change in oxygenation that occurs when a task is carried out, e.g., arithmetic, perception of sensory or visual stimuli, real or imagined movements. This change in oxygenation follows a specific pattern over time and is called the haemodynamic response function (HRF). The sensitivity of MRI measurements to oxygen changes is called the blood-oxygen-level-dependent (BOLD) effect. As the oxygenation levels change there is a change in the MR signal of a few percent thus indicating the areas of the brain where the activity is occurring.

This chapter explains the physics behind MRI and the technique of fMRI.

4.2 The Physics of MRI

MRI relies on interactions with the magnetic moments of nuclei. Protons and neutrons have an intrinsic spin (angular momentum) which is associated with a magnetic moment. In nuclei where there is an even number of protons and neutrons the nucleons combine in pairs producing no net angular momentum or magnetic moment and the NMR experiment is not possible, but most elements have isotopes of non zero spins which allow NMR. However, in biological applications only a few of these isotopes are present in large enough quantities to produce a useful NMR signal, so there is a limit to the number of elements that can be used. Hydrogen is the most abundant atom in the human body and consists of a nucleus of one proton (spin 1/2) and one electron. It binds to other elements to form water and fat molecules and dominates the NMR signal when imaging. (Hydrogen in other biomolecules, which offer a less 'liquid-like' environment, is less easily detected). Different tissues have different concentrations of hydrogen (different proton density) and this produces contrast in the images allowing different structures to be identified.

The net magnetic moment of the nucleus is aligned in the same direction as the angular momentum. Both quantities are vectors, having direction and magnitude. The ratio of them is called the gyromagnetic ratio γ and has a specific value for different elements/isotopes.

When nuclei are placed in an external magnetic field they align either parallel or anti-parallel to it and the Boltzmann factor, Equation 10, predicts that there will be slightly more spins aligned in the parallel direction as this is the lower energy state.

$$\frac{N_b}{N_a} = e^{-\frac{E_b - E_a}{kT}} \tag{10}$$

N_a is the number of protons aligned parallel to the field with energy E_a and N_b is the number of protons aligned anti-parallel with energy E_b, k is Boltzmann's constant and T is temperature; in medical imaging this is body temperature. In

the applied field the spins precess with random phases and produce a small net longitudinal magnetisation aligned parallel to the field.

When a radio frequency pulse is applied some of the energy will be absorbed by the nuclei and the spins tip away from the applied field towards the transverse plane; this can be detected by a receiver coil and is described by the Bloch equation, Equation 11, where M is the net magnetization, B_0 is the strength of the external magnetic field and T_1 and T_2 are the longitudinal and transverse relaxation times, respectively (see below).

$$\frac{d\underline{M}}{dt} = \gamma \underline{M} \times \underline{B}_0 - \frac{M_x \underline{\hat{x}} + M_y \underline{\hat{y}}}{T_2} - \frac{(M_z - M_0)\underline{\hat{z}}}{T_1} \tag{11}$$

When considering the transverse and longitudinal components separately Equation 11 has the form:

$$\frac{dM_x}{dt} = \gamma B_0 M_y - \frac{M_x}{T_2} \tag{12}$$

$$\frac{dM_y}{dt} = -\gamma B_0 M_x - \frac{M_y}{T_2} \tag{13}$$

$$\frac{dM_z}{dt} = -\frac{M_z - M_0}{T_1} \tag{14}$$

The frequency of the exciting radio frequency pulse is determined by the precessional frequency of the nuclei. In an applied magnetic field the nuclear spins precess around the field at a frequency proportional to the strength of the field. This is given by the Larmor equation and is derived from the first term on the right hand side of the Bloch equation (Equation 11):

$$\omega_0 = \gamma B_0 \tag{15}$$

where ω_0 is the Larmor frequency in Hz. This shows that the precessional frequency increases as the strength of the magnetic field increases. For example, the precessional frequency of protons in a 1.5 T magnetic field is 63.86 MHz. The duration and amplitude of the pulse can be chosen to produce a particular tip

angle, and pulses are often described by the angle they produce, e.g., 90° pulse. Once the pulse is switched off the spins return to their normal unperturbed state with a characteristic relaxation time T_1 also called the spin-lattice relaxation time. This change in the magnetization over time is given by solving Equation 14:

$$M_z(t) = M_0[1 - e^{\frac{-t}{T_1}}] \tag{16}$$

The pulse also has the effect of bringing the spins into phase as their net magnetisation precesses around the direction of the field in the transverse plane. If the applied magnetic field includes inhomogeneities, the spins will precess with slightly different frequencies causing dephasing. Therefore as coherence is lost the net magnetisation signal will decay (faster than the T_1 decay) with a characteristic time T_2 also called the spin-spin relaxation time, Equation 17. This process is demonstrated in Figure 13.

$$M_{xy}(t) = M_0 e^{\frac{-t}{T_2}} \tag{17}$$

In addition to the dephasing characteristic of a particular tissue, the nuclei are also influenced by non-uniformities in the B_0 field, either intrinsic inhomogeneities or related to a difference in magnetic susceptibility between tissue boundaries. These effects alter the spin dephasing but they can be calculated using Equation 18. The time with which the magnetisation decays accounting for these effects is denoted T_2^*.

$$\frac{1}{T_2^*} = \frac{1}{T_2} + \frac{1}{T_{2inhomo}} + \frac{1}{T_{2suscept}} \tag{18}$$

4.2.1 Image Encoding

Slice selection and phase and frequency encoding are applied in order to define the region to be imaged. Slice selection allows the width of a slice through a body to be defined; this is the image plane, usually denoted the z axis. It is carried out by applying another magnetic field to B_0 which is spatially varying

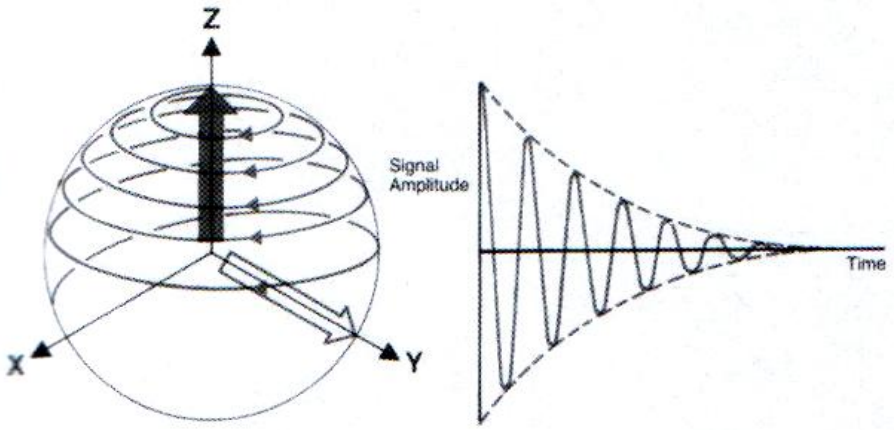

Figure 13: Free Induction Decay: As the spins dephase and return to their unperturbed state the signal decreases exponentially over a characteristic time, T_2. In an inhomogeneous field the signal decays more quickly, over a characteristic time T_2^* [41].

with a linear gradient G. As the gradient varies then the Larmor frequency will also vary. A RF pulse is tailored to a narrow band of frequencies (bandwidth) which is centred on a frequency, f_0. This allows the image plane to be defined. The relationship between the slice thickness, the gradient and the bandwidth are shown in Equation 19.

$$z = 2\pi \frac{f_1 - f_2}{\gamma G_z} \tag{19}$$

Both the gradient and bandwidth can be varied to select the appropriate thickness. In practice, the bandwidth is kept small and the gradient is adjusted as necessary.

Phase and frequency encoding is applied during the receiving of the MR signal to distinguish point sources of signal in the image plane (here taken as the x, y plane). This is done by applying another two magnetic field gradients, one in the x direction and one in the y direction.

The y direction gradient linearly varies the phases of the nuclei. Before the gradient is applied the spins of the nuclei are in phase. When it is applied the frequency or speed of the spins change along the gradient, either becoming faster

or slower, causing dephasing. When the gradient is turned off the phase angle of the spins between nuclei remain the same but the speed reverts to its original frequency. This is phase encoding.

A similar process can be carried out for frequency encoding in the x direction. The applied gradient produces a linearly varying precessional frequency. During the application of the gradient the MR signal is sampled at different time points. At each point (in time) there is a different amount of phase change producing a different spatial frequency.

In summary, phase encoding is the rate of change of the phases between one phase encoding step and another. Frequency encoding is the rate of change of the phases within a single step.

These steps produce a data matrix of spatial frequencies with different amplitudes. Fourier theory states that an image may be decomposed into a spectrum of sinusoidal spatial frequencies - k-space. Each point of raw data creates a point in k-space, although not spatially the same point. High frequency information about the signal to noise and contrast is concentrated at the centre of the image and the low frequency information about image resolution is located towards the edges. By applying a 2D Fourier transform to the raw data a 2D normal image of the object can be formed, see Figure 14

4.2.2 Image Sequence

In MRI there are two main image sequences: spin echo and gradient echo. Spin echo, demonstrated schematically in Figure 15, involves first sending a RF pulse to tip the spins away from the longitudinal magnetic field. The transverse magnetic field signal is then received but the spins soon become dephased as they are rotating at different frequencies. Another RF pulse is then applied to tip the spins by 180°. This has the effect of keeping the transverse magnetic field signal whilst reversing the direction the nuclei are spinning. Therefore the nuclei which are spinning faster are now behind the slower ones and they eventually catch them up causing the spins to rephase and produce an increase in the signal. Hence an

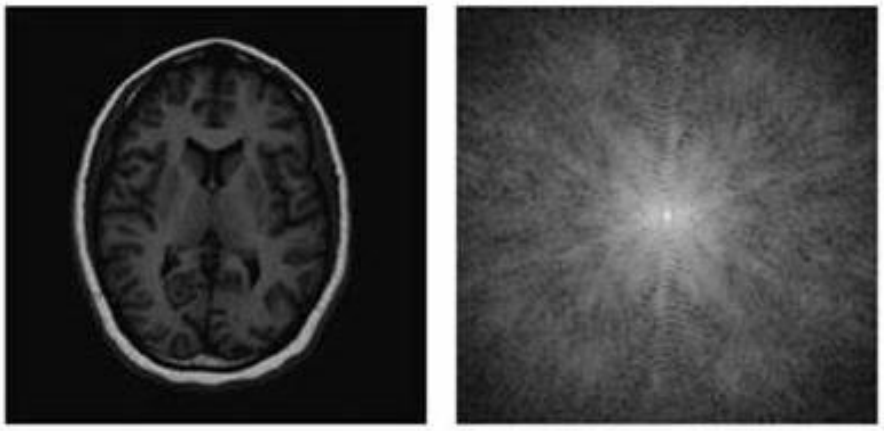

Figure 14: Left: MRI T_1 weighted image of the brain. Right: corresponding k-space image [79].

echo is observed as shown in Figure 15. This process can be repeated many times but the signal becomes weaker each time due to the free induction decay of T_2. The signal decays with relaxation time T_2, rather than T_2^*, as the dephasing effect of field non-uniformity (Equation 18) has been removed. Spin echo imaging is dependent on the T_1 of the material which makes the process slow. In conventional MRI, each RF excitation produces one line in the 2D k-space data matrix, and multiple excitations are required to complete the matrix and hence produce an image. The overall process typically takes tens of seconds.

In contrast the gradient echo technique depends on the T_2 property and can be carried out much faster. It uses similar principles to spin echo with the exception that a magnetic field gradient is applied instead of a RF pulse. Firstly, once the spins are in the transverse plane, the gradient is applied for a short time producing greater magnetic field inhomogeneities which causes the spins to dephase even faster. Another gradient is then applied but in the opposite direction and the spins then reverse by 180°. The signal then recovers as before as the phases refocus producing an echo.

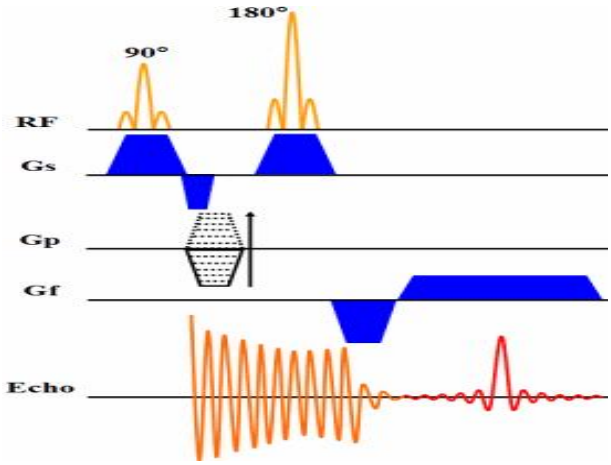

Figure 15: In spin echo imaging a RF pulse is first applied to tip the spins by 90° and then another RF pulse is applied to tip the spins by 180° bringing the spins into phase again and creating the echo in the readout [80].

4.2.3 Single Shot Echo Planar Imaging

Echo planar imaging (EPI) is a fast imaging technique which has applications in functional MRI where we wish to image changing physiological processes, e.g., changes in blood flow in different organs in the body. It allows a single slice of the body to be acquired in fractions of a second with a resolution of a few millimetres. A full 3D brain image can be acquired in a matter of 2 - 3 seconds.

As mentioned in the previous section, in conventional MRI a single line in k-space is acquired for each RF pulse that is transmitted to the sample. Single shot EPI allows the entire k-space data matrix to be acquired from just one pulse. This is achieved by rapidly switching the polarity of the frequency encoding gradient in combination with the normal phase encoding gradient, see Figure 16. The lines in k-space are built from a continuous path which moves to the next line when the polarity is reversed. This is demonstrated in Figure 17.

All fMRI studies in this project were carried out using single shot EPI.

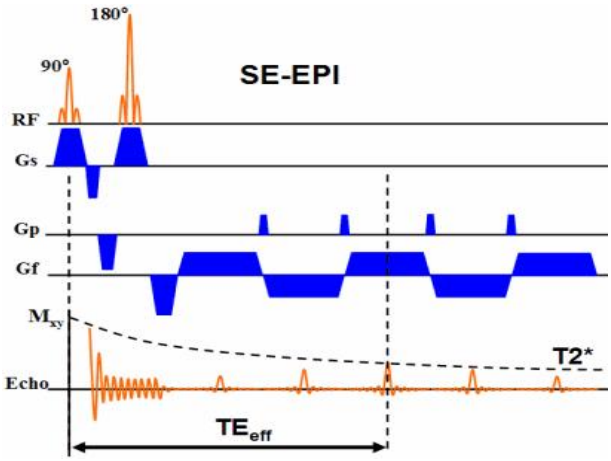

Figure 16: In echo planar imaging the polarity of the frequency and phase encoding gradients, G_f and G_p, are rapidly switched in order to build up lines in k-space using a single RF pulse [81].

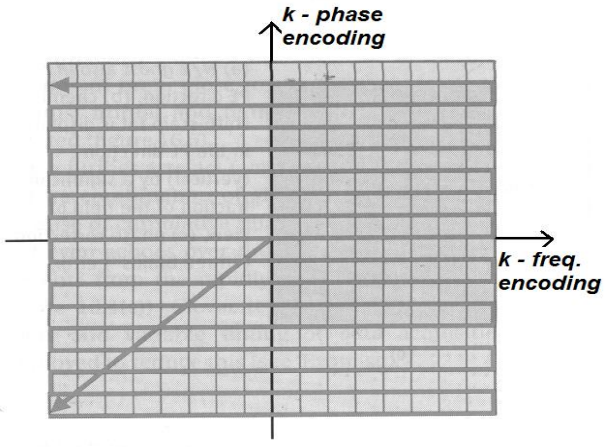

Figure 17: k-space trajectory in EPI [82].

4.2.4 Functional MRI and the BOLD Effect

Neuronal activity in the brain is inferred by detecting changes in the amount of oxygenated blood that is present in the arteries, veins and capillary beds surrounding the nerve cells. The red blood cells in the body contain haemoglobin which oxygen is able to combine with, forming oxyhaemoglobin, and be transported around the body. The oxygen is then extracted by the tissues and the molecules return to their deoxygenated state. When a task is not being carried out, about 40 % of the oxygen that reaches the capillary bed in the brain is extracted by the tissues leaving a large fraction of the blood in the capillaries as deoxyhaemoglobin [83].

Oxyhaemoglobin is a weakly diamagnetic molecule, where as deoxyhaemoglobin is paramagnetic due to the four unpaired electrons of the iron component. The change in magnetic susceptibility associated with the paramagnetic state influences the T_2^* signal causing it to decay faster; thus we see a reduction in the MR signal when blood becomes more deoxygenated. Conversely, when there is more oxyhaemoglobin in a region of the brain an increase in the MR signal is observed. As mentioned above, this is known as the blood-oxygen-level-dependent (BOLD) effect.

When a task is carried out the cerebral metabolic rate of oxygen ($CMRO_2$) increases slightly to meet the increased demands of the tissues. The vessels react and supply more blood at a faster rate, i.e., the cerebral blood flow (CBF) and the cerebral blood volume (CBV) increase, as demonstrated in Figure 18. These changes follow a characteristic time course. The $CMRO_2$ is the first process to spring into action. The higher rate of oxygen extraction initially produces a higher fraction of deoxyhaemoglobin in the blood therefore the MR signal will decrease, shown by the undershoot at the beginning of the HRF shown in Figure 19. (Note: this is the usual interpretation for the cause of the initial dip however due to the small signal change it is difficult to detect, especially at 1.5 T, and there is conflicting evidence for its existence and its origin - [83, 84]). The vessels then

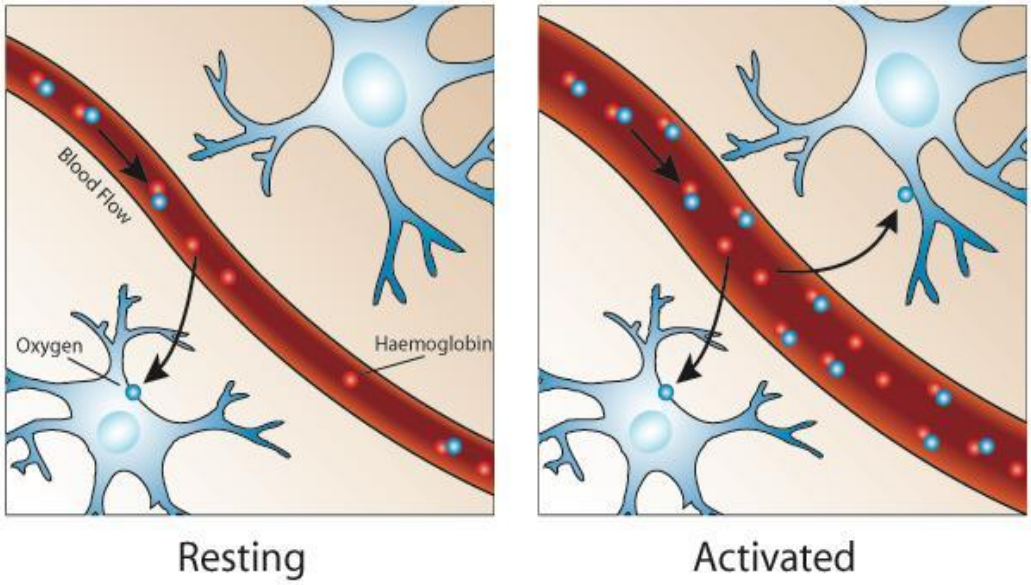

Figure 18: When a task is carried out the vessels make extra oxygen available to the tissues by increasing the CBF and CBV [87].

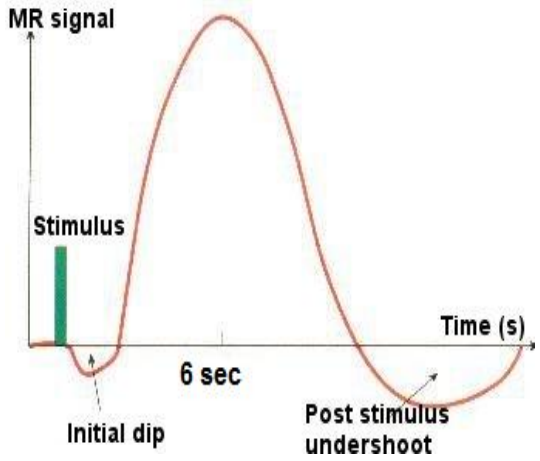

Figure 19: The haemodynamic response function associated with the BOLD effect follows a characteristic time course peaking at approx 3 - 6 seconds after the stimulus/task is commenced and can last for up to 60 seconds after the task has ended [88].

react increasing the volume and flow, to the extent that the increased oxygen supply is more than is needed by the tissues; blood oxygenation is higher than in the resting state and so the MR signal increases. The 'overshoot' takes about 3 - 6 seconds to peak and this can last for the duration of the task. Once the task is finished it can take up to 60 seconds (typically 10 seconds) for the vessels to return to normal and the MR signal slowly decreases during this time. Towards the end of the response (Figure 19) there is a post stimulus undershoot of the signal, attributed to a persistence of the increased $CMRO_2$ after the vessels' reaction has diminished. It should be noted that the signal only increases by a few percent at its peak and is related to the field strength. At 1.5 T the signal change is approximately 1 - 2 % and it increases to 5 - 6 % difference at 7 T [85].

The blood-brain barrier prevents blood directly penetrating the brain tissue and oxygen and other molecules diffuse across the barrier providing the tissues with essential nutrients. There is a contribution to the MR signal from both the tissues (extravascular) and the blood in the vessels (intravascular). The intravascular component dominates the signal and can spread into the extravascular compartment. At low field fMRI (1.5 T) it is difficult to distinguish between the intravascular and extravascular components. Blood affects the T_2^* relaxation and it is easier to differentiate it at higher field strengths (3 T and above) [83, 86].

The contribution to the MR signal from the smaller microvessels are generally cancelled out due to their random orientations. This is not always true of macrovessels. A single artery may respond to the increased demand in oxygen (by increasing the CBF and CBV) causing an increase in the MR signal producing a strong activation that is likely to be distant to the site of the neuronal activity. Additionally, the signal from the veins must also be considered. Due to the paramagnetic qualities of deoxyhaemoglobin inhomogeneities are created in the magnetic field and a difference in magnetic susceptibility results. This causes a decrease in the MR signal in the capillaries, venules and veins. At rest, a 40 % difference in blood oxygenation can be observed. When a neuron activates the oxygen saturation of the blood in the capillaries, venules and veins is comparable

to that in the arteries and arterioles. The 'draining' vein can then produce another large activation that is also removed from the site of the neuronal activity, in a similar way to the artery.

The time lag of the HRF limits the temporal resolution of any fMRI experiment and allowance for this must be built into the design of any paradigm. It should also be noted that if the task is continued for too long then the neurons can accommodate to the activity and oxygenation changes will be weaker. Therefore the ideal fMRI experiment involves a short period of task/stimulus (e.g., 10 - 30 seconds) followed by a short period of inactivity (e.g., 15 - 45 seconds). Due to the inherently noisy signal that is picked up by the receiver coil it is generally necessary to repeat the experiment many times.

Detection of the BOLD signal within the data relies on a statistical analysis, usually after data collection is complete. The images are generally processed to remove spatial artifacts caused by movement of the subject. In fMRI the data often has to be temporally corrected as well. One slice through the brain can be acquired in approximately 100 milliseconds but it usually takes 2 - 3 seconds to acquire all the slices to form a full 3D brain image. Therefore there is 2 - 3 seconds difference between the first and last slices acquired which is on the order of the temporal response of the blood oxygenation.

The time course of signal changes in the brain is modelled on the basis of the known time course of the stimulus taking into account the time lag of the HRF. Each voxel of the corrected data is then statistically interrogated using, for example, a t-test, to determine the statistical significance of any detected signal changes which follow the time course of the model. The statistical parameters are usually plotted on a brain template to localise the activity. The preprocessing and statistical analysis of the data are discussed in detail in Chapter 5.

4.3 Artifacts and Noise

The two main sources of noise in MRI are thermal noise and physiological fluctuations. Thermal noise in the receiver is produced by stray ionic currents in the body or fluctuations in the receiver system itself. It takes the form of uniform random Gaussian noise and is present in all voxels. There are also noise sources with systematic spatial and temporal features, e.g., from rhythmic physiological fluctuations [83]. Artifacts and noise in the signal can be improved by limiting motion of the subject, changing certain imaging parameters and choosing a well designed receiver coil. These are described below.

4.3.1 Physiological Fluctuations

In the human physiological system, pressure waves are created from cardiac pulsations and lung expansion and contraction. The pressure waves can cause pulsations not only in the blood that travels to the brain but also in the cerebrospinal fluid that fills the ventricles and surrounds the brain. These pulsations produce very small movements in the arteries and capillaries which in turn can produce a signal change of up to 1 % which is comparable to the BOLD change in signal at 1.5 T [83]. There is also a non-periodic fluctuation in the blood oxygen level which occurs even at rest so there are always temporal and spatial random oscillations in the signal intensity [89].

It is also possible for quasi-periodic physiological processes, such as the cardiac cycle to appear aliased in the k-space data [90], as shown schematically in Figure 20. (The Nyquist criterion states that to reliably detect a frequency, f, then the sampling rate needs to be at least $2f$). All data in this project was acquired with an acquisition time of 3 s so aliasing could be present.

There are a number of ways that physiological noise can be removed from fMRI data. For example, acquiring volumes with a TR $\leq$ 0.5 s or to monitor and record the pulse and respiration cycles during scanning and then use a retrospective correction technique during the processing of the data to remove them, e.g.

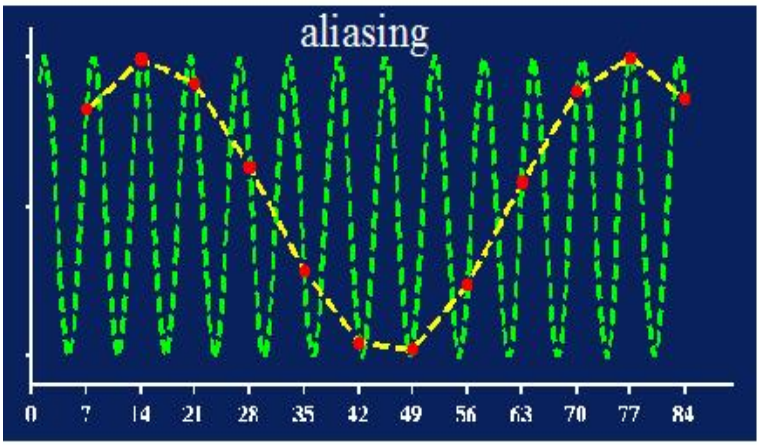

Figure 20: Aliasing. If an oscillation is sampled at a slow rate it can appear to have a different frequency [90].

RETROICOR [91].

4.3.2 Thermal Noise

The signal to noise ratio (SNR) is dependent on the radio frequency coil that is used to acquire the data. A small surface coil placed over the region of interest reduces the ionic currents picked up from the rest of the body but it also limits the area that can be imaged. Thus larger coils are often used which surround the whole head or body part. To improve the SNR they are often composed of multiple coils that work together providing more than one receiver channel.

The intrinsic SNR is changed by the strength of the magnetic field; if the magnetisation, M, is increased then the signal is less noisy. The voxel volume, ΔV, also influences the SNR; the strength of the signal is directly proportional to the number of protons contributing to the signal therefore the larger the voxel, the better the SNR. Also the acquisition time, T, has an effect; scanning for longer periods reduces the noise by a factor of $\sqrt{T}$.

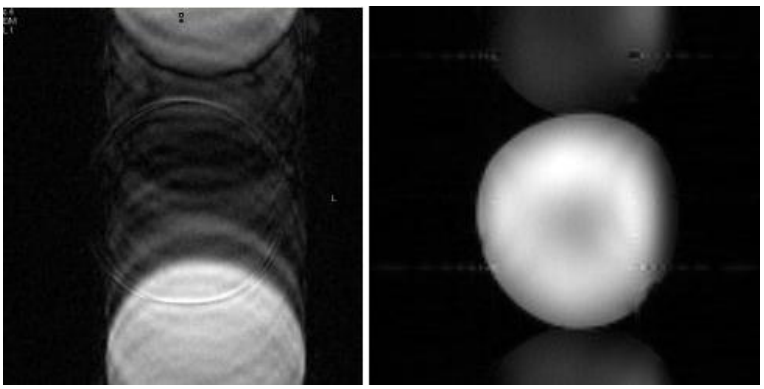

Figure 21: The image on the left shows the effects of motion during image acquisition in the phase encoding direction [92]. The right hand image shows a $N/2$ ghost [93].

4.3.3 Image Artifacts

Artifacts can be caused in the images from slight imbalances in the gradients. Consider how k-space is acquired in EPI (Figure 17), one line is formed by scanning left and the next by scanning right. If there is a slight difference between the gradients for the odd and even lines then the k-space echo can be displaced and a ghost is seen in the images displaced by $N/2$ pixels in the phase encoding direction, where N is the number of voxels in this direction. This is often called a $N/2$ ghost, see Figure 21.

The fMRI signal is also sensitive to the T_2^* properties of the different tissues and if the acquisition time is less than T_2^* then blurring occurs in the image. This occurs in a non-uniform manner as different tissues are being imaged at the same time.

Artifacts can also arise from the person moving slightly during scanning. Small motions can produces signal intensity changes in the order of a few percent especially if the voxel lies very close to a boundary, e.g., air - bone, grey matter - fluid, and this is comparable to the change in BOLD signal. Motion artifacts also appear as ghosts or diffuse blurring in the images in the phase encoding direction, Figure 21. The movement causes a misalignment in the k-space scanning so

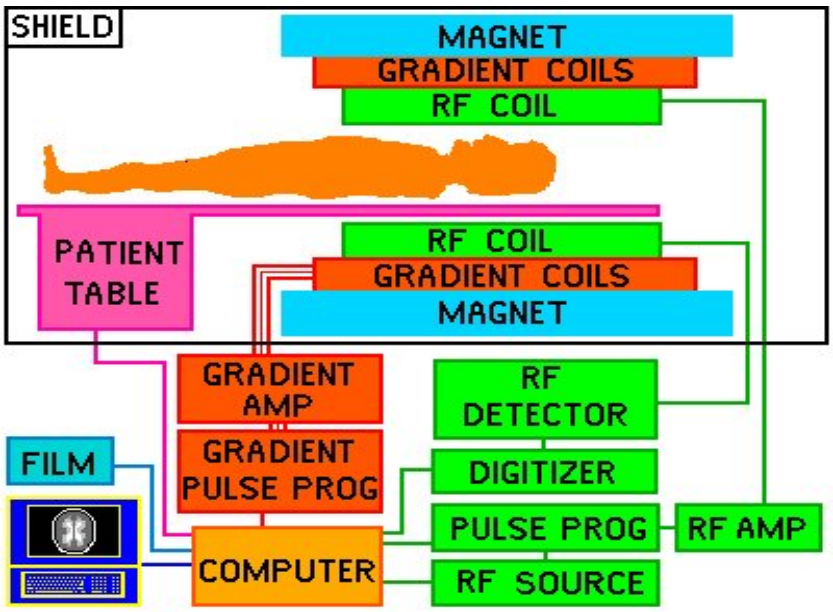

Figure 22: The above schematic shows the basic MRI instrumentation that is required to form a working MR imager [94].

wave patterns do not completely cancel and artifacts can appear over the image. The frequency encoding direction samples at a much faster rate and is usually unaffected by motion.

4.4 MRI Instrumentation

There are a range of MR imagers available but all have similar hardware, shown in Figure 22. Low field MR imagers usually contain a permanent magnet but high field, above 1 T, use a superconducting magnet to generate the magnetic field, B_0. The magnet is formed from coils of wire that are cooled by liquid helium to 4 K and an electric current is passed through them generating a magnetic field. Due to the superconductivity there is no resistance or heat production.

Within the main coil are the gradient coils, arranged in pairs, which vary the strength of the magnetic field with position. These coils are used to achieve spatial localisation within the image.

Radio frequency coils are located within the gradient coils and are used to transmit the RF waves and receive the MR signal from the excited nuclei. The RF coils built into the scanner are 'volume' coils and allow a large area to be imaged at the expense of increased SNR compared to the smaller surface coils, placed directly over the area to be imaged (see above). For fMRI of the brain a purpose-built head coil is often used. This sits around the head like a helmet and offers an appropriate receptive field with a high 'filling factor', i.e., reduced distance to the target and so improved signal. RF coils are often composed of a multiple phased array where two or more coils are coupled together. In principle, the same RF coil can be used to transmit and receive, although in the present study the body coil was used to transmit and the head coil to receive. This produces a better signal to noise ratio.

During imaging the subject/patient lies in the centre of the coils, usually on a computer controlled moveable table. The RF signal received from the tissue is on the order of μwatts therefore it is necessary to shield the room from any outside RF waves that might interfere with the MR signal.

All data for this project was acquired using a 1.5 T Philips Intera MR imager at the Peninsula MR Research Centre at the University of Exeter, Figure 23. This is a dedicated research scanner with an inside bore diameter of 60 cm and a maximum gradient strength of 60 mT/m. A SENSE coil was used throughout which is a phased array head coil, composed of 6 elements. This allows parallel imaging to be carried out. Parallel imaging involves acquiring fewer lines of k-space from each coil, causing the k-space images to be wrapped in the phase encode direction. The images are then reconstructed using a sensitivity map that is performed before the main scans. The SENSE reduction factor describes the reduction in the number of phase encoding steps. A SENSE reduction factor of 2 was used in all studies.

This chapter has covered the physics of MRI and the possible artifacts and

Figure 23: Philips 1.5 T Magnetic Resonance Imager at the Peninsula MR Research Centre at the University of Exeter. The SENSE head coil is shown insitu on the moveable table [95].

noise that may be present in the MR signal. The basic instrumentation required to obtain fMRI images has also been described. The next chapter explains the data processing required to be able to interpret the fMRI data.

Chapter 5

Data Processing

5.1 Introduction

During fMRI a series of 20 - 30 slices are acquired over a few seconds forming a 3D brain image with a resolution usually in the order of a few millimeters. A typical experiment will run for 30 minutes owing to the poor signal to noise ratio present in a MR signal. It is clear there is a vast amount of data produced from a single imaging session and powerful specialised software is needed to convert the raw data into a meaningful format. This chapter describes the processes involved in achieving this.

5.2 Raw Imaging Data

On many commercial scanners the data is exported as a DICOM file which consists of a single file incorporating the header information (e.g., type of scan, image dimensions, etc) and the image data itself. Raw data from the scanner used in this project was exported as Philips *.par* and *.rec* files. The *.par* file contains the header information and the *.rec* file contains the 4D image data (spatial and temporal information) about the scanning session. These files were converted to Analyse format (*.hdr* and *.img* files) before any preprocessing was carried out. This puts the data in a generic form allowing it to be read and manipulated by

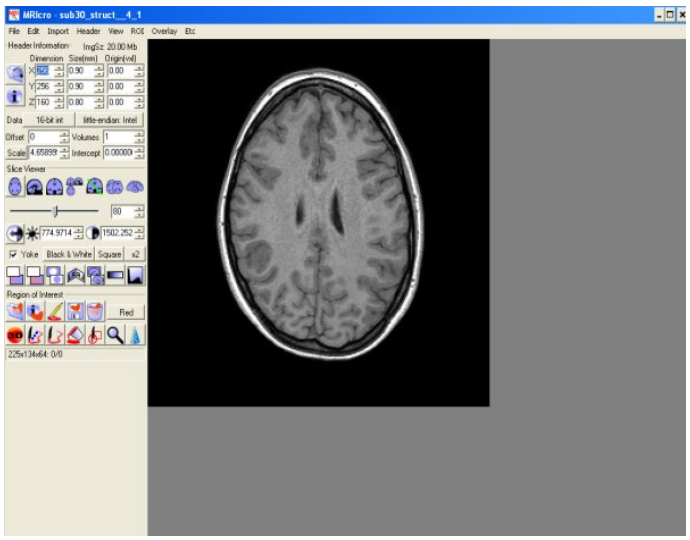

Figure 24: MRIcro desktop [96].

fMRI software. Throughout this project this conversion was carried out using software called MRIcro [96]. This is a standalone freeware programme that allows medical images to be viewed on a PC (see Figure 24). It is available from:

http://www.sph.sc.edu/comd/rorden/mricro.html

The Analyse files were then converted into 3D files before they were preprocessed in Statistical Parametric Mapping (SPM) software. The result is a *.img* and *.hdr* file containing the x, y and z information for each dynamical scan that was acquired during the session.

5.3 Preprocessing

Preprocessing involves temporally correcting and spatially aligning the scans. This is carried out using SPM [97] which was developed by the Functional Imaging Laboratory of the Wellcome Department of Imaging Neuroscience at University College London and is freely available from:

http://www.fil.ion.ucl.ac.uk/spm/

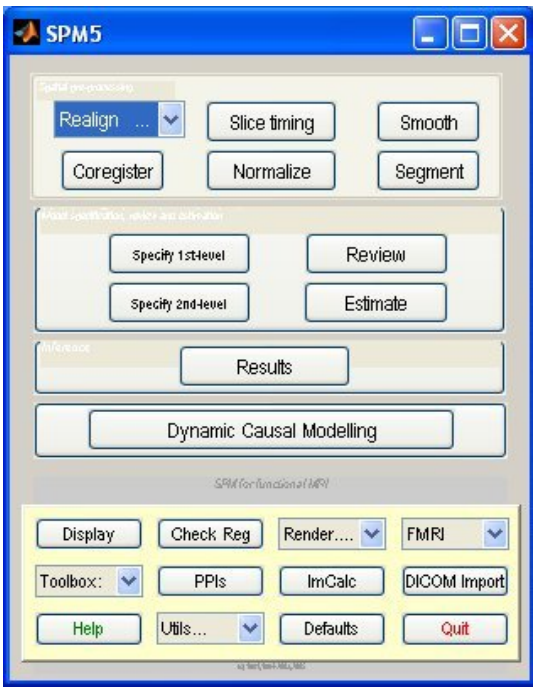

Figure 25: Graphical user interface of SPM software [97].

Version 5 was used throughout this project. It consists of a package of Matlab functions and subroutines which are initiated through a graphical user interface shown in Figure 25. Matlab, short for Matrix Laboratory, is a mathematical programming environment and language that can be used for many applications and it is used as a platform for running SPM. Matlab is available from Mathworks [98] and version 7.4.1 (R2007b) was used throughout.

5.3.1 Slice Timing

In fMRI, each dynamical scan is a 3D image of the brain and is constructed from data obtained in slices which are then stacked together. The slices can be acquired in a number of different sequences. For the purposes of these experiments 30 or 35 slices were acquired in a contiguous interleaved 'bottom-up' fashion, e.g., 1, 3, 5, ..., 29, 2, 4, 6, ..., 30. This sequence has two advantages, firstly, it reduces cross talk. There may be some overlapping of the slices so when adjacent slices

are excited it is possible that some of the tissues are being excited twice in quick succession which can lead to saturation effects and a loss in signal. Interleaving also reduces slice timing bias. Each dynamical scan takes nearly 3 sec to acquire thus there is a temporal lag in the responses recorded in the first slice and the last slice. The interleaved acquisition attempts to provide data across the brain at a more frequent interval [49].

Regardless of the acquisition sequence there is still an inherent lag in the data which increases with every slice that is acquired. It is possible to temporally align the scans using slice timing correction. This method uses sinc interpolation to shift the phases of the responses so that each dynamical scan relates to one point in time instead of a 3 second period [97].

When slice timing is applied SPM creates another file for each dynamical scan with the prefix 'a' before the name to indicate what has been performed.

5.3.2 Realignment

The temporally corrected files were then spatially aligned to correct the images for any movement from the participant during scanning. Random head movement can cause changes in the signal and add extra noise but head movements which correlate with the task condition can produce extra activations, usually at the peripheries of the brain images. Realigning the scans removes these artifacts. SPM does this by using a least squares routine and a 6 parameter rigid body spatial transformation - 3 translations and 3 rotations in x, y and z planes. In most cases movement was often limited to only 1 or 2° of rotation and 1 - 2 mm of translation which was not enough to cause severe artifacts. The scans were realigned with the first scan of the session and an image of the mean motion was created [97]. SPM, again, created another file for each scan but this time with the prefix 'r'.

5.3.3 Normalisation

People have different sized heads and their own unique shape. To assess the images on a common basis and to allow the images from different participants to be compared the scans were normalised to a template. The T_2-weighted imaging template MNI152 developed by the Montreal Neurological Institute [49] was used throughout (see Chapter 2.7). The scans were normalised by using a sum of least squares routine and minimising the difference between the template and the data. A 12 parameter affine transformation is used to estimate the linear differences by matching specific points in the data to the template, 3 translations, 3 rotations, 3 shear and 3 zoom. The non-linear estimations were then carried out. SPM outputted files with the prefix 'w' [97].

5.3.4 Smoothing

Spatial smoothing is often applied to fMRI data when investigating activations on a group level. It is useful way to overcome the differences between individual anatomy, for example differences in the position and shape of the sulci. A Gaussian filter specified by its full width at half maximum (FWHM) is usually used (at least twice the voxel size). Smoothing has the effect of suppressing the noise from the signal by blurring and enlarging the activations but it may also lower the statistical significance of each activation [50]. It is useful when comparing group data as the increased volumes mean it is more likely that the activations will overlap between the participants. It is less useful when reviewing data from an individual participant, particularly when looking for fine or small details as smoothing may cause two activations to appear as one. Therefore when interpreting each participant's data on an individual level smoothing was not applied but when looking at the group data smoothing was applied. The SPM smoothed file had the prefix 's'.

5.4 Modelling of fMRI Data

5.4.1 Fixed Effects Analysis

At the end of the preprocessing the original 3D files now had a prefix of 'wra' or 'swra' indicating what had been carried out and in what order. These files were then processed on the basis of an activation model for the stimulus sequence in order to extract the fMRI information.

A model was specified to test the null hypothesis and this was done using the first level or fixed effects analysis in SPM. The number of conditions were specified and the onsets and durations were entered into the software (see Figure 26). A box car design was used in all experiments and thus stimuli can be represented graphically as box functions. SPM convolves the resulting box functions with the haemodynamic response function (HRF) to produce a model of the ideal signal we would expect to see in response to the stimuli. SPM uses a univariate approach and the general linear model (GLM) to calculate the statistics for each individual voxel. The GLM is described for a single voxel by:

$$y_j = x_{j1}\beta_1 + x_{jL}\beta_L + \epsilon_j \tag{20}$$

where y_j are the data for scan j, x_{jL} are the explanatory variables/regressors where $l = 1, \ldots, L$, β_L refers to the regression slopes and fixed effects and ϵ_j is the independent and identically distributed residual error [90]. The equation in matrix form is given by:

$$y = X\beta + \epsilon \tag{21}$$

where X is the design matrix. The design matrix consists of a column for each condition or regressor and a row for each scan. An example of this is shown in Figure 26. Throughout the analysis in this project the onsets of both the 'on' and the 'off' conditions were modelled although this is not strictly needed as SPM will make the assumption that any scans that are not covered by the 'task' onsets and

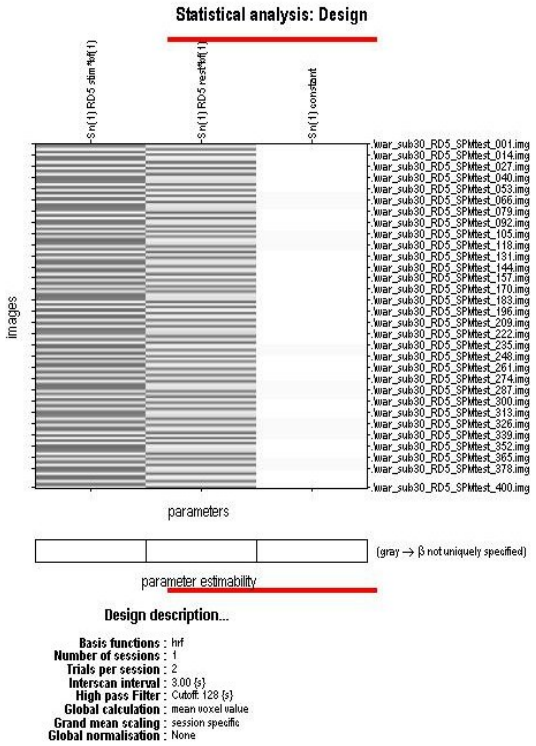

Figure 26: Example of the SPM design matrix for a fixed effects analysis. The first column represents the 'on' condition, the second is the 'off' condition and the third is the confounds. This a single session for one participant.

durations are the 'off' condition [99]. The 'off' conditions were included in the analysis in this instance to provide flexibility in the contrasts between the various conditions.

It is possible to process the data using the time and dispersion derivatives of the HRF as well as the HRF itself. Grand mean scaling of the signal also needs to be carried out to account for variations in the signal in a single scan and across all scans of that session as well as scaling the voxel values to enable differences to be identified more easily [83]. The default option in SPM was used so that SPM first calculates the average signal within each scan and then takes the average of these to find the grand mean value (GMV) for each voxel throughout the session. It then multiplies each data point by 100/GMV [97].

Most of the noise in the MR signal is low frequency, e.g., cardiac and respiratory biorhythms (approx. 0.25 to 1 Hz), therefore using a high-pass filter at 128 seconds period is helpful in reducing artifacts. This is a way of removing confounds - effects of no interest - without determining their parameters [97]. Serial correlation can also be included in the model and is another way of removing the contributions of physiological fluctuations. This option was not selected in the models used here.

Once the model is complete then the statistics need to be estimated for the data. This is done by using a least squares approach to find the maximum likelihood estimates and assumes each voxel has the same error and uses the independent and identically distributed error model, shown below:

$$\hat{\beta} = (X^T X)^{-1} X^T y \tag{22}$$

where $\hat{\beta}$ is the parameter estimates [90, 99].

Once the model had been estimated contrasts were specified in the SPM contrast manager which then performs either a Student two sample t-test or a one sample F-test to test the null hypothesis and make inferences about the data. F-tests are useful for showing the overall effects of a condition and will show all voxels with a value significantly different from the baseline. It is also necessary to use them when interrogating the time and dispersion derivatives with the HRF. The t-test introduces direction in the results and depending on the contrasts defined will show those voxels with a value significantly increased from baseline, or those significantly decreased. The resulting statistically significant voxels are then displayed as a grey scale map overlaid on saggital, coronal and axial views of the MNI glass brain.

A probability threshold also needed to be applied to the contrast to enable an estimate to be made of the likelihood of a particular voxel being a false positive. In SPM there are two options for this 1) uncorrected p value and 2) corrected p value (family wise error). The uncorrected p value looks at the statistics of each voxel individually to determine if it is statistically significant. Consider a typical

brain image with 100,000 voxels, if an uncorrected p value = 0.005 is specified then there could be as many as 500 false positives in the image. The family wise error involves a multiple comparison test using Random Field Theory and is based on the Bonferroni correction. The statistics are repeated many times to reduce the error rate so that a corrected p value = 0.05 would give a rate of 5 false positives in 100 SPMs [97].

5.4.2 Random Effects Analysis

The fixed effects analysis involves using a fixed variable based on the within-subject variance and inferences can be made about the sample population only. The random effects analysis, also called second level analysis, is useful for making inferences about the general population because it takes into account the differences within-subject *and* between subjects.

The contrast estimates from the fixed effects analysis for each participant was used to generate another design matrix. The contrasts need to be identical for the analysis to be carried out. If one population is being investigated then a one sample t-test can be used. If there is more than one population then a two sample t-test is used. If there is more than one condition to be tested then a full factorial matrix can be specified. All data is assumed to be independent between levels and have unequal variance in each level. A restricted maximum likelihood calculation was used to estimate these parameters.

Once the matrix was formulated the parameters were estimated, as with the fixed effects analysis, and the contrasts and thresholds were specified as before. The resulting maps show the statistical significance of the active voxels for the population as a whole.

In Chapters 4 and 5 the physics of MRI and the statistical processing of fMRI data have been covered. The next chapter describes the hardware of the stimulation devices used in the experiments to produce the brain activations and how the stimulation paradigm is based around the BOLD effect.

Chapter 6

Vibrotactile Stimulator

6.1 Introduction

The vibrotactile stimulators used in this project were built in-house by the author, at the University of Exeter Physics Department, for the purpose of these experiments. They use piezoelectric bimorphs to generate the vibration and the design and electronics are based on previous vibrotactile stimulators constructed within the department by a research assistant, Mr Alan Brady.

Many other types of stimulators have been used by other groups using MRI to study somatosensory activity within healthy controls and patients [6, 9, 10, 16, 24, 100]. These range from a commercially bought toothbrush which was brushed along the fingertip by the investigator during scanning, to air jets and air filled diaphragms which balloon to contact the fingertip. Francis et al (2000) [1] used a similar device to that used in the present study, also constructed from piezoelectric bimorphs with good results determining the location and separations of most of the individual Brodmann activations of digits 2 - 5 (index - little finger).

This chapter gives an overview of the equipment and describes its basic components.

6.2 Stimulator Design

In section 4.2.4 the BOLD effect was discussed and suitable stimulation paradigms were suggested to produce a strong signal. This involves alternating short burst of stimulation followed by slightly longer periods of no stimulation or 'rest'. This demands that the vibrotactile stimulator be capable of generating a robust, reliable and repeatable sequence. Also, the aim of this project was to determine the location of D1 and D5 on the cerebral cortex therefore it required the hardware to be able to comfortably accommodate both digits.

With these aims in mind two stimulator units were designed and built, one with a horizontal contactor surface for D5 and one angled to accommodate D1. These are shown in Figure 27. The vibrotactile stimulation was generated via four piezoelectric cantilevers that run the length of each unit and were isolated from the user by a contactor attached to a square of plastic which is fixed to the tip of each cantilever. The contactors were constructed of wood with approximate dimensions 2 x 2 x 20 mm and a small amount of Norland optical adhesive was used to smooth the tips that contact with the skin. When the cantilevers were not oscillating the contactors sat flush with the perforated surface that the fingertip rests on, this is the raised platform with the four holes at the end of the units shown in Figure 27.

The units were attached to individual stabilizer boards so that they sat comfortably on the abdomen during imaging. The unit bases were also lined with foam to dampen stray vibrations and minimise the amount of stimulation that might be felt through the abdomen. The electronics and computer that control the generation of the stimulation sat in the control room next to the scanner room and each unit was connected to them by several metres of twisted wire that were covered in screening copper tape. This wire was fed through a fixed wave guide in the wall to the control room.

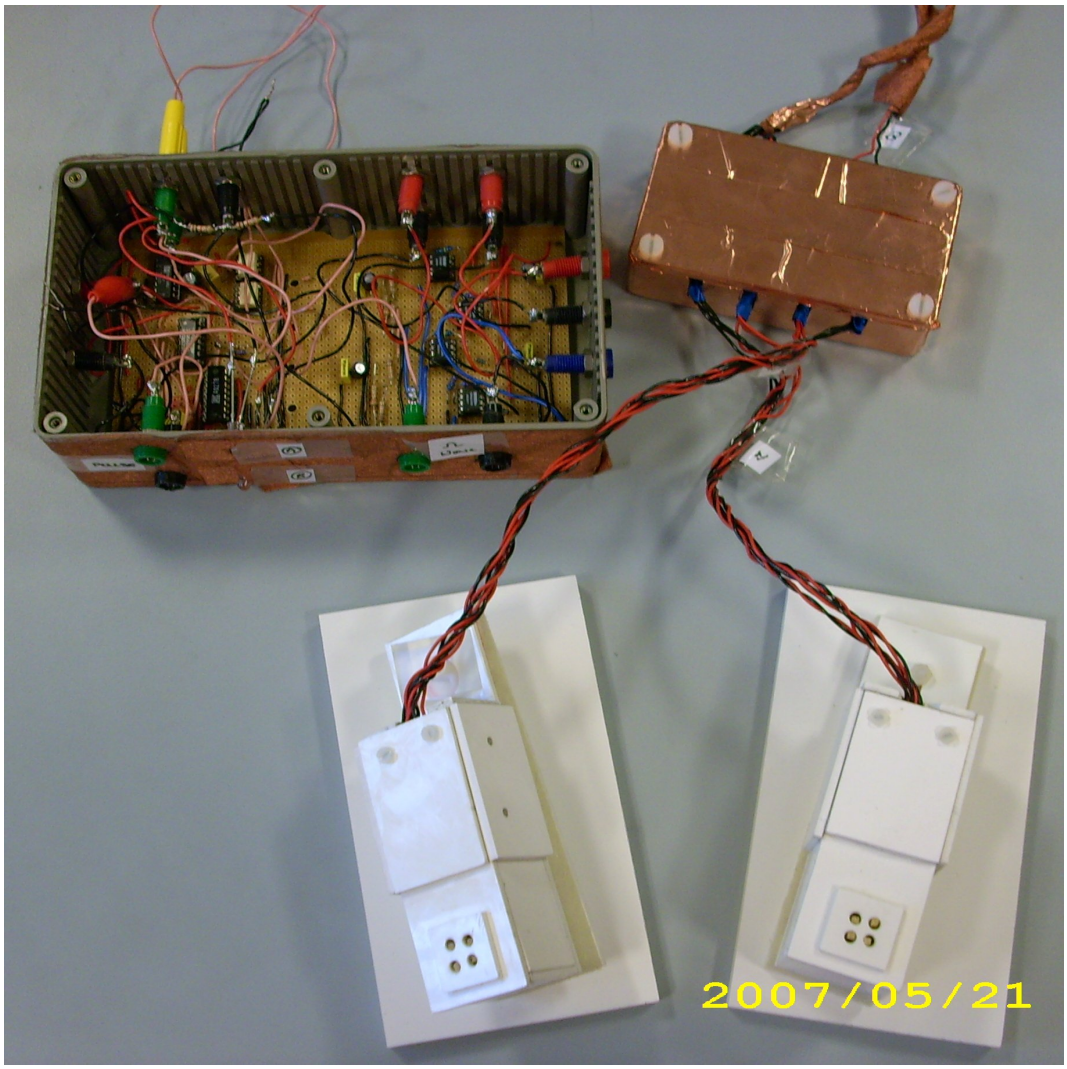

Figure 27: The two stimulator units are shown, one is angled to accommodate the thumb and the other accommodates the little finger. The electronics that controls them is also shown.

6.3 Control of Stimulus Timing

The start of the generation sequence began with the MRI control hardware, which was configured to output a trigger pulse at the start of a volume scan, i.e., every 3 seconds or at integral multiples of this period. This pulse was picked up by a commercial pulse generator (TTi TGP110 10 MHz Pulse Generator), used as a pulse stretcher to provide a longer pulse necessary to reliably trigger the standard PC which controlled the vibrotactile stimuli.

The PC was a stand-alone computer with Microsoft Windows NT operating system. The software used to detect the stretched pulse and generate the output signals (logic '1' to enable the stimulus and logic '0' to disable it, in either the D1 or D5 channels) was developed in-house by Mr Brady. The software used a text input file to determine the timing, duration, pattern of the output signal and the channel through which it should be directed. D1 and D5 were never stimulated at the same time so that the BOLD activity could be clearly separated. The timing element allowed the output signal to be delayed by a variable amount with respect to the trigger pulse, thereby building in a randomness to the occurrence of the stimulation. This was done to prevent the brain from becoming 'adjusted' to the sequence and reducing its BOLD response. The duration of the output signal was always 9 s, i.e., the time required for 3 complete volume scans. Two types of output sequence could be generated: 1) continuous stimulus, specified by logic '1' maintained for 9 s, 2) intermittent stimulus by a repeated pattern of logic '1' for 0.5 s followed by logic '0' for 0.5 s, i.e., a 1 Hz square wave.

6.4 Electronic Drive Circuitry

The control signals in the D1 and D5 channels were then passed to the purpose built electronic circuitry which provided drive signals for the two stimulators. A diagram of the circuitry is shown in Figure 28. Each channel is identical and consists of an LED, an opto-isolator and two operational amplifiers. The LED's

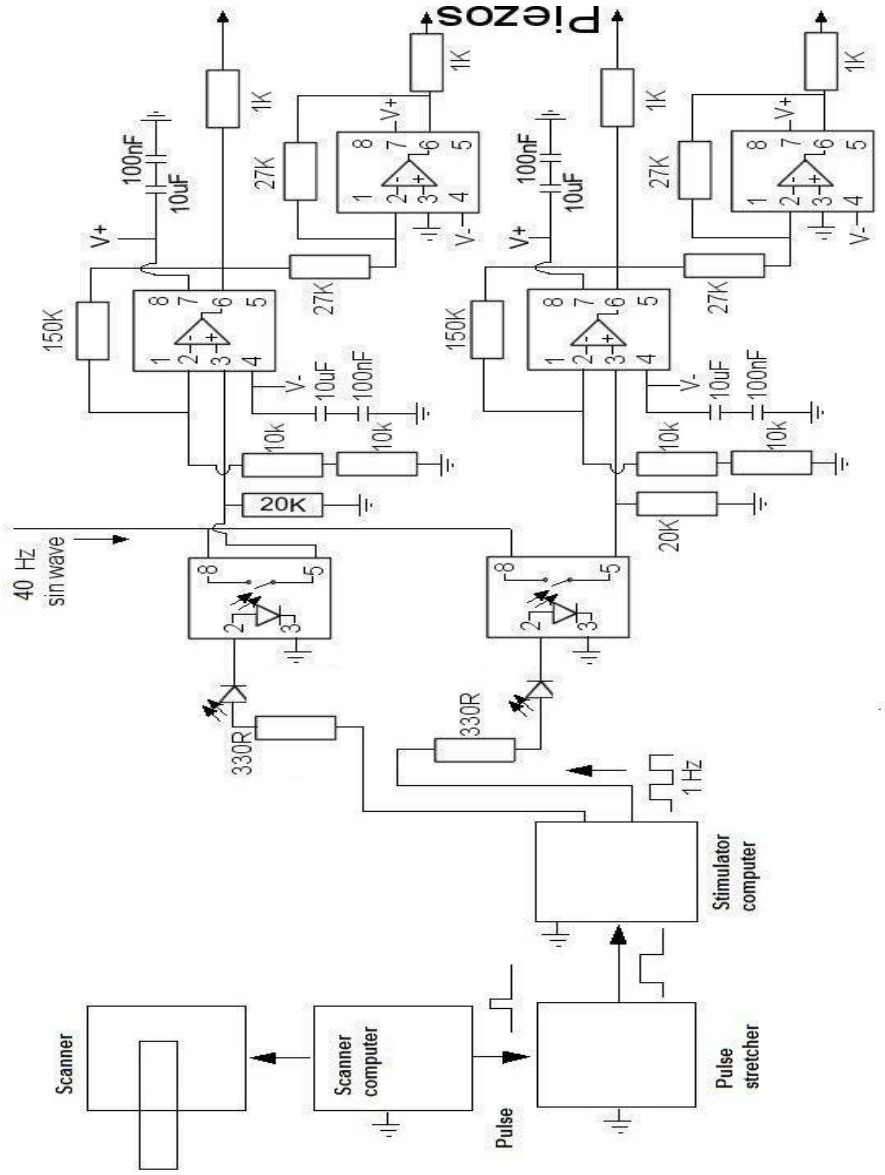

Figure 28: Schematic of the systems and electronics involved in generating the vibrotactile stimulation.

were built into the circuit simply to indicate which channel was being used, to facilitate system checking and fault finding. The opto-isolators were included in the design to minimise the amount of electromagnetic interference that was fed directly to the MRI room. The output signal from the PC (logic levels) was sent into the opto-isolator which was used to switch the 40 Hz sine wave from a commercial signal generator, Feedback FG600. Depending on the software output mode this produced a 40 Hz oscillation for 0.5 s on, 0.5 s off, for a duration of 9 s or simply a 9 s burst at 40 Hz. This is demonstrated in Figure 29.

The sine wave output of the opto-isolator was sent to two operational amplifiers which were configured as bridge amplifiers in each of the two channels. The maximum amplitude of the signal, determining the force amplitude applied to the fingertip, was limited by the power supply which has a maximum setting of 30 V. The power packs were commercially available Weir 400. The signal was then passed to the piezoelectric cantilever which bent back and forth moving the contactor in response to the 40 Hz drive signal. This generated a sensation on the fingertip of the participant, producing activity in the somatosensory cortices.

This chapter concludes the background to the thesis. The next chapter describes the procedure of each experiment carried out, the results are presented in Chapter 8 and discussed in Chapter 9.

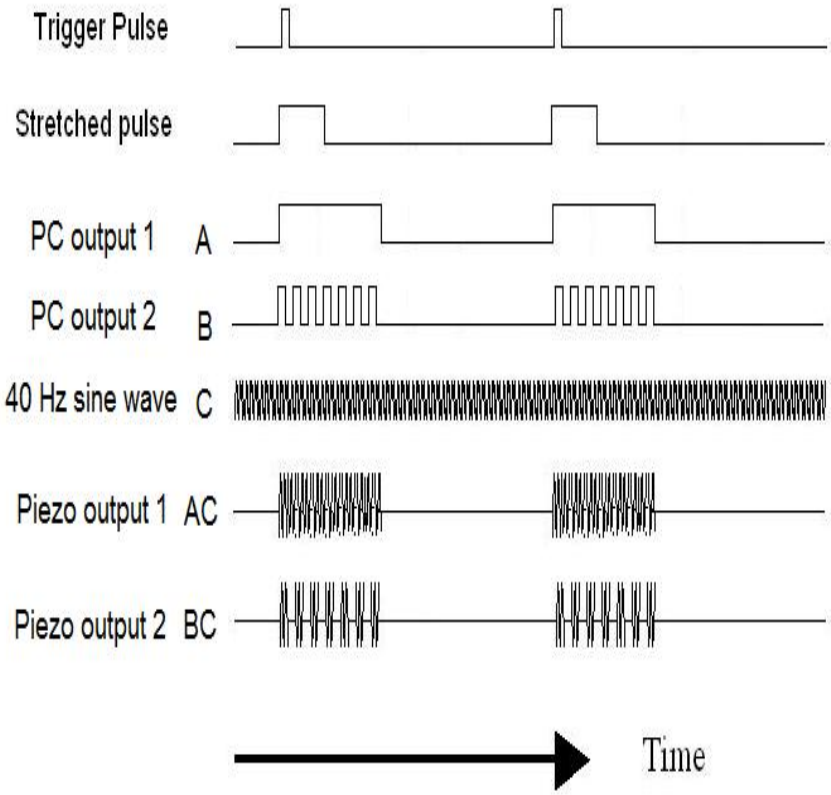

Figure 29: Input signals and the resultant output.

Chapter 7

Studies 1 - 5: Experimental Procedure

7.1 Studies 1 to 4

A number of preliminary tests followed by 4 group studies were carried out to investigate the effectiveness of the vibrotactile devices and determine the stimulation and scanning protocols needed to reliably detect cortical SI activity. Healthy volunteers participated in all four studies and ethics approval was obtained from the School of Physics Ethics Committee at the University of Exeter prior to scanning. Volunteers were recruited predominantly from the postgraduate community and staff in the department. Before being scanned each participant was given an information leaflet describing the nature of MRI and its associated risks. They also received a description of the study protocol and all information was verbally explained before they were asked to sign a consent form. All participants also completed an MRI Safety Checklist before entering the scanner room. A sample of all documentation can be found in Appendix A.1.

7.2 Protocol

The scanner/stimulator interface, scanning protocol and the duration of a scanning session required to detect the SI activations was firstly investigated by carrying out several experiments. From assessing the data at different points in time it was found that a minimum of 25 stimulation events per digit were needed which equates to a scanning time of approximately 12 - 15 minutes per digit, dependent upon the frequency of the stimulus presentation. Four formal studies were then carried out on healthy volunteers to further refine the scanning and stimulation protocols to reliably and consistently detect the activations and determine the D1 - D5 cortical separation for the left and right hands. Digits 1 and 5 were chosen for investigation as they have the greatest separation on the cortex. These studies formed the basis for a later CRPS patient study therefore the stimulation and scanning protocols had to be appropriate for patients.

The maximum amplitude of the vibration was ascertained by testing the stimulus on three patients outside of the scanner and their details are summarised in Table 4. CRPS was present in the right hand of each patient and each suffered from allodynia. Patient (ii) also experienced intermittent numbness. Various intensities were tested and the patients' comments were noted for each level, including the duration they were able to tolerate it for. The maximum drive amplitude that each was able to tolerate for a sustained duration of 10 - 12 minutes was $\pm$ 36 V ($\sim$ 100 - 200 microns piezoelectric bimorph displacement). This level was adopted and used in study 1.

The frequency of the vibrotactile stimuli was chosen on the basis of a previous study carried out by Sleigh et al. [101] who investigated how the SI and SII fMRI signal changed in response to increasing frequency using a piezoelectric bender. They found that the fMRI signal from the SI activations was greater at lower frequencies and reduced as the frequency increased. The opposite was found of the fMRI signal from the SII activations. The frequency where the SI and SII fMRI signals crossed was approximately 40 Hz and this frequency was adopted

Table 4: Patient details for investigation of tolerance to stimuli. M - male, F - female, R - right.

Pat	Age	Gender	Duration of disease	Location	Symptoms
i	39	M	$\geq$ 2 yrs	R hand, forearm and foot	Allodynia Hyperalgesia Phantom sensation
ii	57	F	9 mths	R hand	Allodynia Intermittent numbness Tingling sensation
iii	49	F	$\geq$ 2 yrs	R hand	Allodynia hyperalgesia

and used in all experiments.

The 1.5 T Philips Intera MR imager at the Peninsula MR Research Centre at the University of Exeter was used for all scanning sessions. The fMRI scanning protocol was based on the standard Philips fMRI paradigm. A series of T_2^* echo-planar images with BOLD contrast were acquired. The parameters used in the studies are summarised in Table 5. In studies 1 and 2 a repetition time (TR) of 3 s and an echo time (TE) of 40 ms was used with a 240 mm field of view. In studies 3 and 4 the TE was increased slightly to 45 ms to improve the contrast in the images. A voxel size of approximately 3 $\times$ 3 $\times$ 3 mm was chosen for all studies as a balance between being able to determine the small separation of the digits and the reduction in the MRI signal as a consequence of the smaller voxel volume. A sequence of either 30 or 35 slices was acquired contiguously across the brain providing data of all areas with the exception of the cerebellum and brain stem. A SENSE factor of 2 was also used throughout. An anatomical T_1 weighted 3D gradient echo image was also acquired for each subject consisting of 160 slices with a voxel size of 0.9 $\times$ 0.9 $\times$ 0.8 mm, TR = 25 ms and TE = 4.1 ms.

During scanning the volunteers lied supine on the patient table with the SENSE volume coil placed around their head. Movement was minimised by packing foam blocks between the head and the coil. The stimulation units were placed

Table 5: FMRI parameters used in studies 1 - 5.

Study	1	2	3	4	5
TR (s)	3	3	3	3	3
TE (ms)	40	40	45	45	45
Field of view (mm)	240	240	240	240	240
Matrix	80 × 80	80 ×80	96 × 96	96 × 96	96 × 96
Slice thickness (mm)	3	3	3.5	3.5	3.5
Voxel size (mm)	2.9 × 2.9 × 3.0	2.9 × 2.9 × 3.0	2.5 × 2.5 × 3.5	2.5 × 2.5 × 3.5	2.5 × 2.5 × 3.5
Number of slices	35	35	30	30	30

comfortably across the abdomen with the D1 and D5 fingertips, of either the left or right hand, gently resting on the contactors. The other digits were positioned so that they were comfortable and not in contact with the units. Where necessary the unused digits, the elbow and wrist were supported by foam cushions. The patient table was then positioned so that the volunteers' head was at the centre of the bore.

The experimenter was able to speak to the volunteer via an intercom system and the subject was given a call button to be able to alert the experimenter to any problems during scanning. The subject was asked to follow a number of instructions:

1) To keep all digits still during scanning and to keep D1 and D5 in contact with the devices but not to apply undue pressure as this would dampen the vibrations.

2) To give full attention to the fingertip stimulation when felt and to divert their attention to other things the rest of the time.

3) To continuously visually focus on a dot projected onto a screen that was positioned at the foot of the patient table in order to suppress visual activations from the data.

This forms the basis of the experimental protocols for the 4 formal studies. Certain parameters were adjusted to investigate the effect on the detection and

Table 6: Details of volunteers who participated in studies 1 and 2. M - male, F - female.

Age	Gender	Study 1	Study 2
23	F	S1	S1
24	F	S2	
30	F	S3	
23	F		S2
25	F		S3
25	M	S4	S4
29	M	S5	S5
22	M	S6	S6
26	F		S7

description of the SI and SII activations and the resultant cortical digit separations. The specifics of each study are described in the following sections and are summarised in Table 10 at the end of this chapter.

7.2.1 Study 1

Six healthy, right handed volunteers were recruited, 3 male, age range 22 - 30 years, see Table 6. Subjects were positioned in the scanner as described previously with the vibrotactile devices resting comfortably across the abdomen. Each participated in 2 scanning sessions of 30 minutes duration. In one session digits 1 and 5 of the right hand were stimulated and in the other session digits 1 and 5 of the left hand. The order of handedness was varied to reduce any ordering effect that might present itself in the group analysis.

Within each session, digits 1 and 5 were stimulated in a random sequence that was defined by the experimenter prior to the start of the session. The same random order was used for the stimulation to each hand. The stimulation was triggered by a pulse that was emitted from the scanner every 12 volume scans (36 s) and was passed through a pulse stretcher before being detected by the computer that controlled the vibrotactile devices. The computer then sent a logic '1' signal along the relevant channel to enable stimulation at either D1 or D5. A

stimulation paradigm of 9 s stimulation (on condition) and 27 s rest (off condition) was used. During the on condition the vibration at 40 Hz was switched on and off every 0.5 s. Each digit was stimulated a total of 25 times and 600 dynamic scans were acquired per session.

Subjects were given time to relax outside of the scanner room between sessions. All subjects could clearly feel the vibration and there were no reports of the stimulation being uncomfortable or painful (unsurprisingly, as these were normal controls and levels had been set to be acceptable to CRPS patients).

7.2.2 Study 2

The protocol for study 2 was designed using the results from study 1 with modifications to improve the detection of the SI activations. These are presented and discussed in detail in Chapters 8 and 9. In summary, contralateral SI activity was detected in all subjects at an uncorrected p value of ≤ 0.001. However the cortical digit separations were smaller than expected in many cases at the individual level. Both digits were stimulated during the session and it was possible that both D1 and D5 activations were appearing together making it impossible to separate out the clusters of activity. Since the calculation of the separations relies on the centre of mass of the SI clusters this effect could produce small separations. Therefore study 2 was carried out using another stimulation sequence to eliminate this possibility by stimulating only one digit per session.

The scanning sessions were reduced to 12 minutes and a total of 4 sessions were carried out allowing data to be obtained for the 4 digits. Each digit received a total of 30 stimulation events. The 40 Hz stimulus remained at 9 s duration, switching on and off every 0.5 s, but the interstimulus interval was randomised with a duration between 9 and 27 s. Again, the sequence of intervals was defined by the experimenter prior to commencement of the sessions. Different sequences were used for the left and right hands. The stimulation was triggered by a pulse emitted from the scanner every 8 scans (24 s). A total of 240 dynamic scans per session (per digit) were acquired.

Seven right handed subjects were recruited, 3 male, age range 22 - 29 years. Four had previously participated in study 1, see Table 6. The subjects were positioned in the scanner as described in study 1 and the fingers were positioned so that only the little finger or thumb was resting on a stimulator at any given time and the unused fingers were positioned away from the stimulator and supported by foam cushions as necessary. The subjects were not removed from the scanner after every session. Session 1 was carried out then there was a few minutes pause in scanning to allow repositioning of the units and digits before session 2 was started. Subjects were given time to relax outside of the scanner environment before commencement of sessions 3 and 4 which were carried out in the same manner. The ordering of the digits was varied to minimise any ordering effects.

7.2.3 Study 3

Study 3 was designed around the results of studies 1 and 2 (presented and discussed in Chapters 8 and 9). In summary, contralateral SI activity was detected less frequently in study 2 at a threshold of uncorrected p value ≤ 0.001 compared to study 1; study 1: 100 % and study 2: 89 %. The T-scores were also lower on average in study 2 reducing the likelihood of the activation being 'real'. The cortical digit separations from the individual data were often smaller than expected. Stimulation of both digits in a single scanning session, used in study 1 but not study 2, was therefore discounted as a cause of these smaller-than-expected digit separations. In an attempt to produce increased levels of cortical activation, the protocol of study 2 was adapted for study 3. The scanning time was increased to 20 minutes per digit and the amplitude of the vibration was increased by 3 dB making it more noticeable to the participants ($\sim$ 300 - 400 microns piezoelectric bimorph displacement). Due to the extended time only data from D1 and D5 of the right hand were acquired and a total of 50 repetitions of the stimulus was applied to each digit using a similar random interstimulus interval sequence. The use of a foam gutter was introduced to support the arm, wrist and unused digits.

Table 7: Details of volunteers who participated in studies 3 and 4. M - male, F - female.

Age	Gender	Study 3	Study 4
24	F	S1	S1
23	F	S2	S2
36	M	S3	S3
24	M	S4	S4
26	F	S5	S5
42	F	S6	S6
26	M	S7	S7
23	M	S8	S8

The edges at one end were cut away to allow the vibrotactile devices to be positioned close to the thumb or little finger. A total of 400 dynamic scans per digit were obtained and subjects were given time to relax between sessions outside of the scanner environment. Eight right handed volunteers were recruited to this study, 4 male, age range 23 - 42 years, see Table 7.

7.2.4 Study 4

The protocols of study 4 were based on the results of the previous experiments. In study 3, increasing the stimulus amplitude had the effect of increasing the statistical significance of the contralateral SI activations with a detection rate of 100 % at an uncorrected p value threshold of ≤ 0.001, and a detection rate of 87 % at a corrected p value threshold of ≤ 0.05. The effect of extending the duration of the data acquisition increased the T-scores even further. Neither condition affected the Euclidean separations which were generally smaller-than-expected and were consistent with studies 1 and 2.

Study 4 was carried out to improve the SI activity detection rate at a corrected threshold of ≤ 0.05 and to investigate the effect of changing the stimulus pattern. In the previous 3 studies the stimulus switched on and off every 0.5 s for the duration of the 9 s presentation. It is believed this switching has the benefit of engaging the subject's attention but the digit actually only receives 4.5 s of

stimulation which may have the effect of reducing or limiting the SI activation. This theory was investigated by repeating study 3 using the same protocols with the exception that the switching was removed from the 40 Hz vibration to give 9 s of continuous vibratory stimulation. The same eight subjects from study 3 were recruited.

7.3 Study 5: CRPS Patients

Another tactile fMRI study was also carried out with CRPS patients to investigate the hypothesis of cortical reorganisation in the SI area being present in this chronic pain condition. Ethics approval was obtained from the NHS Devon and Torbay Research Ethics Committee prior to approaching the patients. Each patient was given a leaflet detailing the study procedure and information regarding MRI and its associated risks. The study procedure and risks were also verbally explained by Dr Richard Haigh, Consultant Rheumatologist at the Royal Devon and Exeter Hospital, before the patients gave informed consent. The patient's GP was also notified of their participation and informed that the study would not interfere with their treatments and that the patient would not receive any additional treatments throughout the study. Patients were also required to complete an MRI Safety Checklist prior to entering the scanner room. A sample of the documentation can be found in Appendix A.2.

7.3.1 Protocol

The protocol for this study was based on the results of the previous four experiments and the limitations imposed by the presence of the disease. Studies 3 and 4 produced results comparable to study 1 in terms of the detection rate at an uncorrected p value threshold of ≤ 0.001; however they required longer scanning durations and higher stimulus amplitude. In view of the amount of discomfort that some patients may experience from the length of scanning time it was decided to keep the scanning time as short as possible and use the protocol that produced

good SI activations at a low stimulus level. Therefore the protocol from study 1 was adopted. Patients were asked to test the vibrotactile equipment before being placed in the scanner to find the stimulus level that was tolerable and non-painful to them, up to a maximum drive voltage of ± 52 V. The same level was used for both the diseased and unaffected hands for that patient and for the initial and follow up scans.

Studies 3 and 4 tested the effect of changing the vibration from an intermittent pattern (at 1 Hz) to a continuous pattern. The results showed no significant difference in the SI activations or cortical digit separations. Therefore, the stimulus from study 4 was chosen for the patient study due to a particular symptom that some patients experience: sometimes an intermittent stimulus can 'overexcite' the sense of touch and produce an unpleasant ongoing sensation that can last several minutes. Often people with CRPS are able to tolerate a continuous stimulus better as it minimises this effect.

Patients were made comfortable in the scanner as described previously. The arm, wrist and unused digits were supported by a foam gutter and the patients were given the same instructions as before. They were also given a call bell to alert the experimenter to any problems or if they wished to stop the experiment.

Digits 1 and 5 of the right and left hands were stimulated in two 30 minute sessions using the scanning parameters shown in Table 5. A TR of 3 s and a TE of 45 ms were used. A total of 600 dynamic scans per digit were collected consisting of 30 slices each (except 28 slices for patient 1, see description of patients). A T_1 weighted structural scan was also obtained consisting of 160 slices with a voxel size of 0.9 × 0.9 × 0.8 mm, TR = 25 ms and TE = 4.1 ms.

Note: a substantial upgrade of the MRI scanner was undertaken during the patient study. A number of components were replaced including the 6 element SENSE coil, replaced by a new 8 element SENSE coil. The extra 2 channels of data had the effect of improving the SNR in the data. The data from the repeat scans of patients 3 and 4 and the control group were acquired with the new coil.

Patients

Four patients were recruited from the Royal Devon and Exeter Hospital, all female, age range 50 - 60 years. The diagnosis of CRPS was confirmed according to IASP criteria (see Chapter 3.4) by Dr Haigh who also assessed their suitability for the research prior to referral to the project. Patients were initially scanned within 7 months of the onset of their symptoms. All had received a few weeks of the standard treatments (pain medication and occupational therapy involving desensitisation and a motor imagery program, see Chapter 3.5.2) offered by the Royal Devon and Exeter Hospital and their GP prior to the first scans. The patients were then invited to be scanned again approximately 4 months later to assess any changes that may have occurred within the cortical digit representations and correlate it with improvement or worsening of their symptoms. A summary of their details is given in Table 8 and their symptoms are described individually below:

Patient 1: A left handed 59 year old lady with CRPS of the right hand caused by a fractured wrist with abnormal sensations being felt soon after the wrist was put in a cast. The patient described the sensation of a phantom enlargement of the hand in a glove-like distribution and was sometimes unable to locate the injured hand without a visual input. Symptoms of allodynia, hyperalgesia, swelling, discolouration, and stiffness were also present. Other sensory disturbances included textures feeling different compared to the unaffected hand. There was no reaction to warmth and cold and no referred sensations. The patient was able to tolerate the stimulus at a drive voltage of $\pm$ 52 V and did not report the sensation as being painful.

At the second scans the patient reported a reduction in the amount of pain experienced in her hand and there was no sign of swelling or discolouration. The sensation of the phantom enlargement had also gone but there was still residual stiffness and sensory disturbances. A

slight sensitivity to warmth was also present in the centre of the palm.

Note: Due to the past medical history of the patient (internal fixation of right shoulder and a pin inserted into one hip) the switching gradient of the scanner was reduced from maximum to minimum to reduce any heating effects that may have occurred. This reduced the number of slices per dynamical scan from 30 to 28.

Patient 2: A right handed 55 year old lady with CRPS of the right hand caused by a soft tissue injury to the wrist. Symptoms included a glove-like phantom enlargement of the hand, tingling, slight discolouration, allodynia and hyperalgesia. A sensitivity to warmth was also present, where a tepid temperature felt burning hot in the thumb area. No referred sensations were present. This patient had difficulty tolerating the stimulus so it was reduced to a drive voltage of $\pm$ 26 V which the patient was able to tolerate for the duration of the experiment even though it still induced some pain.

When the second scans were carried out 3 months later, she reported a greater than 50 % improvement. The allodynia and hyperalgesia had decreased in most of the hand with the exception of the thumb area which remained very painful and sensitive to warmth. The phantom enlargement was still present although reduced and the tingling sensations still persisted. The hand was also still prone to periods of discolouration. The stimulus was kept at the same drive voltage as the first scans and the patient reported it still induced some pain (in the thumb).

Patient 3: Right handed 60 year old lady with CRPS of the left hand. The inciting event was a fracture sustained to the wrist. Although pain was felt from the injury there were no symptoms of allodynia or hyperalgesia. Swelling and discolouration were present and the patient reported a glove-like phantom enlargement of the hand with no referred

sensations. The patient also described non painful 'strange sensations' in her hand but was unable to describe them. For the experiment the higher stimulus drive voltage of ± 52 V was used with no reports of pain being felt.

By the second scans, 5 months later, the patient was not experiencing pain and the sensation of the phantom enlargement was much reduced but the strange sensations persisted. The hand no longer became discoloured but there was still a small amount of swelling present. The patient also reported an ongoing heightened sensitivity to touch in the fingertips.

Patient 4: A right handed 50 year old lady with CRPS of the right hand triggered by hand joint surgery (trapeziectomy) for osteoarthritis. The patient experienced a glove-like phantom enlargement but no referred sensations. Swelling, discolouration and hyperalgesia were also present as well as an ongoing tingling sensation. The patient was able to tolerate the stimulus at a drive voltage of ± 52 V. Although pain was reported afterwards this was due to the hand being immobilised for the duration of the experiment rather than due to the stimulus itself.

At the second scans, the pain had reduced and the phantom enlargement had disappeared but the tingling sensation persisted. Some discolouration was still present but the swelling had gone.

Controls

Initially, the CRPS data were compared to the data for the patient's own healthy hand as a control condition. Ideally it should also be compared to an age and gender matched control group of healthy volunteers. Due to the time constraints of the project it was not possible to source these matched volunteers but it was possible to scan a group of healthy controls to represent a general population. Their details are summarised in Table 9. Four subjects were recruited, 3 male,

Table 8: Details of patients 1 - 4 who participated in study 5. F - female, R - right, L - left, OT - occupational therapy.

Patient	1	2	3	4
Age	59	55	60	50
Gender	F	F	F	F
Handedness	L	R	R	R
Initial insult	Fracture wrist & shoulder	Soft tissue injury	Fracture wrist	Surgery
Location	R hand	L hand	R hand	R hand
Duration at scan 1 at scan 2	 7 mth 11 mth	 4 mth 7 mth	 3 mth 8 mth	 4 mth 8 mth
Improvement at scan 2	Yes	Yes	Yes	Yes
Medication	Protolos Calcichew Amitriptyline Paracetamol	Diclofenic Codeine Phosphate Fludrocortisone Omeprazole	Alendronate Adcal Ibuprofen Paracetamol	Omeprazole Dicloflex Livial Ulesco Salbutamol Amitriptyline Tramadol Paracetamol Gabapentin
Therapies	OT	OT	OT	OT

Table 9: Details of healthy volunteers who participated in the patient control study. M - male, F - female, R - right.

Control	Age	Gender	Handedness
1	28	F	R
2	33	M	R
3	28	M	R
4	26	M	R

age range 26 - 33 years. The same protocols from the patient study were used. A stimulus drive voltage of ± 52 V was used in all instances.

7.4 Data Processing

All data from studies 1 - 5 were processed in the same manner. Firstly, the raw data were converted to Analyse format using MRIcro software and converted to 3D files creating a *.img* and *.hdr* file for each dynamic scan. These were then preprocessed in SPM5 software. This involved applying slice timing correction to each scan and the time sequence was registered to slice 1. These images where then spatially realigned and an image was created of the mean position. The temporally and spatially realigned images were resliced and normalised to the standard MNI EPI template with a 2 × 2 × 2 mm resolution, see sections 2.7 and 5.3.3 for more information. For use in the group analysis only, smoothing was also applied using a 6 × 6 × 6 mm mask for studies 1 and 2, and a 5 × 5 × 7 mm mask for studies 3 to 5.

For the first level analysis, a model was created by convolving the haemodynamic response function with a boxcar function based on the timings for the various conditions. The time frame was registered to slice 1 of each scan. For studies 1 and 5, four conditions were specified, in seconds:

1) stimulation to D5 (9 s)

2) rest (27 s)

3) stimulation to D1 (9 s)

4) rest (27 s).

For studies 2 to 4, only two conditions were needed:

1) stimulation to digit (9 s)

2) rest (9 - 27 s)

Grand mean scaling was performed and a high pass filter of 128 s was applied but no serial correlations or global corrections were carried out. Once the design matrix was created an estimate of the statistical significance of each voxel in each dynamical scan was calculated.

The data were modelled twice at the first level as the individual and group analyses required different preprocessing. When the data were interrogated on the subject level it was modelled with the unsmoothed normalised images in order to preserve the resolution and allow detection of the individual Brodmann areas. The group analysis required a small amount of blurring to enlarge the activations and increase the chance of overlapping between subjects, therefore the smoothed normalised images were used in this instance.

The SPMs were created by applying a two sample t-test to the contrasts and specifying a statistical threshold - either an uncorrected p value or a family wise error (corrected p value) - and overlaying the activity on a glass brain in the medial/lateral (x axis), anterior/posterior (y axis) and superior/inferior (z axis) views. The clusters that appeared when the 'on' condition was contrasted against the 'off' condition were considered to be associated with the stimulation to that digit. The statistics for each cluster lying within the SI and SII regions were obtained including the size of the cluster, the coordinate of the most activated voxel and its associated T-score. These were then tabulated and analysed further to calculate the cortical digit separations.

A second level analysis was carried out to investigate the statistical significance of common activations between the subjects. This was done using the

contrasts from the smoothed SPMs ('on' condition versus 'off' condition, as described above). Again, a two sample t-test was carried out contrasting the digit against the other digits in the sample. A threshold of uncorrected p value ≤ 0.001 was applied and the statistics of each cluster were obtained for further analysis.

7.5 Calculation of Cortical Digit Separations

The Euclidean separations between the cortical D1 and D5 representations were calculated using the centre of mass of all SI activations that were identified for each digit. This was done using Equations 23 - 25.

$$X_{CoM} = \frac{T_1X_1 + ... + T_nX_n}{T_{total}} \tag{23}$$

$$Y_{CoM} = \frac{T_1Y_1 + ... + T_1Y_n}{T_{total}} \tag{24}$$

$$Z_{CoM} = \frac{T_1Z_1 + ... + T_1Z_n}{T_{total}} \tag{25}$$

Where X_1 is the x coordinate from cluster 1 for a particular digit with a T-score of T_1, X_n is the x coordinate for the nth cluster and T_n is its respective T-score. T_{total} is the sum of all the clusters T-scores for that digit. The same calculations were carried out for the y and z coordinates. The difference between the D1 and D5 centre of mass coordinates was then calculated as shown in Equations 26 - 28.

$$X_{dif} = X_{CoMD1} - X_{CoMD5} \tag{26}$$

$$Y_{dif} = Y_{CoMD1} - Y_{CoMD5} \tag{27}$$

$$Z_{dif} = Z_{CoMD1} - Z_{CoMD5} \tag{28}$$

Finally, the Euclidean separation was calculated using simple trigonometry:

$$EucSep = \sqrt{{X_{dif}}^2 + {Y_{dif}}^2 + {Z_{dif}}^2}. \quad (29)$$

Table 10: Summary of procedures for studies 1 to 5.

Study	1	2	3	4	5
No. of subjects	6	7	8	8	4 patients 4 controls
No. of sessions	2	4	2	2	2
Session duration	30 mins	12 mins	20 mins	20 mins	30 mins
Dyn. scans per session	600	240	400	400	600
Digits stim. in session	LD1 +LD5 or RD1 +RD5	LD1 or LD5 or RD1 or RD5	RD1 or RD5	RD1 or RD5	LD1 +LD5 or RD1 +RD5
Stimulus	Puls. vib. 40 Hz ±36 V	Puls. vib. 40 Hz ±36 V	Puls. vib. 40 Hz ±52 V	Cont. vib. 40 Hz ±52 V	Puls. vib. 40 Hz ±52 V
Protocol	9 s on 27 s off Rand. alt. D1-D5	9 s on Rest duration 9 - 27 s	9 s on Rest duration 9 - 27 s	9 s on Rest duration 9 - 27 s	9 s on 27 s off Rand. alt. D1-D5

Chapter 8

Results

8.1 Introduction

The results of studies 1 - 5 are reported in this chapter. Results are presented on the individual subject level and at the group level for each study and there is a brief summary at the end of each section, indicating how the results affected the protocols for the following studies.

8.2 Study 1

Six right handed subjects participated in study 1 which consisted of two 30 minute scanning sessions. In one session digits 1 and 5 of the left hand were stimulated and in the other session digits 1 and 5 of the right hand were stimulated. A switching stimulus was used with a drive voltage of $\pm$ 36 V, and it was presented to the fingertips for 9 s duration followed by 27 s rest. The stimulation randomly alternated between D1 and D5. Each digit received 25 stimulation events. A total of 600 dynamic scans were acquired per session.

8.2.1 Individual Analysis

For stimulation of LD1, LD5, RD1 and RD5, contralateral SI activity was detected for all digits in all 6 subjects at a threshold of uncorrected p value ≤ 0.001 (T-score ≥ 3.11). The T-score of the most statistically significant SI and SII activations for each stimulation site are listed in Table 11. Obviously, the higher the T-score, the more likely it is that the activation is 'real'. The maximum value in the table is 10.39, and 59 % of the activations in Table 11 would survive a corrected p value threshold of ≤ 0.05 (T-score ≥ 5.1).

Ipsilateral SI activity was also detected in all digits for all subjects (at uncorrected p value ≤ 0.001) with the exception of LD1 in subject 1. The T-scores are, generally, lower than their respective contralateral SI counterparts and over half would not appear at the higher threshold (corrected p value ≤ 0.05). Ipsilateral SI and SII activity has been observed in other tactile studies [1, 10] and may be explained by the transcallosal fibres which connect the two hemispheres.

Figure 30 shows the brain activity for a representative subject (subject 5) displayed on the template brain for digits 1 and 5 of the left and right hands. Dense regions can be seen in the contralateral SI area, indicated by a red arrow, and either bilateral or unilateral SII areas.

For each subject, the cluster centres which were identified as being in the general vicinity of the primary somatosensory area S1 (Brodmann areas 1, 2 and 3) are shown in Figures 31 to 36. The regions considered are defined in MNI coordinates by $-45 \leq y \leq -5$ and $35 \leq z \leq 66$, with $x \leq -30$ for the left side of the brain and $x \geq 32$ for the right side of the brain. Shown in the graphs in Figures 31 to 36 is the extent of the Brodmann area 1 (BA1, yellow), and a 4 mm error margin either side of BA1 (in blue) to allow for differences between the Talairach brain and each subject's normalised brain. The extent of BA1 was determined using an electronic version of the Talairach atlas [109], with the resulting Talairach coordinates converted to MNI coordinates using the algorithm proposed by Brett [49], mentioned in Chapter 2.7 and Equation 6. BA3 (BA3a and 3b) lies next to BA1,

Table 11: The highest T-scores for contralateral and ipsilateral SI and SII activations for subjects 1 - 6 in study 1. The location of the activations is indicated in Figures 31 to 36. Contra = contralateral, Ipsi = ipsilateral, - = activity not detected at uncorrected p value threshold of ≤ 0.001 (T-score ≥ 3.11). T-scores ≥ 5.1 (a corrected p value threshold of ≤ 0.05) are highlighted in bold. The mean and standard deviation for each digit for the group are given at the bottom of the table. The two columns on the far right show the ratio of contralateral SI/ipsilateral SI activity and contralateral SII/ipsilateral SII activity.

Subject	Digit stim.	Contra SI	Ipsi SI	Contra SII	Ipsi SII	Contra V Ipsi SI	Contra V Ipsi SI
1	LD1	3.84	-	**5.79**	3.92	-	1.48
	LD5	4.38	3.22	**5.54**	-	1.36	-
	RD1	5.05	3.91	4.34	3.98	1.29	1.09
	RD5	**6.41**	4.25	**6.28**	**5.87**	1.51	1.07
2	LD1	**6.27**	4.35	4.80	3.53	1.44	1.36
	LD5	4.42	4.85	**5.76**	4.15	0.91	1.39
	RD1	**8.20**	**6.78**	**6.88**	**8.26**	1.21	0.83
	RD5	**6.92**	**6.35**	**6.80**	4.53	1.09	1.50
3	LD1	**8.19**	**6.95**	**10.39**	**8.05**	1.18	1.28
	LD5	**6.10**	**6.65**	**8.84**	4.26	0.92	2.08
	RD1	**6.42**	4.94	**7.39**	4.33	1.30	1.71
	RD5	**6.72**	**6.95**	**8.74**	**7.10**	0.97	1.23
4	LD1	5.09	3.72	3.73	4.36	1.37	0.86
	LD5	5.04	3.29	4.72	-	1.53	-
	RD1	**5.61**	**5.22**	**6.76**	5.03	1.07	1.34
	RD5	**5.84**	**5.22**	**6.43**	**5.36**	1.12	1.20
5	LD1	**8.48**	3.85	**6.08**	**7.19**	2.20	0.85
	LD5	**9.01**	**5.11**	**6.10**	**9.38**	1.76	0.65
	RD1	**7.08**	**6.75**	**6.65**	3.81	1.05	1.75
	RD5	**9.04**	**7.34**	**10.06**	**5.65**	1.23	1.77
6	LD1	4.71	4.06	**5.96**	**6.25**	1.16	0.95
	LD5	3.66	4.58	4.21	4.43	0.80	0.95
	RD1	**7.02**	5.07	**7.14**	**5.10**	1.38	1.40
	RD5	**6.09**	4.68	**6.60**	5.00	1.30	1.32
Mean & standard deviation	LD1	6.10	4.59	6.11	5.55		
		1.90	1.34	2.24	1.88		
	LD5	5.44	4.62	5.86	5.56		
		1.93	1.28	1.62	2.55		
	RD1	6.56	5.45	6.53	5.09		
		1.13	1.12	1.10	1.64		
	RD5	6.84	5.80	7.48	5.59		
		1.15	1.26	1.53	0.88		

to the left on the left hand side (LHS) of the brain and to the right on the right hand side (RHS). BA2 lies on the opposite side to BA3. The LHS graphs are shown with the right D1 and D5 activations overlaid and the RHS graphs contain the corresponding activations for the left hand. Those activations which fall close to (i.e., within the yellow and blue regions) BA1 are shown with larger markers and are coloured red if they also have a T-score ≥ 4.

As can be seen in Figures 31 to 36, there are multiple activations detected in the contralateral SI region ranging between 4 - 23 foci. Although results from previous studies (see Chapter 1.2.1) are inconsistent, on the basis of these one might expect a D1 activation in BA1 at z $\sim$ 40 - 45 and a D5 activation in BA1 at z $\sim$ 50 - 55. The data in Figures 31 to 36 were often difficult to reconcile with this expectation. Considering only those activations close to BA1 (large icons on the graphs), and within the limits in the z direction, it can be seen that there are often more than one activation for each digit. Some subjects demonstrate one or two BA1 activations common to D1 and D5 but there does not appear to be a systematic pattern to the location of the activations for either digit.

In an attempt to summarise these data, values for the Euclidean separation of D1 and D5 activations were determined by first calculating the centre of mass of all the activations associated with a particular stimulus, weighted by the cluster's associated T-score, and then calculating the distance on the cortex between these centres of mass. (The T-score was used rather than the number of activated voxels as the cluster size will change as the threshold is raised or lowered but the T-score will remain constant). The separations are listed in Table 12. Two of the separations are similar to the distances ($\sim$ 10 - 18 mm) obtained in other studies (see Chapter 1.2.1) - subject 1: left D1-D5 and subject 3: right D1-D5. The other separations are 2 - 3 times smaller than the range of values expected. In an effort to improve this, the Euclidean separations were recalculated using only the clusters which fell close to BA1 (i.e., within the blue and yellow zones in the Figures). These are also listed in Table 12. It was not possible to calculate all the separations using this method as not all the digits for each subject had an

Table 12: Euclidean separations for the left and right hands for each subject in study 1. The centre of mass was calculated using the coordinates (estimated error ± 2 mm) that fell within specific Brodmann areas and were weighted according to their T-score.

Subject	BA1,2,3 and vicinity		BA1	
	LD1-D5 mm	RD1-D5 mm	LD1-D5 mm	RD1-D5 mm
1	13.7	4.7	10.2	8.5
2	7.4	8.0	9.9	-
3	6.2	11.2	-	-
4	9.1	2.3	3.9	3.4
5	4.9	5.8	6.8	9.7
6	5.8	9.0	7.3	9.6
Average	7.9	6.8	7.6	7.8

activation close to BA1. Where the separations could be calculated, some values have increased but others have decreased and so, overall, there is no appreciable difference using this method.

As the data were difficult to assess in terms of the individual digits, the T-scores were also interrogated for side to side differences between the dominant and non-dominant hands; all subjects were right handed. An unpaired two-tailed student t-test was carried out using the ratios of the contralateral SI activity contrasted with the ipsilateral SI activity for the left and right hands, column 7 in Table 11. No statistically significant differences were found for the dominant and non-dominant hands ($p = 0.36$, t = 0.95, 21 degrees of freedom). A similar statistical analysis was carried out for the contralateral SII/ipsilateral SII activity (column 8, Table 11). Again no statistically significant differences were found ($p = 0.29$, t = 1.09, 21 degrees of freedom).

8.2.2 Group Analysis

A second level analysis was carried out for each digit using the data from all the subjects in this study. The resulting SPMs are shown in Figure 37. Contralateral

Table 13: The SI activation centres (most activated coordinates) for the digits are listed with their respective T scores for the contralateral SI activations for the group analysis for subjects 1 - 6 in study 1. Threshold of uncorrected p value of ≤ 0.001 was used.

Stimulation	x	y	z	T-score
LD1	54	-12	44	6.61
	46	-14	52	5.68
	54	-20	48	5.48
	34	-12	66	3.80
	38	-16	50	3.56
Average	45	-15	52	
LD5	50	-26	62	4.06
RD1	-56	-10	48	5.20
	-44	-42	56	4.43
	-44	-8	60	4.20
	-50	-16	52	4.03
Average	-49	-19	54	
RD5	-42	-22	64	4.27

SI activation can be seen for all digits, indicated by the red arrow. The SI coordinates are listed with their T-scores in Table 13 and have been overlaid on the graphs shown in Figure 38.

The LD1 and RD1 data reveal multiple clusters of activity but only 1 cluster each for LD5 and RD5. The contralateral SI T-scores range from 3.56 to 6.61. The Euclidean separations were calculated based on all clusters in the vicinity of SI, and reveal a left hand cortical digit distance of 16.1 mm and for the right hand 12.8 mm. Both of these values are within the range expected on the basis of previous studies.

A closer inspection of the results for the left hand (RHS brain) shows there is one activation per digit which lies within BA1, D1: (54 -20 48) and D5: (50 -26 62). Calculating the separations using only these two activations produces a new value of 15.7 mm, which is also in line with expectation. This suggests that the group data may provide a more reliable representation of the differences between D1 and D5 activations. The right hand stimulation (LHS activation) has no D5 element

in BA1 but there is a D1 marker in a similar position to that found for the left hand, (-50 -16 52), lending support to this suggestion. (It would be plausible to assume that the right D5 activation would be in a similar position to the left). However, on revisiting the individual data (Figures 31 to 36), it is disappointing that there are only a few cases in which single-subject activations can be seen in similar locations to activations in the group data. The group data also suggests the D5 BA1 activation is located higher in the brain than the D1 BA1 activation, ($z \sim 48$ versus $z \sim 62$). To compare this to the individual data, for each subject the centre of mass (weighted by the T-score) of all the activations within BA1 for each digit were plotted on the graphs in Figure 39. D1 and D5 are shown by the same markers as before and are joined by a line to indicate each subject's data. For the RHS brain (left hand stimulation) the centres move around within a small region of BA1 and in four of the five subjects which displayed activations within BA1, the z-value increases from D1 to D5. In the LHS brain (right hand stimulation) three of the four D1 activation centres are clustered in one area, although in a different location to the RHS (LHS: $y \sim -28$, $z \sim 54$ versus RHS: $y \sim -22$, $z \sim 50$). The LHS D5 activation centres are less organised and are scattered throughout BA1 with z-value ranging from 48 to 64. In two of the four subjects the activation centre has a smaller z-value for D5 indicating a movement in the opposite direction.

8.2.3 Summary of Study 1

The results are discussed in the following chapter. A possible explanation of the lack of consistent movement on the cortex between D1 and D5 stimulation is that activations relating to D1 stimulation were evoked by D5 stimulation, and vice versa. In an effort to eliminate this possibility, in study 2, D1 and D5 stimulation were arranged in separate scanning sessions.

Figure 30: The brain activations for a representative subject (subject 5), study 1, for right D1 and D5, and left D1 and D5 overlaid on the template brain. A corrected p value threshold of ≤ 0.05 was applied. The SI activations for each digit is indicated by the red arrow.

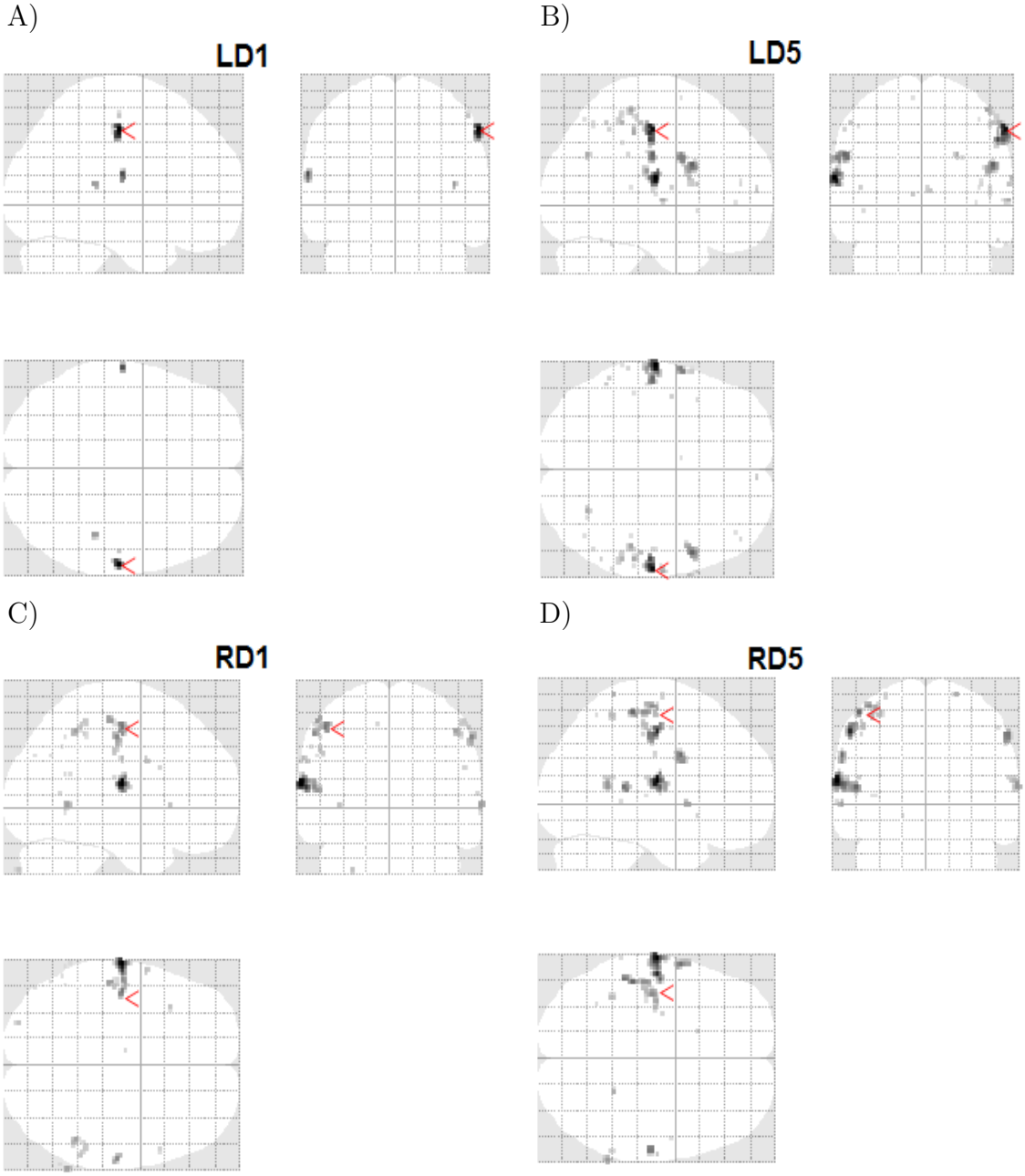

Figure 31: The SI activations for subject 1, study 1, plotted over the extent of Brodmann area 1 (yellow) with a 4 mm error margin in x and y (blue). The mean location of the SI activation for each digit was determined from other studies (Table 1) and are shown by the large green markers. An uncorrected p value threshold of ≤ 0.001 was applied (T-score ≥ 3.11). The activations which fall within the area bounded by blue in x, y and z are denoted by a larger marker. Those which also have a T-score ≥ 4 are coloured red. All data plotted in MNI coordinates. D1 activation = '+', D5 activation = 'X'.

A)

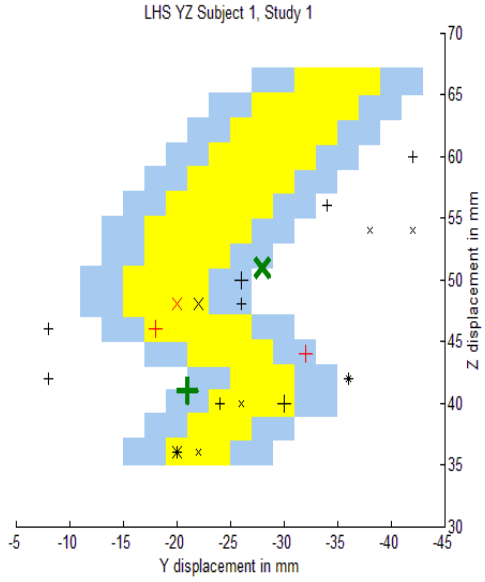

B)

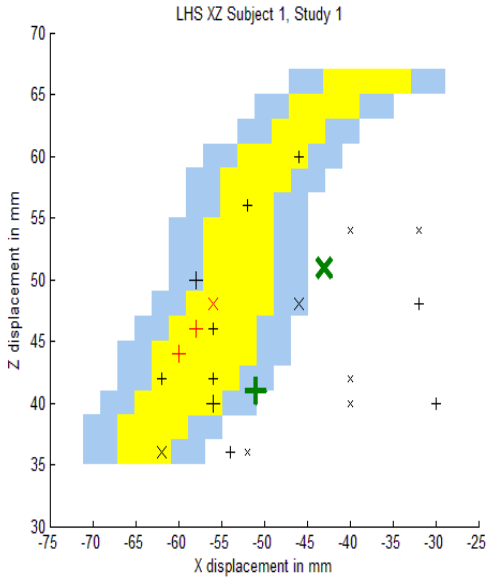

C)

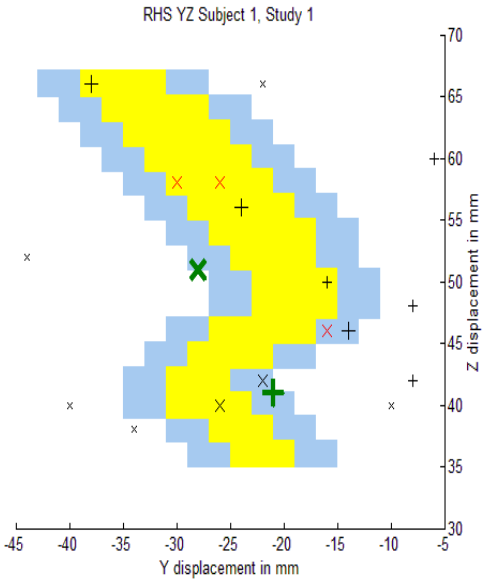

D)

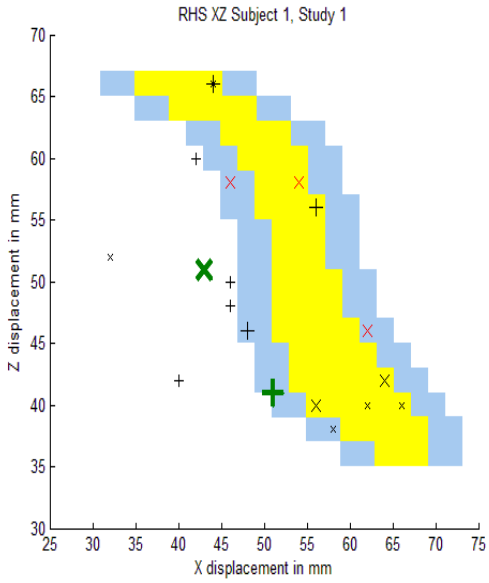

Figure 32: The SI activations for subject 2, study 1, plotted over the extent of Brodmann area 1 (yellow) with a 4 mm error margin in x and y (blue). The mean location of the SI activation for each digit was determined from other studies (Table 1) and are shown by the large green markers. An uncorrected p value threshold of ≤ 0.001 was applied (T-score ≥ 3.11). The activations which fall within the area bounded by blue in x, y and z are denoted by a larger marker. Those which also have a T-score ≥ 4 are coloured red. All data plotted in MNI coordinates. D1 activation = '+', D5 activation = 'X'.

A)

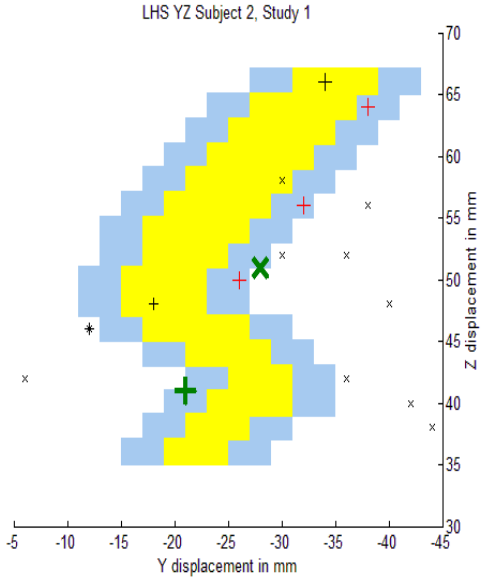

B)

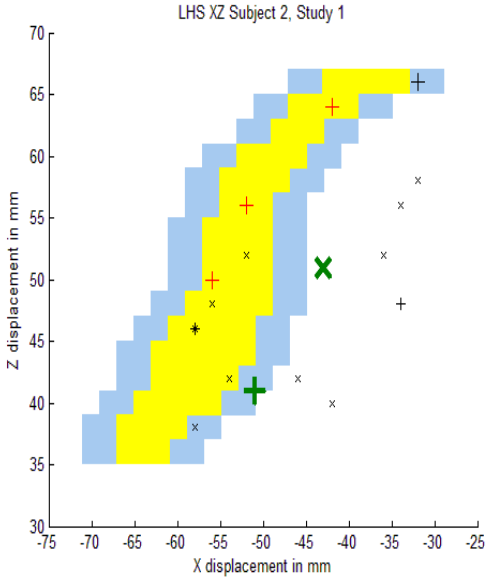

C)

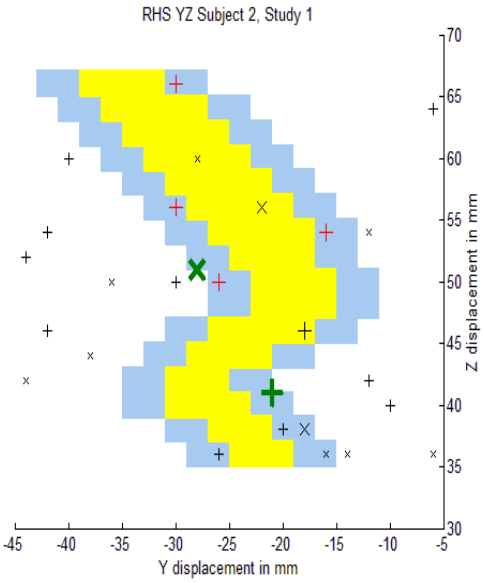

D)

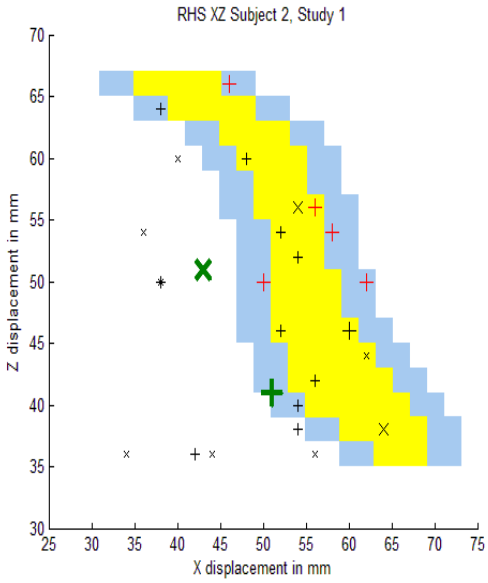

Figure 33: The SI activations for subject 3, study 1, plotted over the extent of Brodmann area 1 (yellow) with a 4 mm error margin in x and y (blue). The mean location of the SI activation for each digit was determined from other studies (Table 1) and are shown by the large green markers. An uncorrected p value threshold of ≤ 0.001 was applied (T-score ≥ 3.11). The activations which fall within the area bounded by blue in x, y and z are denoted by a larger marker. Those which also have a T-score ≥ 4 are coloured red. All data plotted in MNI coordinates. D1 activation = '+', D5 activation = 'X'.

A)

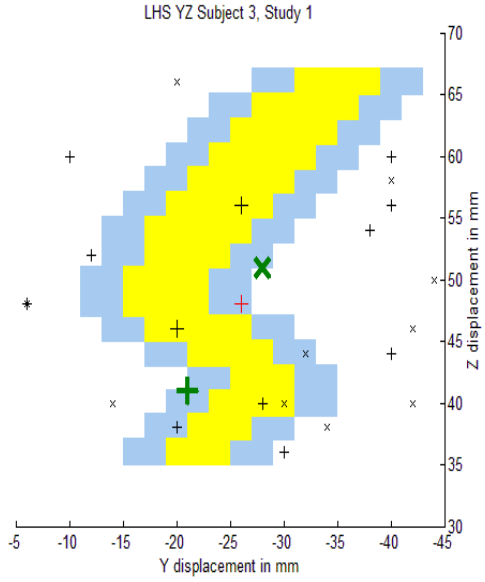

B)

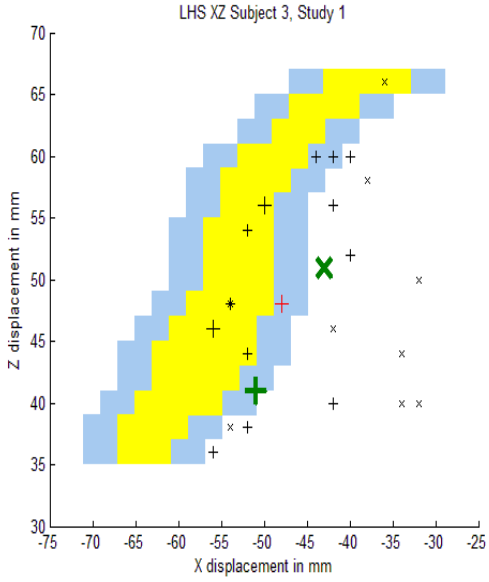

C)

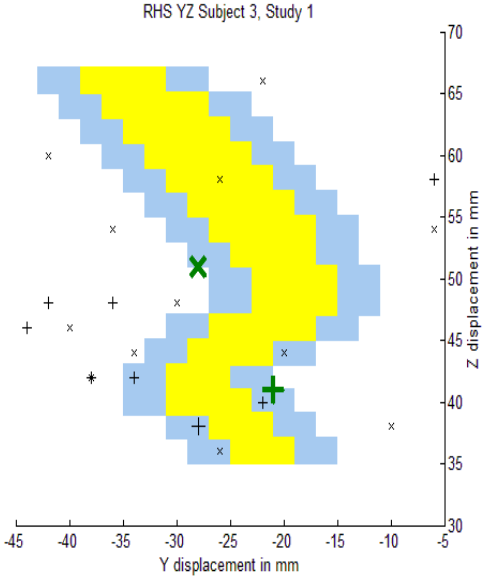

D)

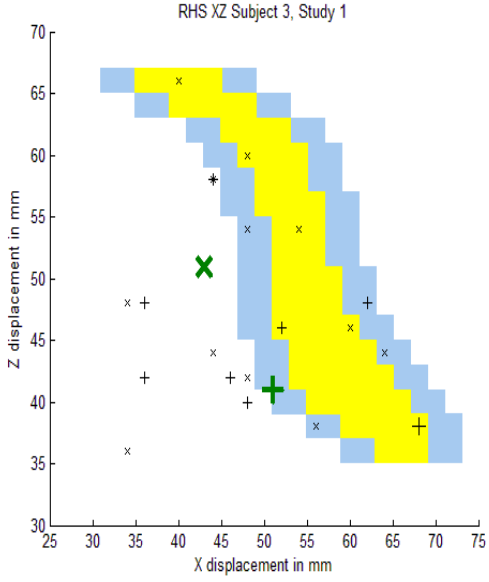

Figure 34: The SI activations for subject 4, study 1, plotted over the extent of Brodmann area 1 (yellow) with a 4 mm error margin in x and y (blue). The mean location of the SI activation for each digit was determined from other studies (Table 1) and are shown by the large green markers. An uncorrected p value threshold of ≤ 0.001 was applied (T-score ≥ 3.11). The activations which fall within the area bounded by blue in x, y and z are denoted by a larger marker. Those which also have a T-score ≥ 4 are coloured red. All data plotted in MNI coordinates. D1 activation = '+', D5 activation = 'X'.

A)

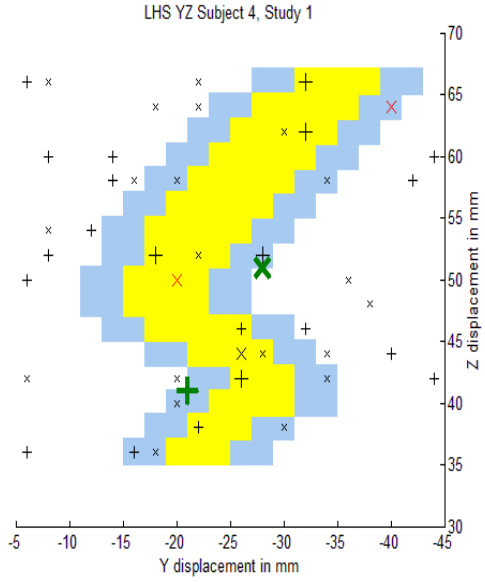

B)

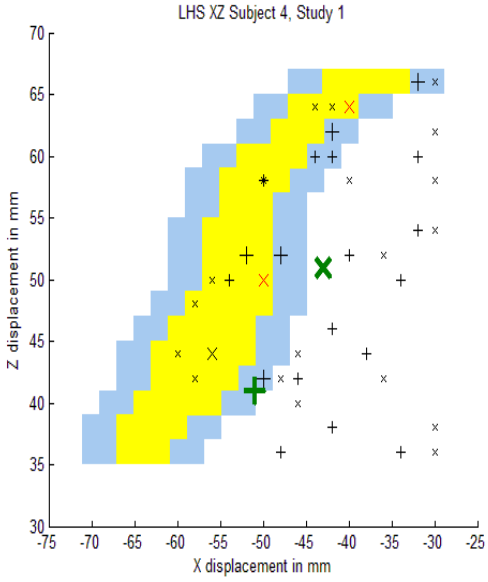

C)

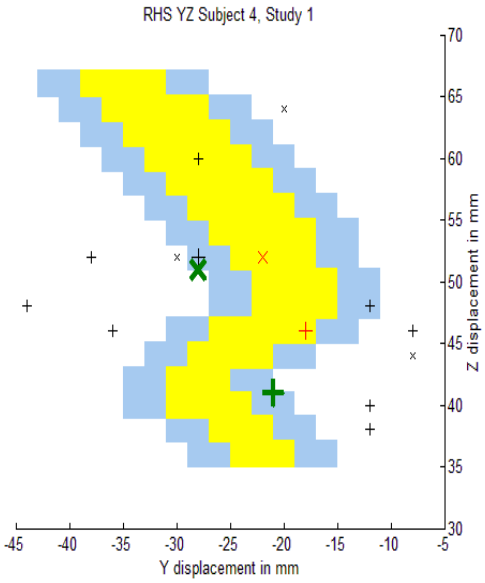

D)

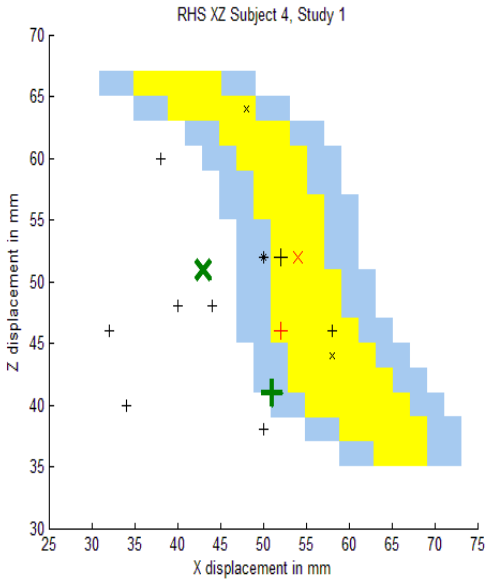

Figure 35: The SI activations for subject 5, study 1, plotted over the extent of Brodmann area 1 (yellow) with a 4 mm error margin in x and y (blue). The mean location of the SI activation for each digit was determined from other studies (Table 1) and are shown by the large green markers. An uncorrected p value threshold of ≤ 0.001 was applied (T-score ≥ 3.11). The activations which fall within the area bounded by blue in x, y and z are denoted by a larger marker. Those which also have a T-score ≥ 4 are coloured red. All data plotted in MNI coordinates. D1 activation = '+', D5 activation = 'X'.

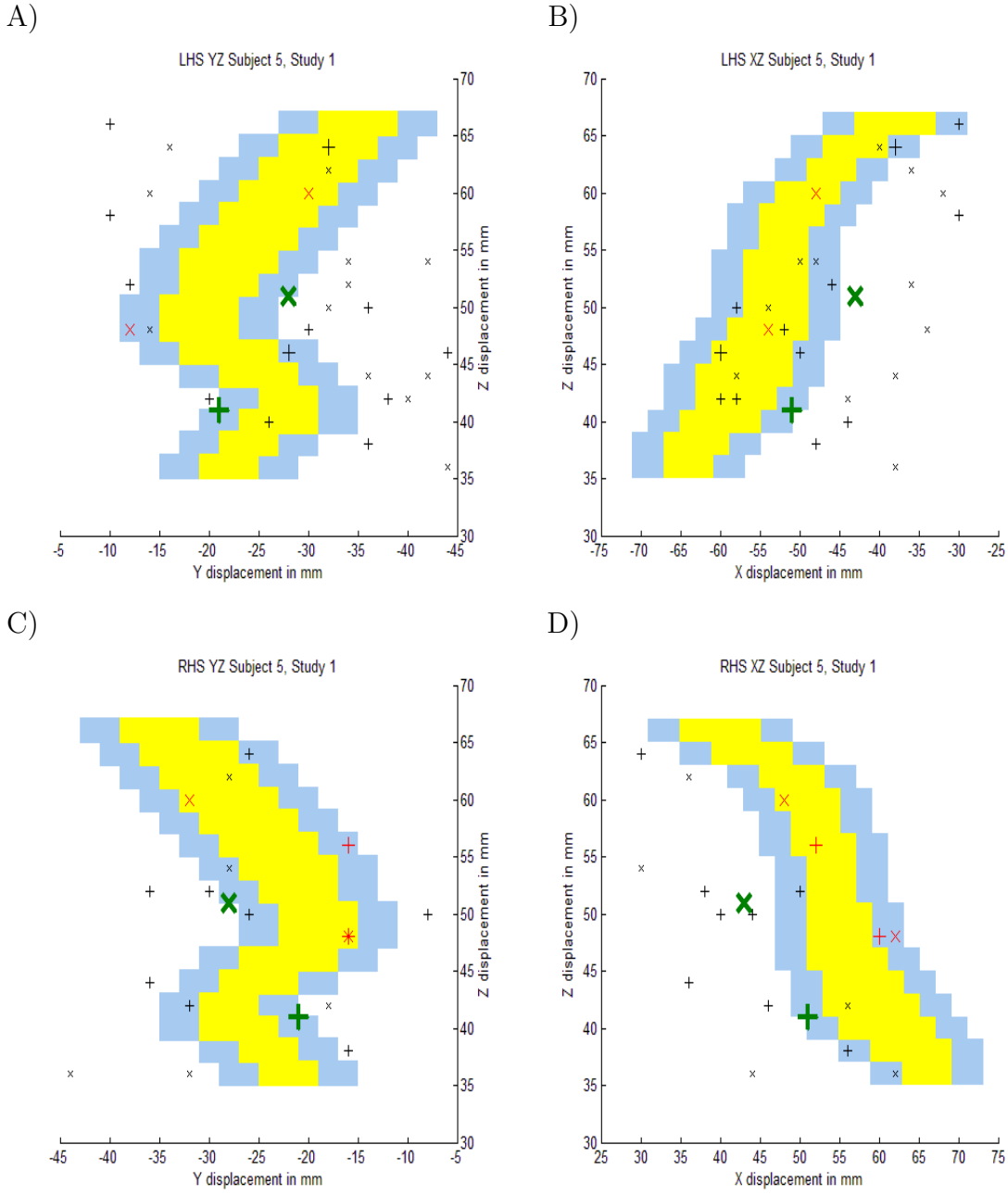

Figure 36: The SI activations for subject 6, study 1, plotted over the extent of Brodmann area 1 (yellow) with a 4 mm error margin in x and y (blue). The mean location of the SI activation for each digit was determined from other studies (Table 1) and are shown by the large green markers. An uncorrected p value threshold of ≤ 0.001 was applied (T-score ≥ 3.11). The activations which fall within the area bounded by blue in x, y and z are denoted by a larger marker. Those which also have a T-score ≥ 4 are coloured red. All data plotted in MNI coordinates. D1 activation = '+', D5 activation = 'X'.

A)

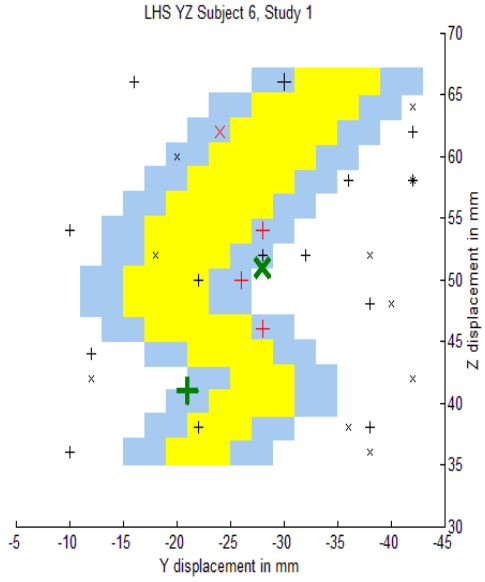

B)

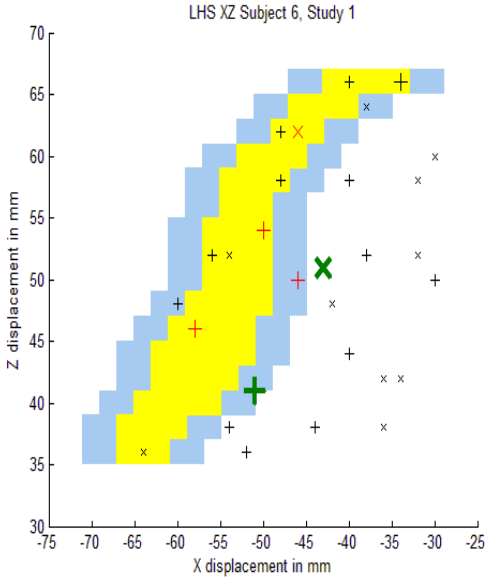

C)

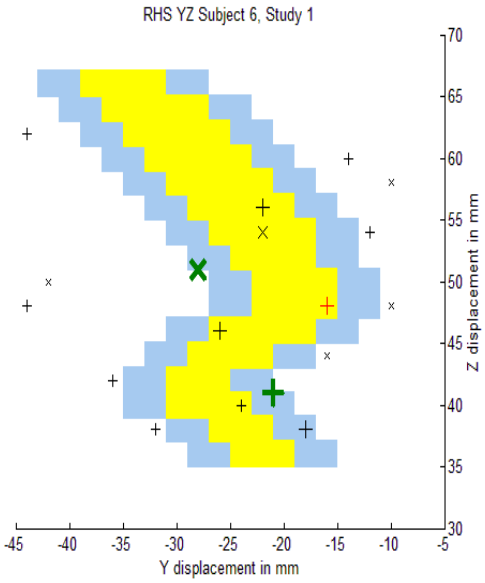

D)

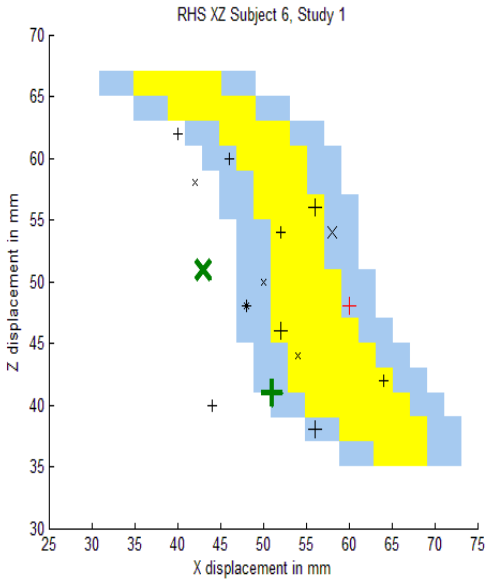

Figure 37: The results from the second level analysis of study 1, using data from subjects 1 to 6, for each digit on the template brain. Threshold uncorrected p value ≤ 0.001. SI activations for each digit is indicated by the red arrow.

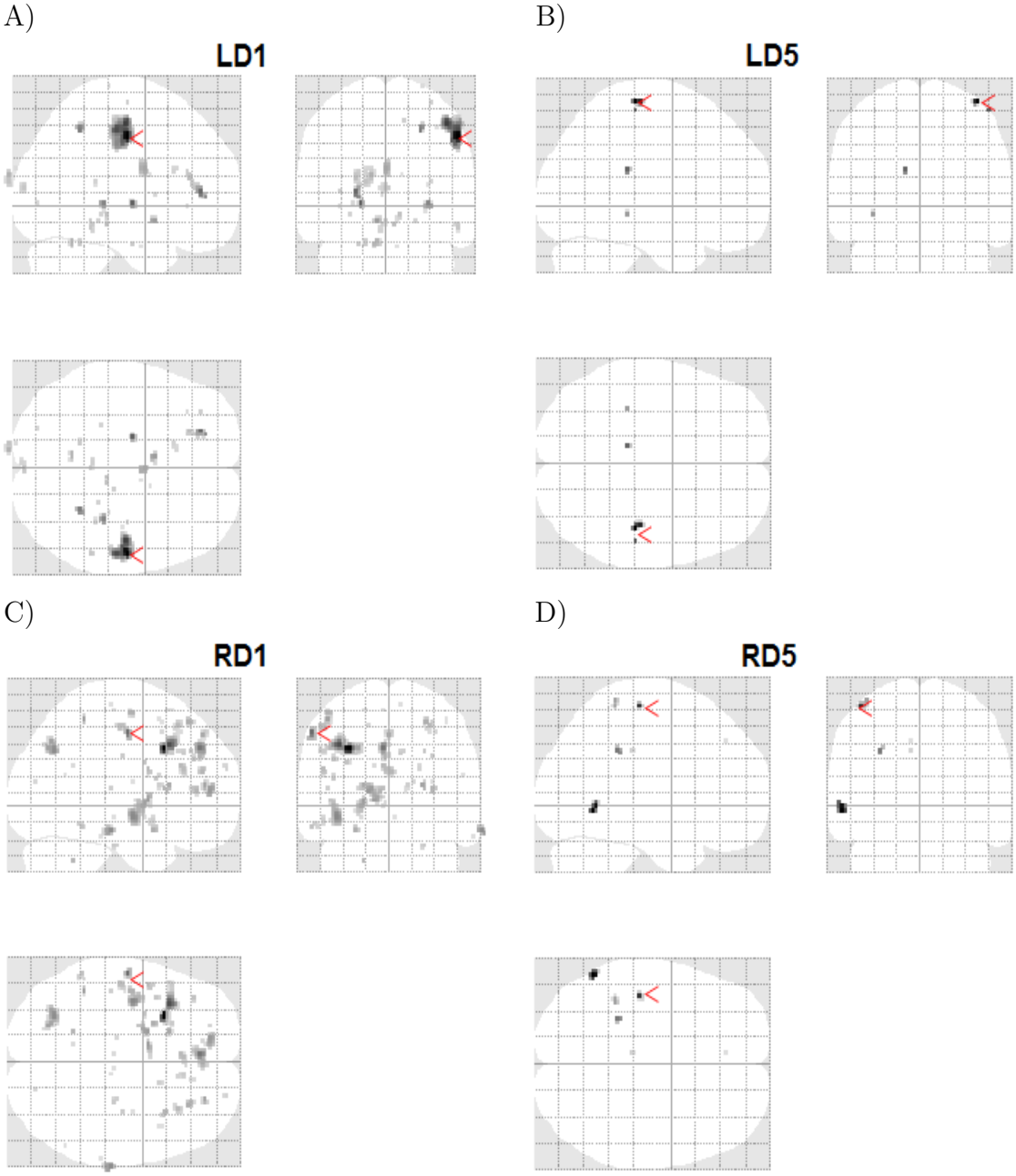

Figure 38: The SI activations from the group analysis for study 1 overlaid on BA1 (yellow), 4 mm error margin in x and y (blue), plotted in MNI coordinates. D1 = '+' and D5 = 'X'. The mean location of the SI activation for each digit was determined from other studies (Table 1) and are shown by the large green markers. An uncorrected p value threshold of ≤ 0.001 was applied (T-score ≥ 3.11). The activations which fall within the area bounded by blue in x, y and z are denoted by larger markers and those which also have a T-score ≥ 4 are coloured red.

A)

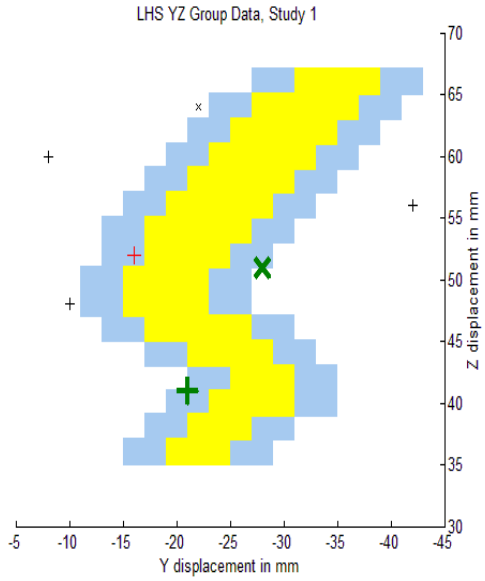

B)

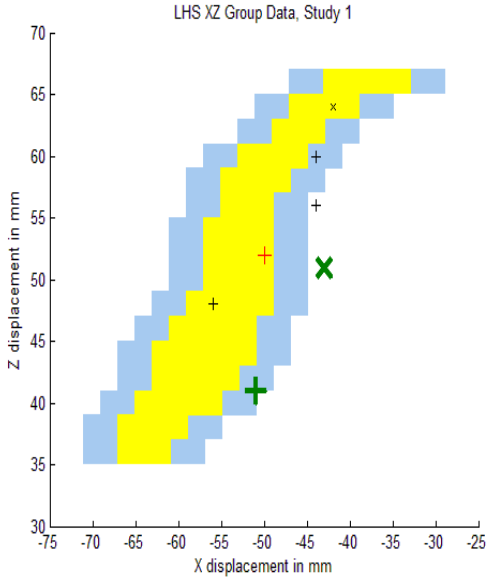

C)

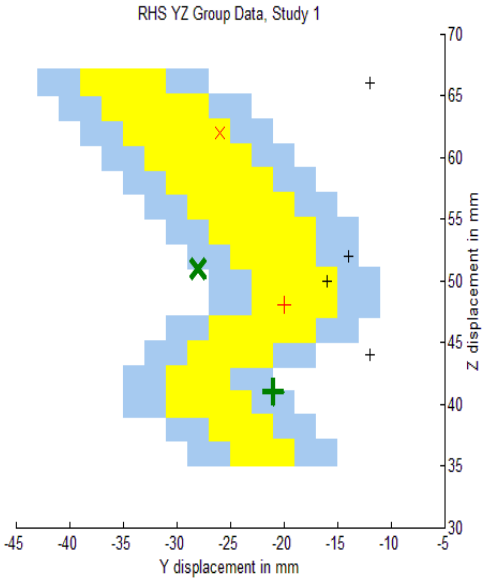

D)

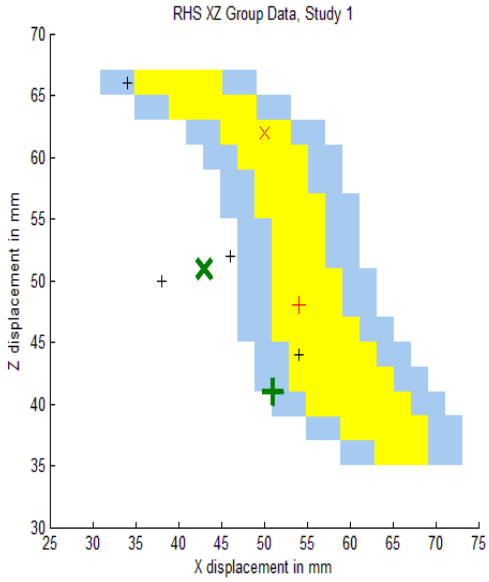

Figure 39: The centre of mass of all activations within BA1 for each subject in study 1, plotted over BA1. D1 data is indicated by '+' and D5 data by 'X'. Lines show each subject's data. All data plotted in MNI coordinates.

A)

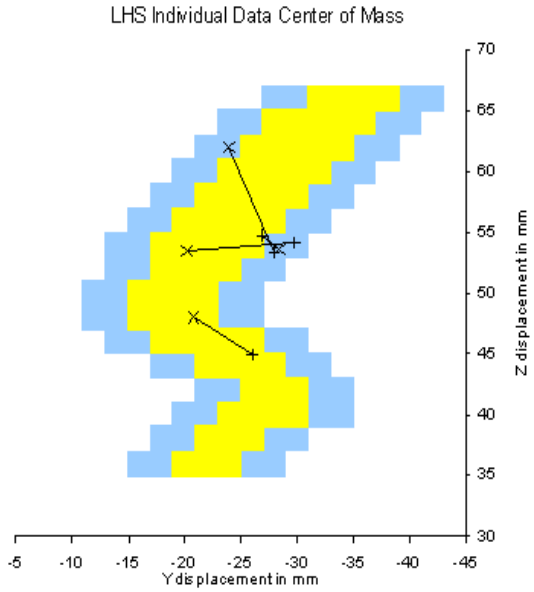

B)

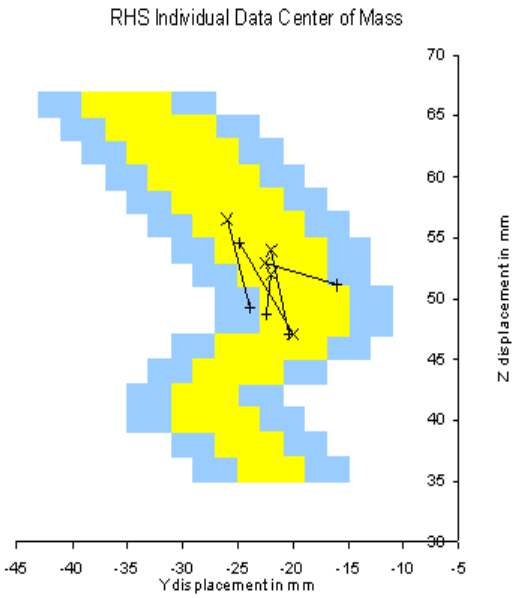

8.3 Study 2

This experiment was carried out over four 12 minute scanning sessions (instead of two 30 minute sessions as in study 1). Previously, the stimulation was applied to two digits in each scanning session, here, stimulation was restricted to one digit only per session (either LD1, LD5, RD1 and RD5). The duration of the stimulation was kept at 9 s and was delivered with a random interstimulus interval between 9 and 27 s (as opposed to a regular 27 s 'off' pattern). The 40 Hz drive voltage remained at $\pm$ 36 V, and 240 dynamic scans were acquired per session. Seven right handed subjects were recruited.

8.3.1 Individual Analysis

The results of subjects 1 to 7 of study 2 are presented here. The T-score value of the most activated voxels in SI and SII, for each stimulation site, are listed in Table 14 for stimulation to LD1, LD5, RD1 and RD5. Contralateral SI activity was detected in all but 3 cases (LD5 in subjects 1, 4 and 7) at an uncorrected p value threshold ≤ 0.001. Comparing the T-scores to study 1, the average value for all the activations is lower (5.84 versus 4.57) and the maximum T-score is also lower (10.39 versus 8.74). Only 22 % of the activations in Table 14 would survive a corrected p value threshold ≤ 0.05 (T-score ≥ 5.1). Four of the subjects participated in both studies (subjects 1, 4, 5, and 6) and it is possible to directly compare the average T-scores for each subject. In all four subjects, the average T-scores were more than 15 % lower in study 2.

Ipsilateral SI activity was not detected in 3 subjects in the group and the T-scores are lower on average than their respective contralateral counterparts. The average T-scores are also lower than those for the ipsilateral SI activations in study 1 (5.14 versus 4.13). Contralateral and ipsilateral SII activity was detected in all digits for all subjects but the T-scores are lower, in general, than in the previous study.

The brain activations for a representative subject (subject 3) are displayed

Table 14: The highest T-scores for contralateral and ipsilateral SI and SII activations for subjects 1 - 7 in study 2. The location of the activations is indicated in Figures 41 to 47. Contra = contralateral, Ipsi = ipsilateral, - = activity not detected above uncorrected p value threshold of ≤ 0.001. T-scores ≥ 5.1 (a corrected p value threshold of ≤ 0.05) are highlighted in bold. The mean and standard deviation for each digit for the group are given at the bottom of the table. The two columns on the far right show the ratio of contralateral SI/ipsilateral SI activity and contralateral SII/ipsilateral SII activity.

Subject	Digit stim.	Contra SI	Ipsi SI	Contra SII	Ipsi SII	Contra V Ipsi SI	Contra V Ipsi SI
1	LD1	3.78	4.99	4.02	4.86	0.76	0.83
	LD5	-	-	3.24	3.81	-	0.85
	RD1	4.11	-	4.39	3.78	-	1.16
	RD5	4.49	4.30	**6.40**	4.19	1.04	1.53
2	LD1	**8.40**	**5.40**	**6.28**	5.00	1.56	1.26
	LD5	3.73	4.40	4.15	4.28	0.85	0.97
	RD1	**5.15**	3.47	4.27	4.12	1.48	1.04
	RD5	3.48	4.07	4.72	4.19	0.86	1.13
3	LD1	**6.87**	4.70	**6.68**	**6.60**	1.46	1.01
	LD5	**7.04**	3.54	**7.32**	**6.66**	1.99	1.10
	RD1	**6.23**	4.65	**6.77**	4.20	1.34	1.61
	RD5	4.57	4.87	**8.74**	**6.70**	0.94	1.30
4	LD1	5.00	3.60	4.08	3.98	1.39	1.03
	LD5	4.29	3.39	4.04	3.80	1.27	1.06
	RD1	3.35	3.51	4.44	3.28	0.95	1.35
	RD5	3.55	3.53	3.75	3.36	1.01	1.12
5	LD1	**7.12**	5.00	3.68	4.44	1.42	0.83
	LD5	4.16	3.51	3.34	4.32	1.19	0.77
	RD1	**5.59**	**5.52**	**7.02**	3.15	1.01	2.23
	RD5	3.82	4.82	**6.07**	4.43	0.79	1.37
6	LD1	**5.67**	4.40	**5.33**	4.99	1.29	1.07
	LD5	-	3.62	3.43	3.56	-	0.96
	RD1	**5.21**	4.23	4.77	3.94	1.23	1.21
	RD5	3.37	-	3.57	4.09	-	0.87
7	LD1	5.05	4.23	4.67	4.33	1.19	1.08
	LD5	-	-	3.82	3.19	-	1.20
	RD1	4.38	3.17	3.46	4.09	1.38	0.85
	RD5	4.23	3.18	3.50	4.29	1.33	0.82
Mean & standard deviation	LD1	5.98	4.62	4.96	4.89		
		1.57	0.60	1.17	0.85		
	LD5	4.81	3.69	4.19	4.23		
		1.51	0.40	1.42	1.14		
	RD1	4.86	4.09	5.02	3.79		
		0.97	0.89	1.35	0.42		
	RD5	3.93	4.13	5.25	4.46		
		0.50	0.68	1.94	1.04		

on the template brain in Figure 40. The SI activations are indicated by the red arrows. The SI activations for each digit and subject are displayed on the graphs showing the outline of BA1 and its vicinity in Figures 41 to 47. Those activations close to BA1 (yellow and blue regions) are shown by a large marker and they are also coloured red if the T-score is ≥ 4. Again, multiple activations were detected for stimulation to the digits with up to 15 foci being present. Some activations appear in the same location for both D1 and D5 in some subjects whilst some appear in different locations, but again, no systematic pattern is obvious in the locations of the SI activity for either digit. A few activations for the left and right hands for some subjects appear in a similar location to the LD1, LD5 and RD1 BA1 activations from the group data in study 1.

The Euclidean separations were calculated in two ways. The centre of mass weighted to the T-score was obtained from all the SI activations for each digit and also from those only within the area defined as BA1 in the graphs. The separations are shown in Table 15. As SI activity was not detected in all digits for all subjects it was not possible to calculate separations in 3 cases, and separations could not be calculated in 5 cases using the BA1 coordinates. For BA1, 2, 3 and the vicinity four values are within the expected range $\sim$ 15 mm (subjects 1, 2 and 6: right hand, and subject 3: left hand). The rest are smaller than expected. The Euclidean separations calculated from only the BA1 activations reveal two values within the expected range, subject 1: right hand, and subject 5: left hand. The separation for the left hand of subject 2 is twice the value expected whilst the rest are smaller. The SI area and BA1 separations for subjects 1, 4, 5 and 6 can be directly compared to the values obtained in study 1, Table 12. The separations differ between the two studies and show the amount of variability demonstrated by both groups in both studies.

The ratios of the T-scores were also assessed for any laterality differences between the dominant and non-dominant hands; all subjects were right handed. An unpaired two-tailed student t-test was carried out using the ratios of the SI

Table 15: Euclidean separations for the left and right hands for subjects 1 to 7 in study 2. The centre of mass was calculated using the coordinates (estimated error ± 2 mm) that fell within specific Brodmann areas and were weighted according to their T-score.

	BA1,2,3 and vicinity		BA1	
Subject	LD1-D5 mm	RD1-D5 mm	LD1-D5 mm	RD1-D5 mm
1	-	13.7	-	14.7
2	6.8	17.4	32.1	9.7
3	16.7	6.1	9.2	3.4
4	7.7	9.1	4.8	-
5	5.5	4.9	16.3	2.9
6	-	19.4	-	-
7	-	8.9	-	8.2
Average	9.2	11.4	15.6	7.8

activity for the left and right hands (column 7, Table 14). No statistically significant differences were found for the dominant and non-dominant hands ($p = 0.12$, t = 1.63, 21 degrees of freedom). A similar statistical analysis was carried out for the SII activity ratios (column 8, Table 14). A slight statistically significant difference was found between the dominant and non-dominant hands ($p = 0.02$, t = 2.41, 26 degrees of freedom) implying the contralateral SII area is more active when the dominant hand is stimulated.

8.3.2 Group Analysis

The brain activations resulting from the second level analysis are shown in Figure 48. SI activations were detect for stimulation to LD1, RD1 and RD5 but no activations (SI or otherwise) were detected for stimulation to LD5 at uncorrected p value ≤ 0.001. The SI clusters are listed in Table 16. These activations are plotted on the graphs in Figure 49. There are several activations for the stimulation to LD1 but only 1 centre is within the yellow and blue regions in the graphs, (52 -32 40). For the RD1 stimulation, only 1 activation was detected and it falls

Table 16: The most activated coordinates of the SI activations for the digits are listed with their respective T scores for the contralateral SI activations for the group analysis for subjects 1 - 7 in study 2. Threshold is uncorrected p value of ≤ 0.001.

Digit	x	y	z	T-score
LD1	52	-12	56	6.63
	48	-12	46	5.58
	46	-32	52	4.44
	34	-28	60	4.12
	46	-24	36	3.8
	52	-32	40	3.53
	38	-28	40	3.51
	52	-30	36	3.49
Average	46	-25	46	
LD5				
RD1	-54	-20	54	4.16
RD5	-30	-30	50	4.49
	-44	-44	36	3.86
Average	-37	-37	43	

within the vicinity of BA1, (-54 -20 54). It is in a similar location to that detected in the group analysis in study 1 for the RD1 stimulus. Both centres detected for RD5 stimulation are outside the area on the graphs defined as BA1. The Euclidean separations were calculated using all the SI activations for RD1 and RD5 and reveal a distance of 26.2 mm, well above the expected range.

The centre of mass coordinates for the stimulation to D1 and D5 from the individual subject data are shown in Figure 50. The markers are connected by a line indicating the D1 and D5 subject pairs. The D1 centre of mass coordinates for the right hand (LHS brain) are located very close together in y and z (y $\sim$ -18 to -24 and z $\sim$ 50 to 55) and are in a similar location to the D1 activation from the group analysis in studies 1 and 2. However, the D5 centre of mass coordinates are more spread out and the direction of the activation movement in the brain from D1 to D5 shows no obvious pattern. The left hand (RHS brain) shows no clustering of the D1 or D5 centre of mass activations and 2 of the 4 subjects show a decrease in z when moving from D1 to D5.

8.3.3 Summary of Study 2

These results are discussed in the following chapter. In terms of the digit separations, there was no significant effect of changing the protocol between study 1 and study 2. In an attempt to produce stronger activations, study 3 involved increasing the stimulator drive voltage and longer scanning sessions.

Figure 40: The brain activations for a representative subject (subject 3), study 2, for the right and left hands for D1 and D5, overlaid on the template brain. The SI area is indicated by the red arrow in panels A, B and C. SI activity was not present in panel D at this threshold. A corrected p value threshold of ≤ 0.05 was applied to all data.

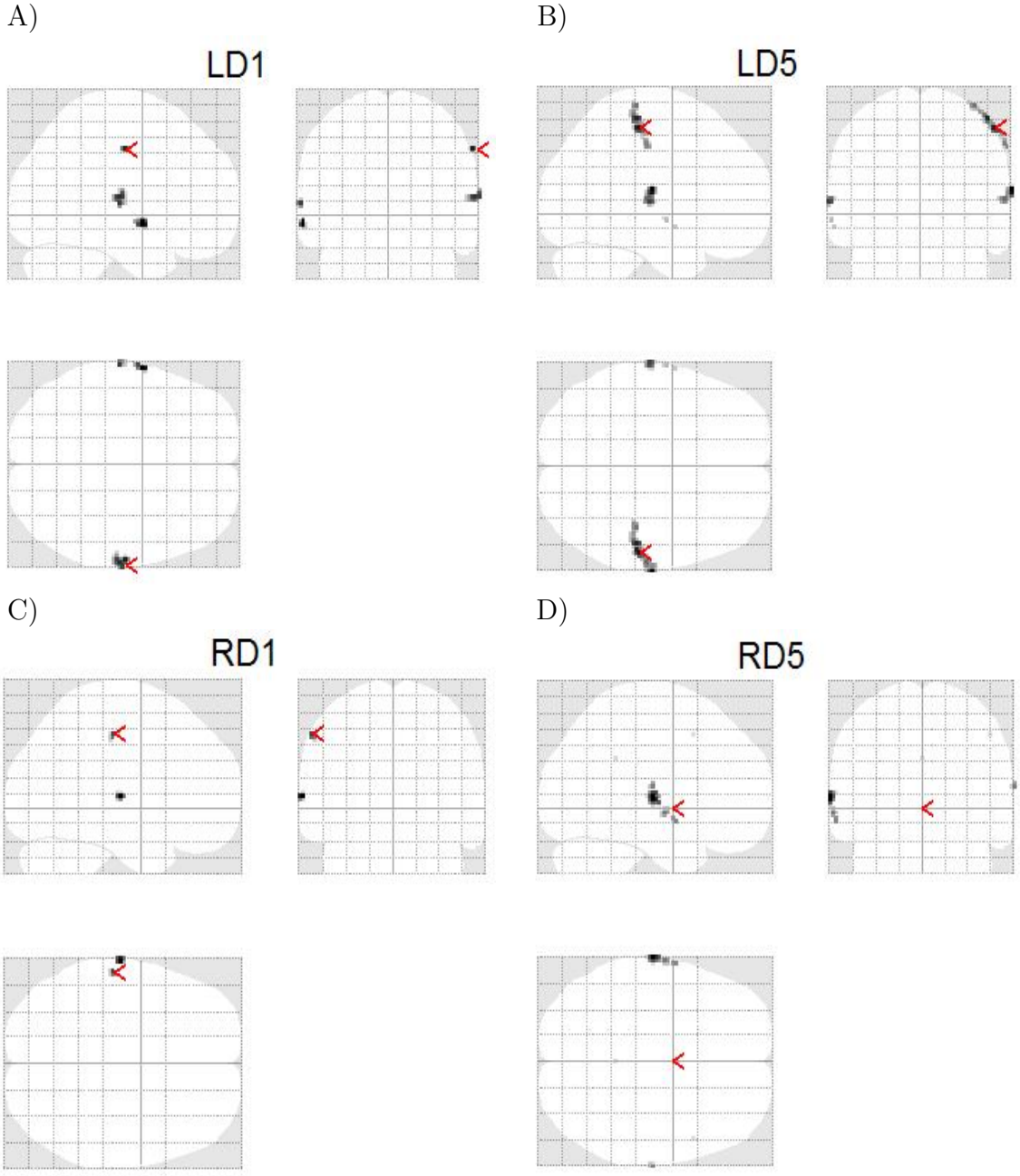

Figure 41: Brodmann area 1 (yellow) with a 4 mm error margin in x and y (blue), and SI activations for subject 1, study 2, overlaid. The mean location of the SI activation for each digit was determined from other studies (Table 1) and are shown by the large green markers. An uncorrected p value threshold of ≤ 0.001 was applied (T-score ≥ 3.11). The activations which fall within the area bounded by blue in x, y and z are denoted by a larger marker. Those which also have a T-score ≥ 4 are coloured red. All data plotted in MNI coordinates. D1 activation = '+', D5 activation = 'X'.

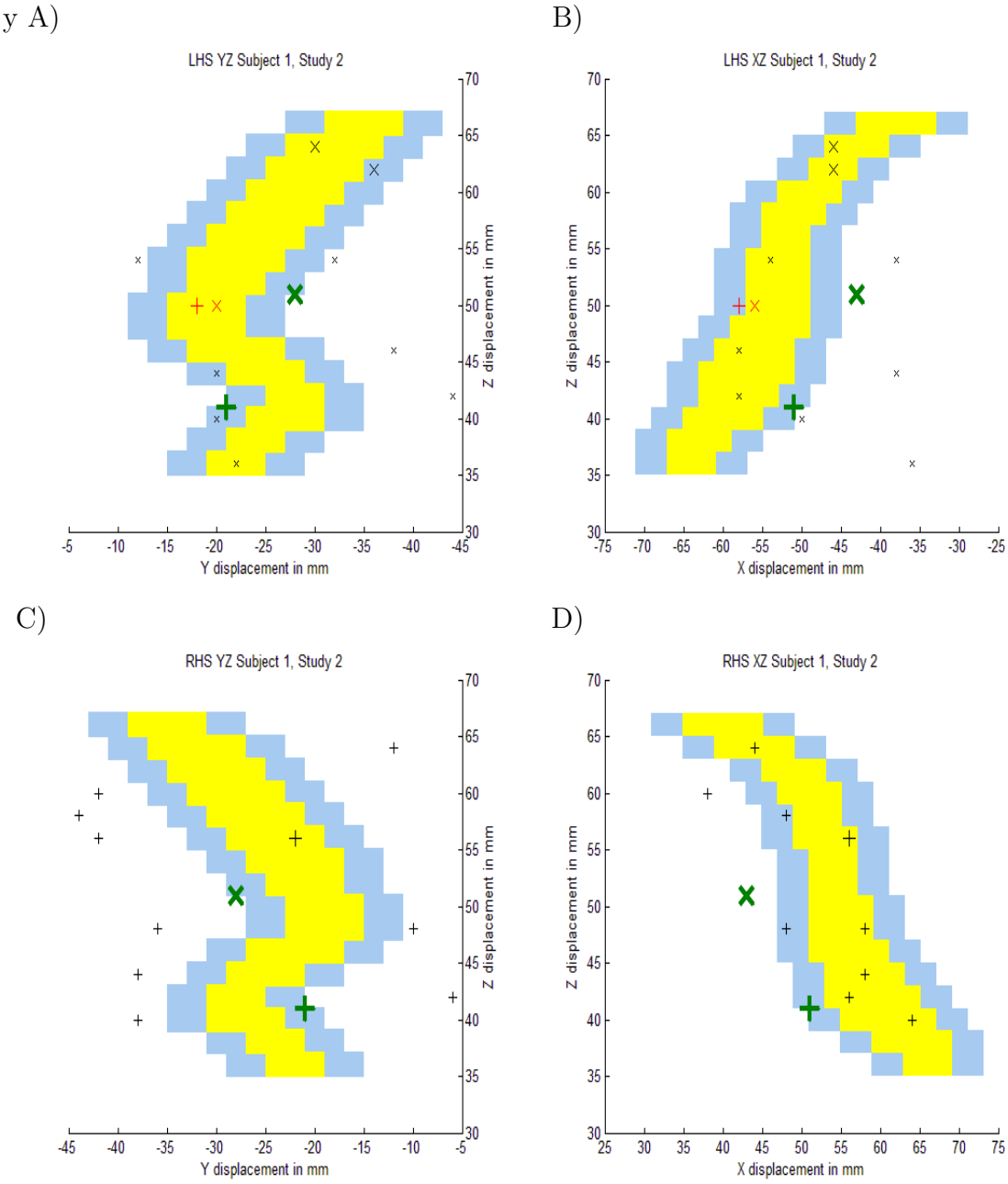

Figure 42: Brodmann area 1 (yellow) with a 4 mm error margin in x and y (blue), and SI activations for subject 2, study 2, overlaid. The mean location of the SI activation for each digit was determined from other studies (Table 1) and are shown by the large green markers. An uncorrected p value threshold of ≤ 0.001 was applied (T-score ≥ 3.11). The activations which fall within the area bounded by blue in x, y and z are denoted by a larger marker. Those which also have a T-score ≥ 4 are coloured red. All data plotted in MNI coordinates. D1 activation = '+', D5 activation = 'X'.

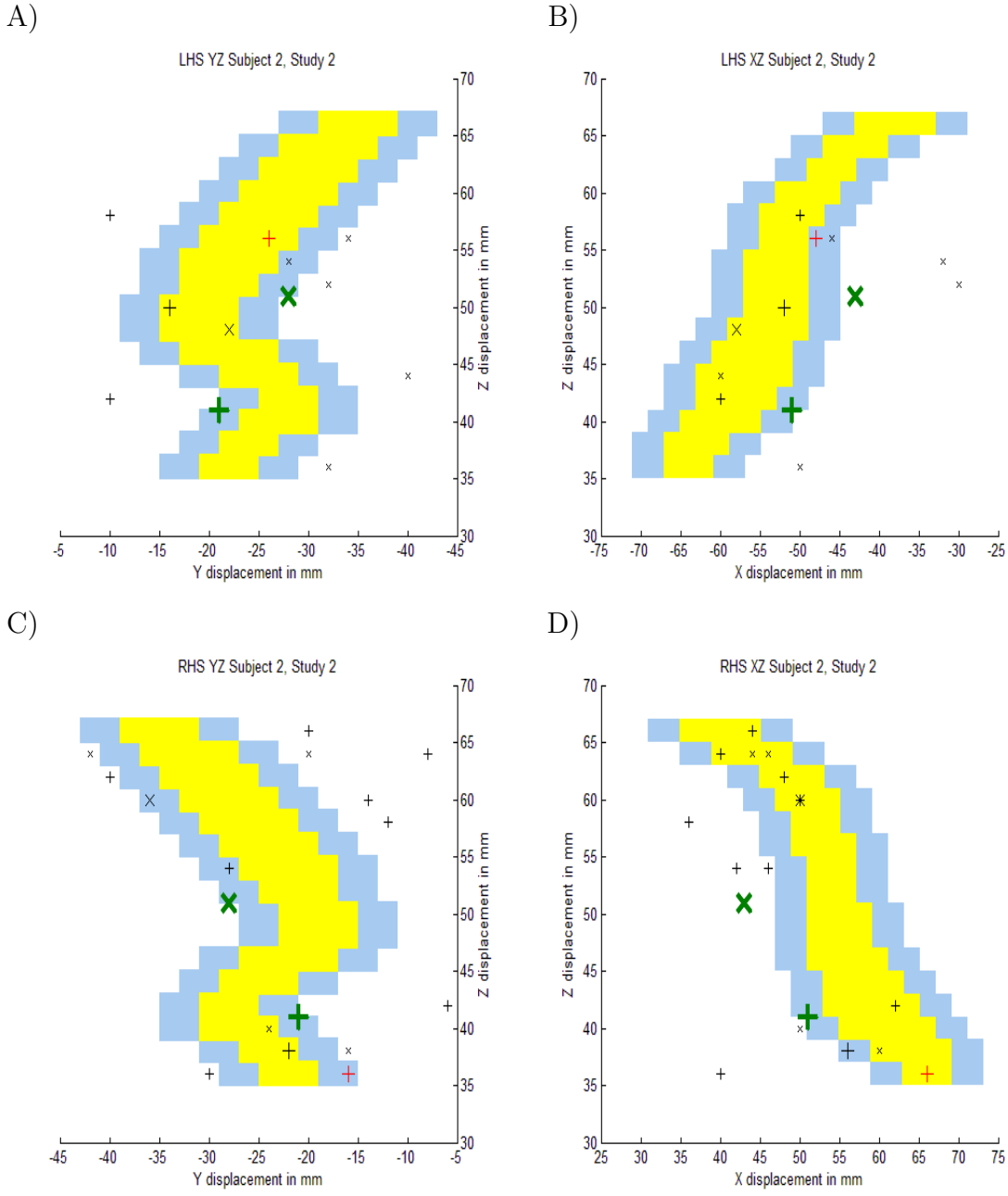

Figure 43: Brodmann area 1 (yellow) with a 4 mm error margin in x and y (blue), and SI activations for subject 3, study 2, overlaid. The mean location of the SI activation for each digit was determined from other studies (Table 1) and are shown by the large green markers. An uncorrected p value threshold of ≤ 0.001 was applied (T-score ≥ 3.11). The activations which fall within the area bounded by blue in x, y and z are denoted by a larger marker. Those which also have a T-score ≥ 4 are coloured red. All data plotted in MNI coordinates. D1 activation = '+', D5 activation = 'X'.

A)

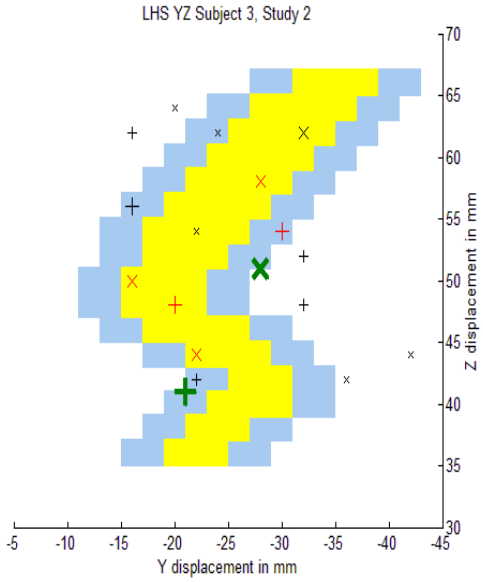

B)

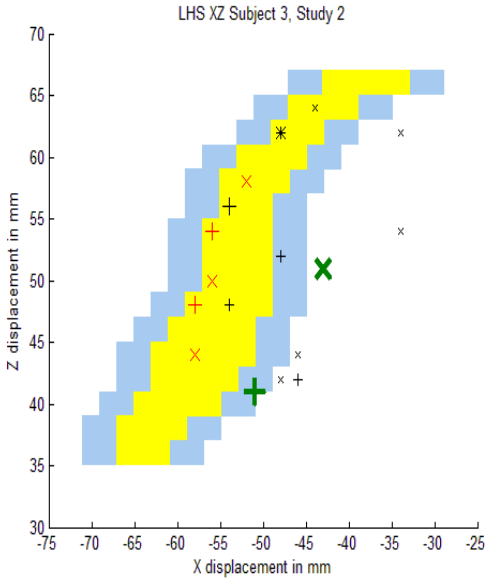

C)

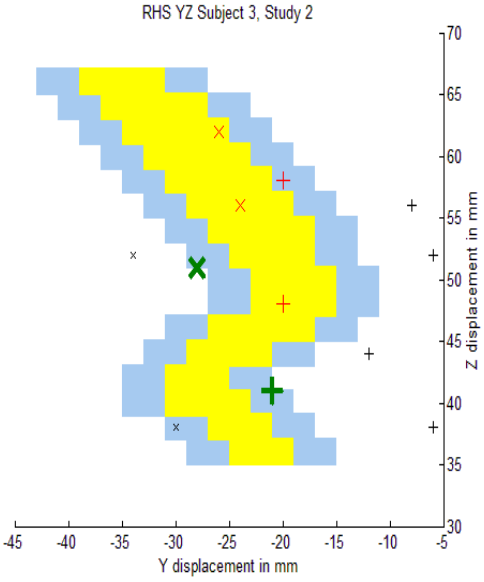

D)

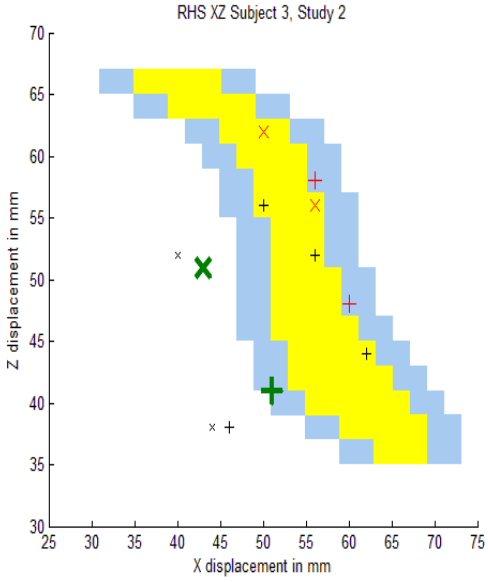

Figure 44: Brodmann area 1 (yellow) with a 4 mm error margin in x and y (blue), and SI activations for subject 4, study 2, overlaid. The mean location of the SI activation for each digit was determined from other studies (Table 1) and are shown by the large green markers. An uncorrected p value threshold of ≤ 0.001 was applied (T-score ≥ 3.11). The activations which fall within the area bounded by blue in x, y and z are denoted by a larger marker. Those which also have a T-score ≥ 4 are coloured red. All data plotted in MNI coordinates. D1 activation = '+', D5 activation = 'X'.

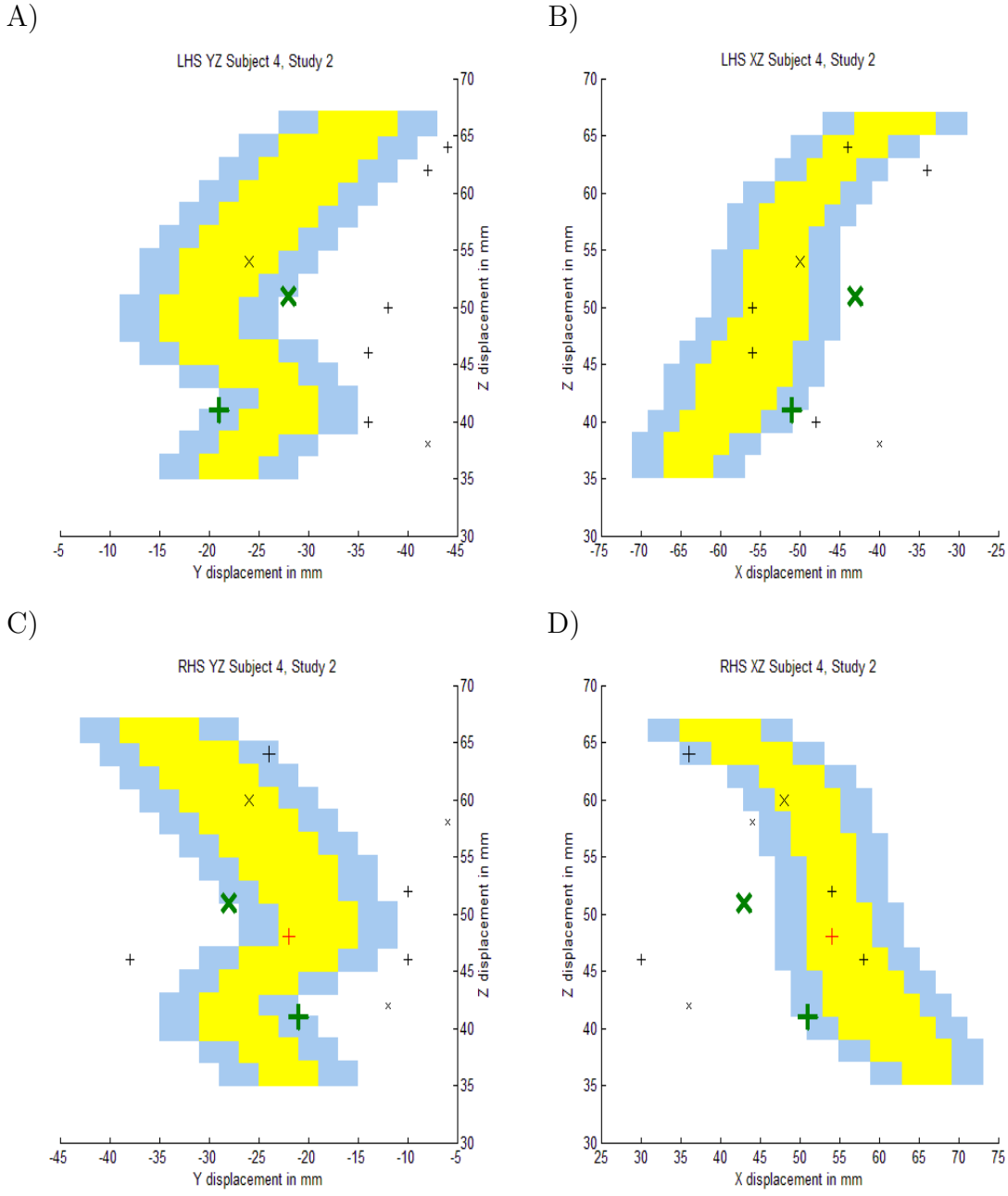

Figure 45: Brodmann area 1 (yellow) with a 4 mm error margin in x and y (blue), and SI activations for subject 5, study 2, overlaid. The mean location of the SI activation for each digit was determined from other studies (Table 1) and are shown by the large green markers. An uncorrected p value threshold of ≤ 0.001 was applied (T-score ≥ 3.11). The activations which fall within the area bounded by blue in x, y and z are denoted by a larger marker. Those which also have a T-score ≥ 4 are coloured red. All data plotted in MNI coordinates. D1 activation = '+', D5 activation = 'X'.

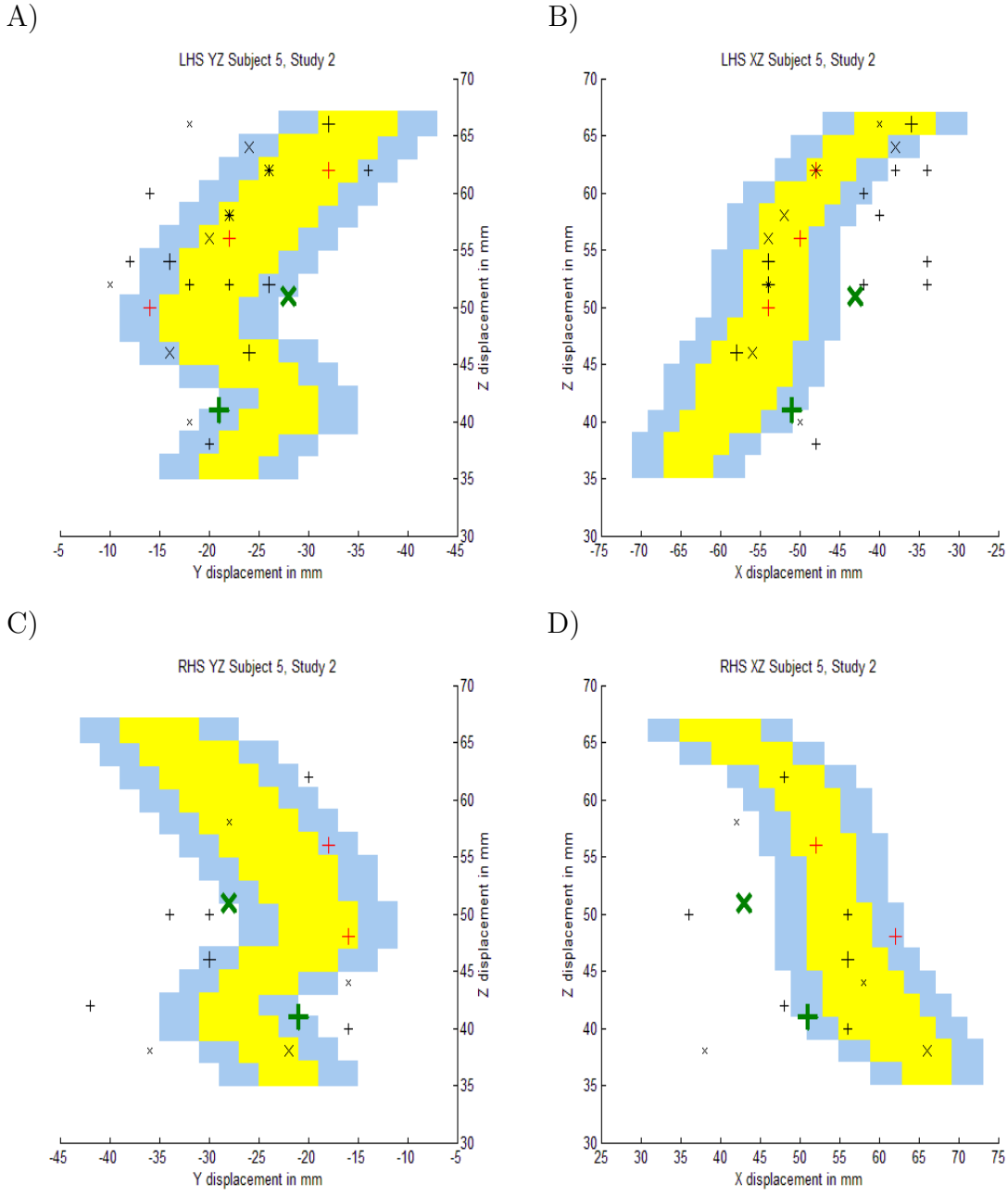

Figure 46: Brodmann area 1 (yellow) with a 4 mm error margin in x and y (blue), and SI activations for subject 6, study 2, overlaid. The mean location of the SI activation for each digit was determined from other studies (Table 1) and are shown by the large green markers. An uncorrected p value threshold of ≤ 0.001 was applied (T-score ≥ 3.11). The activations which fall within the area bounded by blue in x, y and z are denoted by a larger marker. Those which also have a T-score ≥ 4 are coloured red. All data plotted in MNI coordinates. D1 activation = '+', D5 activation = 'X'.

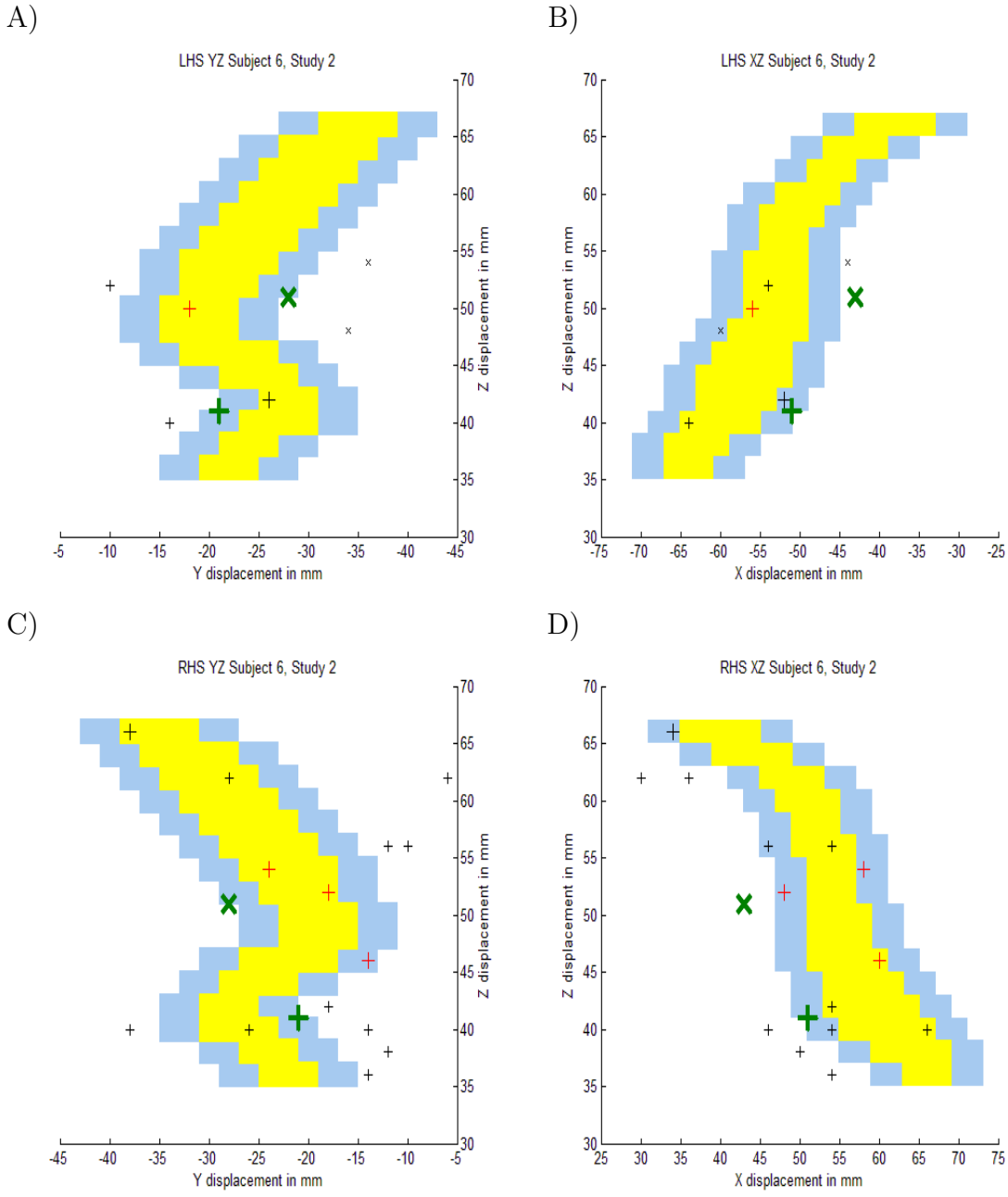

Figure 47: Brodmann area 1 (yellow) with a 4 mm error margin in x and y (blue), and SI activations for subject 7, study 2, overlaid. The mean location of the SI activation for each digit was determined from other studies (Table 1) and are shown by the large green markers. An uncorrected p value threshold of ≤ 0.001 was applied (T-score ≥ 3.11). The activations which fall within the area bounded by blue in x, y and z are denoted by a larger marker. Those which also have a T-score ≥ 4 are coloured red. All data plotted in MNI coordinates. D1 activation = '+', D5 activation = 'X'.

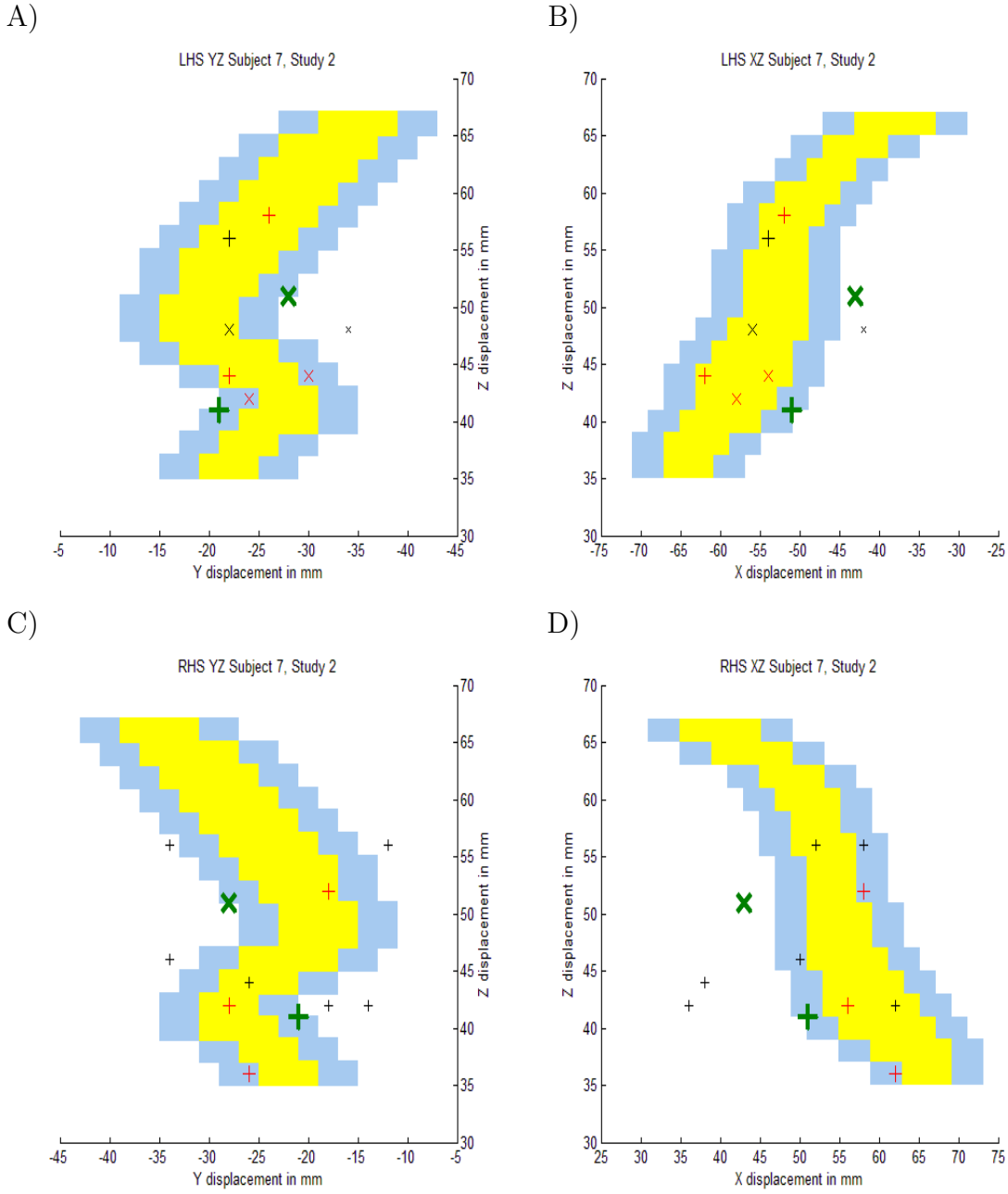

Figure 48: The results from the second level analysis of study 2, using data from subjects 1 to 7, for each digit on the template brain. Threshold uncorrected p value ≤ 0.001.

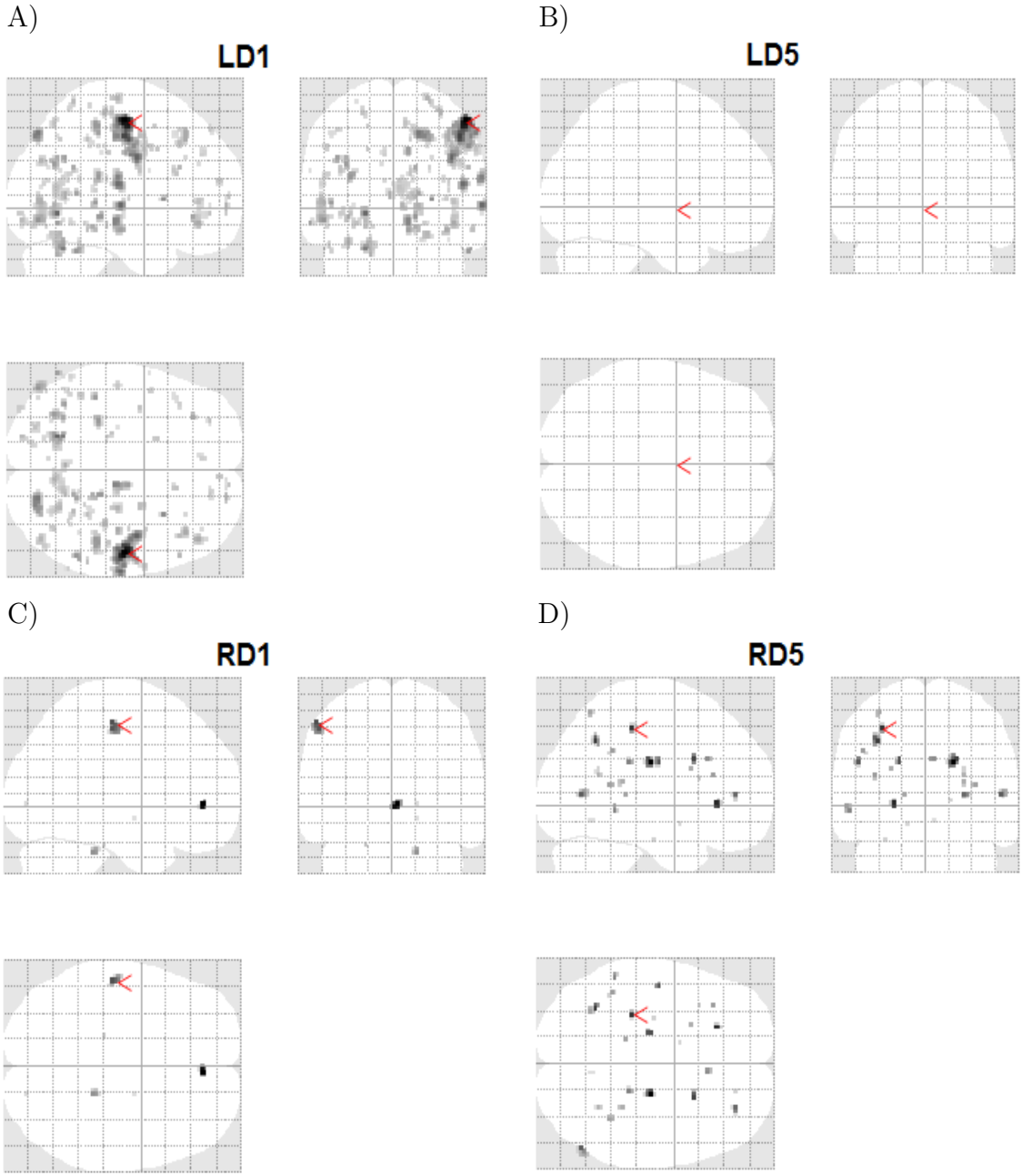

Figure 49: The SI activations from the group analysis for study 2 overlaid on BA1 (yellow), 4 mm error margin in x and y (blue), plotted in MNI coordinates. D1 = '+' and D5 = 'X'. The mean location of the SI activation for each digit was determined from other studies (Table 1) and are shown by the large green markers. An uncorrected p value threshold of ≤ 0.001 was applied (T-score ≥ 3.11). The activations which fall within the area bounded by blue in x, y and z are denoted by larger markers and those which also have a T-score ≥ 4 are coloured red.

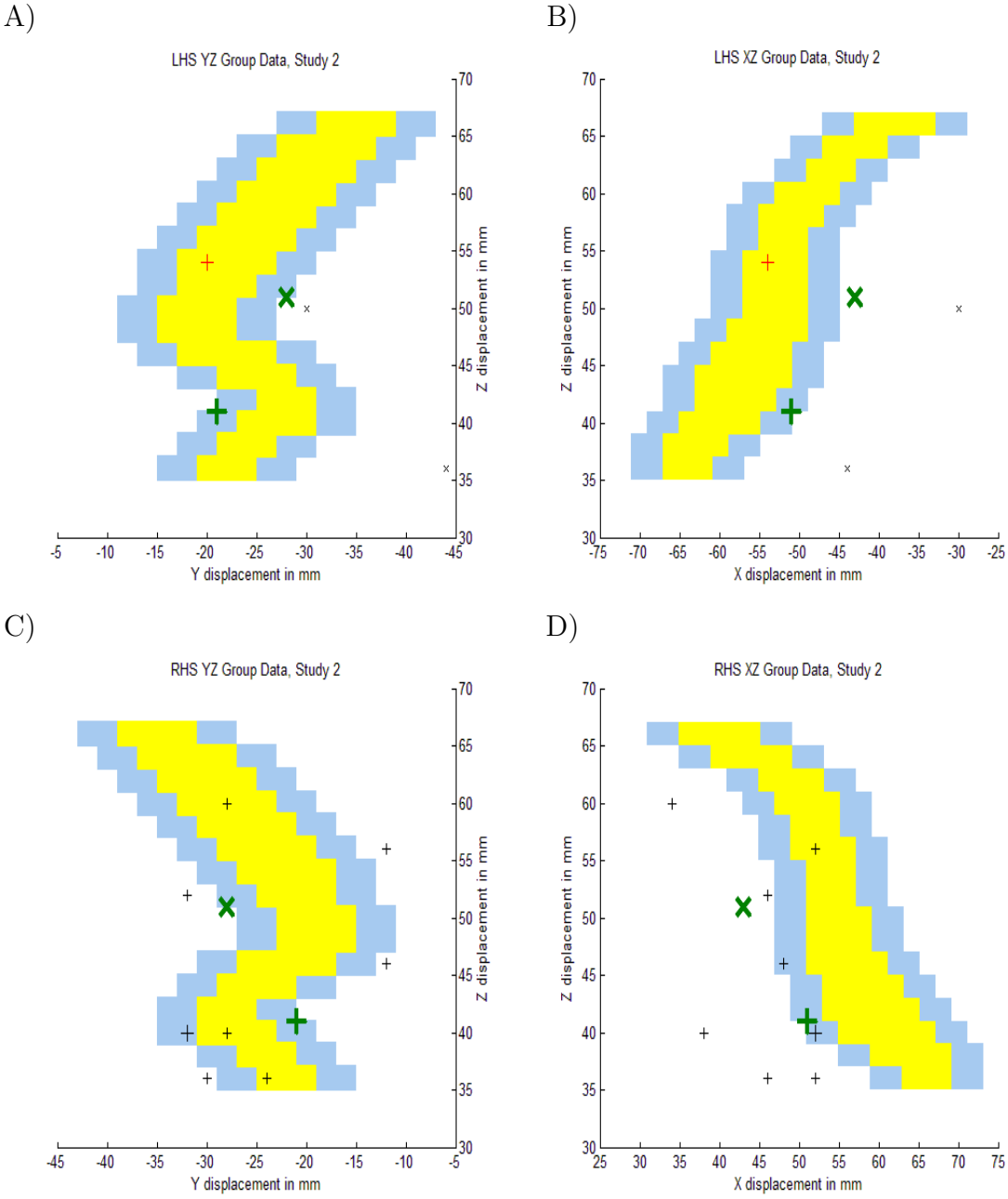

Figure 50: The centre of mass of all activations within BA1 for each subject in study 2, plotted over BA1. D1 data is indicated by '+' and D5 data by 'X'. Lines show each subject's data. All data plotted in MNI coordinates.

A)

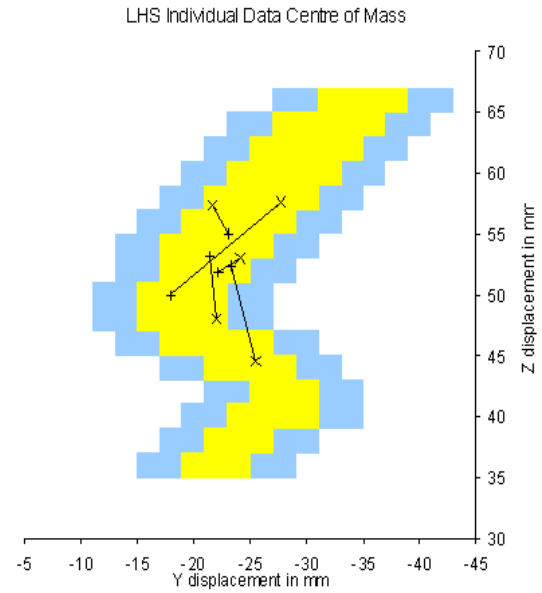

B)

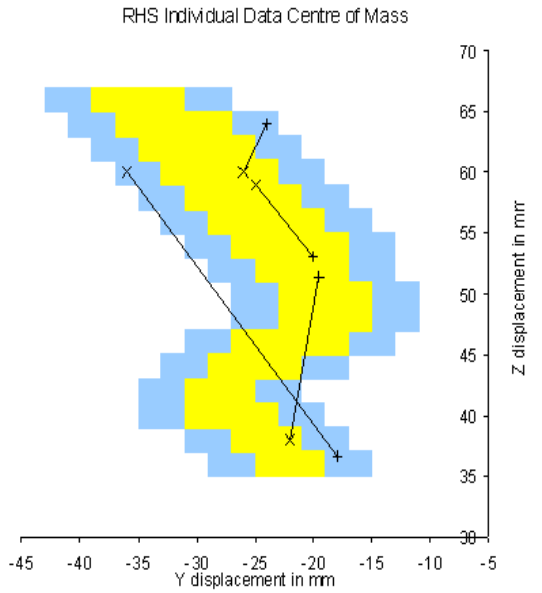

8.4 Study 3

Study 3 was carried out to improve the T-scores of the contralateral SI activations. Two sessions were performed, one session involved stimulation to RD1 and the other session involved stimulation to RD5. The scanning time per digit was extended from 12 minutes in study 2 to 20 minutes in study 3. Due to the extra scanning time the experiment was not performed for LD1 or LD5. Also, the 40 Hz drive voltage was increased from ± 36 V to ± 52 V. To evaluate the effect of increasing the stimulus amplitude a model was created to assess the first 12 minutes (first 240 scans) of each session. Another model was also created to assess the full 20 minutes (400 scans) of data to investigate the effect of extending the scanning time. Eight right handed subjects participated in the study.

8.4.1 Individual Analysis

12 minute session

At an uncorrected p value threshold of ≤ 0.001, the increased stimulus amplitude produced detectable contralateral SI activity in all subjects for stimulation to RD1 and RD5, compared to a detection rate of 89 % in study 2. The contralateral SI T-score for the most activated voxel for each digit is shown in Table 17, the values are ≥ 4 for all digits. The average T-score value has improved significantly from 4.57 in study 2 to 6.69; this is also higher than in study 1 (5.84). The maximum T-score value is also higher, 12.71 versus 8.4. 75 % of the activations in Table 17 would survive a corrected p value threshold of ≤ 0.05 (T-score ≥ 5.1); recall that only 59 % of the digit activations in Table 11 (study 1) would survive this level and as little as 22 % in Table 15 (study 2). The higher rate of detection and increased statistical significance in the contralateral SI cortex is reflected in the T-scores for the ipsilateral SI activity and also the contralateral and ipsilateral SII activity, also shown in Table 17.

The activations for a representative subject (subject 1) are shown on the template brain in panels A and B of Figure 51. A corrected p value threshold of ≤ 0.05

Table 17: The highest T-scores for contralateral and ipsilateral SI and SII activations for subjects 1 - 8 in study 3 after 12 minutes of data collection. The location of the activations is indicated in panels A and B of Figures 52 to 59. Contra = contralateral, Ipsi = ipsilateral, - = activity not detected above uncorrected p value threshold of ≤ 0.001. T-scores ≥ 5.1 (a corrected p value threshold of ≤ 0.05) are highlighted in bold. The mean and standard deviation for each digit for the group are given at the bottom of the table. The two columns on the far right show the ratio of contralateral SI/ipsilateral SI activity and contralateral SII/ipsilateral SII activity.

Subject	Digit stim.	Contra SI	Ipsi SI	Contra SII	Ipsi SII	Contra V Ipsi SI	Contra V Ipsi SI
1	RD1	**12.71**	**6.45**	**11.39**	**11.76**	1.97	0.97
	RD5	**8.15**	4.08	**8.92**	**7.60**	2.00	1.17
2	RD1	**9.63**	**7.79**	**8.82**	**7.96**	1.24	1.11
	RD5	**8.53**	**6.65**	**8.67**	**6.73**	1.28	1.29
3	RD1	**6.86**	**5.27**	**8.42**	**5.92**	1.30	1.42
	RD5	**5.95**	**13.39**	**12.19**	**7.64**	0.44	1.44
4	RD1	**8.51**	4.59	4.89	**5.36**	1.85	0.91
	RD5	**7.20**	4.21	**6.37**	4.85	1.71	1.31
5	RD1	**9.91**	**6.39**	**10.86**	**9.67**	1.55	1.12
	RD5	**5.17**	3.91	**5.98**	4.79	1.32	1.25
6	RD1	**6.73**	**5.20**	**5.23**	3.69	1.29	1.42
	RD5	**5.84**	**6.31**	**6.74**	**5.44**	0.93	1.24
7	RD1	**5.36**	-	**6.73**	3.19	-	2.11
	RD5	4.63	**5.80**	**5.94**	**5.43**	0.80	1.09
8	RD1	4.02	4.81	4.46	4.13	0.84	1.08
	RD5	**5.63**	3.53	4.14	4.18	1.59	0.99
Mean & standard deviation	RD1	7.97	5.79	7.60	6.46		
		2.79	1.14	2.69	3.07		
	RD5	6.39	5.99	7.37	5.83		
		1.41	3.22	2.48	1.33		

has been applied to the data. The red arrow points to the SI activity which can be seen as a dense black region. Bilateral SII activity is also present. The location of the SI activations within the somatosensory area are shown in panels A and B of Figures 52 to 59 for subjects 1 to 8. The number of foci varied between 1 - 22 clusters and demonstrated no systematic distribution for either digit. Some D1 and D5 activations are common to both digits in a few subjects whilst the other activations appear/disappear. This is consistent with the previous two studies.

The Euclidean digit separations in the brain were calculated for each subject using the centre of mass of all the SI clusters detected (BA1, 2, 3 and vicinity). These are shown in Table 18. They range from 2.2 to 12.4 mm with only two of the separations being within the expected range (10 to 18 mm) the rest being smaller. The Euclidean separations were also calculated using the activations that fell within the BA1 region marked on the graphs. Contrary to the previous studies, all digits contained an activation within this area allowing all the separations to be recalculated and compared. The resulting average values are also shown in Table 18 and are slightly higher than the average values from the larger set of SI activations. All the separations are consistent with the values obtained in studies 1 and 2.

The group analysis reveals no SI activations for stimulation to RD1 and only one SI activation for stimulation to RD5 at (-34 -40 38). These coordinates are outside the area defined as BA1 in the graphs but similar to the coordinates for stimulation to RD5 from the group analysis in study 2.

For each subject, the centre of mass coordinate from the BA1 activations for RD1 and RD5 are shown in Figure 60. The RD1 and RD5 subject pairs are linked by a black line showing the movement of the centre of mass between the two digits. As can be seen, the locations of RD1 and RD5 (shown by '+' and 'X' respectively) are distributed with no consistent pattern through the Brodmann area. The movement between the centre of mass for the two digits is also random in the y and z axis.

Table 18: Euclidean separations for the left and right hands for subjects 1 to 8 in study 3 at 12 minutes and 20 minutes of data collection. The centre of mass was calculated using the coordinates (estimated error ± 2 mm) that fell within specific Brodmann areas and were weighted according to their T-score.

Subject	BA1,2,3 and vicinity RD1-D5 (12 mins) mm	BA1,2,3 and vicinity RD1-D5 (20 mins) mm	BA1 RD1-D5 (12 mins) mm	BA1 RD1-D5 (20 mins) mm
1	2.2	6.2	6.4	4.1
2	6.4	6.5	2.2	1.2
3	12.4	11.2	15.4	15.0
4	3.7	9.1	10.1	10.6
5	9.4	8.0	8.0	7.1
6	6.8	9.2	5.8	7.7
7	12.3	3.0	4.0	22.8
8	5.2	2.6	6.1	5.8
Average	7.3	7.0	8.1	10.3

20 minute session

Assessing the data using the 400 volume scans from each session reveals that, at an uncorrected p value threshold of ≤ 0.001, contralateral SI activity was detected in all subjects for stimulation to RD1 and RD5. As must be expected the most significant difference to the 12 minute data set is the increase in the T-scores of the digit activations, listed in Table 19. The maximum T-score value has increased from 12.71 to 16.69 and the average has also risen from 6.69 to 7.14. However, in one quarter of the subjects the average T-score decreased with the extra 8 minutes of data acquisition.

For comparison with the 12 minute data in Figure 51, panels A and B, the brain activations of the same representative subject (subject 1) are shown on the template brain in panels C and D of Figure 51. The same corrected p value threshold of ≤ 0.05 has been applied. The two images appear to be very similar for this subject, however, when the SI activations (indicated by the red arrow) are plotted on the BA1 graphs in Figure 52 (panels A and B: 12 minutes of data,

Table 19: The highest T-scores for contralateral and ipsilateral SI and SII activations for subjects 1 - 8 in study 3 after 20 minutes of data collection. The location of the activations is indicated in panels C and D of Figures 52 to 59. An uncorrected p value threshold of ≤ 0.001 was applied. Contra = contralateral, Ipsi = ipsilateral. T-scores ≥ 5.1 (a corrected p value threshold of ≤ 0.05) are highlighted in bold. The mean and standard deviation for each digit for the group are given at the bottom of the table. The two columns on the far right show the ratio of contralateral SI/ipsilateral SI activity and contralateral SII/ipsilateral SII activity.

Subject	Digit stim.	Contra SI	Ipsi SI	Contra SII	Ipsi SII	Contra V Ipsi SI	Contra V Ipsi SI
1	RD1	**16.69**	**6.07**	**13.29**	**13.83**	2.75	0.96
	RD5	**9.81**	**5.48**	**11.57**	**9.45**	1.79	1.22
2	RD1	**11.90**	**7.41**	**9.56**	**8.12**	1.61	1.18
	RD5	**10.16**	**6.97**	**9.81**	**8.39**	1.46	1.17
3	RD1	**6.11**	4.85	**8.50**	**5.93**	1.26	1.43
	RD5	**6.87**	**13.76**	**10.52**	**7.79**	0.50	1.35
4	RD1	**9.99**	**5.65**	**5.55**	**5.66**	1.77	0.98
	RD5	**7.74**	4.10	**6.86**	4.31	1.89	1.59
5	RD1	**11.76**	**6.63**	**12.25**	**11.30**	1.77	1.09
	RD5	4.35	4.72	**6.80**	5.02	0.92	1.35
6	RD1	**9.09**	4.39	**5.95**	4.30	2.07	1.38
	RD5	**6.18**	**5.29**	**7.22**	**5.60**	1.17	1.29
7	RD1	4.49	3.20	**6.45**	3.95	1.40	1.63
	RD5	**5.26**	4.93	**6.90**	4.43	1.07	1.56
8	RD1	4.34	4.26	3.74	4.71	1.02	0.79
	RD5	**5.41**	3.33	4.18	3.76	1.62	1.11
Mean	RD1	9.30	5.31	8.17	7.23		
&		4.24	1.39	3.37	3.60		
standard	RD5	6.97	6.07	7.98	6.09		
deviation		2.13	3.28	2.44	2.15		

panels C and D: 20 minutes of data) it can be seen that they are not exactly the same. For the other subjects, the SI activations at 20 minutes are shown in panels C and D of Figures 53 to 59. Again multiple foci were detected and the activations demonstrated no consistent pattern in location for either digit. It can be seen that there are also some differences between the 12 minute and 20 minute data.

The Euclidean separations were recalculated using the 20 minute data and are shown in Table 18. Due to the differences in the location of the SI activations the new values for each subject are different to those calculated with the 12 minutes of data but they remain within a similar range.

When the group analysis was carried out it revealed similar results as for the 12 minute data set. No SI activations for stimulation to RD1 were present and only one activation for stimulation to RD5 was detected at (-32 -40 40). Although no further SI activations were gained at the group level from the extra scanning time, the T-score of the one SI activation did increase from 4.84 to 8.8.

The centre of mass of the BA1 activations for RD1 and RD5 for each subject are displayed in panel B of Figure 60. The RD1 and RD5 subject pairs are linked by a black line. The coordinates of the centre of mass for both digits are different to the coordinates calculated for the 12 minute data set but are distributed in a similar inconsistent fashion. The directions of the centre of mass movements from RD1 to RD5 are also inconsistent.

8.4.2 Summary of Study 3

These results are discussed in the following chapter. As expected the increased drive voltage and scan time in study 3 produced stronger activations. In an attempt to establish the optimum timing pattern for stimulation, study 4 involved continuous stimulation, in contrast to the intermittent (1 Hz) stimulation in study 3.

Figure 51: The brain activations for a representative subject (subject 1), study 3, for the right hand for D1 and D5 after 12 (panels A and B) and 20 (panels C and D) minutes of data collection, overlaid on the template brain. The SI area is indicated by the red arrow. A corrected p value threshold of ≤ 0.05 was applied to all data.

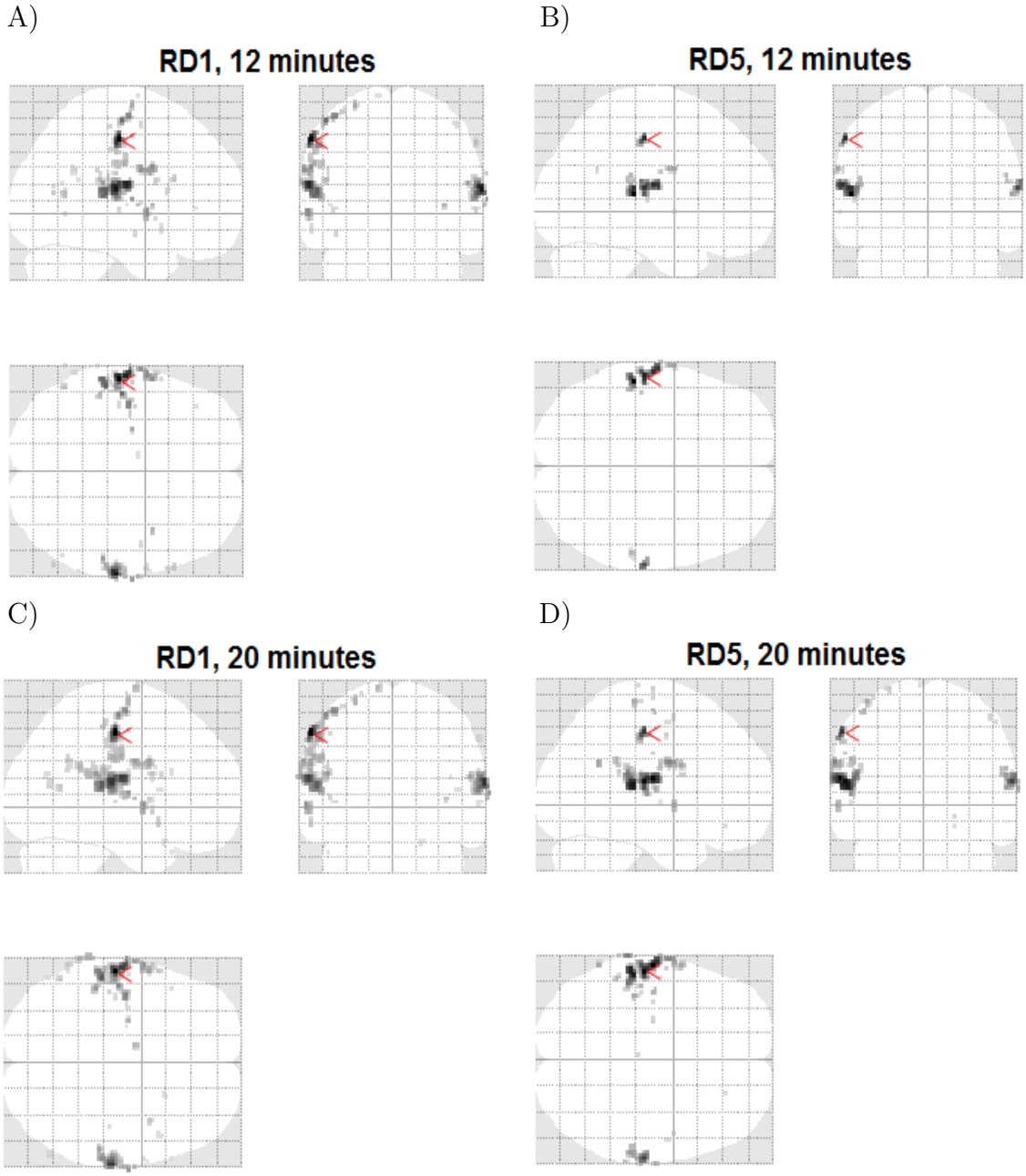

Figure 52: Brodmann area 1 (yellow) with a 4 mm error margin in x and y (blue). The RD1 and RD5 SI activations for subject 1, study 3 after 12 minutes of data acquisition are overlaid in panels A and B. The full data set (20 minutes of data acquisition) is shown in panels C and D. An uncorrected p value threshold of ≤ 0.001 was applied (T-score ≥ 3.11). The activations which fall within the area bounded by blue in x, y and z are denoted by a larger marker. Those which also have a T-score ≥ 4 are coloured red. The mean location of the SI activation for each digit was determined from other studies (Table 1) and are shown by the large green markers. All data plotted in MNI coordinates. D1 activation = '+', D5 activation = 'X'.

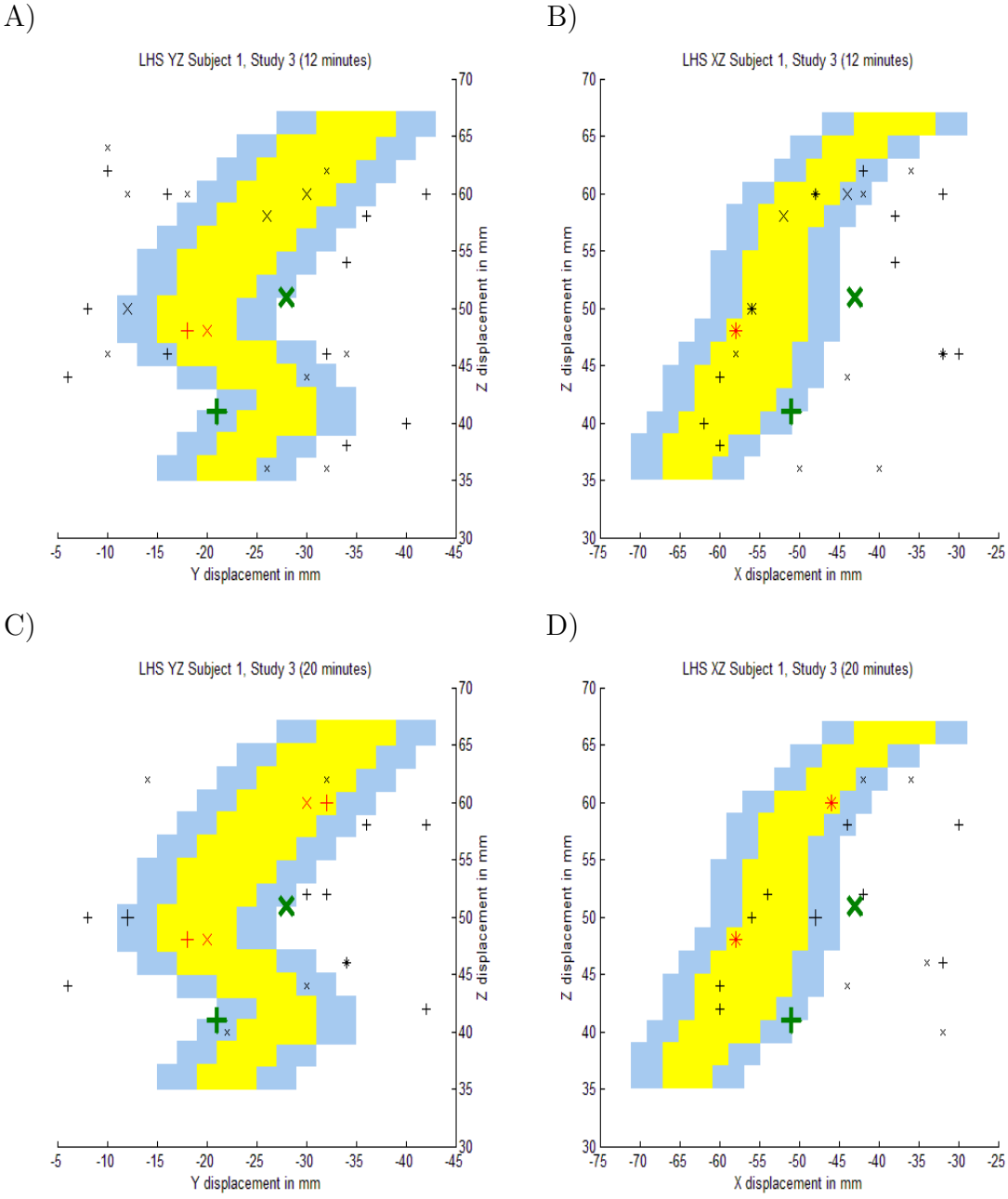

Figure 53: Brodmann area 1 (yellow) with a 4 mm error margin in x and y (blue). The RD1 and RD5 SI activations for subject 2, study 3 after 12 minutes of data acquisition are overlaid in panels A and B. The full data set (20 minutes of data acquisition) is shown in panels C and D. An uncorrected p value threshold of ≤ 0.001 was applied (T-score ≥ 3.11). The activations which fall within the area bounded by blue in x, y and z are denoted by a larger marker. Those which also have a T-score ≥ 4 are coloured red. The mean location of the SI activation for each digit was determined from other studies (Table 1) and are shown by the large green markers. All data plotted in MNI coordinates. D1 activation = '+', D5 activation = 'X'.

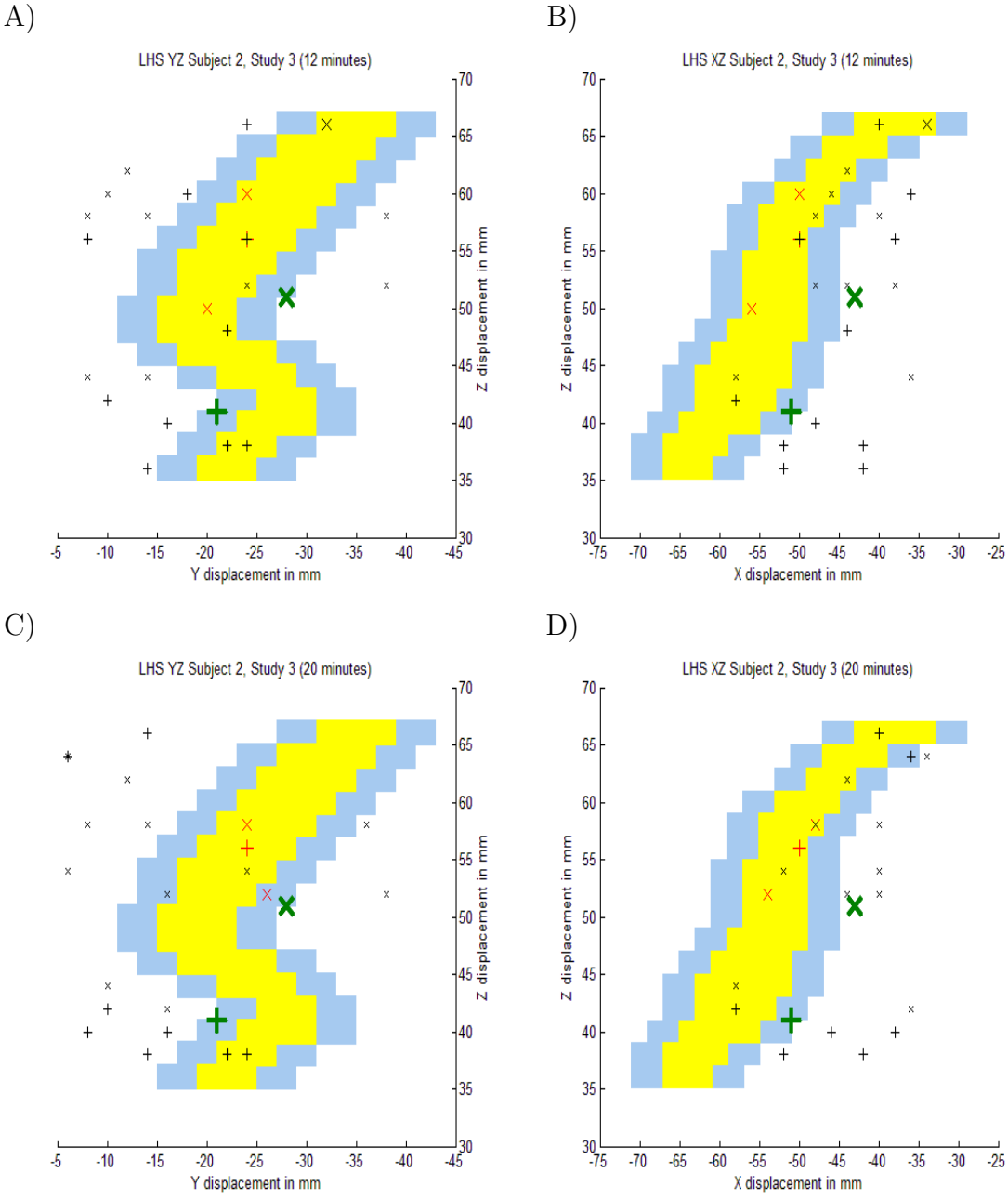

Figure 54: Brodmann area 1 (yellow) with a 4 mm error margin in x and y (blue). The RD1 and RD5 SI activations for subject 3, study 3 after 12 minutes of data acquisition are overlaid in panels A and B. The full data set (20 minutes of data acquisition) is shown in panels C and D. An uncorrected p value threshold of ≤ 0.001 was applied (T-score ≥ 3.11). The activations which fall within the area bounded by blue in x, y and z are denoted by a larger marker. Those which also have a T-score ≥ 4 are coloured red. The mean location of the SI activation for each digit was determined from other studies (Table 1) and are shown by the large green markers. All data plotted in MNI coordinates. D1 activation = '+', D5 activation = 'X'.

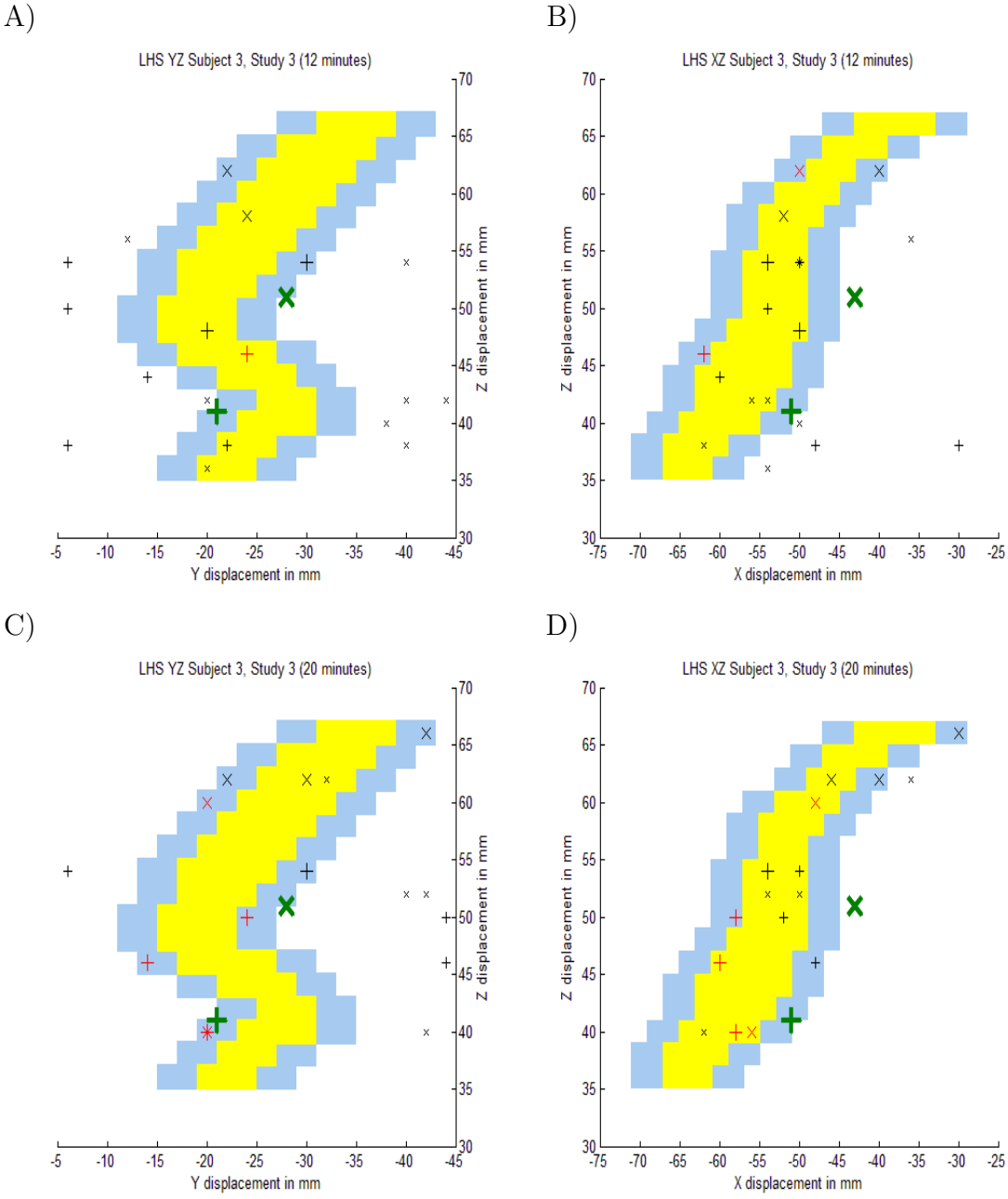

Figure 55: Brodmann area 1 (yellow) with a 4 mm error margin in x and y (blue). The RD1 and RD5 SI activations for subject 4, study 3 after 12 minutes of data acquisition are overlaid in panels A and B. The full data set (20 minutes of data acquisition) is shown in panels C and D. An uncorrected p value threshold of ≤ 0.001 was applied (T-score ≥ 3.11). The activations which fall within the area bounded by blue in x, y and z are denoted by a larger marker. Those which also have a T-score ≥ 4 are coloured red. The mean location of the SI activation for each digit was determined from other studies (Table 1) and are shown by the large green markers. All data plotted in MNI coordinates. D1 activation = '+', D5 activation = 'X'.

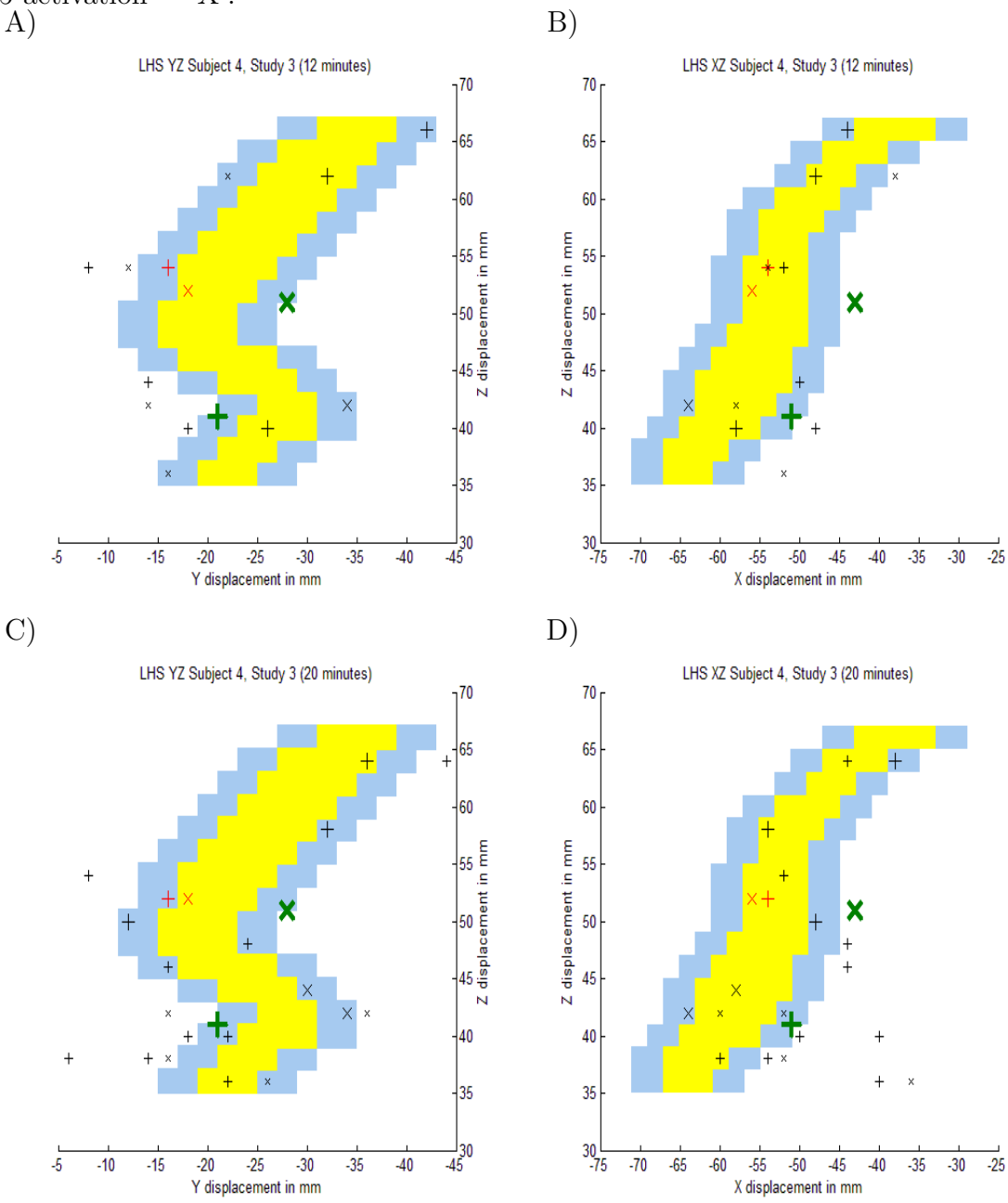

Figure 56: Brodmann area 1 (yellow) with a 4 mm error margin in x and y (blue). The RD1 and RD5 SI activations for subject 5, study 3 after 12 minutes of data acquisition are overlaid in panels A and B. The full data set (20 minutes of data acquisition) is shown in panels C and D. An uncorrected p value threshold of ≤ 0.001 was applied (T-score ≥ 3.11). The activations which fall within the area bounded by blue in x, y and z are denoted by a larger marker. Those which also have a T-score ≥ 4 are coloured red. The mean location of the SI activation for each digit was determined from other studies (Table 1) and are shown by the large green markers. All data plotted in MNI coordinates. D1 activation = '+', D5 activation = 'X'.

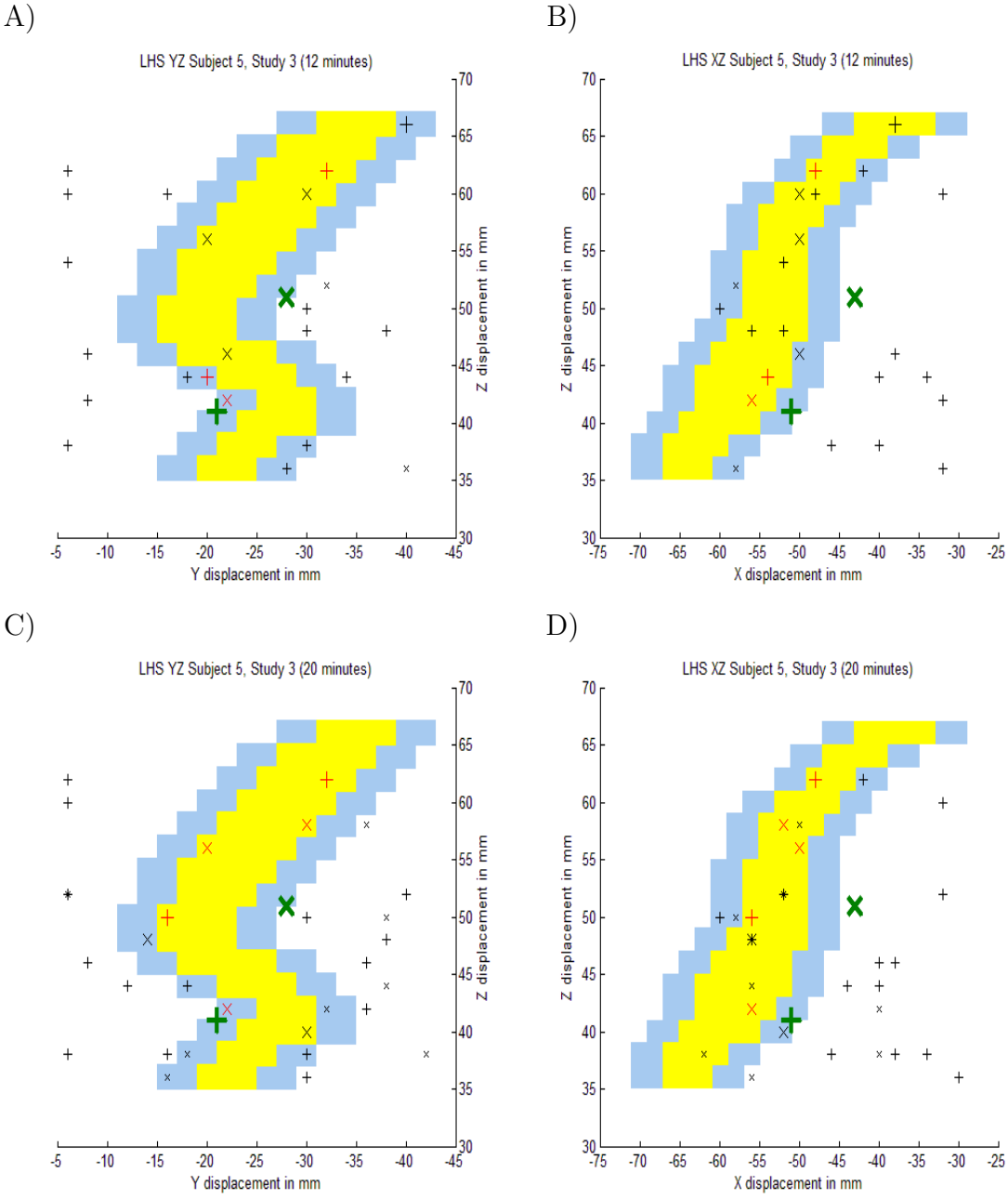

Figure 57: Brodmann area 1 (yellow) with a 4 mm error margin in x and y (blue). The RD1 and RD5 SI activations for subject 6, study 3 after 12 minutes of data acquisition are overlaid in panels A and B. The full data set (20 minutes of data acquisition) is shown in panels C and D. An uncorrected p value threshold of ≤ 0.001 was applied (T-score ≥ 3.11). The activations which fall within the area bounded by blue in x, y and z are denoted by a larger marker. Those which also have a T-score ≥ 4 are coloured red. The mean location of the SI activation for each digit was determined from other studies (Table 1) and are shown by the large green markers. All data plotted in MNI coordinates. D1 activation = '+', D5 activation = 'X'.

A)

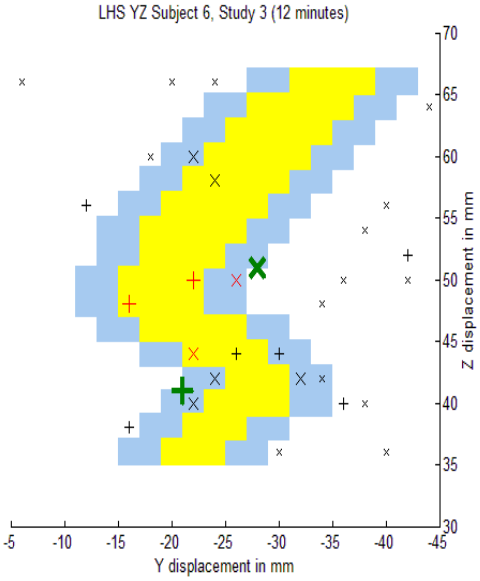

B)

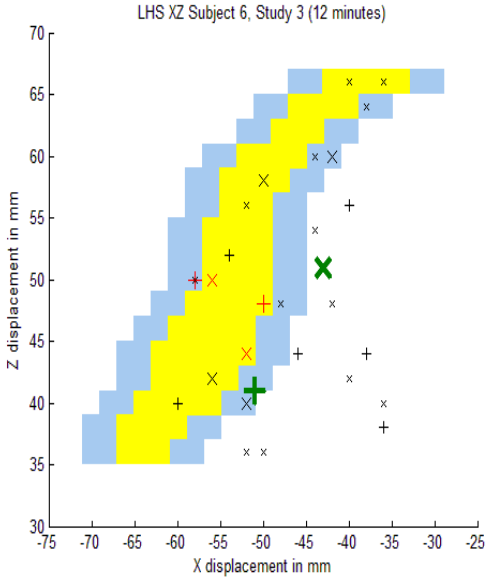

C)

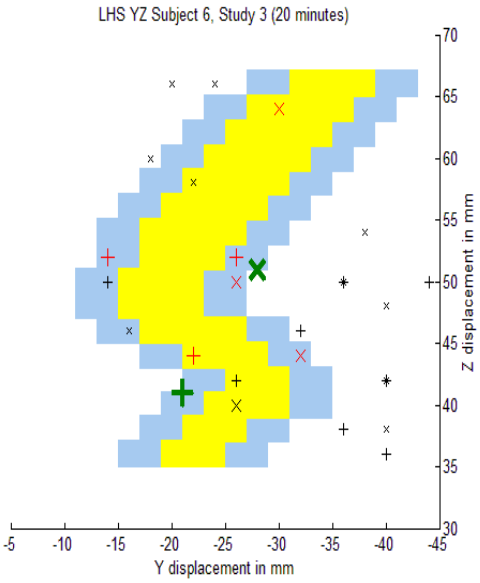

D)

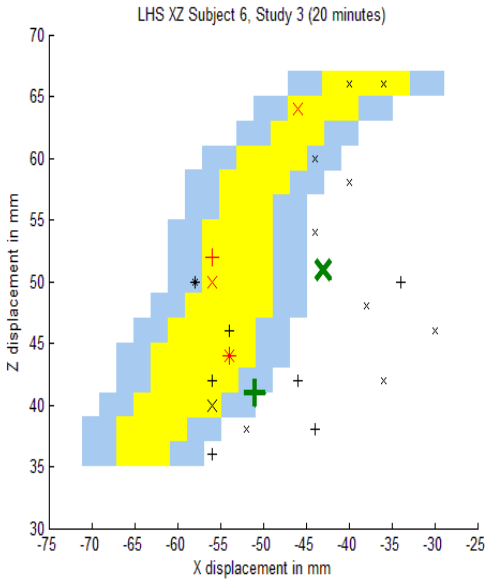

Figure 58: Brodmann area 1 (yellow) with a 4 mm error margin in x and y (blue). The RD1 and RD5 SI activations for subject 7, study 3 after 12 minutes of data acquisition are overlaid in panels A and B. The full data set (20 minutes of data acquisition) is shown in panels C and D. An uncorrected p value threshold of ≤ 0.001 was applied (T-score ≥ 3.11). The activations which fall within the area bounded by blue in x, y and z are denoted by a larger marker. Those which also have a T-score ≥ 4 are coloured red. The mean location of the SI activation for each digit was determined from other studies (Table 1) and are shown by the large green markers. All data plotted in MNI coordinates. D1 activation = '+', D5 activation = 'X'.

A)

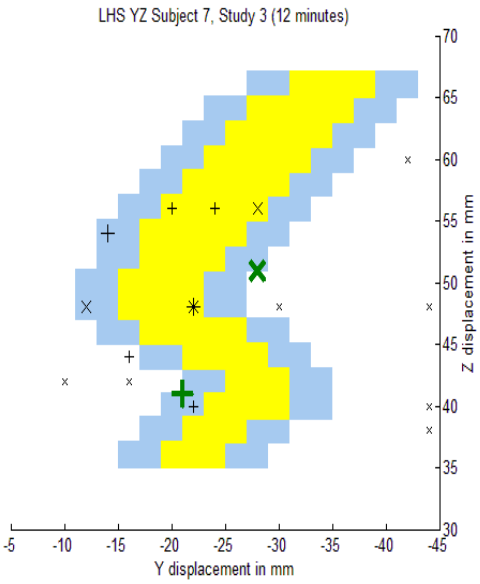

B)

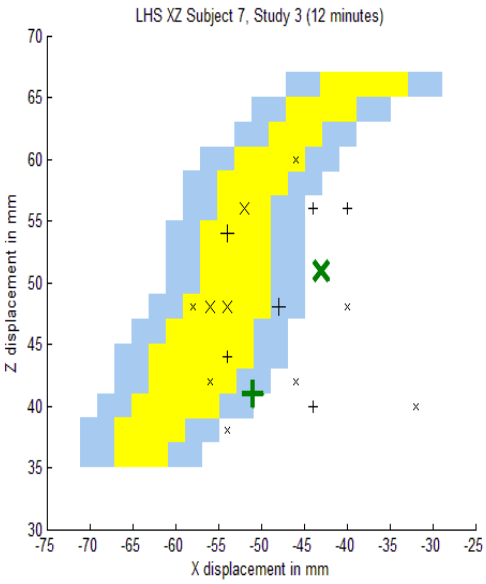

C)

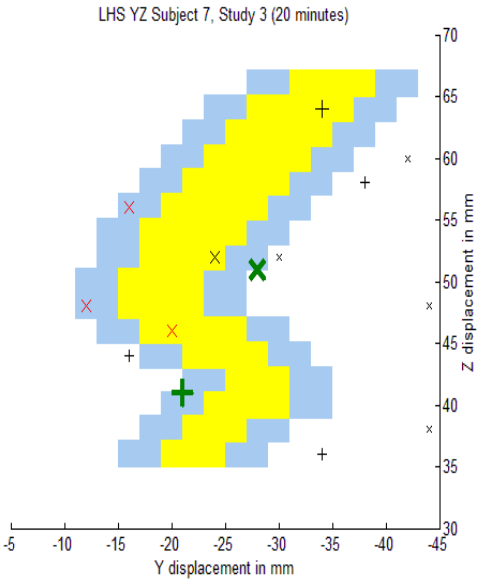

D)

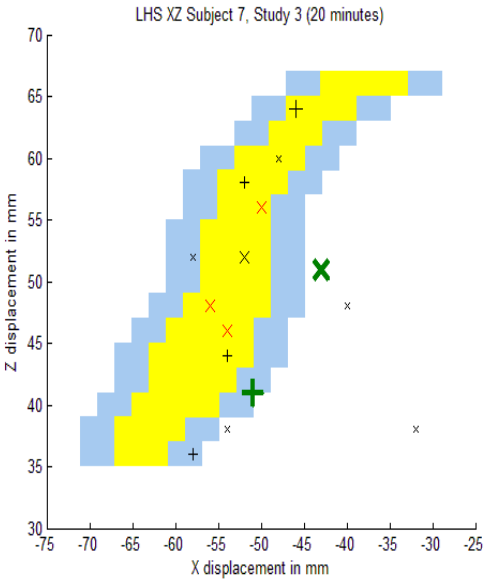

Figure 59: Brodmann area 1 (yellow) with a 4 mm error margin in x and y (blue). The RD1 and RD5 SI activations for subject 8, study 3 after 12 minutes of data acquisition are overlaid in panels A and B. The full data set (20 minutes of data acquisition) is shown in panels C and D. An uncorrected p value threshold of ≤ 0.001 was applied (T-score ≥ 3.11). The activations which fall within the area bounded by blue in x, y and z are denoted by a larger marker. Those which also have a T-score ≥ 4 are coloured red. The mean location of the SI activation for each digit was determined from other studies (Table 1) and are shown by the large green markers. All data plotted in MNI coordinates. D1 activation = '+', D5 activation = 'X'.

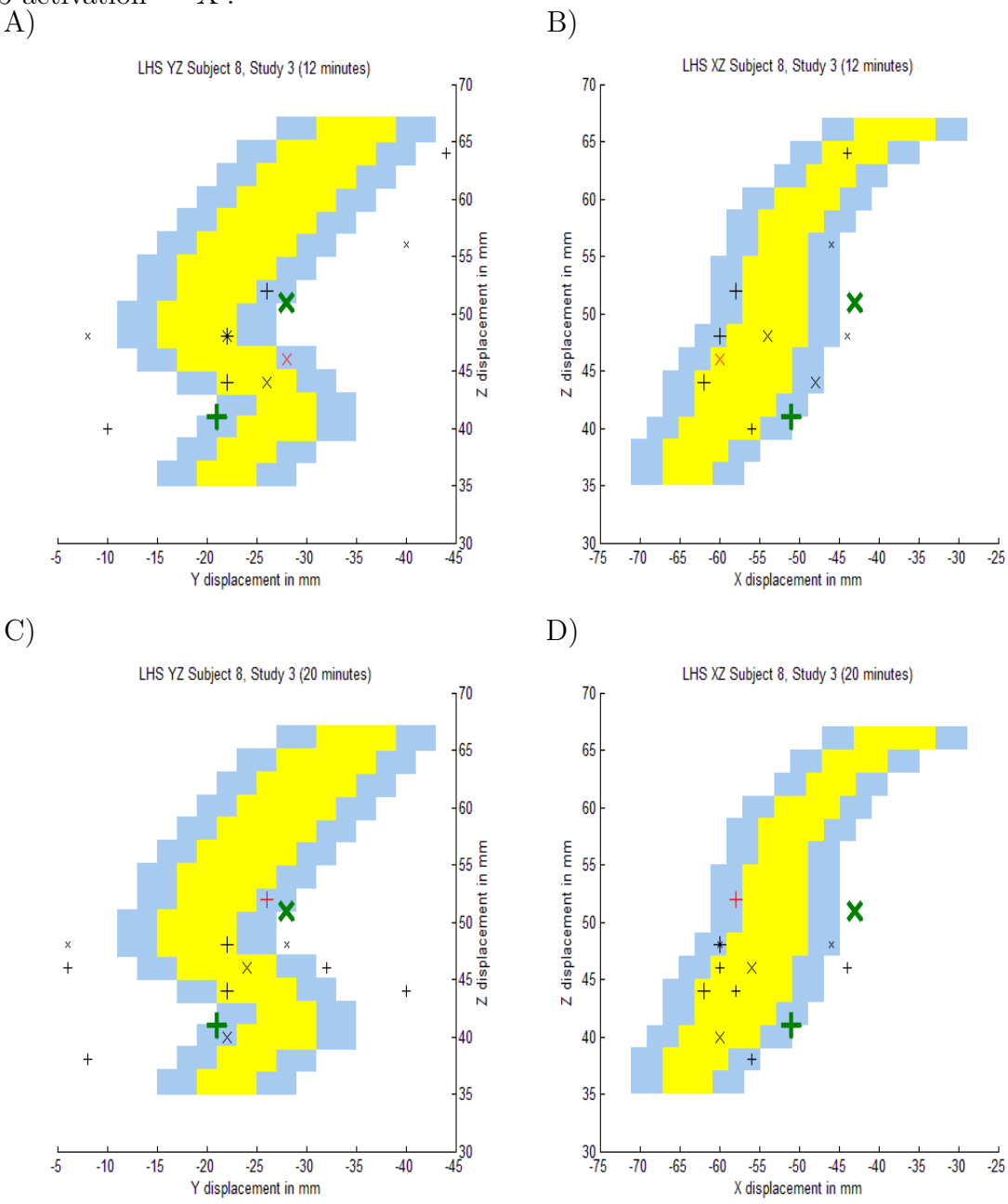

Figure 60: The centre of mass of all activations within BA1 for each subject in study 3 after 12 (A) and 20 minutes (B) of scanning, plotted over BA1. D1 data is indicated by '+' and D5 data by 'X'. Lines show each subject's data. All data plotted in MNI coordinates.

A)

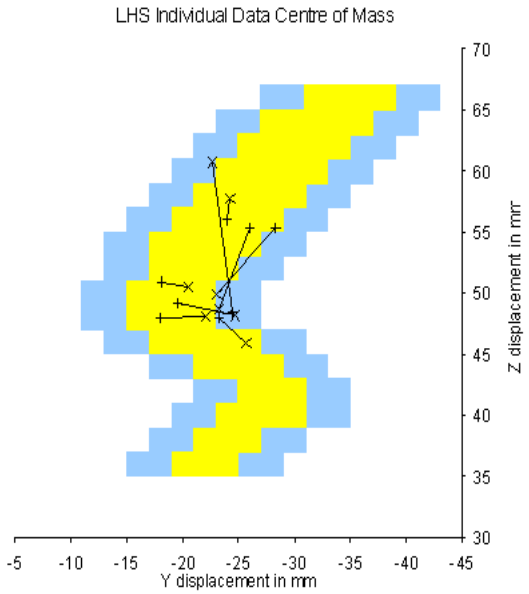

B)

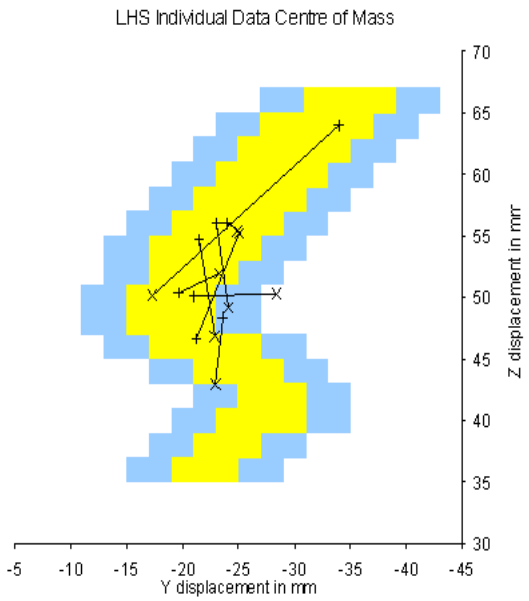

8.5 Study 4

In study 4 the same protocols were used that were employed in study 3. Two 20 minute scanning sessions were carried out with stimulation being applied to one digit per session, either RD1 or RD5. A variable interstimulus interval between 9 and 27 seconds was used. The 40 Hz drive voltage remained at ± 52V but the intermittent stimulus pattern was changed to a continuous vibration. The same eight subjects from study 3 were imaged.

8.5.1 Individual Analysis

For stimulation to RD1 and RD5 SI activity was detected for all digits for all subjects at an uncorrected p value threshold of ≤ 0.001. At a corrected p value threshold of ≤ 0.05 (T-score ≥ 5.1), contralateral SI activations are not detected in 2 instances which is comparable to study 3 (3 instances after 20 minutes of data collection). The T-score of the most activated voxel for each digit is listed in Table 20. The average T-score has decreased from 7.14 to 6.91 between the two studies and the maximum T-score has fallen from 16.69 to 15.47. Directly comparing the average T-score for each subject between study 3 and study 4 shows that the average T-score decreased in half the subjects.

Ipsilateral SI activity was not detected in 3 instances at an uncorrected p value threshold ≤ 0.001, compared to a 100 % detection rate in study 3 (after 20 minutes). The detection rate and T-scores of the most activated voxels for contralateral and ipsilateral SII activity are also similar to study 3 (after 20 minutes). A statistical analysis comparing the contralateral/ipsilateral SI T-score ratios from study 3 (20 minutes) to those of study 4 (column 7, Tables 19 and 20) reveals a slight statistical difference (unpaired two-tailed t-test, $p = 0.02$, t = 2.35, 27 degrees of freedom) indicating that the contralateral SI response was stronger in study 4. A similar analysis carried out using the SII ratios (column 8, Tables 19 and 20) shows there is no difference between the two studies for this parameter (unpaired two-tailed t-test, $p = 0.07$, t = 1.86, 30 degrees of freedom).

Table 20: The highest T-scores for contralateral and ipsilateral SI and SII activations for subjects 1 - 8 in study 4. The location of the activations is indicated in Figures 62 to 65. Contra = contralateral, Ipsi = ipsilateral, - = activity not detected above uncorrected p value threshold of ≤ 0.001. T-scores ≥ 5.1 (a corrected p value threshold of ≤ 0.05) are highlighted in bold. The mean and standard deviation for each digit for the group are given at the bottom of the table. The two columns on the far right show the ratio of contralateral SI/ipsilateral SI activity and contralateral SII/ipsilateral SII activity.

Subject	Digit stim.	Contra SI	Ipsi SI	Contra SII	Ipsi SII	Contra V Ipsi SI	Contra V Ipsi SI
1	RD1	**12.65**	3.60	**8.54**	4.86	3.51	1.76
	RD5	**11.04**	-	**8.10**	4.26	-	1.90
2	RD1	**11.60**	**6.66**	**8.60**	**6.85**	1.74	1.26
	RD5	**8.97**	4.38	**7.46**	**7.58**	2.05	0.98
3	RD1	4.87	-	4.89	4.23	-	1.16
	RD5	**6.69**	4.30	**6.43**	3.89	1.56	1.65
4	RD1	**10.94**	4.99	**7.49**	4.86	2.19	1.54
	RD5	**8.11**	3.83	**6.07**	4.72	2.12	1.29
5	RD1	**15.47**	**9.52**	**12.31**	**8.13**	1.63	1.51
	RD5	**9.06**	3.25	**8.83**	**6.47**	2.79	1.36
6	RD1	**13.36**	**7.31**	**9.39**	**5.97**	1.83	1.57
	RD5	**7.68**	4.54	**8.72**	**5.57**	1.69	1.57
7	RD1	**6.10**	-	**8.16**	4.46	-	1.83
	RD5	4.91	3.44	**6.68**	3.55	1.43	1.88
8	RD1	**8.86**	4.43	**6.12**	**7.62**	2.00	0.80
	RD5	**5.48**	3.81	**5.59**	**5.29**	1.44	1.06
Mean	RD1	10.48	6.09	8.19	5.87		
&		3.64	2.18	2.22	1.51		
standard	RD5	7.74	3.94	7.24	5.17		
deviation		2.02	0.49	1.23	1.36		

Figure 61 shows the brain activations overlaid on the template brain for the same representative subject from study 3 (subject 1). The area of the SI activity is indicated by the red arrow. With the same corrected p value threshold of ≤ 0.05 being applied to the data as in study 3 (Figure 51) it can be seen that there are less activations and the ipsilateral SII activity is absent. This trend is not true of all subjects in this study. The SI activations from all the subjects have been plotted in Figures 62 to 65. As the same subjects participated in both study 3 and study 4 it is possible to directly compare the locations for each subject. Although some SI activations for stimulation to RD1 and RD5 do appear in the same positions in this study as in study 3 (Figures 52 to 59), there are also differences, with more or fewer activations being detected in different locations. These differences still do not show a consistent distribution for either digit. The centre of mass of the BA1 activations for each digit were calculated and plotted on the graph in Figure 66. As can be seen, the RD1 and RD5 distribution is different to that of study 3 (shown in Figure 60), but again is inconsistent. Also the direction of the movement of the centre of mass from one digit to the other is no more consistent than in study 3 (or studies 1 and 2).

The Euclidean separations were calculated using the centre of mass of all the SI activations (BA1, 2, 3 and vicinity) as well only those within the BA1 region defined in the graphs. The separations are listed in Table 21. For each set of calculations, there are 2 values in the expected range but the rest are 2 - 3 times smaller. This is consistent with the results obtained in the previous 3 studies.

Despite the strong SI activity in response to the stimulus no SI clusters were detected at an uncorrected p value threshold of ≤ 0.001 in the group analysis.

8.5.2 Summary of Study 4

In terms of detecting and separating out the individual digit data there was no significant effect of changing between the intermittent stimulation in study 3 and the continuous stimulation in study 4. However, as outlined in the previous chapter, continuous stimulation was found to be advantageous for some patients, and

Table 21: Euclidean separations for the left and right hands for subjects 1 to 8 in study 4. The centre of mass was calculated using the coordinates (estimated error ± 2 mm) that fell within specific Brodmann areas and were weighted according to their T-score.

Subject	BA1,2,3 and vicinity RD1-D5 mm	BA1 RD1-D5 mm
1	5.4	12.9
2	3.5	9.8
3	14.1	10.9
4	4.2	4.6
5	1.9	3.1
6	5.0	8.2
7	8.5	7.1
8	12.6	6.9
Average	6.9	7.9

so was used in study 5.

Figure 61: The brain activations for a representative subject (subject 1), study 4, for D1 and D5 of the right hand, overlaid on the template brain. The SI area is indicated by the red arrow. A corrected p value threshold of ≤ 0.05 was applied to all data.

A)

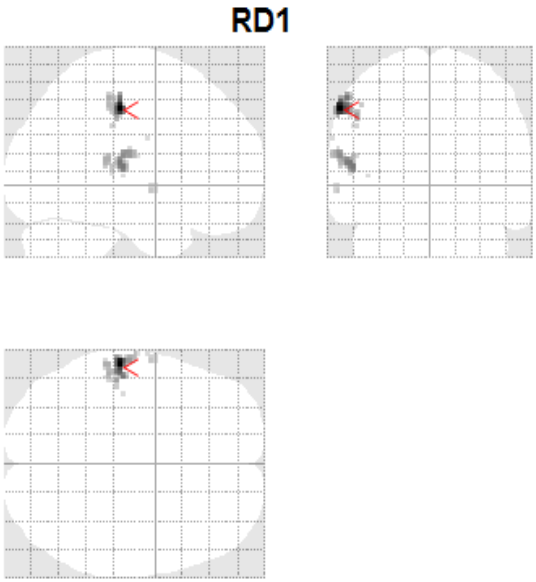

B)

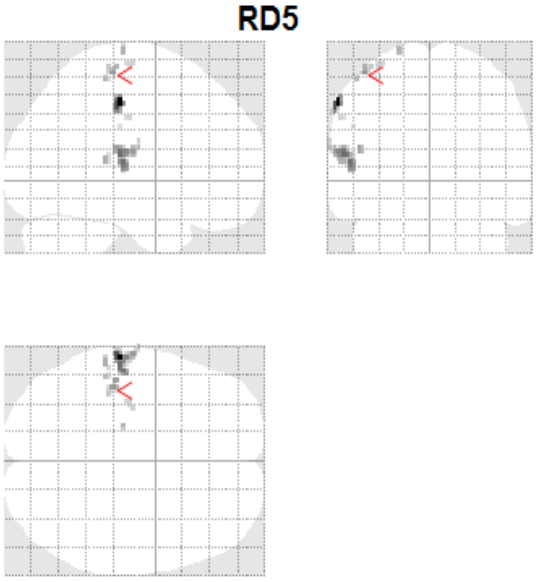

Figure 62: Brodmann area 1 (yellow) with a 4 mm error margin in x and y (blue). The RD1 and RD5 SI activations for subject 1, study 4 are overlaid in panels A and B. The same data for subject 2 is shown in panels C and D. An uncorrected p value threshold of ≤ 0.001 was applied (T-score ≥ 3.11). The activations which fall within the area bounded by blue in x, y and z are denoted by a larger marker. Those which also have a T-score ≥ 4 are coloured red. The mean location of the SI activation for each digit was determined from other studies (Table 1) and are shown by the large green markers. All data plotted in MNI coordinates. D1 activation = '+', D5 activation = 'X'.

A)

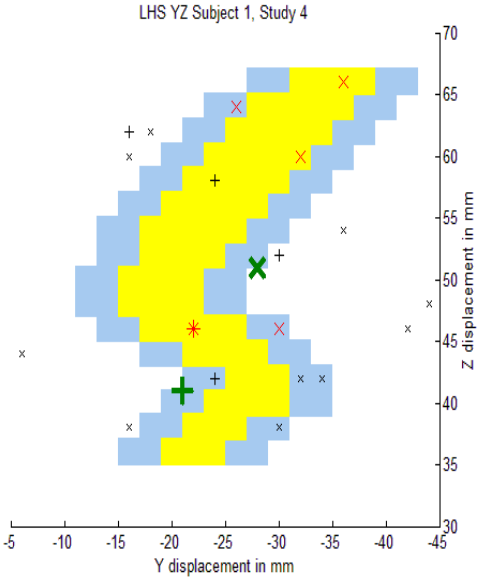

B)

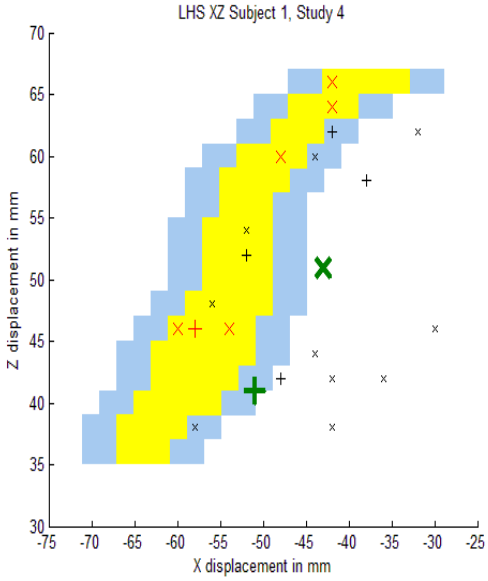

C)

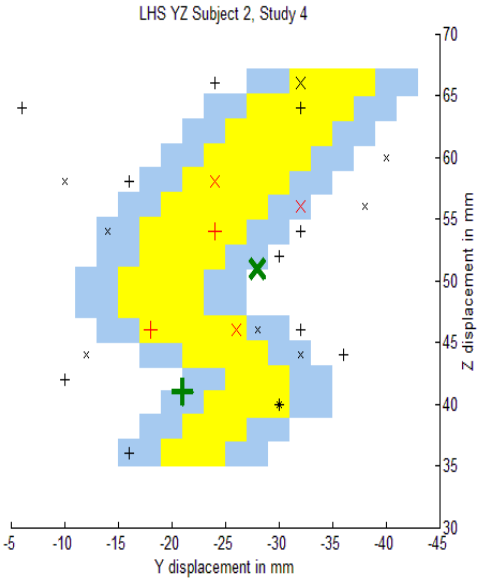

D)

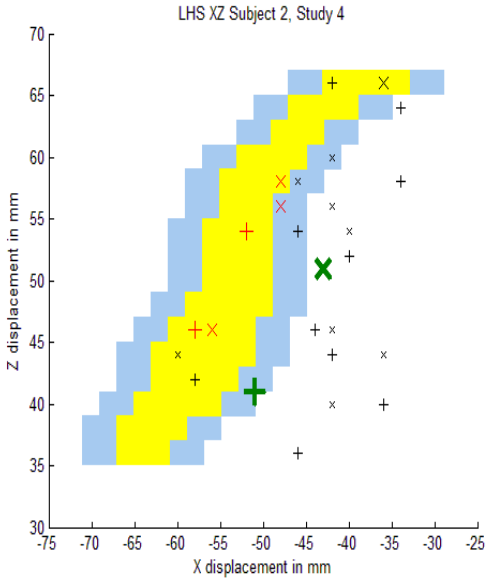

Figure 63: Brodmann area 1 (yellow) with a 4 mm error margin in x and y (blue). The RD1 and RD5 SI activations for subject 3, study 4 are overlaid in panels A and B. The same data for subject 4 is shown in panels C and D. An uncorrected p value threshold of ≤ 0.001 was applied (T-score ≥ 3.11). The activations which fall within the area bounded by blue in x, y and z are denoted by a larger marker. Those which also have a T-score ≥ 4 are coloured red. The mean location of the SI activation for each digit was determined from other studies (Table 1) and are shown by the large green markers. All data plotted in MNI coordinates. D1 activation = '+', D5 activation = 'X'.

A)

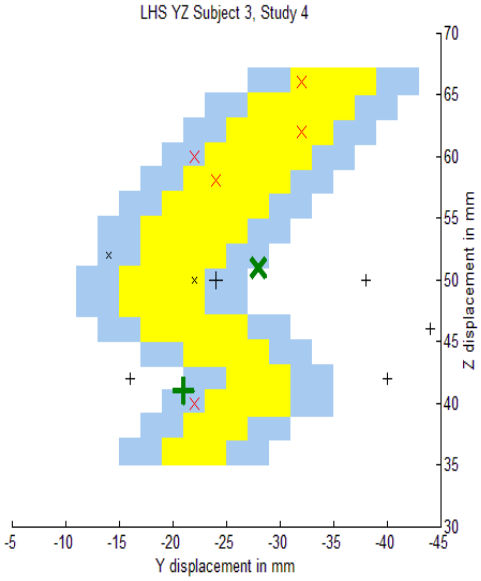

B)

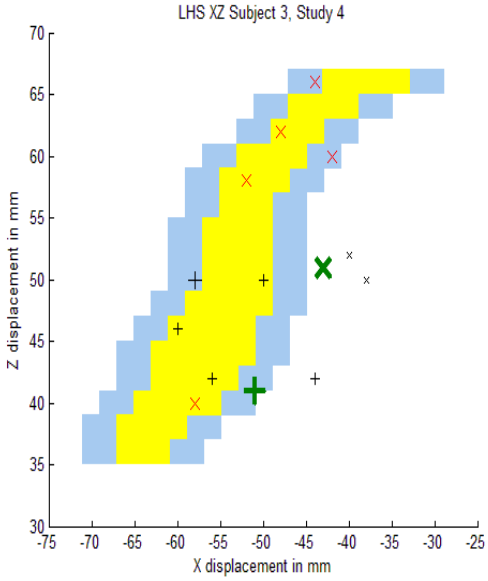

C)

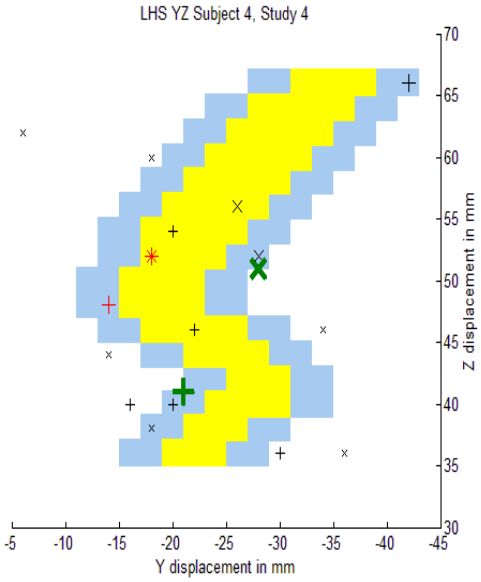

D)

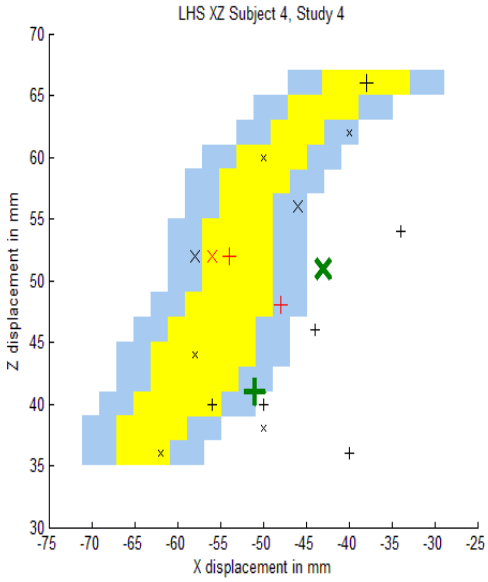

Figure 64: Brodmann area 1 (yellow) with a 4 mm error margin in x and y (blue). The RD1 and RD5 SI activations for subject 5, study 4 are overlaid in panels A and B. The same data for subject 6 is shown in panels C and D. An uncorrected p value threshold of ≤ 0.001 was applied (T-score ≥ 3.11). The activations which fall within the area bounded by blue in x, y and z are denoted by a larger marker. Those which also have a T-score ≥ 4 are coloured red. The mean location of the SI activation for each digit was determined from other studies (Table 1) and are shown by the large green markers. All data plotted in MNI coordinates. D1 activation = '+', D5 activation = 'X'.

A)

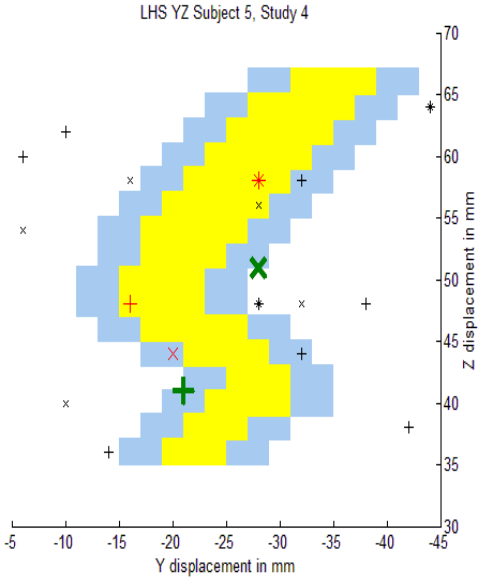

B)

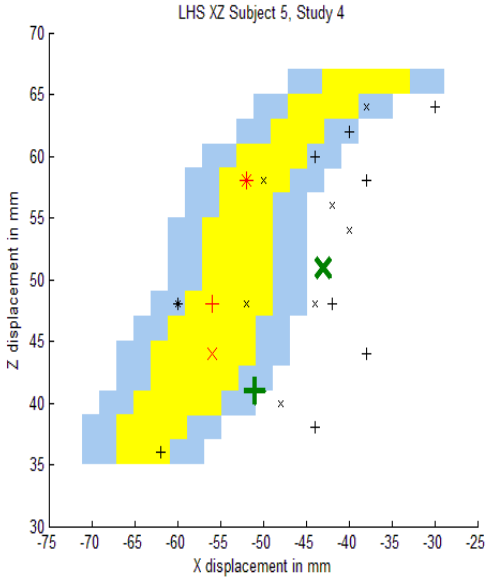

C)

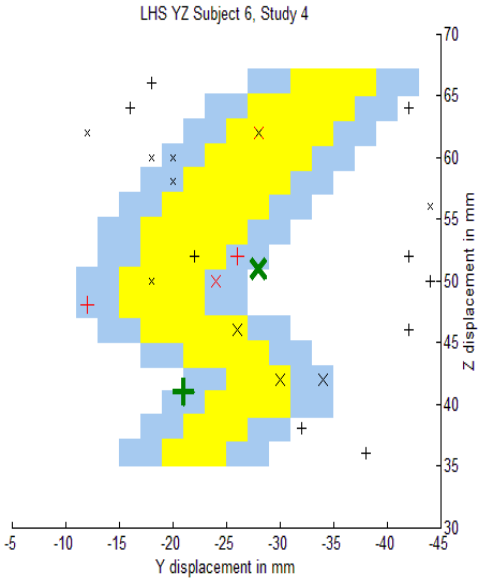

D)

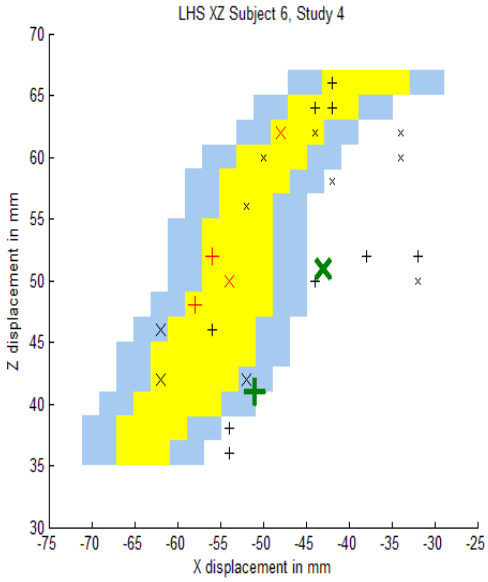

Figure 65: Brodmann area 1 (yellow) with a 4 mm error margin in x and y (blue). The RD1 and RD5 SI activations for subject 7, study 4 are overlaid in panels A and B. The same data for subject 8 is shown in panels C and D. An uncorrected p value threshold of ≤ 0.001 was applied (T-score ≥ 3.11). The activations which fall within the area bounded by blue in x, y and z are denoted by a larger marker. Those which also have a T-score ≥ 4 are coloured red. The mean location of the SI activation for each digit was determined from other studies (Table 1) and are shown by the large green markers. All data plotted in MNI coordinates. D1 activation = '+', D5 activation = 'X'.

A)

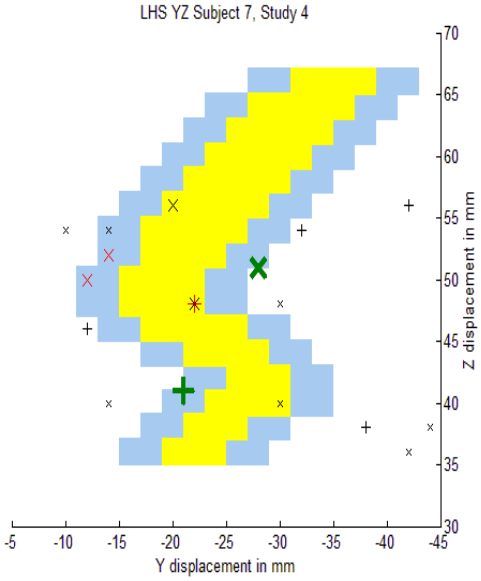

B)

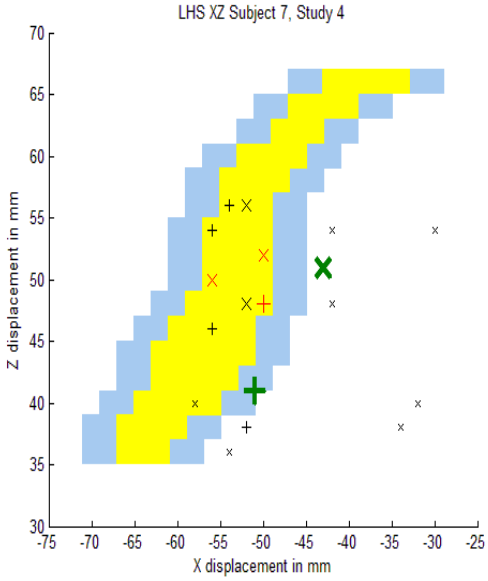

C)

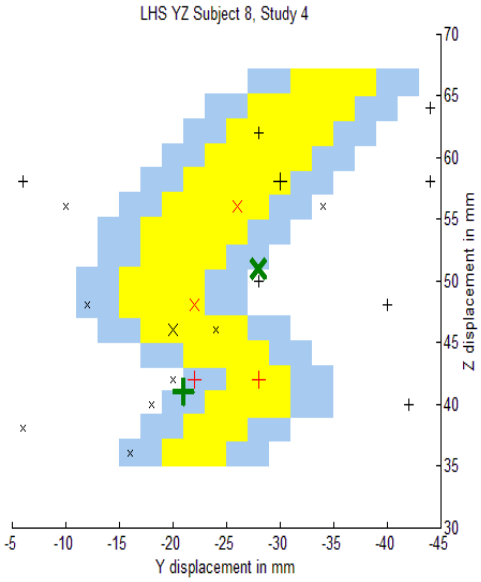

D)

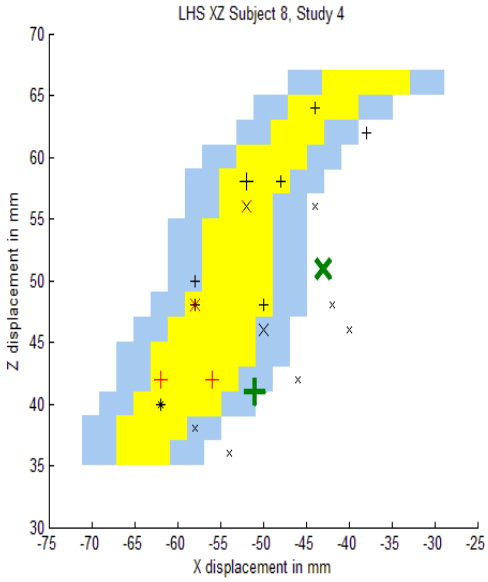

Figure 66: The centre of mass of all activations within BA1 for each subject in study 4, plotted over BA1. D1 data is indicated by '+' and D5 data by 'X'. Lines show each subject's data. All data plotted in MNI coordinates.

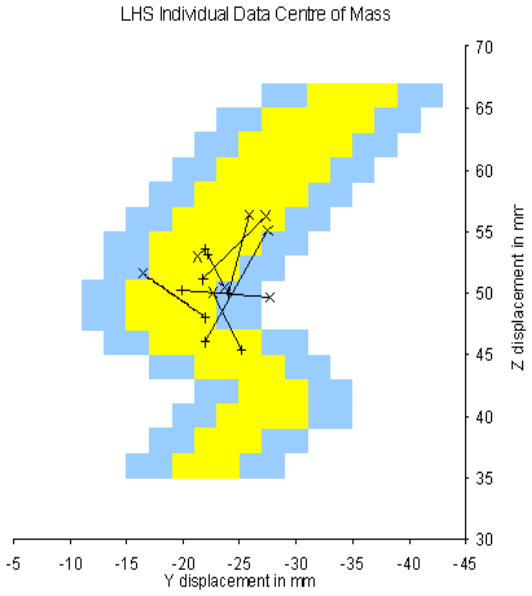

8.6 Study 5

The protocol from study 1 was used for the patient study. This involved two 30 minute scanning sessions where D1 and D5 of the left hand were stimulated in one session and the same digits of the right hand were stimulated in the other session. The stimulus alternated randomly between D1 and D5 and the continuous vibratory stimulus from study 4 was used, presented in a regular 9 s 'on' and 27 s 'off' pattern. The drive voltage remained at ± 52 V - except for experiments relating to patient 2 who required a lower setting of ± 26 V. The patients were initially imaged soon after diagnosis and the scans were repeated approximately 4 months later to assess for any changes in the somatosensory cortex and possibly correlate them with changes in the patients' symptoms. A control group was also imaged.

The objective of the patient study was to determine if there were changes in the finger representations in the primary somatosensory cortices in CRPS patients. It was hypothesised that the D1 and D5 representations for a CRPS affected hand would be in a different position on the cortex (producing smaller or larger cortical separations between the digits) compared to the patient's unaffected hand and compared to D1/D5 representations for a control group. It was also hypothesised that changes might be detected in the size of the SI activations, either larger or smaller, compared to the unaffected hand or to the control group. Additionally, these changes in location and size of the activations would reverse as the disease improved.

8.6.1 Individual Analysis

The initial patient scans are denoted by the suffix 'a' (P1a, P2a, P3a and P4a). The results of the initial scans reveal contralateral SI activity for stimulation to LD1, LD5, RD1 and RD5 in all patients at an uncorrected p value threshold of ≤ 0.001. If the threshold is raised to a corrected p value of ≤ 0.05, contralateral SI activity is detected in all instances except for LD1 and LD5 (unaffected hand) of

patient 4. The repeat patient scans carried out a few months later are denoted by the suffix 'b'. They show similar detection rates and T-score values to the initial data. [Note: when the second patient scans were carried out all patients reported an improvement in their symptoms compared to the first scans].

The T-scores of the most activated voxels in the contralateral and ipsilateral SI and SII regions for the patients are shown in Tables 22 and 23 and the corresponding control subject data are shown in Table 24. The T-scores for the patients have a similar range to that found in the control subject data. An inspection of the data in Table 22 and 23 suggests that there are no significant differences in the T-scores for the CRPS digits compared to the unaffected digits (CRPS affected the right hand of patients 1, 3 and 4 and the left hand of patient 2). Both hands demonstrate a high T-score in most instances and are within the same range as the control subject data. The average T-score values for the CRPS digits are 7.23 and 7.01 for the first and second patient scans respectively, compared to the control group average of 7.33. Interestingly, the T-score average for the *unaffected* hands in the patient group is lower at 6.46 and 6.09 for the first and second scans respectively. A paired two-tailed student t-test comparing the patient values for the CRPS and unaffected hands show this difference is not statistically significant for the first scans ($p = 0.14$, t = 1.66, 7 degrees of freedom) and the second scans ($p = 0.10$, t = 1.89, 7 degrees of freedom).

Comparing the patient average T-scores for the affected and unaffected hands in more detail, for patients 1 and 2 both the affected and unaffected averages are lower in the second scans. The upgrades to the scanner were carried out between the first and second scans for patients 3 and 4. The T-score averages for the affected and unaffected hands are higher in the second scans, as expected with the improvements to the hardware. The control group scans were also carried out after the upgrades and it is likely that the T-score average of 7.33 would have been lower if carried out with the original hardware. This suggests that the T-score averages for the unaffected hands in the first and second scans might be in line with the control group and that the averages for the CRPS digits are actually

Table 22: The highest T-scores for contralateral and ipsilateral SI and SII activations for patients 1 to 4 in study 5 for the first patient scans, denoted by 'a'. The underlined digits indicate those affected by CRPS. The location of the activations is indicated in Figures 69 to 76. An uncorrected p value threshold of ≤ 0.001 was applied. Contra = contralateral, Ipsi = ipsilateral. The mean and standard deviation for each digit for the group are given at the bottom of the table. The two columns on the far right show the ratio of contralateral SI/ipsilateral SI activity and contralateral SII/ipsilateral SII activity.

Subject	Digit stim.	Contra SI	Ipsi SI	Contra SII	Ipsi SII	Contra V Ipsi SI	Contra V Ipsi SI
Pat 1a	LD1	13.88	3.70	10.10	6.44	3.75	1.57
	LD5	13.61	8.13	13.37	3.69	1.76	3.62
	RD1	13.84	7.36	11.07	12.29	1.88	0.90
	RD5	12.54	13.05	6.61	4.22	0.96	1.57
Pat 2a	LD1	9.82	4.36	6.39	4.40	2.25	1.45
	LD5	6.12	4.56	5.24	5.41	1.34	0.97
	RD1	8.83	8.30	8.49	4.44	1.06	1.91
	RD5	7.89	3.53	5.13	4.96	2.24	1.03
Pat 3a	LD1	6.42	4.09	4.26	5.04	1.57	0.85
	LD5	8.86	5.79	6.74	6.03	1.53	1.12
	RD1	10.19	5.43	6.32	4.17	1.88	1.52
	RD5	10.15	4.61	6.19	3.50	2.20	1.77
Pat 4a	LD1	4.88	4.53	5.69	4.56	1.08	1.25
	LD5	3.63	4.04	3.38	4.16	0.90	0.81
	RD1	8.07	6.28	8.43	7.55	1.29	1.12
	RD5	7.49	4.47	6.70	4.53	1.68	1.48
Mean & standard deviation	D1 (healthy)	8.50	5.16	7.14	5.12		
		3.94	2.12	2.64	0.92		
	D5 (healthy)	8.50	5.37	7.16	4.71		
		4.10	2.08	4.36	1.02		
	D1 (CRPS)	10.48	5.86	8.05	7.10		
		2.42	1.27	2.24	3.79		
	D5 (CRPS)	9.08	6.67	6.19	4.42		
		2.85	4.25	0.67	0.79		

Table 23: The highest T-scores for contralateral and ipsilateral SI and SII activations for patients 1 to 4 in study 5 for the second patient scans, denoted by 'b'. The underlined digits indicate those affected by CRPS. The location of the activations is indicated in Figures 69 to 76. An uncorrected p value threshold of ≤ 0.001 was applied. Contra = contralateral, Ipsi = ipsilateral. The mean and standard deviation for each digit for the group are given at the bottom of the table. The two columns on the far right show the ratio of contralateral SI/ipsilateral SI activity and contralateral SII/ipsilateral SII activity.

Subject	Digit stim.	Contra SI	Ipsi SI	Contra SII	Ipsi SII	Contra V Ipsi SI	Contra V Ipsi SI
Pat 1b	LD1	10.42	4.40	5.13	5.32	2.37	0.96
	LD5	8.37	4.25	6.57	4.81	1.97	1.37
	RD1	15.40	5.61	5.40	5.66	2.75	0.95
	RD5	10.42	5.45	3.34	3.80	1.91	0.88
Pat 2b	LD1	6.76	3.49	3.88	3.95	1.94	0.98
	LD5	6.06	3.28	5.14	6.02	1.85	0.85
	RD1	7.46	5.23	6.37	4.13	1.43	1.54
	RD5	9.10	6.25	6.07	4.94	1.46	1.23
Pat 3b	LD1	11.00	5.09	6.87	6.93	2.16	0.99
	LD5	3.50	6.31	6.76	7.11	0.55	0.53
	RD1	12.54	6.56	4.51	8.10	1.91	0.56
	RD5	10.60	6.10	8.57	11.55	1.74	0.74
Pat 4b	LD1	7.97	6.18	6.83	4.33	1.29	1.58
	LD5	5.33	3.33	4.44	3.99	1.60	1.11
	RD1	11.61	8.17	11.72	8.64	1.42	1.36
	RD5	6.78	5.26	5.72	4.33	1.29	1.32
Mean	D1 (healthy)	9.21	5.23	6.30	5.18		
&		1.76	0.73	0.81	1.28		
standard	D5 (healthy)	6.58	5.04	5.21	5.21		
deviation		2.62	1.49	1.33	1.33		
	D1 (CRPS)	11.58	5.96	6.38	6.59		
		3.59	1.96	3.62	2.18		
	D5 (CRPS)	9.47	5.02	5.69	6.43		
		2.38	1.22	2.17	3.55		

Table 24: The highest T-scores for contralateral and ipsilateral SI and SII activations for control subjects 1 - 4 in study 5. The location of the activations is indicated in Figures 77 to 80. An uncorrected p value threshold of ≤ 0.001 was applied. Contra = contralateral, Ipsi = ipsilateral. The mean and standard deviation for each digit for the group are given at the bottom of the table. The two columns on the far right show the ratio of contralateral SI/ipsilateral SI activity and contralateral SII/ipsilateral SII activity.

Subject	Digit stim.	Contra SI	Ipsi SI	Contra SII	Ipsi SII	Contra V Ipsi SI	Contra V Ipsi SI
Control 1	LD1	12.77	6.80	3.82	10.38	1.86	0.37
	LD5	11.19	4.50	11.32	10.24	2.49	1.11
	RD1	11.14	9.19	5.79	7.58	1.21	0.76
	RD5	6.04	3.45	6.04	4.25	1.75	1.21
Control 2	LD1	12.18	5.28	3.83	4.00	2.31	0.96
	LD5	9.90	4.40	10.33	4.56	2.25	2.27
	RD1	9.29	5.60	7.98	5.13	1.66	1.55
	RD5	6.33	3.69	5.67	3.97	1.72	1.43
Control 3	LD1	11.37	8.41	10.63	6.73	1.35	1.58
	LD5	3.52	3.74	7.02	5.15	0.94	1.36
	RD1	9.22	7.79	6.33	7.98	1.18	0.79
	RD5	6.17	5.73	6.81	6.92	1.08	0.98
Control 4	LD1	10.00	6.71	8.77	6.91	1.49	1.27
	LD5	11.35	8.14	3.66	10.31	1.39	0.35
	RD1	10.71	6.30	8.06	7.55	1.70	1.07
	RD5	9.81	5.98	7.19	7.31	1.64	0.98
Mean	LD1	11.58	6.82	6.76	7.01		
&		1.20	1.28	3.48	2.61		
standard	LD5	8.99	5.20	8.08	7.57		
deviation		3.70	1.99	3.47	3.14		
	RD1	11.14	9.19	5.79	7.58		
		0.98	1.60	1.15	1.30		
	RD5	7.09	4.71	6.43	5.61		
		1.82	1.33	0.70	1.75		

higher than the norm.

The data were also assessed for laterality effects between the CRPS and patient healthy hands and the CRPS and control group hands using the data collectively from both the initial and repeat scans. An unpaired two-tailed t-test was carried out using the SI T-score ratios in column 7 of Tables 22 to 24. There was no statistical difference between the CRPS and patient healthy hands ($p = 0.63$, t = 0.51, 30 degrees of freedom) or the CRPS and control group hands ($p = 0.37$, t = 0.90, 30 degrees of freedom). The test was repeated for the SII ratios (column 8, Tables 22, 23, and 15) and no statistically significant differences were found (CRPS/patient healthy hands $p = 0.34$, t = 0.97, 30 degrees of freedom, CRPS/control group hands $p = 0.94$, t = 0.07, 30 degrees of freedom).

The size of the largest SI cluster for stimulation to each digit in the patient and control groups are summarised in Table 25 and are given in detail in Appendix B.5. The cluster sizes relating to the CRPS digits have been underlined in the Table. In the control subjects, the size of the largest cluster for stimulation to each digit is, generally, in the region of a few hundred voxels. The minimum and maximum cluster sizes for each digit in the control data may be used to estimate a normal range for each digit. Each patient is summarised individually below. [In interpreting these observations, it must be born in mind that the control data (and the second scans of patients 3 and 4) were acquired after the scanner upgrade and hinder the comparison between the normal range and the patient data. Due to the time course of the disease and the aim of the investigation to determine the level of cortical reorgansation in the early stages of the disease and track them as the disease progresses it was not possible to repeat the first scans. No phantom data was acquired prior to the upgrade to allow a comparison of the SNR before and after in the images. Also many of the observed changes may be incidental, perhaps relating to 'normal' physiological variation, or uncontrolled aspects of the measurements. These factors and the small number of control subjects also lead to uncertainty in estimating normal ranges.]

Patient 1: The CRPS hand demonstrates large cluster sizes, near to

1000 voxels for both RD1 and RD5. A similar size cluster is also seen for LD5 of the unaffected hand but the size of the activation for LD1 is below the normal range for that digit. The second scans carried out a few months later show little change for the CRPS hand; LD5 of the unaffected hand has returned to within the normal range but LD1 remains small. It would be reasonable to assume that if the data had been acquired after the scanner upgrade the cluster sizes would be larger. This suggests that the cluster sizes for LD1 might be within the normal range and the CRPS clusters would be even larger.

Patient 2: The unaffected right hand is within the normal ranges in both scans but the size of the activations for the CRPS digits is smaller than the unaffected hand and below the normal range in the first scans. In the data from the second scans, the cluster size for LD5 is on the lower limit of the normal range but the cluster size for LD1 has shrunk even further. It is possible that the cluster sizes would be larger if the data had been acquired with the new equipment suggesting the cluster sizes of the CRPS digits might be within the normal range in both scans. However, compared to the unaffected hand, the CRPS cluster sizes are consistently lower.

Patient 3: The CRPS cluster sizes are within the normal limits in the first scans whereas by the second scans (with improvement of symptoms and after the scanner upgrade) RD1 remains within normal limits but RD5 is larger than the normal range. For the unaffected hands, the cluster sizes for LD5 are in the normal range for both scans but for LD1 are smaller in both scans than the normal range.

Patient 4: For both unaffected digits, cluster sizes are smaller than the normal range in both scans, although some improvement is seen in the second scans possibly as a result of the new equipment. For the CRPS hand, cluster sizes are also below normal for the initial scans,

Table 25: The sizes (in 2 mm^3 voxels) of the largest clusters in the contralateral SI region of the brain for the first (a) and second (b) patient scans and for the patient controls. The values underlined indicate the digits affected by CRPS. An uncorrected p value threshold of ≤ 0.001 was applied to the data.

Subject	LD1	LD5	RD1	RD5
P1a	186	1067	<u>922</u>	<u>838</u>
P2a	<u>69</u>	<u>18</u>	348	115
P3a	34	132	<u>178</u>	<u>129</u>
P4a	14	3	<u>70</u>	<u>18</u>
P1b	101	67	<u>1268</u>	<u>970</u>
P2b	<u>39</u>	<u>35</u>	288	312
P3b	96	92	<u>215</u>	<u>412</u>
P4b	97	21	<u>228</u>	<u>57</u>
C1	594	258	416	61
C2	411	133	236	42
C3	424	37	132	37
C4	337	466	385	212

as in patient 2. However, by the second scans both digits have larger cluster sizes bringing them within the normal range. It is possible that the CRPS digit cluster sizes in the first scans would have been larger had they had been acquired with the new equipment suggesting there might be little change between the two scanning sessions.

To summarise, the CRPS digit cluster sizes were smaller in one patient and larger in one patient than the normal ranges obtained from the control group but, surprisingly, the unaffected digit cluster sizes are also not as expected. The differences are not statistically significant (two-tailed student t-test: $p = 0.71$, t = 0.39, 7 degrees of freedom). Although other CRPS imaging studies have not found differences in the unaffected side [26, 27, 28, 29, 30, 36, 111], a motor task study by Ribber et al. [110] found slightly slower response times for both the CRPS and unaffected sides compared to a control group suggesting that bilateral differences in cortical activity may exist.

The brain activations for a representative patient (patient 3) are shown in Figures 67 and 68 overlaid on the template brain. The top images of Figure 67

(panels A and B) show the data for RD1 and RD5 for the initial scans and the bottom images (panels C and D) are for the same digits from the repeat scans. Figure 68 shows the data for LD1 and LD5 arranged in the same manner. The SI region is indicated by the red arrow. As can be seen, more brain activity was detected in the second scans and there are some differences in the location of the RD5 (CRPS) SI activations between the initial and repeat scans.

The SI activations for each patient are shown in Figures 69 to 76. They are arranged in a similar fashion to Figures 67 and 68 where the data from the first and second scans for a single hand are shown together. The control subject data are shown in Figures 77 to 80.

The Euclidean separations were calculated using the centre of mass of all the activations detected in the SI region (BA1, 2, 3 and vicinity) for each digit in the patient and control subject groups. The values are shown in Table 26 and the values relating to the CRPS digits have been underlined. Most of the control group separations are smaller than expected and have a similar range of values to those calculated in studies 1 to 4. The separations for the patients are similar to the control group and show no correlation to the CRPS or the unaffected digits. The separations were also calculated using the centre of mass of only those activations that fell within the vicinity of BA1 (defined by the blue and yellow regions in the graphs). These separations are also listed in Table 26. Again, there is no correlation with the distance calculated and the laterality of CRPS.

The centre of mass of the BA1 activations for each digit were plotted on the graphs in Figure 87. The LHS and RHS activations for the CRPS digits are shown in panels A and B, and the LHS and RHS activations for the unaffected patient digits are shown in panels C and D. The individual patient and control subject D1/D5 pairs are joined by a line indicating the direction the activation has moved between the digits. The control subjects are shown in black, the CRPS activations from the first scans are shown in red and the CRPS centres from the second scans are shown in green. This convention is also used for the unaffected digit data in panels C and D. All the black and coloured lines are orientated inconsistently for

Table 26: Euclidean separations for the left and right hands for each patient and control subject in study 5. The underlined values indicate the separations relating to the CRPS digits. The centre of mass was calculated using the coordinates (estimated error ± 2 mm) that fell within specific Brodmann areas and were weighted according to their T-score.

	BA1,2,3 and vicinity		BA1	
Subject	LD1-D5 mm	RD1-D5 mm	LD1-D5 mm	RD1-D5 mm
P1a	7.4	<u>6.9</u>	13.0	<u>3.0</u>
P2a	<u>3.9</u>	8.6	<u>3.7</u>	6.0
P3a	8.1	<u>5.3</u>	3.7	<u>6.0</u>
P4a	12.6	<u>6.3</u>	18.6	<u>2.0</u>
P1b	7.2	<u>4.1</u>	13.1	<u>2.9</u>
P2b	<u>11.6</u>	9.4	<u>30.6</u>	20.7
P3b	2.0	<u>7.4</u>	6.3	<u>10.8</u>
P4b	5.0	<u>3.4</u>	-	<u>11.0</u>
C1	9.9	6.9	-	6.3
C2	6.4	8.1	11.9	17.5
C3	5.2	5.2	4.0	5.7
C4	4.7	6.9	-	7.8

both hands, as in the data obtained in studies 1 to 4. The CRPS data from both scans reveals no systematic variation of the movement between the activations in either the initial scans or the follow up scans (after improvement in the patients' symptoms).

8.6.2 Group Analysis

Patients 1, 3 and 4 demonstrated right-side CRPS, but patient 2 demonstrated CRPS on the left side. Hence, before the group analysis was carried out the data of patient 2 were flipped left to right so that the CRPS data from all the patients were in the same hemisphere.

The brain activations from the group data have been overlaid on the template brain and are shown in Figures 81 and 82. The SI activations are indicated by the red arrow. These are listed in Table 27 and are shown in more detail in the graphs in Figures 83 and 84. There was no activity detected for stimulation to LD5 and RD5 at the group level for the initial scans at an uncorrected p value threshold of ≤ 0.001, therefore the group separations could not be determined. In the data from the repeat scans activity was detected for LD1, RD1 and RD5, allowing the cortical separation for the patient CRPS digits to be calculated. This was found to be 15.2 mm which is within the range expected for an unaffected hand (10 - 18 mm).

A group analysis was also carried out with the control group data. The resulting brain activations are shown on the template brain in Figure 85 and have been overlaid in the graphs in Figure 86. The separation between the centre of mass of the cortical digit activity was found to be 18.7 mm for the right hand (LHS) and 8.1 mm for the left hand (RHS). Although the right hand distance is at the upper limit of the expected range, the left hand distance is smaller than expected but is consistent with the values obtained from the individual analysis.

The lack of SI activations in the patient group data may be an indication of the cortical differences found in CRPS. However, it has proved difficult to detect SI activations at the group level in studies 1 to 4 carried out with control subjects.

Table 27: The SI activations centres for the digits with their respective T scores for the contralateral SI activations for the group analysis for patients and control subjects in study 5. The data relating to the CRPS digits is underlined. A threshold of uncorrected p value of ≤ 0.001 was used.

Subject	Stimulation	x	y	z	T-score
Patients	LD1	56	-28	42	4.28
Scans a	LD5				
	RD1	-44	-10	56	5.11
		-44	-14	46	4.47
		-46	-38	60	4.05
	RD5				
Patients	LD1	50	-10	54	5.35
Scans b	LD5				
	RD1	-46	-8	50	6.58
	RD5	-30	-8	46	4.43
		-32	-10	50	4.24
Controls	LD1	40	-14	62	6.25
		42	-16	52	4.27
		34	-34	54	4.89
		30	-38	62	4.73
		36	-38	50	4.11
	LD5	30	-14	50	4.60
		48	-20	58	4.35
		44	-28	56	4.01
	RD1	-40	-18	42	6.17
		-30	-40	42	6.00
		-48	-10	42	5.52
		-52	-8	50	5.36
		-48	-16	50	4.53
		-38	-42	44	4.47
		-54	-20	40	3.97
	RD5	-38	-22	62	6.49

8.6.3 Summary of Study 5

In summary, the locations and separations of the cortical digit representations from the individual and group data do not reveal any differences between the CRPS and unaffected hands or between the CRPS patients and the control group. The movement of the centre of mass of each digit's activation does not show any systematic variation between the CRPS and non-CRPS digits, or with improvement in the patients' symptoms. For the patient group, some changes were observed between the 2 scans with respect to the size of the largest SI activation for the CRPS digits, and this may be related to changes in the patients' symptoms.

Figure 67: The brain activations for a representative subject (patient 3), study 5, for right (CRPS) D1 and D5, overlaid on the template brain. Panels A and B show the data from the first scans and panels C and D show the data from the second scans a few months later after improvement in the patient's symptoms. A corrected p value threshold of ≤ 0.05 was applied. The SI activation for each digit is indicated by the red arrow.

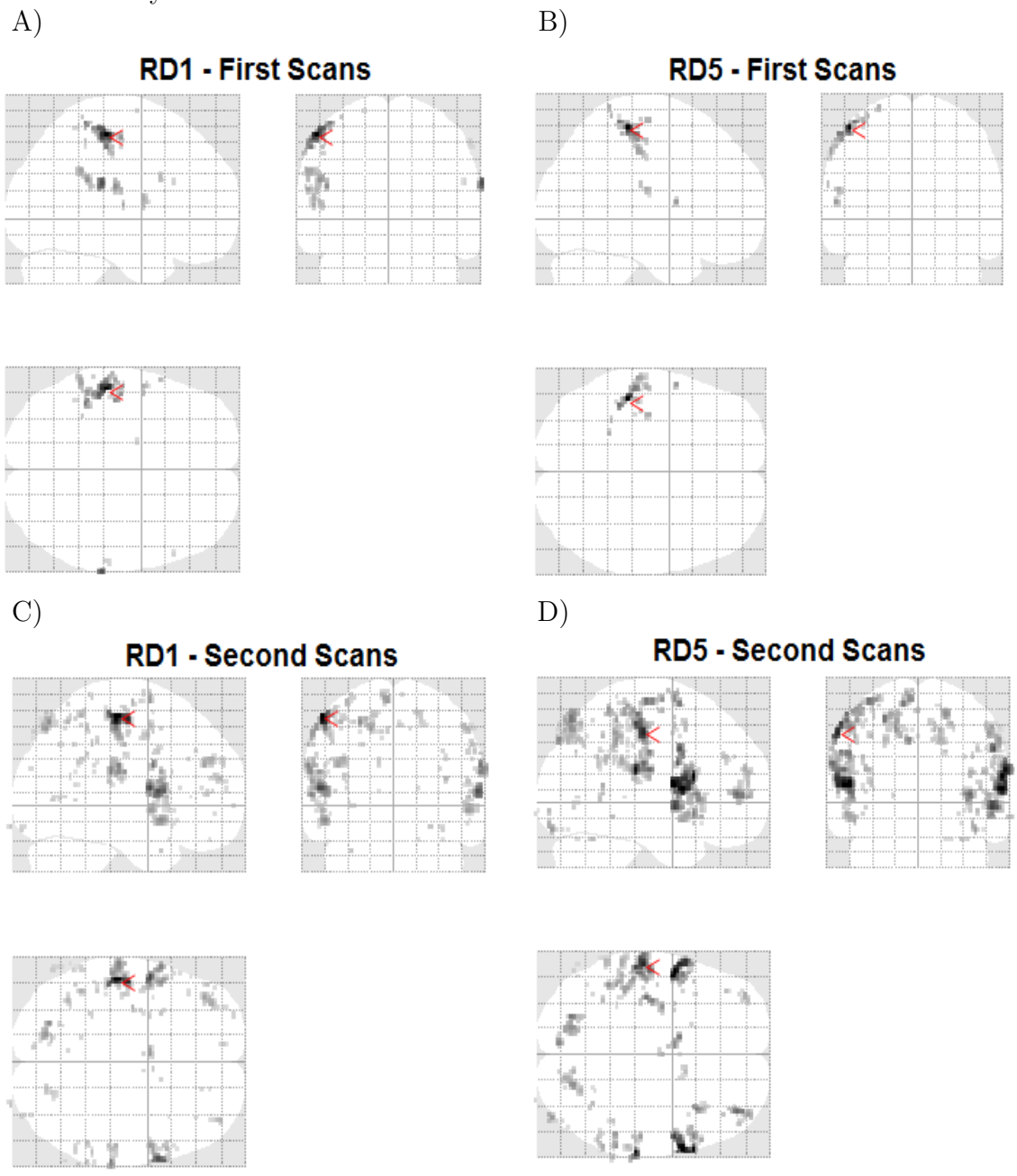

Figure 68: The brain activations for a representative subject (patient 3), study 5, for left (unaffected) D1 and D5, overlaid on the template brain. Panels A and B show the data from the first scans and panels C and D show the data from the second scans a few months later after improvement in the patient's symptoms. A corrected p value threshold of ≤ 0.05 was applied. The SI activation for each digit is indicated by the red arrow.

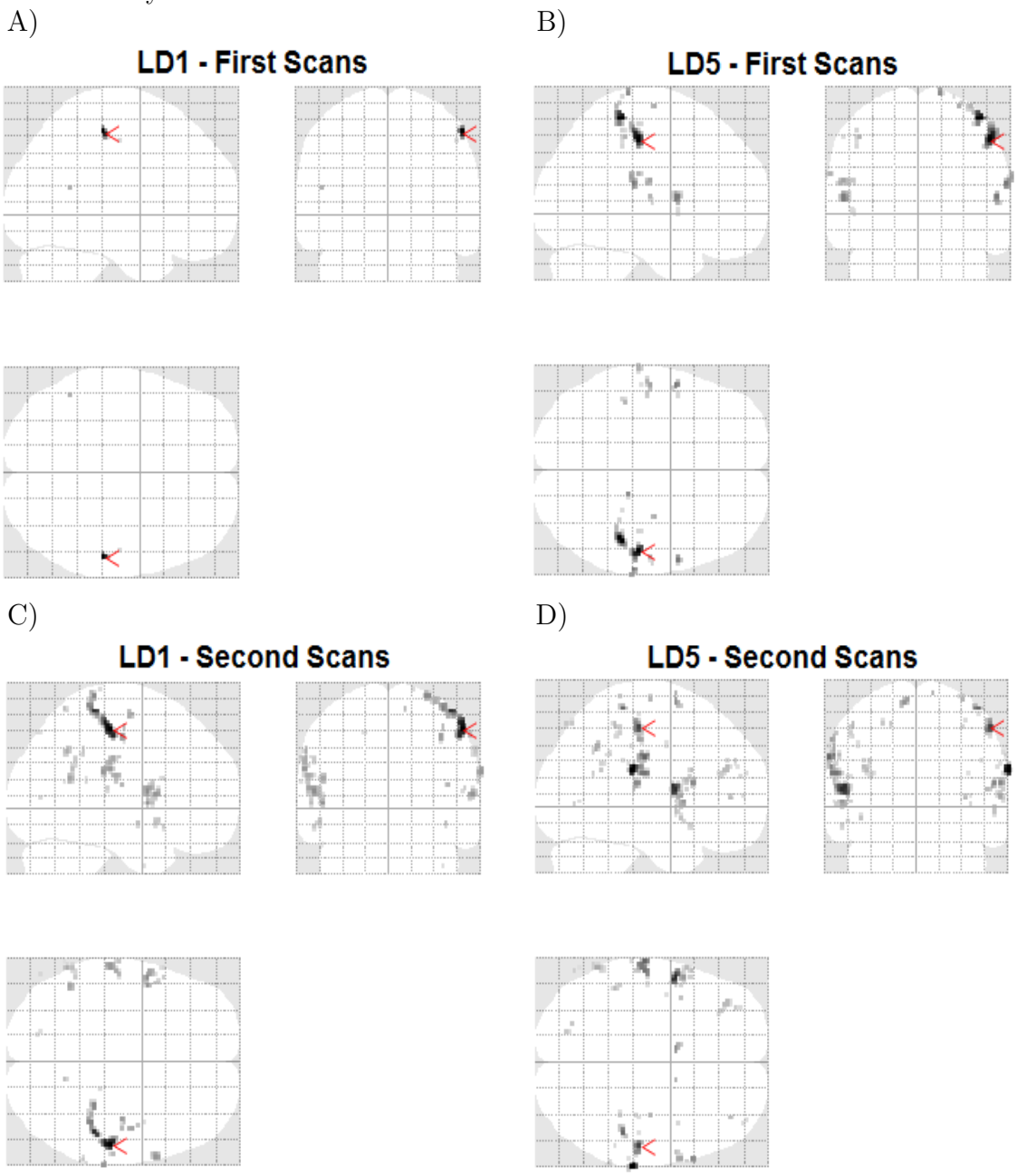

Figure 69: The SI activations for the left hand side of the brain (right *CRPS* D1 and D5) for patient 1, study 5, over Brodmann area 1 (yellow) with a 4 mm error margin in x and y (blue). Panels A and B show the data from the first scans and panels C and D show the data from the second scans taken a few months later after some improvement in the patient's symptoms. An uncorrected p value threshold of ≤ 0.001 was applied (T-score ≥ 3.11). The activations which fall within the area bounded by blue in x, y and z are denoted by a larger marker. Those which also have a T-score ≥ 4 are coloured red. The mean location of the SI activation from other studies (Table 1) are shown by the large green markers. All data plotted in MNI coordinates. D1 activation = '+', D5 activation = 'X'.

A)

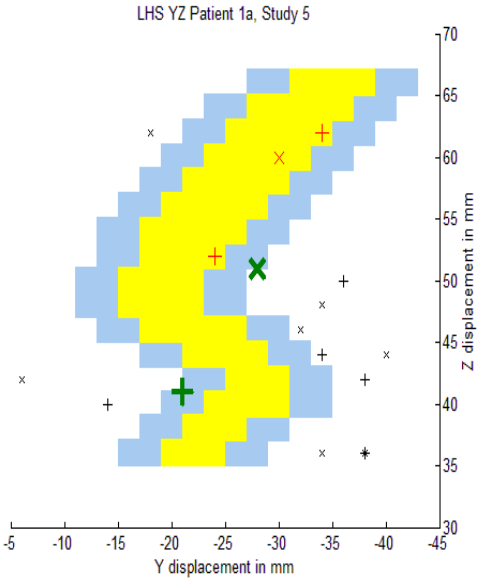

B)

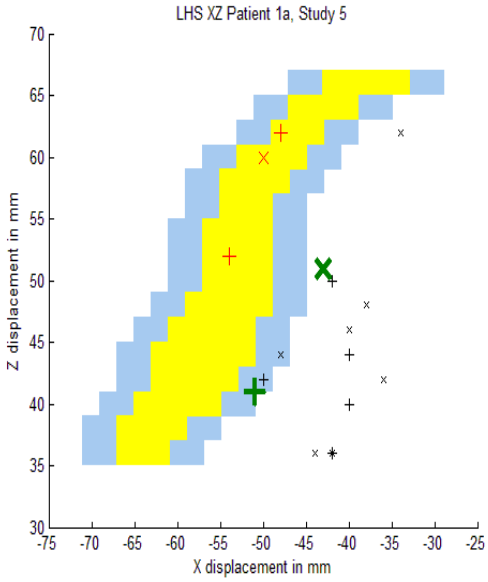

C)

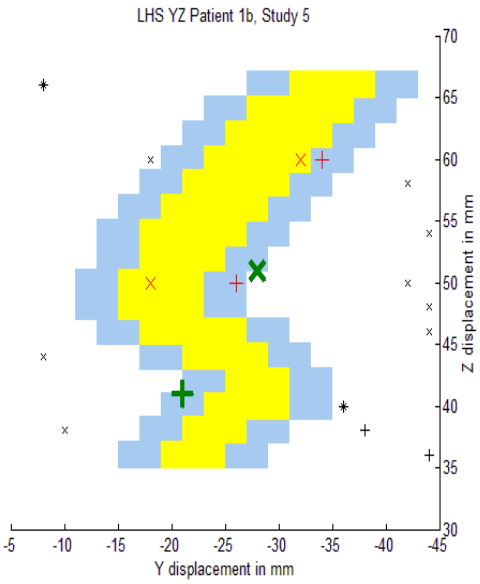

D)

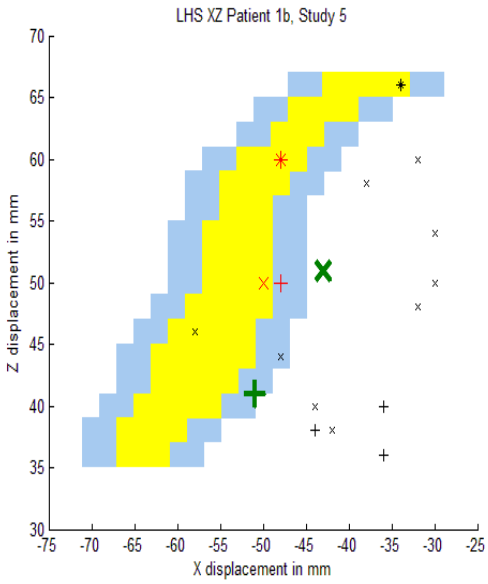

Figure 70: The SI activations for the right hand side of the brain (left *unaffected* D1 and D5) for patient 1, study 5, over Brodmann area 1 (yellow) with a 4 mm error margin in x and y (blue). Panels A and B show the data from the first scans and panels C and D show the data from the second scans taken a few months later after some improvement in the patient's symptoms. An uncorrected p value threshold of ≤ 0.001 was applied (T-score ≥ 3.11). The activations which fall within the area bounded by blue in x, y and z are denoted by a larger marker. Those which also have a T-score ≥ 4 are coloured red. The mean location of the SI activation from other studies (Table 1) are shown by the large green markers. All data plotted in MNI coordinates. D1 activation = '+', D5 activation = 'X'.

A)

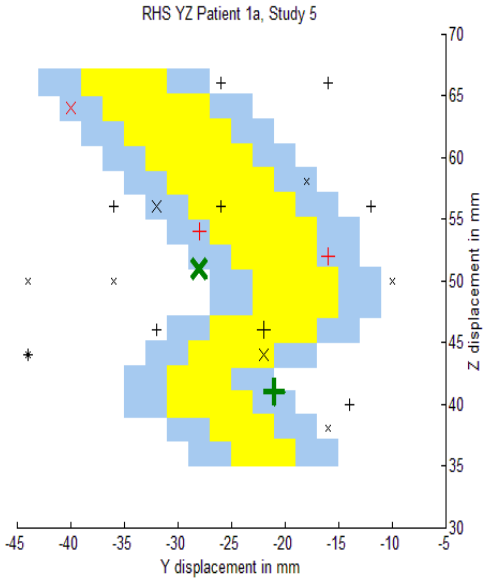

B)

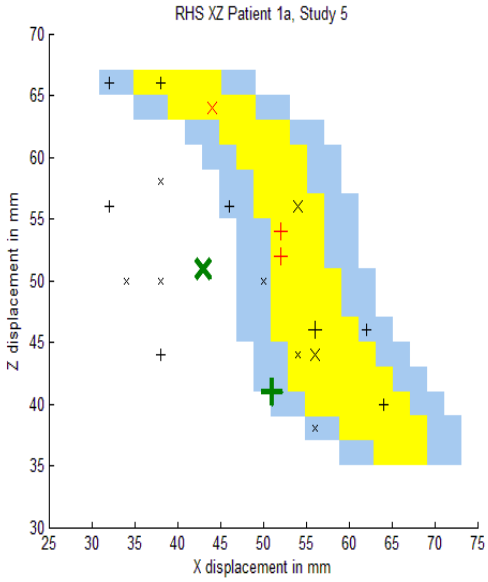

C)

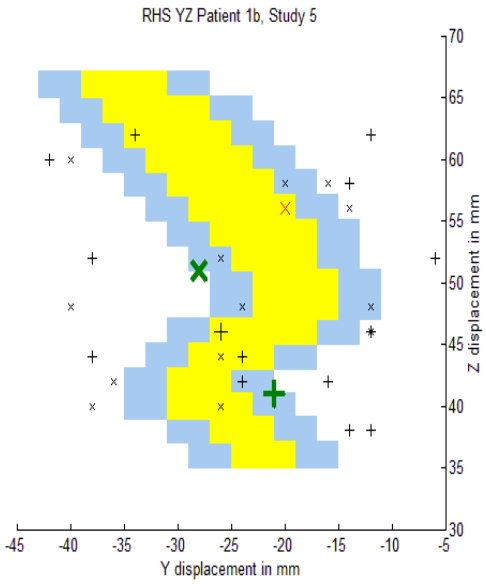

D)

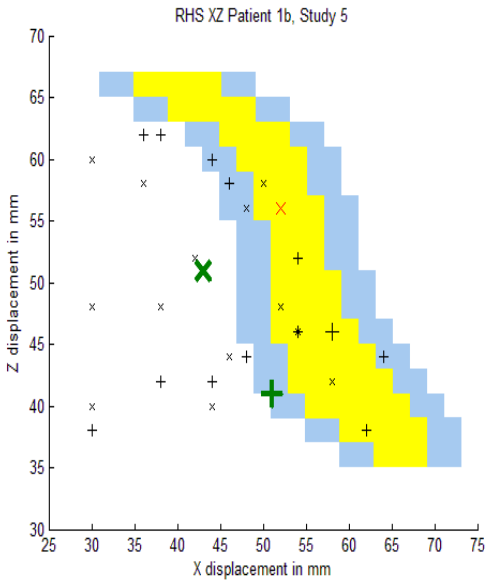

Figure 71: The SI activations for the left hand side of the brain (right *unaffected* D1 and D5) for patient 2, study 5, over Brodmann area 1 (yellow) with a 4 mm error margin in x and y (blue). Panels A and B show the data from the first scans and panels C and D show the data from the second scans taken a few months later after some improvement in the patient's symptoms. An uncorrected p value threshold of ≤ 0.001 was applied (T-score ≥ 3.11). The activations which fall within the area bounded by blue in x, y and z are denoted by a larger marker. Those which also have a T-score ≥ 4 are coloured red. The mean location of the SI activation from other studies (Table 1) are shown by the large green markers. All data plotted in MNI coordinates. D1 activation = '+', D5 activation = 'X'.

A)

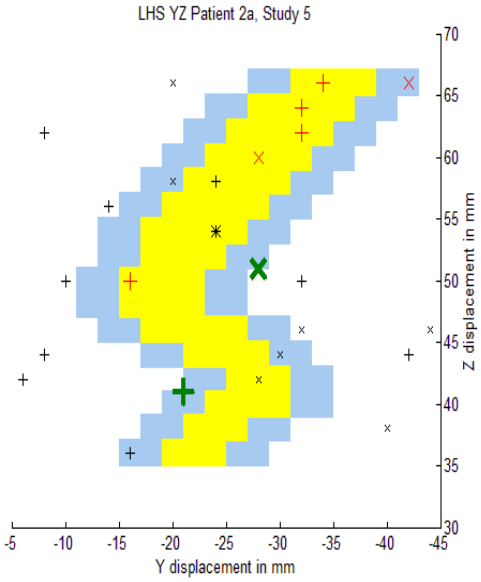

B)

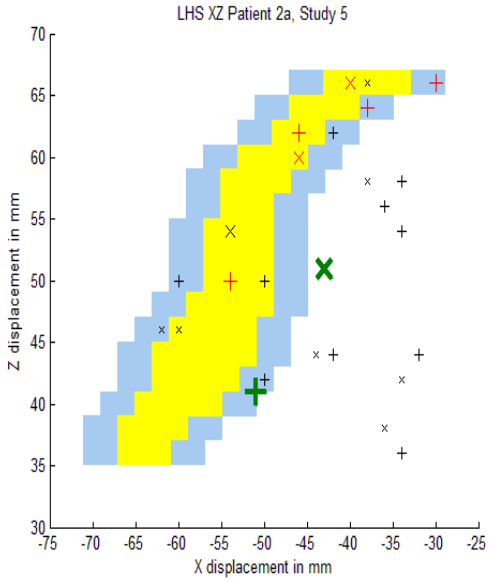

C)

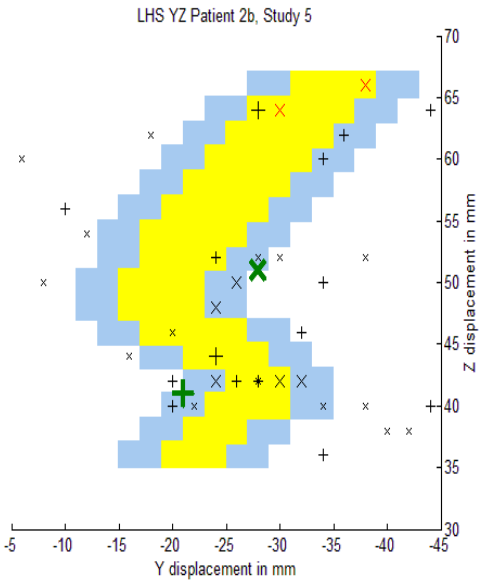

D)

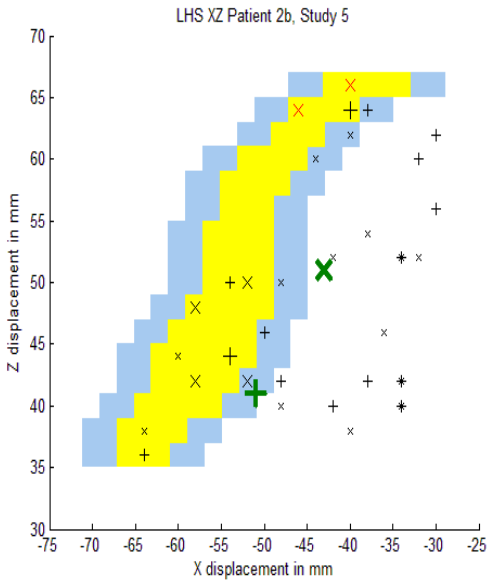

Figure 72: The SI activations for the right hand side of the brain (left *CRPS* D1 and D5) for patient 2, study 5, over Brodmann area 1 (yellow) with a 4 mm error margin in x and y (blue). Panels A and B show the data from the first scans and panels C and D show the data from the second scans taken a few months later after some improvement in the patient's symptoms. An uncorrected p value threshold of ≤ 0.001 was applied (T-score ≥ 3.11). The activations which fall within the area bounded by blue in x, y and z are denoted by a larger marker. Those which also have a T-score ≥ 4 are coloured red. The mean location of the SI activation from other studies (Table 1) are shown by the large green markers. All data plotted in MNI coordinates. D1 activation = '+', D5 activation = 'X'.

A)

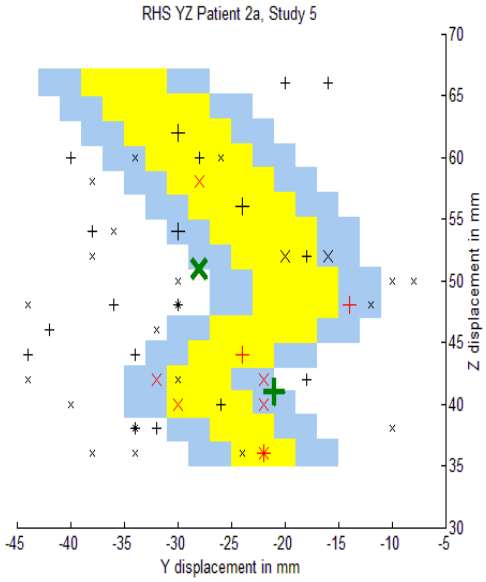

B)

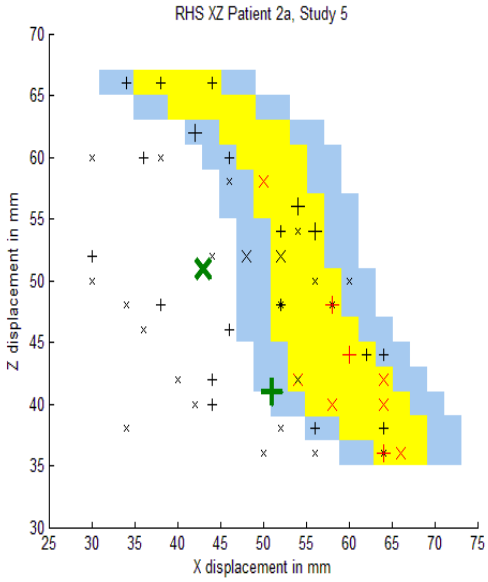

C)

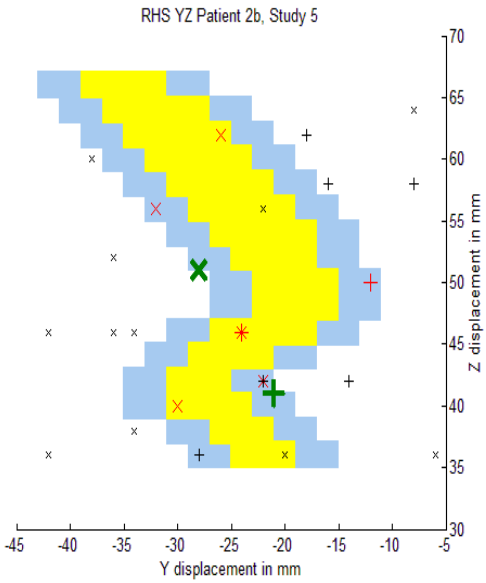

D)

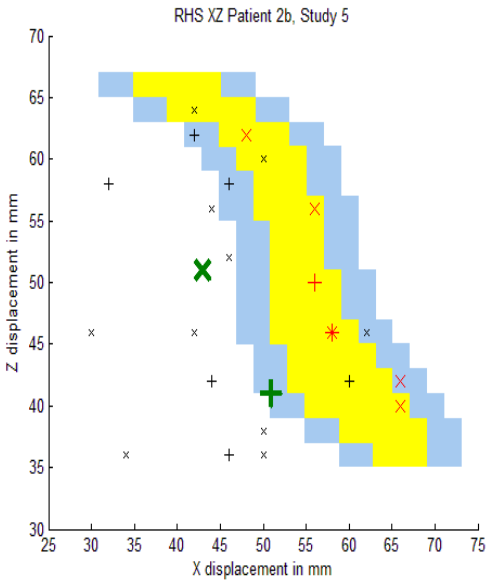

Figure 73: The SI activations for the left hand side of the brain (right *CRPS* D1 and D5) for patient 3, study 5, over Brodmann area 1 (yellow) with a 4 mm error margin in x and y (blue). Panels A and B show the data from the first scans and panels C and D show the data from the second scans taken a few months later after some improvement in the patient's symptoms. An uncorrected p value threshold of ≤ 0.001 was applied (T-score ≥ 3.11). The activations which fall within the area bounded by blue in x, y and z are denoted by a larger marker. Those which also have a T-score ≥ 4 are coloured red. The mean location of the SI activation from other studies (Table 1) are shown by the large green markers. All data plotted in MNI coordinates. D1 activation = '+', D5 activation = 'X'.

A)

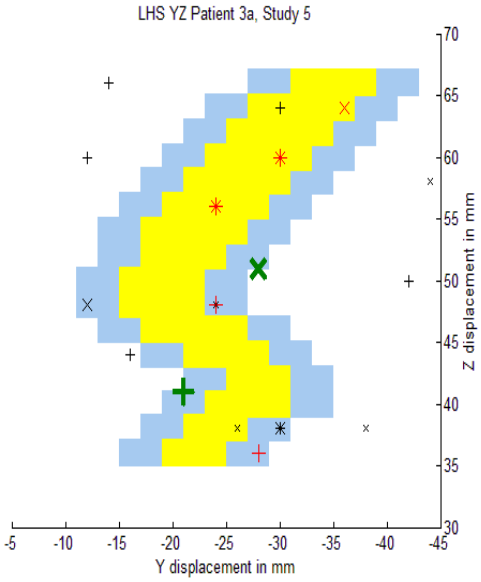

B)

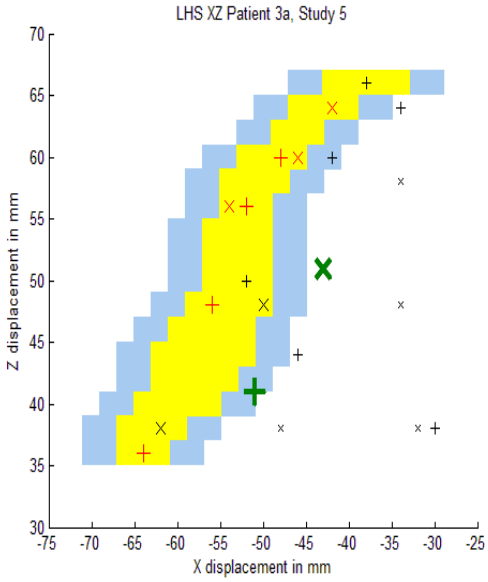

C)

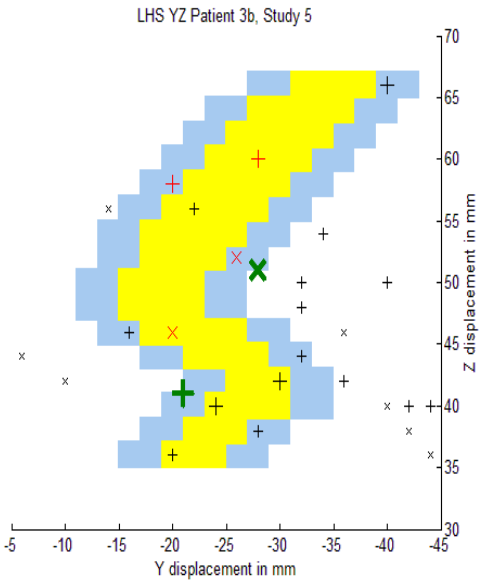

D)

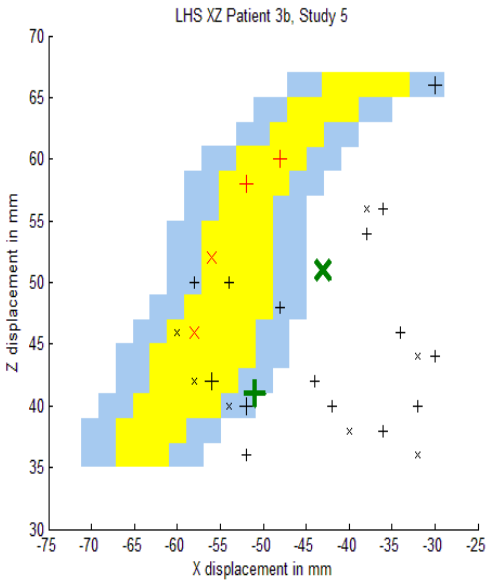

Figure 74: The SI activations for the right hand side of the brain (left *unaffected* D1 and D5) for patient 3, study 5, over Brodmann area 1 (yellow) with a 4 mm error margin in x and y (blue). Panels A and B show the data from the first scans and panels C and D show the data from the second scans taken a few months later after some improvement in the patient's symptoms. An uncorrected p value threshold of ≤ 0.001 was applied (T-score ≥ 3.11). The activations which fall within the area bounded by blue in x, y and z are denoted by a larger marker. Those which also have a T-score ≥ 4 are coloured red. The mean location of the SI activation from other studies (Table 1) are shown by the large green markers. All data plotted in MNI coordinates. D1 activation = '+', D5 activation = 'X'.

A)

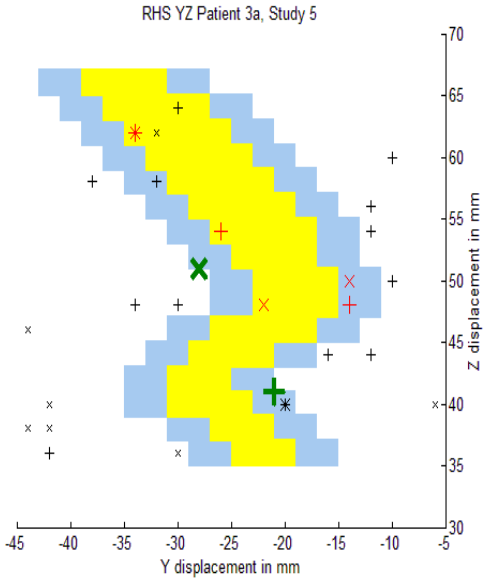

B)

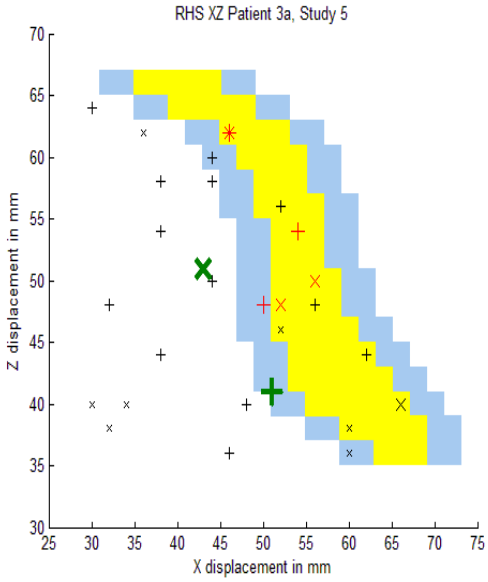

C)

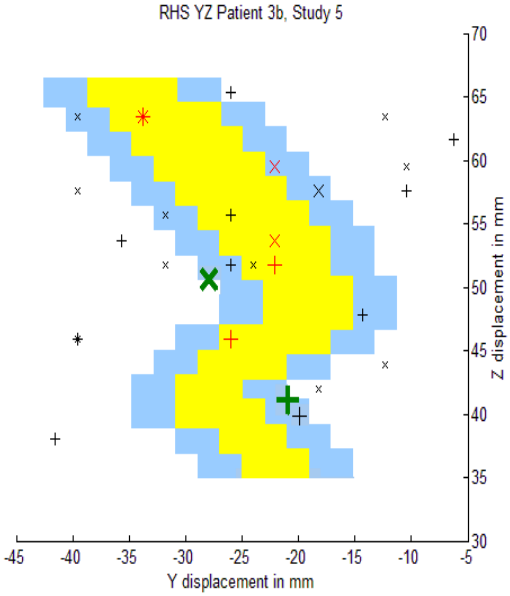

D)

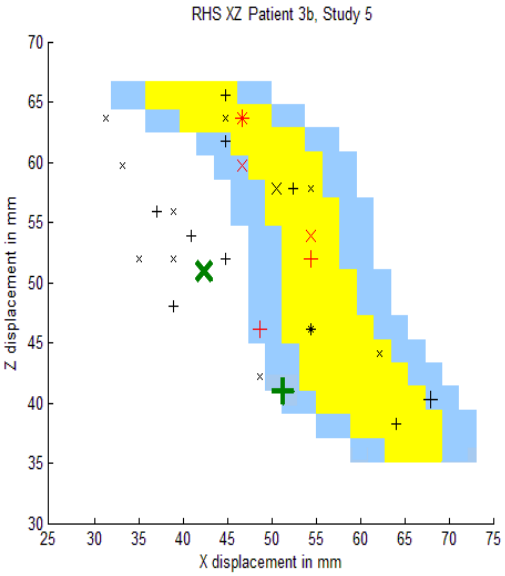

Figure 75: The SI activations for the left hand side of the brain (right *CRPS* D1 and D5) for patient 4, study 5, over Brodmann area 1 (yellow) with a 4 mm error margin in x and y (blue). Panels A and B show the data from the first scans and panels C and D show the data from the second scans taken a few months later after some improvement in the patient's symptoms. An uncorrected p value threshold of ≤ 0.001 was applied (T-score ≥ 3.11). The activations which fall within the area bounded by blue in x, y and z are denoted by a larger marker. Those which also have a T-score ≥ 4 are coloured red. The mean location of the SI activation from other studies (Table 1) are shown by the large green markers. All data plotted in MNI coordinates. D1 activation = '+', D5 activation = 'X'.

A)

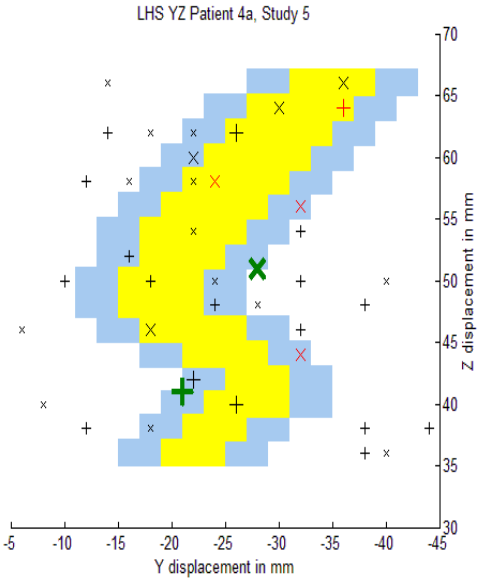

B)

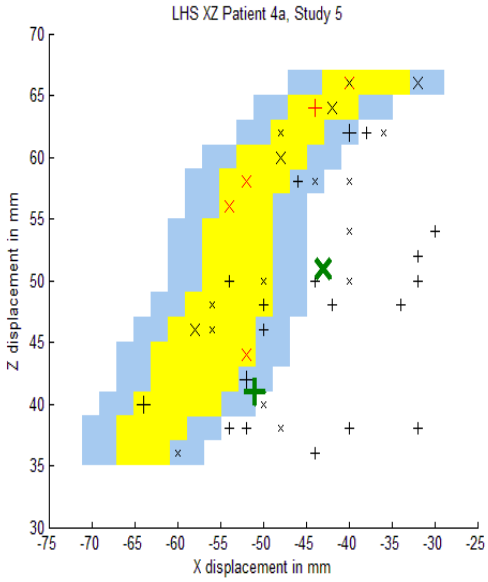

C)

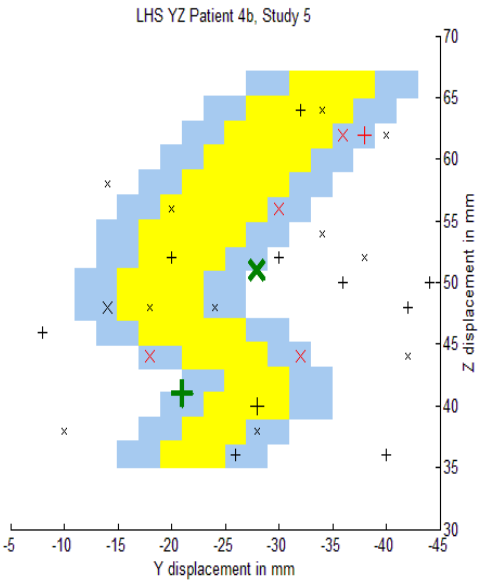

D)

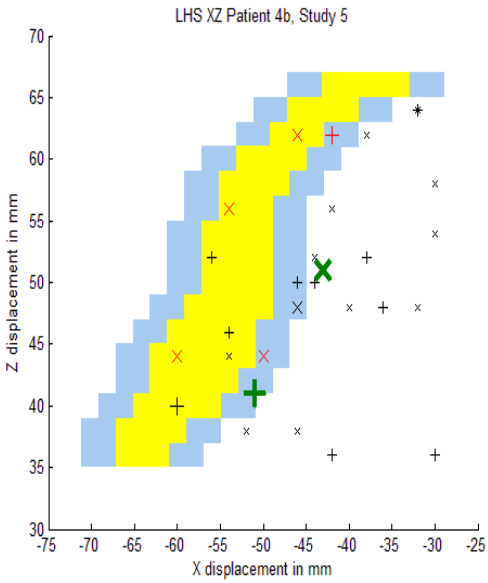

Figure 76: The SI activations for the right hand side of the brain (left *unaffected* D1 and D5) for patient 4, study 5, over Brodmann area 1 (yellow) with a 4 mm error margin in x and y (blue). Panels A and B show the data from the first scans and panels C and D show the data from the second scans taken a few months later after some improvement in the patient's symptoms. An uncorrected p value threshold of ≤ 0.001 was applied (T-score ≥ 3.11). The activations which fall within the area bounded by blue in x, y and z are denoted by a larger marker. Those which also have a T-score ≥ 4 are coloured red. The mean location of the SI activation from other studies (Table 1) are shown by the large green markers. All data plotted in MNI coordinates. D1 activation = '+', D5 activation = 'X'.

A)

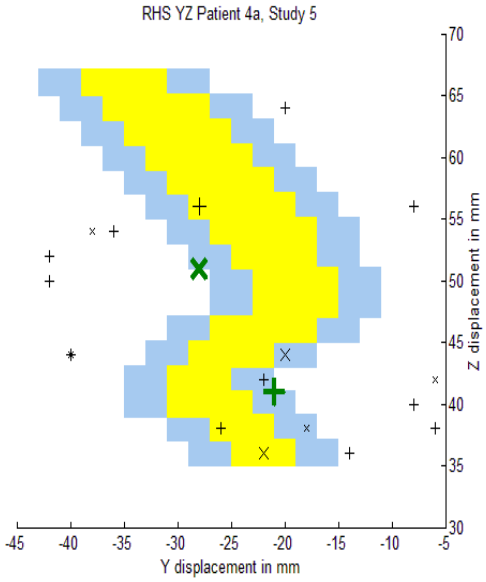

B)

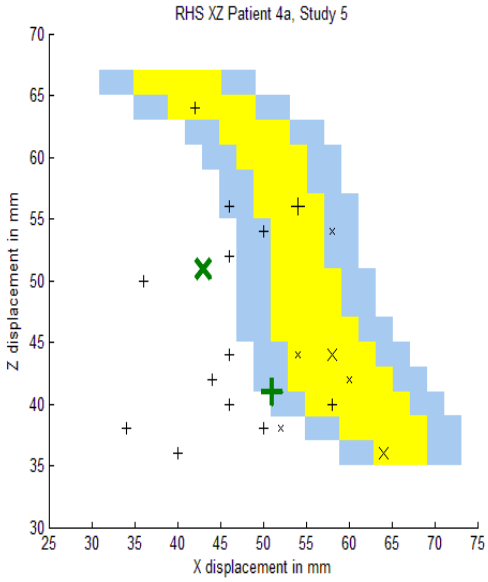

C)

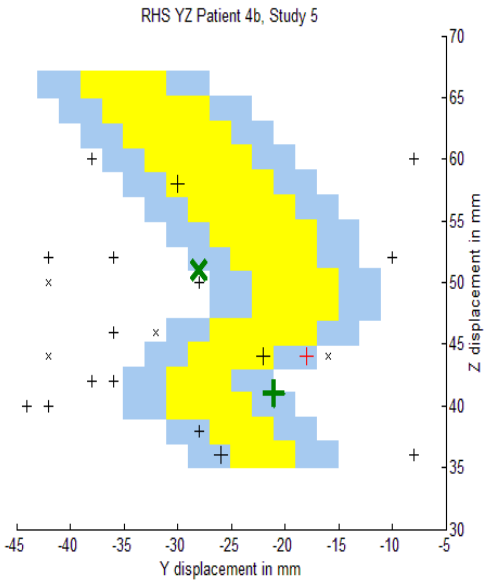

D)

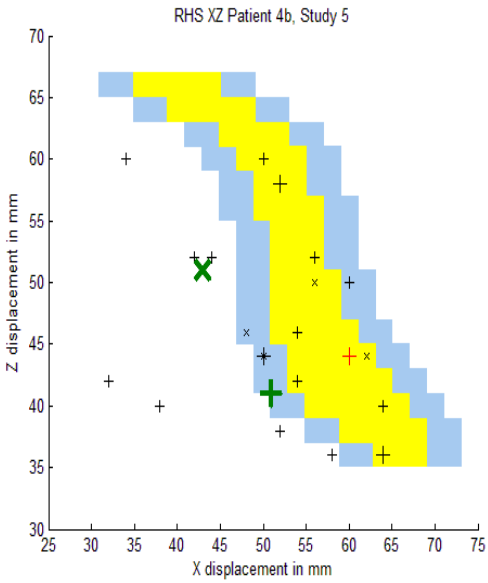

Figure 77: The SI activations for control 1, study 5, over Brodmann area 1 (yellow) with a 4 mm error margin in x and y (blue). An uncorrected p value threshold of ≤ 0.001 was applied (T-score ≥ 3.11). The activations which fall within the area bounded by blue in x, y and z are denoted by a larger marker. Those which also have a T-score ≥ 4 are coloured red. The mean location of the SI activation from other studies (Table 1) are shown by the large green markers. All data plotted in MNI coordinates. D1 activation = '+', D5 activation = 'X'.

A)

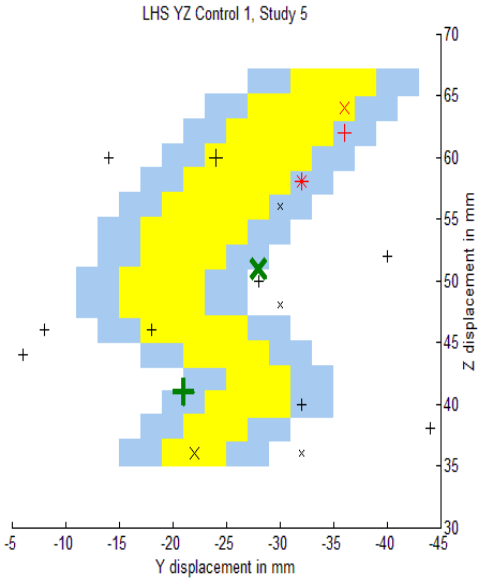

B)

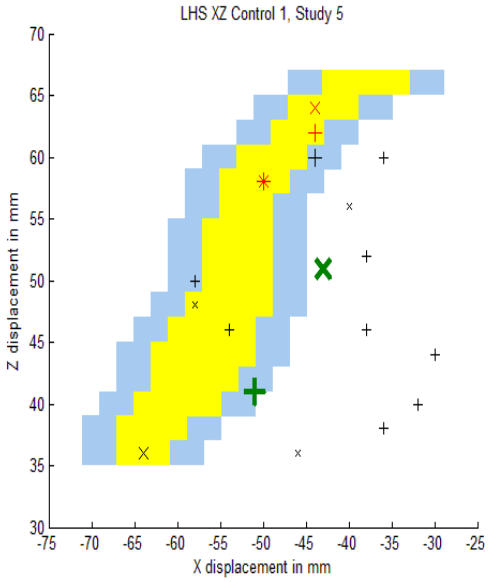

C)

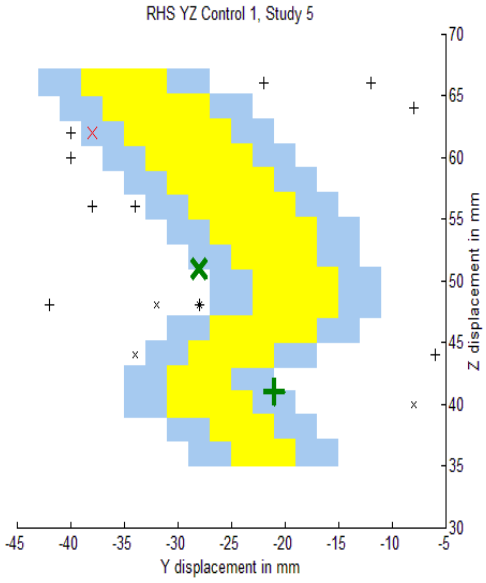

D)

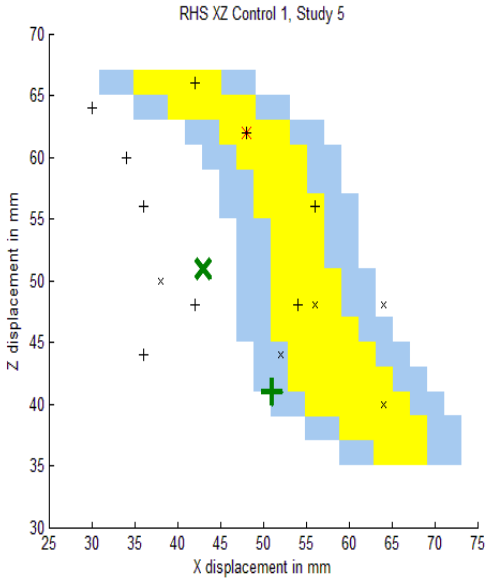

Figure 78: The SI activations for control 2, study 5 over Brodmann area 1 (yellow) with a 4 mm error margin in x and y (blue). An uncorrected p value threshold of ≤ 0.001 was applied (T-score ≥ 3.11). The activations which fall within the area bounded by blue in x, y and z are denoted by a larger marker. Those which also have a T-score ≥ 4 are coloured red. The mean location of the SI activation from other studies (Table 1) are shown by the large green markers. All data plotted in MNI coordinates. D1 activation = '+', D5 activation = 'X'.

A)

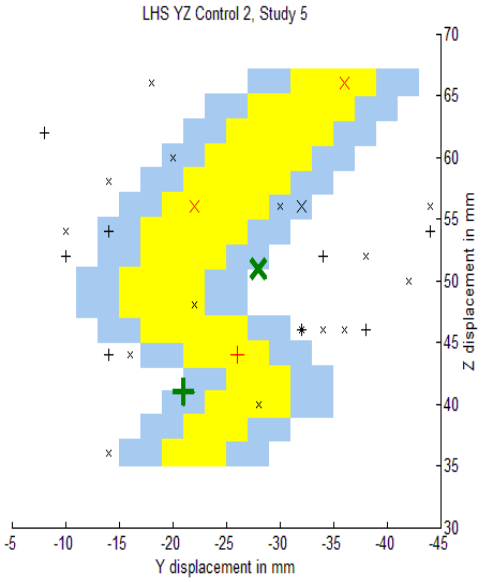

B)

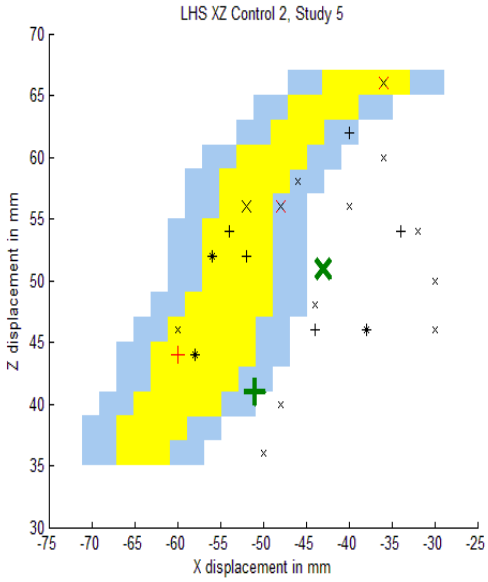

C)

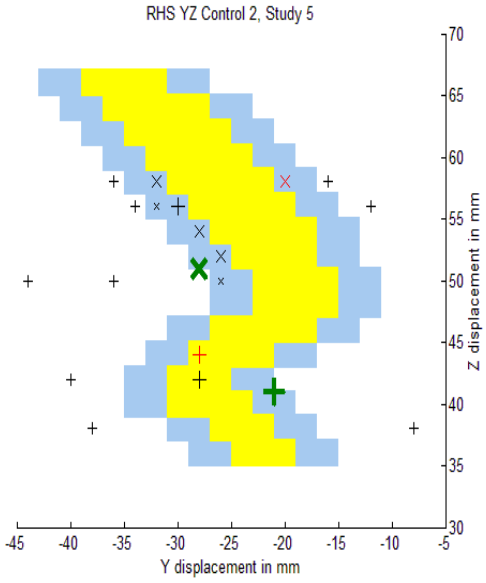

D)

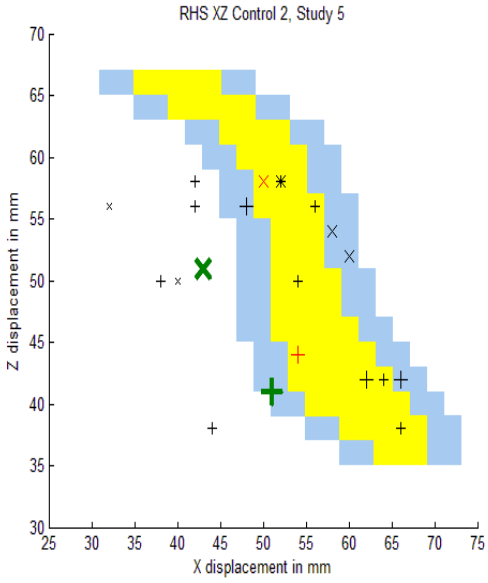

Figure 79: The SI activations for control 3, study 5 over Brodmann area 1 (yellow) with a 4 mm error margin in x and y (blue). An uncorrected p value threshold of ≤ 0.001 was applied (T-score ≥ 3.11). The activations which fall within the area bounded by blue in x, y and z are denoted by a larger marker. Those which also have a T-score ≥ 4 are coloured red. The mean location of the SI activation from other studies (Table 1) are shown by the large green markers. All data plotted in MNI coordinates. D1 activation = '+', D5 activation = 'X'.

A)

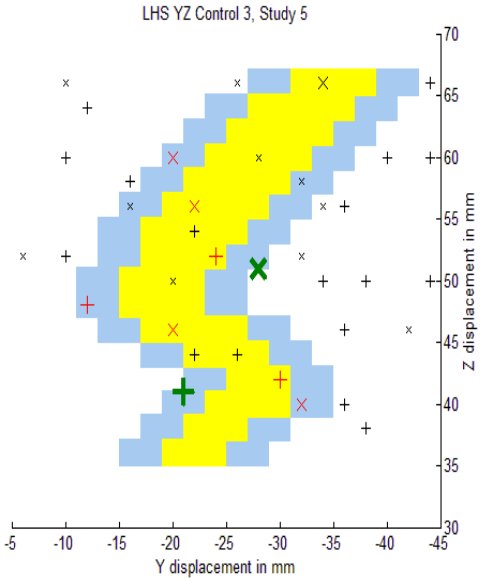

B)

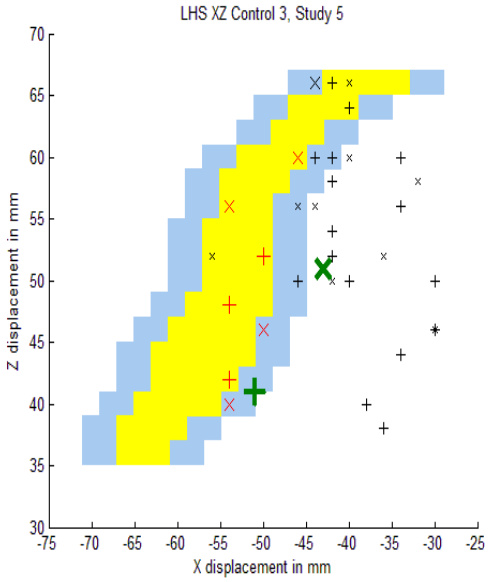

C)

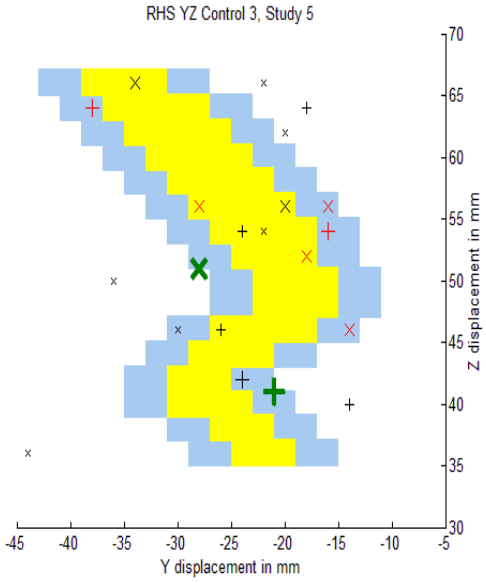

D)

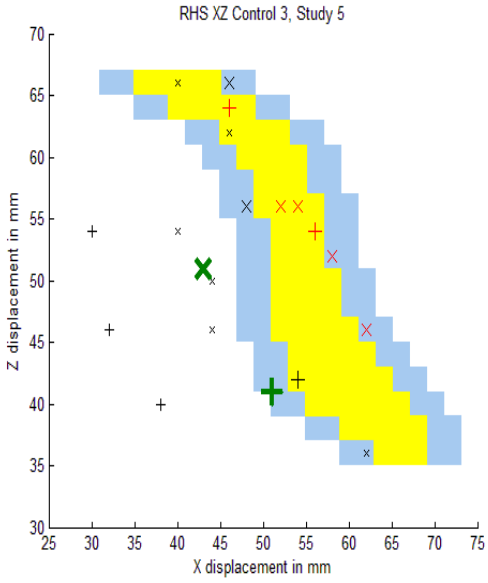

Figure 80: The SI activations for control 4, study 5 over Brodmann area 1 (yellow) with a 4 mm error margin in x and y (blue). An uncorrected p value threshold of ≤ 0.001 was applied (T-score ≥ 3.11). The activations which fall within the area bounded by blue in x, y and z are denoted by a larger marker. Those which also have a T-score ≥ 4 are coloured red. The mean location of the SI activation from other studies (Table 1) are shown by the large green markers. All data plotted in MNI coordinates. D1 activation = '+', D5 activation = 'X'.

A)

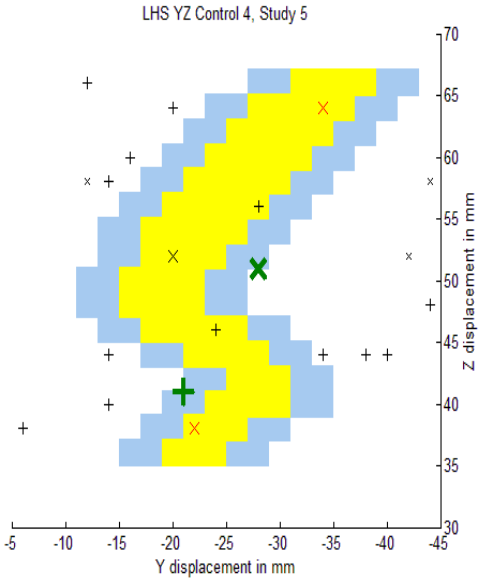

B)

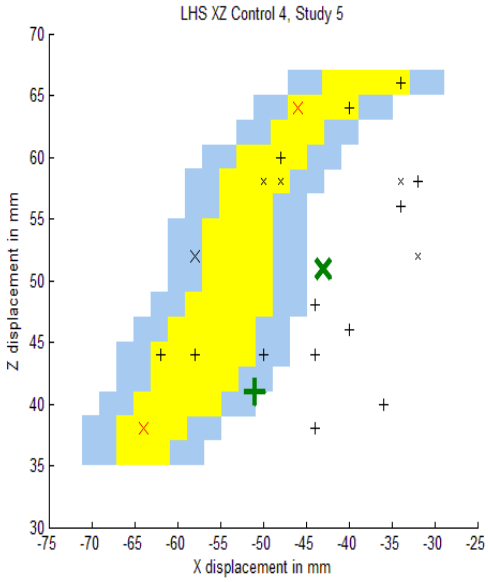

C)

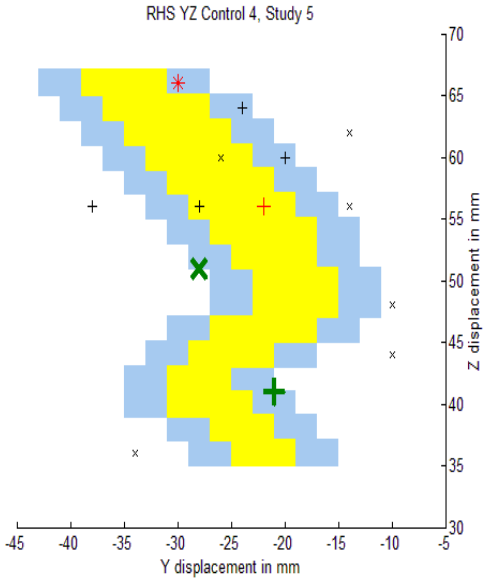

D)

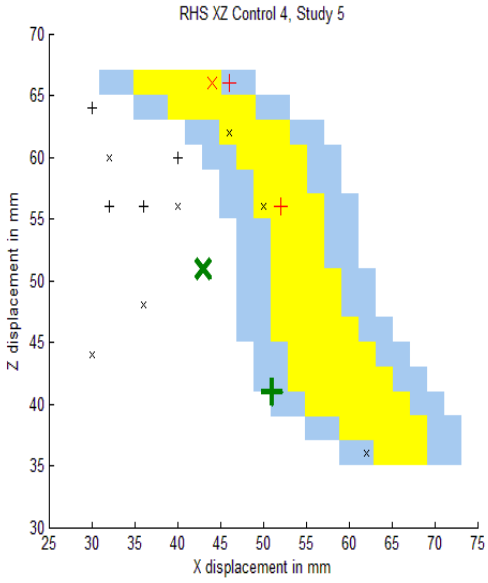

Figure 81: The results from the second level analysis of study 5 for the right CRPS digits 1 and 5 on the template brain. The data of patient 2 was flipped so that the CRPS data matched the same side as the other patients. Thresholded at an uncorrected p value ≤ 0.001. SI activations for each digit is indicated by the red arrow.

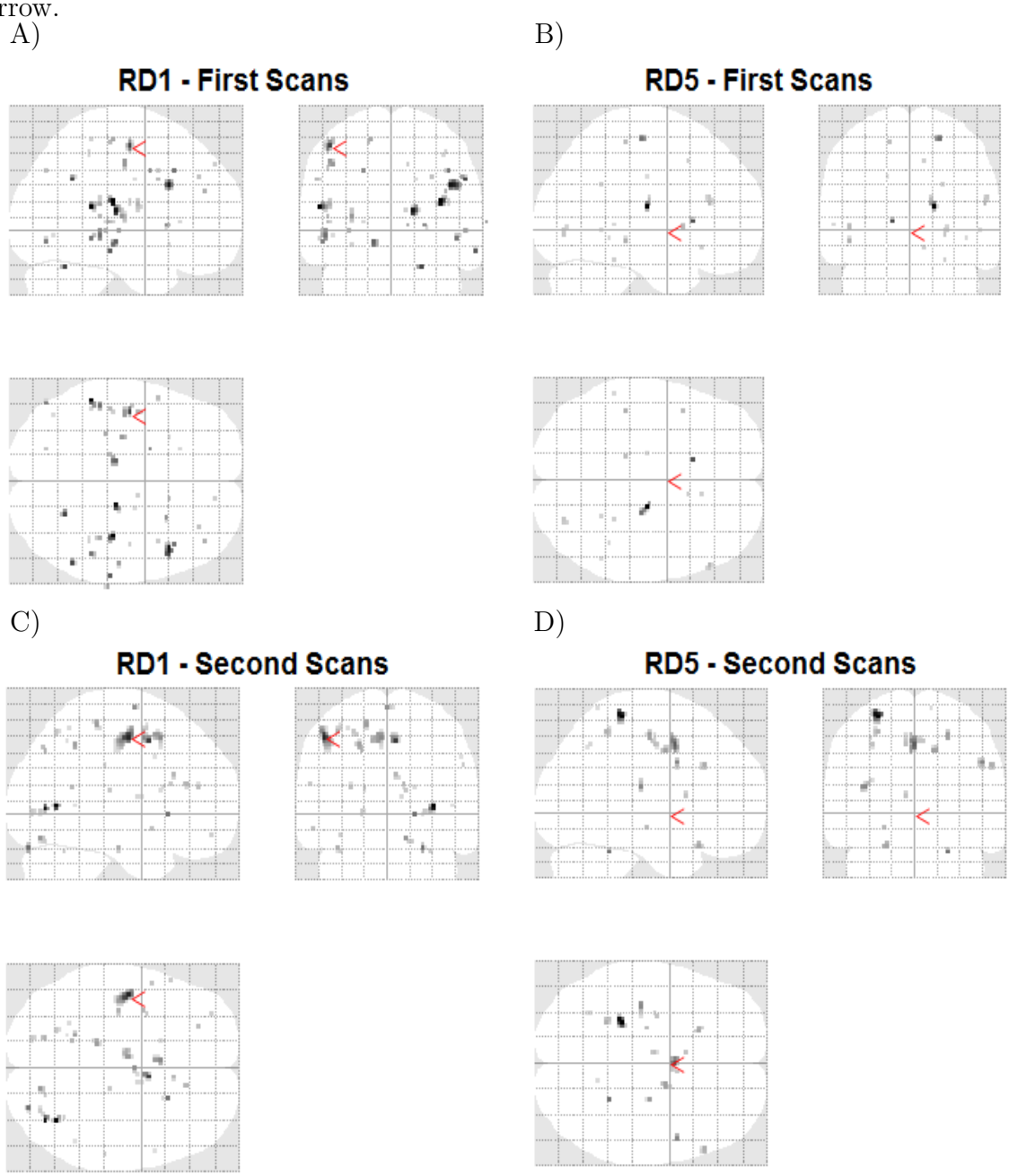

Figure 82: The results from the second level analysis of study 5 for the left unaffected digits 1 and 5 on the template brain. The data of patient 2 was flipped so that the unaffected data matched the same side as the other patients. Thresholded at an uncorrected p value ≤ 0.001. SI activations for each digit is indicated by the red arrow.

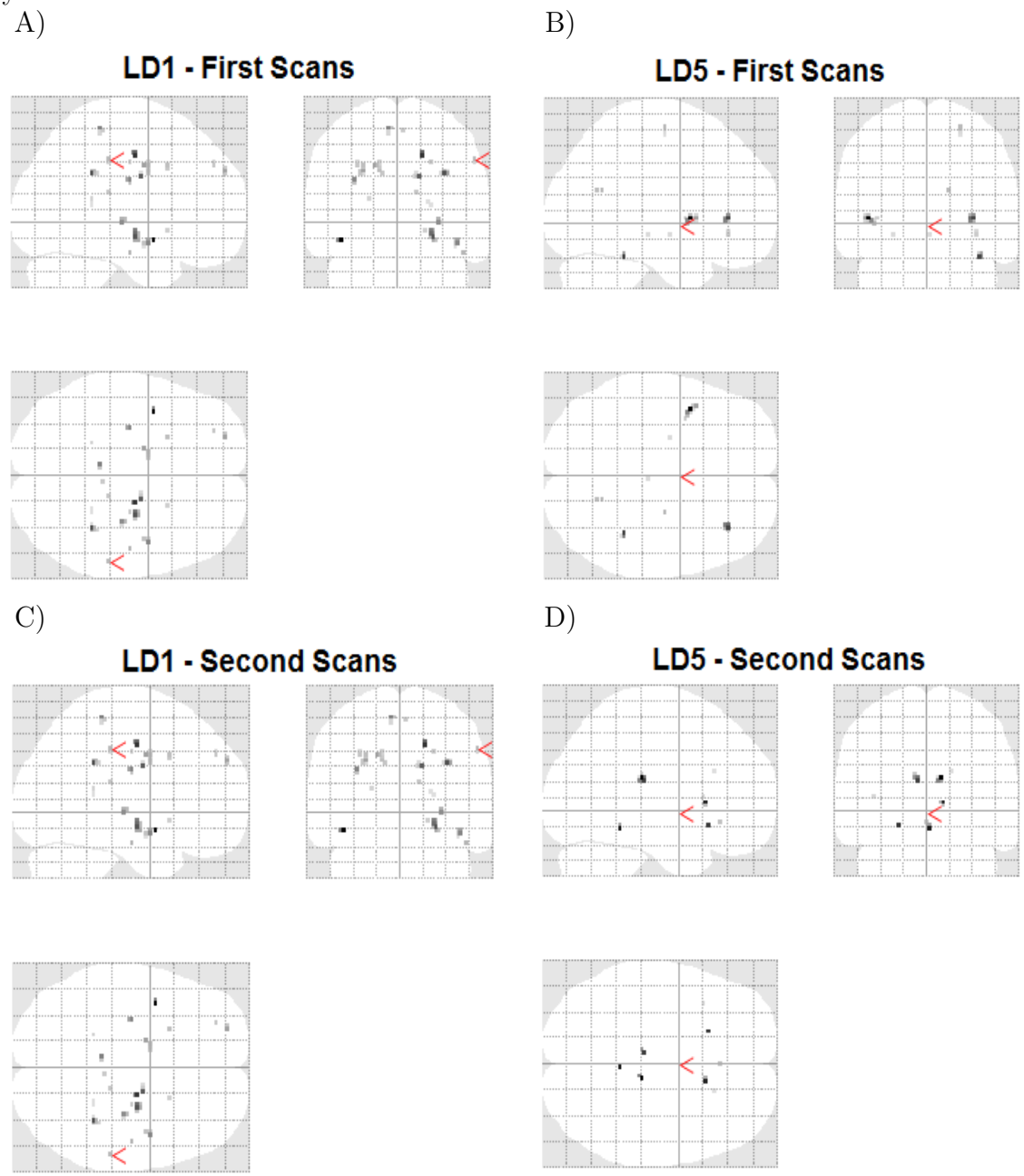

Figure 83: Panels A and B show the group SI activations for the right CRPS digits 1 and 5 overlaid on BA1 (yellow) and determined using the data from the first patient scans in study 5. The data for patient 2 has been flipped so that the CRPS hand data now appears on the LHS of the brain. Panels C and D show the group SI activations for the same hand but determined using the data from the second scans. A 4 mm error margin in x and y (blue) has been added and all coordinates are plotted in MNI coordinates. D1 = '+' and D5 = 'X'. The mean location of the SI activation from other studies (Table 1) are shown by the large green markers. An uncorrected p value threshold of ≤ 0.001 was applied (T-score ≥ 3.11). The activations which fall within the area bounded by blue in x, y and z are denoted by larger markers and those which also have a T-score ≥ 4 are coloured red.

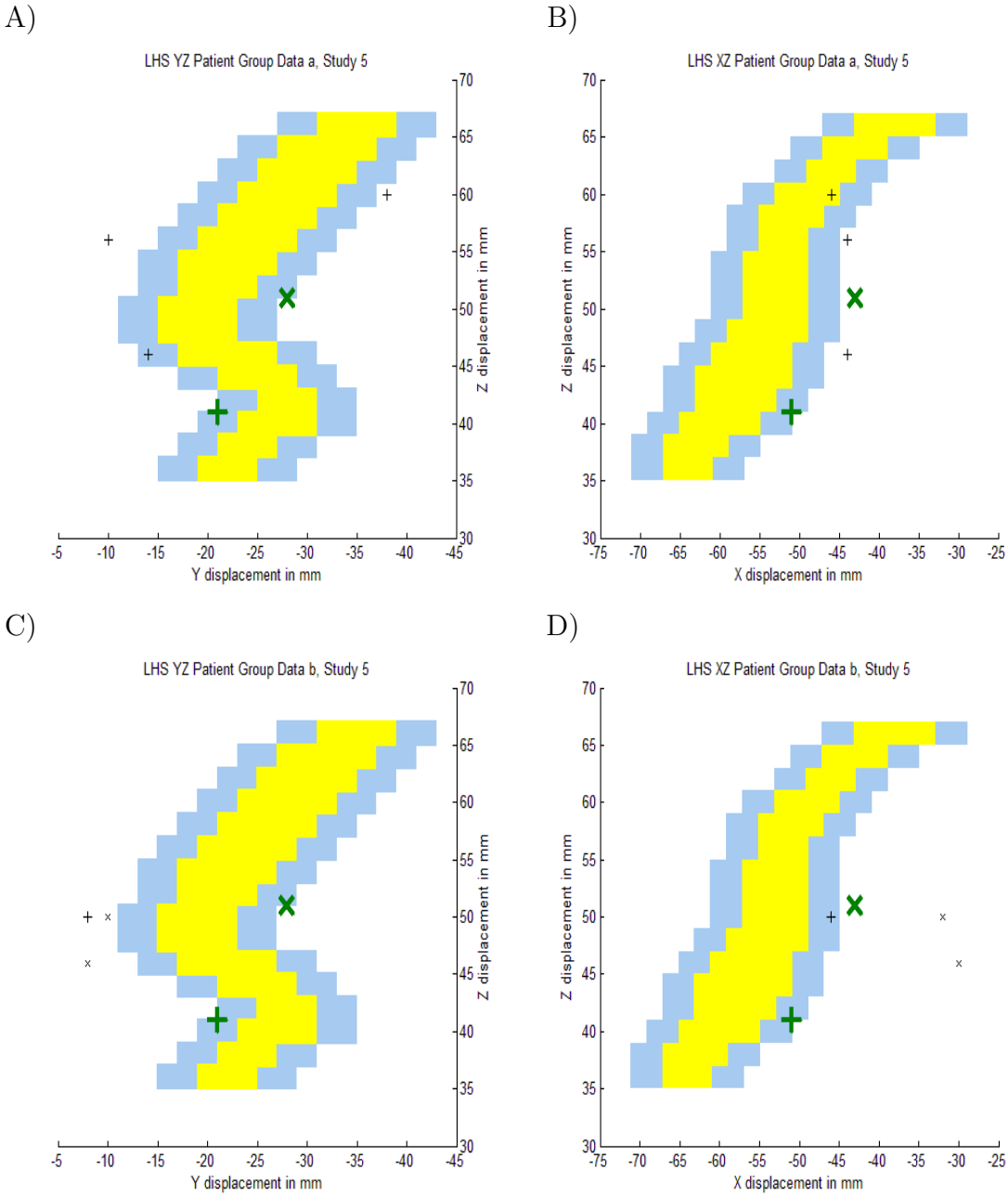

Figure 84: Panels A and B show the group SI activations for the left unaffected digits 1 and 5 overlaid on BA1 (yellow) and determined using the data from the first patient scans in study 5. The data for patient 2 has been flipped so that the unaffected hand data now appears on the RHS of the brain. Panels C and D show the group SI activations for the same hand but determined using the data from the second scans. A 4 mm error margin in x and y (blue) has been added and all coordinates are plotted in MNI coordinates. The mean location of the SI activation from other studies (Table 1) are shown by the large green markers. D1 = '+' and D5 = 'X'. An uncorrected p value threshold of ≤ 0.001 was applied (T-score ≥ 3.11). The activations which fall within the area bounded by blue in x, y and z are denoted by larger markers and those which also have a T-score ≥ 4 are coloured red.

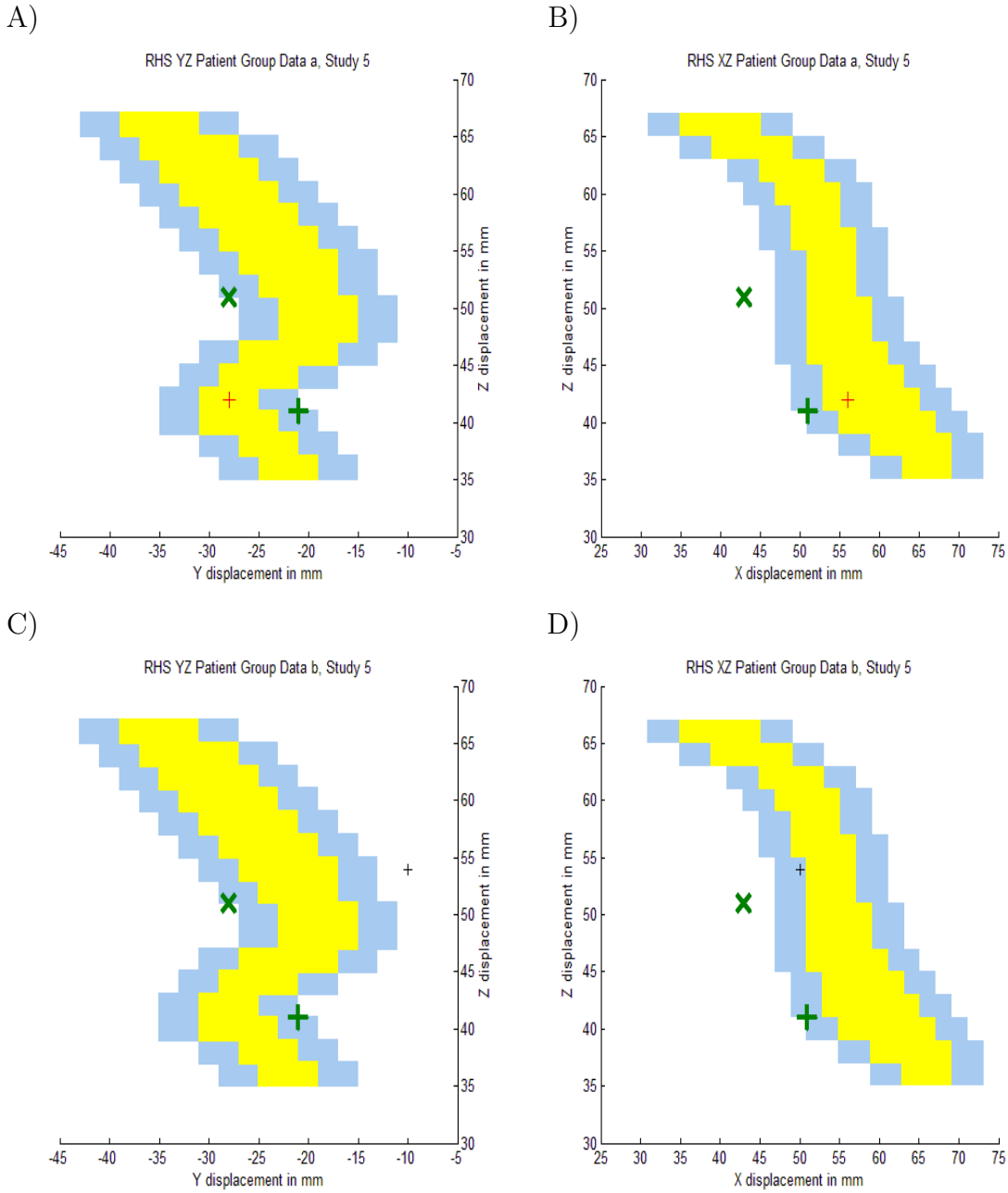

Figure 85: The results from the second level analysis of the control group data, study 5, for each digit on the template brain. Thresholded at an uncorrected p value ≤ 0.001. SI activations for each digit is indicated by the red arrow.

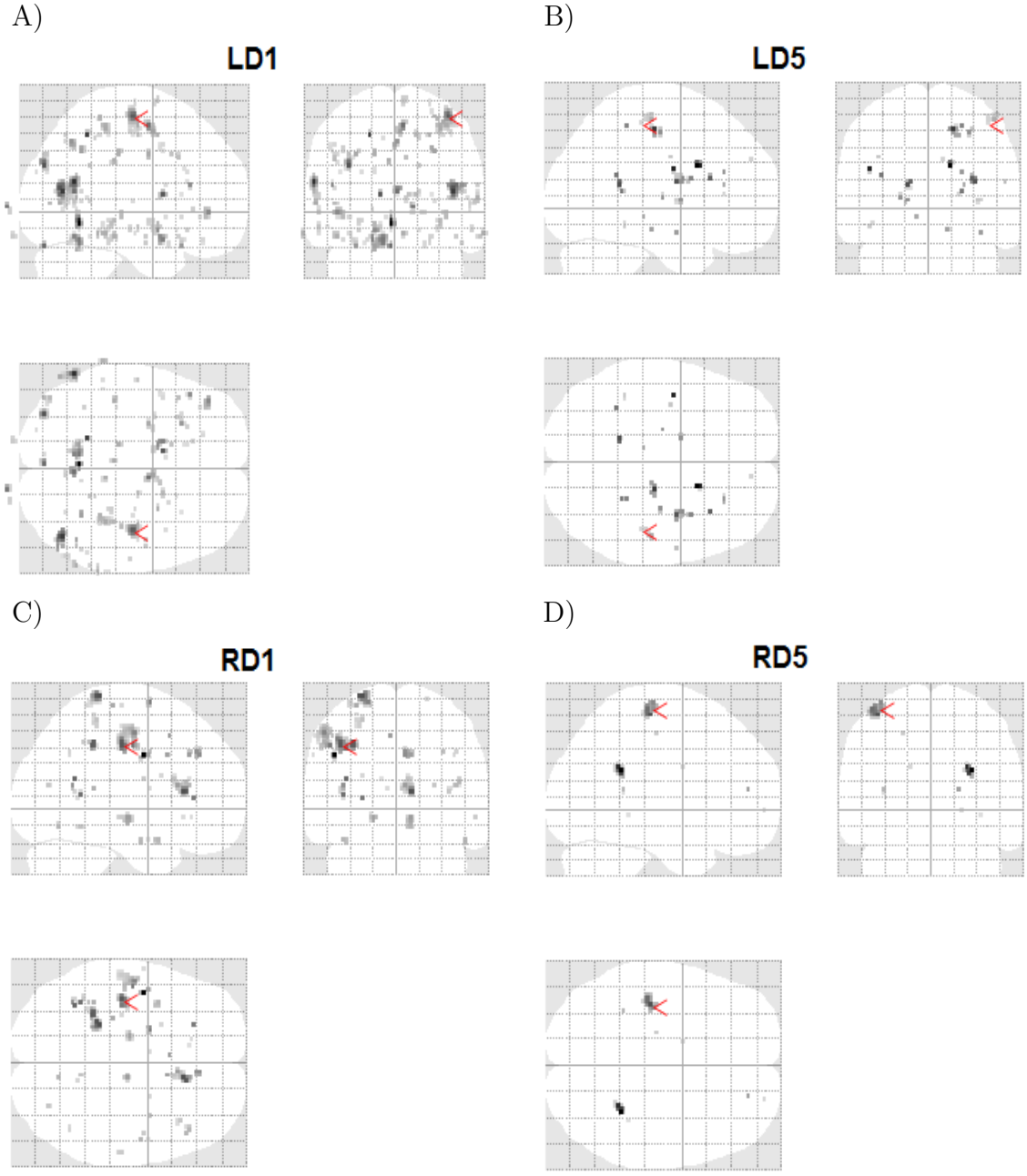

Figure 86: The SI activations from the control group analysis for study 5 overlaid on BA1 (yellow), 4 mm error margin in x and y (blue), plotted in MNI coordinates. D1 = '+' and D5 = 'X'. An uncorrected p value threshold of ≤ 0.001 was applied (T-score ≥ 3.11). The activations which fall within the area bounded by blue in x, y and z are denoted by larger markers and those which also have a T-score ≥ 4 are coloured red. The mean location of the SI activation from other studies (Table 1) are shown by the large green markers.

A)

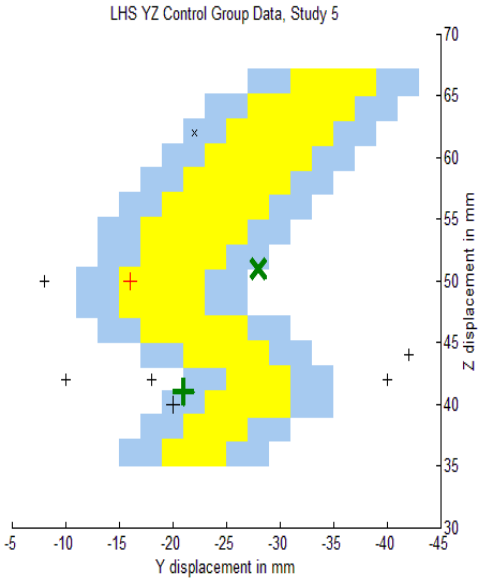

B)

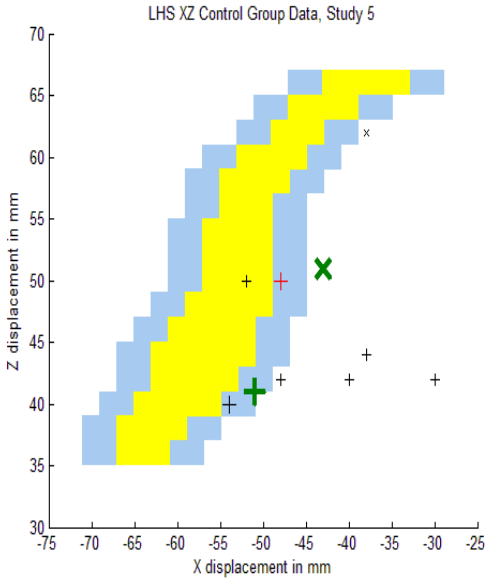

C)

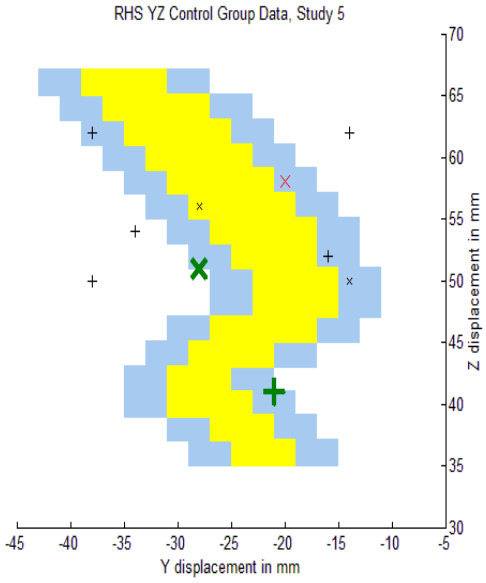

D)

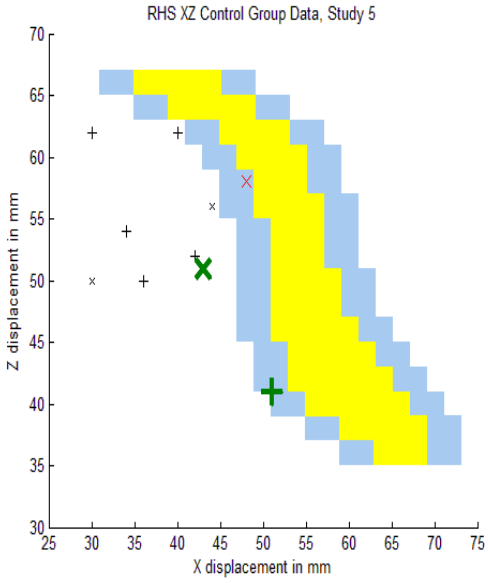

Figure 87: The centre of mass of all activations within BA1 for each patient for the first and second scans and for the patient controls in study 5. They are plotted over BA1. D1 data is indicated by '+' and D5 data by 'X' and each subject pair is connected by a line. The CRPS digit data are in panels A and B, the data from the first scans are in red and the data from the second scans are in green. The control data is also shown in black. Panels C and D show the unaffected patient data, first scans data is in red and the second scans data is in green, control subject data in black. All data plotted in MNI coordinates.

A)

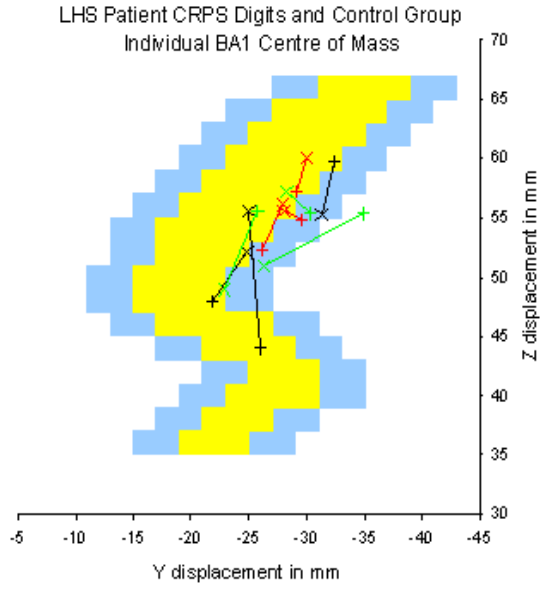

B)

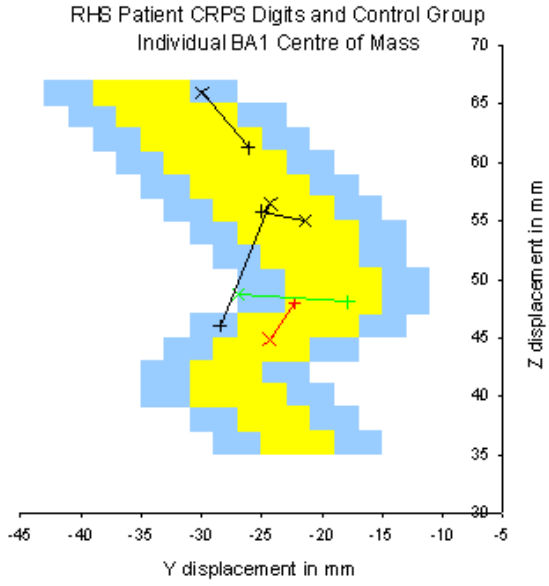

C)

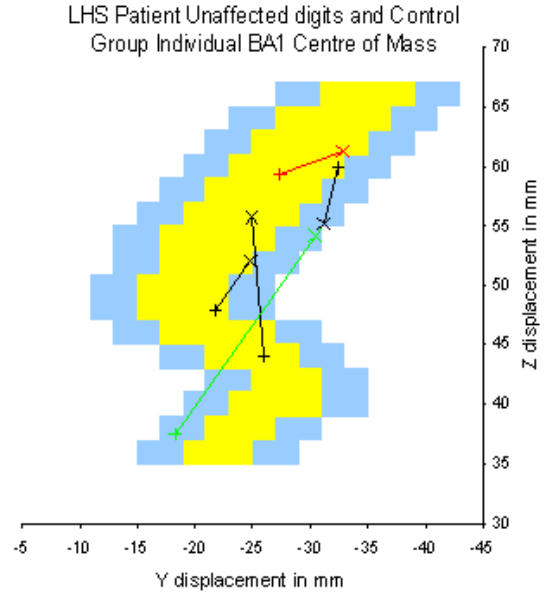

D)

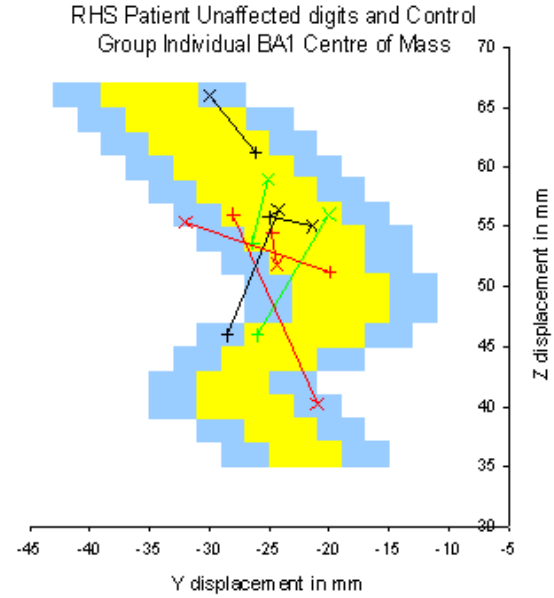

Chapter 9

Discussion

9.1 Introduction

The first aim of this project was to develop a stimulation protocol that reliably produced robust SI activation and allowed the cortical digit separation to be accurately determined from individual subject data. Studies 1 to 4 addressed this aim by testing a number of protocols and the results (Chapter 8) were assessed using various parameters, including the T-scores of the most activated voxels and the locations of the centre of mass of the SI activations. A protocol was successfully developed to produce activity in the somatosensory cortices of subjects, however, it was not possible to reliably measure the separation between the cortical representations of the digits, essentially because of uncertainty in identifying a principal activation site and tracking its movement.

The second aim of the project was to determine if there were differences in the SI activations of complex regional pain syndrome patients compared to a control group. It was hypothesised that in CRPS patients the activations for the affected digits would be of different size than in the control group and that the separations of the cortical representations would be closer together. Study 5 was carried out to look for these possible CRPS-related changes in comparison to control subjects, no differences were detected in the location of the activations or in the cortical separation of the digits. In one patient a smaller SI cluster size was detected, in

one patient there was a larger SI cluster size and in two patients the size of the activation was within normal limits. Also, within the patient group, comparison between the CRPS-affected and unaffected hands showed larger cluster sizes for the affected hand in 3 patients.

The results of each study are discussed in detail below.

9.2 Study 1

In study 1, each scanning session involved stimulation of the two selected digits in a single hand, using a random sequence of D1 and D5 stimulation. Multiple SI activations were found for each digit. The detection of so many activation centres in the single-subject data was, at the time, unexpected. With hindsight, however the idea of multiple activations within each Brodmann area (BA1, BA2, BA3a, BA3b) with each centre showing more or less movement in response to change of stimulus location, seems entirely plausible (see, for example, the detailed studies of BA3b by van Westen et al. [6] and Kurth et al. [10]).

The separations between the digit representations were also smaller than expected as the D1 and D5 SI activations were distributed throughout the region. An overlap between the SI activations of the digits has also been found in other somatosensory imaging studies [3, 7, 10, 112]. However, in this study, as stimulation to both digits was carried out in the same scanning session, it is possible that activations relating to D1 stimulation were evoked by D5 stimulation, and vice versa, perhaps due to anticipation or concentration by the subject. This may also explain the smaller-than-expected cortical separations determined here.

Many somatosensory studies report the ordering of the digits within the SI cortices, with the little finger being more medial, posterior and superior to the thumb (e.g., [2, 3, 6, 7, 10]). A few studies have reported coordinates for either activations within a specific Brodmann area or for the centre of mass of all SI activations [1, 5, 7, 9], and these are shown in Table 1 in Chapter 1.2.1. It is possible to overlay these coordinates on the graph showing the extent of BA1 and

its vicinity and visualise the direction of the movement from D1 to D5, shown in Figure 88. It can be seen that the direction of the movement is not as well defined as some statements in the literature suggest and that the results obtained here are consistent with those obtained by other authors. Of particular relevance are the results obtained by Francis et al. [1], in which it is suggested that RD5 activations are higher in the brain than RD2 activations in the case of four subjects but lower in the brain in the case of two subjects, a similar inconsistency to that seen in all five studies in the present investigation.

9.3 Study 2

In study 2 the stimulation was delivered to a single fingertip (either LD1, LD5, RD1 or RD5) during each scanning session to eliminate the possible effect of D1 and D5 being activated at the same time. The results of this study showed a lower rate of detection of contralateral SI activity and lower T-scores compared to study 1. This could be due to the shorter interstimulus interval that was used. In study 1, the interval was 27 s but in study 2 it was varied between 9 and 27 s. It is possible that a minimum of 9 s was not long enough for the signal from the BOLD response to decrease by a sufficient amount to be detected. However, a fMRI study investigating the pain sensory pathways by Bingel et al. [103] used an interval between 8 to 12 s to produce reliable SI activity. The tactile fMRI study carried out by Kamal [41] employed an interval between 12 to 33 s and the results showed the incidence of SI activity did not increase with increasing duration. This suggests that the longer interstimulus interval in study 1 was not the factor that produced more frequent detection of activity and a random interval between 9 and 27 s was a reasonable period to use. The lower detection rate could also be due to less scans being acquired per digit, 240 versus 300, even though more stimulation events were carried out.

The detection of multiple foci for each digit and the small cortical digit separations were consistent with the results from study 1. As the stimulation to each

Figure 88: The digit SI activations within BA1 that were given by other authors in their papers are plotted on BA1. D1 = '+', D2 = '△', D3 = '◇', D4 = '□' and D5 = 'X'. Lines show each data set. Panel A - LHS of the brain, black [1, 5], red [7]. Panel B - RHS of the brain, black [9]. Where secondary maxima were detected in [9] the average coordinates of the two activations have been plotted. All data plotted in MNI coordinates.

A)

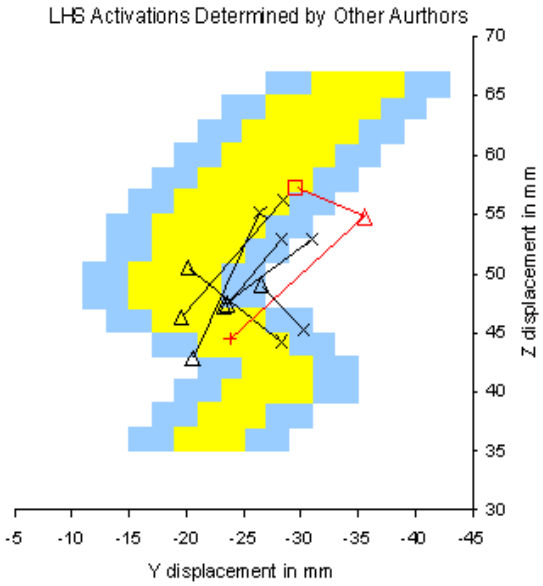

B)

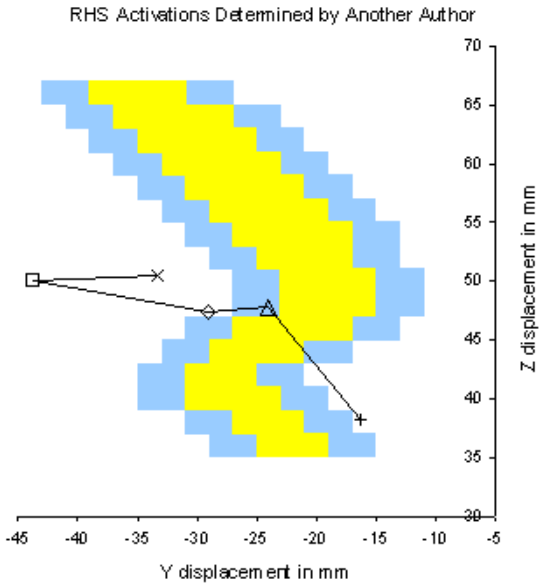

digit was presented in separate scanning sessions in this study the possibility of D1 and D5 being activated at the same time due to the subjects anticipating the next stimulus can be excluded. It is evident in the results published by van Westen et al. [6] that they observed multiple stationary activations in BA3b for stimulation to digits 1 to 5 and one activation which moved when the stimulus changed to another digit. In the present investigation, some subjects demonstrated one to two activations common to D1 and D5 but also show (usually) several activations in different positions for the two digits. This is true of all five studies in this investigation. The observation of many activations moving in an inconsistent pattern in or near BA1 has not been reported in previous similar studies carried out with a similar resolution (e.g., [1, 2, 5, 10, 15, 112]). It is not clear why the present study produces different results.

The detection of one to two stationary activations may be an indication of a contribution from a draining vein (see Chapter 4.2.4). The intravascular signal is larger than the extravascular contributions from the tissues and often appears remote to the site of the neuronal activity. Although this may explain some of what was observed in the data it still does not explain the large number of activations and the problems of clearly separating the cortical digit representations. The draining vein problem can be overcome by acquiring data using a higher magnetic field strength, statistical post-processing methods [113] or by using vascular crushing (applying a bipolar gradient during imaging [114]).

In an effort to discern some consistent pattern in the location of the activity, data from all the non-patient subjects (all subjects from studies 1, 2, 3 and 4, and all subjects in the control group from study 5) were plotted on the region defined as BA1. The data were restricted to RD1 and RD5 activations, in or near BA1, with a T-score ≥ 4, i.e., corresponding to the large red icons in Figures 31 - 36, 41 - 47, 52 - 59, 62 - 65 and 77 - 80. The resulting distribution is shown in Figure 89. A number of the activations are in the same location for both digits, however, in panel A (y direction) a clustering of D1 activations appears in the location $-18 \leq y \leq -14$ and $46 \leq z \leq 52$, indicated by the lower ellipse. This

Figure 89: LHS of the brain showing the region defined as BA1, overlaid with the RD1 and RD5 activations from all non-patient subjects from studies 1 to 5. The data were restricted to those activations that fell within the yellow and blue region and had a T-score ≥ 4. RD1 = blue '+' and RD5 = red 'X'. Areas of RD1 and RD5 clustering are circled in panel A (y direction) but no clustering is apparent in panel B (x direction). All data plotted in MNI coordinates.

A)

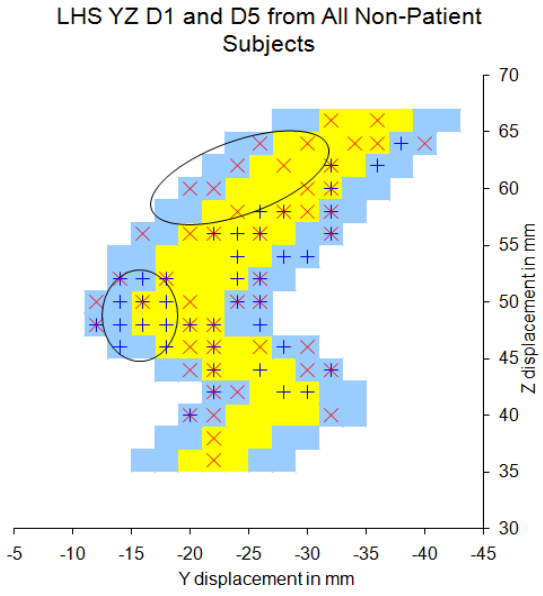

B)

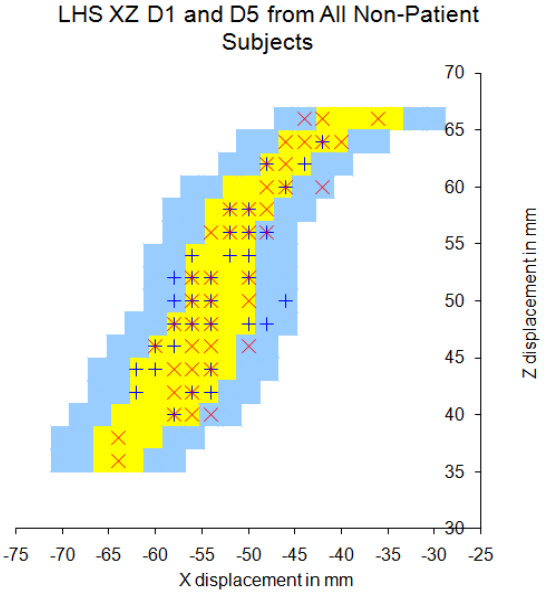

is just outside the z axis limits for D1 gleaned from the other studies plotted in Figure 88 (-23 $\leq$ y $\leq$ -16 and 38 $\leq$ z $\leq$ 44) though still within the hand somatosensory area. A clustering of RD5 activations is also observed in panel A of Figure 89 (y direction) at -30 $\leq$ y $\leq$ -20 and 57 $\leq$ z $\leq$ 64 and is indicated by the upper ellipse. The cluster is located more superior and more posterior to the RD1 clustering of activity which is in agreement with that found in other studies [2, 3, 6, 7, 10]. However, it is outside the z axis limits obtained from Figure 88 for D5 (-34 $\leq$ y $\leq$ -25 and 44 $\leq$ z $\leq$ 56) and is likely to be above (and outside) the hand somatosensory area. It is interesting to note that both clusters are located close to the BA1/BA3 border. The error margins used when defining BA1 are large enough to encompass part of BA3. It is possible that the majority of these activations relate to activity in BA3, and relative few relate to BA1 which was the intended target of the present studies. In a high resolution tactile fMRI study by Panchuelo et al. [115] at 7 T the digit SI activity was highly localised to BA3. The fact that BA1 activity is difficult to observe at 7 T suggests with the benefit of hindsight, that the problems of observing BA1 activity in the present study (at 1.5 T) were only to be expected.

It is possible to more accurately localise the activity to each Brodmann area by normalising the data to the subject's own space and visually identifying the Brodmann areas based on the anatomical topography. This method makes comparing the separations between subjects difficult but it does allow greater accuracy in identifying the SI activity related to each digit; it is possible that not all the activations detected for each subject relate to BA1 activity and they may even relate to other associated sensory areas.

9.4 Study 3

Study 2 did not achieve the aim of improving the cortical digit separations obtained from the individual data therefore study 3 was carried out using the same

protocols but increasing the duration of the scanning session from 12 to 20 minutes per digit (also increasing the number of stimulation events per digit) and increasing the stimulus amplitude by 3 dB.

The 3 dB increase in the stimulus amplitude produced SI activations with a higher T-score value at the individual level compared to the data from studies 1 and 2. Increasing the duration of data acquisition further increased the overall statistical significance of the SI activations at the individual level. The number of activations detected in each subject changed between the two time frames and the locations of the activations also changed in some instances. The activations were distributed in a similar inconsistent fashion to studies 1 and 2. The separation of the digit representations were smaller than the expected range in most instances, also consistent with studies 1 and 2, and were not improved by the changes introduced in the protocols.

Despite the more robust SI activations the second level group analysis results for both conditions showed no SI activity for stimulation to RD1 and only one activation in the vicinity of the somatosensory area for RD5. This disappointing result may be due to the folding nature of the cortex and the highly individual topography. The group results rely on a certain amount of overlap between subject data and it is usually a requirement that the activity for all subjects are normalised to a standard template (e.g., the MNI template). However the squashing and stretching required to fit the data to a template still makes overlapping between subject data difficult. A more useful method may be to normalise to the subject's own anatomical space and use a cortical flattening method. This involves 'inflating' the brain like a balloon to smooth out the folds into a flat surface and it allows a more accurate comparison of activity both at the group and individual levels [116].

9.5 Study 4

It was decided that study 4 would be carried out to improve the SI activity detection rate at a corrected p value threshold ≤ 0.05. This was done by changing the switching vibration to a continuous vibratory sensation to ensure the fingertip received a full 9 s of stimulation per stimulus event.

As the same subjects participated in studies 3 and 4 it was possible to directly compare each subject's data. Differences were found in the number of activations and the locations of the SI activations when using a continuous vibratory stimulus. This might be expected due to the difference in locations found by examining the data of study 3 at different time intervals. This difference did not significantly impact on the locations of the centre of mass of the digits (i.e., they were still randomly distributed) and nor did it significantly impact on the Euclidean separations of the finger representations in the brain. Therefore it can be concluded that there was no significant difference in the SI activations between the continuous vibratory stimulus and a switching stimulus.

The results of all four studies show that, as expected, a stronger stimulus amplitude and a longer scanning duration produce more robust, statistically significant SI activations. Multiple foci were detected for each digit and these changed within a single subject over time. Some of these activations were common to both D1 and D5 whilst other activations appeared in different positions when the stimulus location was changed. Rarely were the same number of activations detected for both digits. Examining the BA1 activations with a T-score $\geq$ 4 of all non-patient data (Figure 89) shows a clustering of activity for RD1 and RD5 near the BA1/BA3 border. (D5 clustering of activity is most likely outside the digit somatosensory area). The effect of multiple activations, lying within the same region of SI for both D1 and D5 stimulation, produced smaller-than-expected separations between the D1 and D5 representations at the individual level. It

proved difficult to identify SI activations at the group level.

9.6 Study 5

The protocol for study 5 was based on that for study 1, but with the higher stimulus amplitude where the patients were able to tolerate it. Also, the continuous vibratory stimulus was used to avoid unpleasant touch sensations in the patients' CRPS hand.

The average T-scores for the CRPS digits appeared to be similar to the average T-score from the control group, however, the control data was acquired using upgraded fMRI scanning equipment which had the effect of improving the SNR and the T-scores. It is possible that if the control data had been acquired before the upgrade then the average T-score may have been lower, suggesting the average T-score for the CRPS data might be slightly higher than the normal range (although not statistically significant). Other CRPS imaging studies include two MEG studies and an fMRI study. The MEG studies show an increased signal strength for the CRPS SI activations [26, 38] and the fMRI study showed decreased T-scores [29].

Differences were found in the maximum cluster sizes for the CRPS digits, with one patient demonstrating smaller activations and one patient demonstrating larger activations. The difference in cluster size is consistent with that observed in other fMRI CRPS imaging studies where smaller activations [30, 111] and larger activations [27] were found in patients. The observed anomalies in the cluster sizes of the *unaffected* digits were unexpected in the results of this study, although not statistically significant. This has not been observed in other CRPS imaging studies. Unfortunately the sample size of both the patients and control subjects used here are too small to determine reliable information about the normal and abnormal ranges. Further investigation is needed.

It was not possible to observe any systematic effect of CRPS on the locations or separations of the digit representations. The separations of the representations in

CRPS patients have only been measured using MEG and EEG imaging modalities [26, 36, 38]. Previous CRPS fMRI studies have focused on stimulation to a single finger or on motor tasks that involve more than one digit at a time. It is believed that fMRI has not been previously used to determine the cortical digit separations in CRPS.

FMRI can provide data about brain activations throughout the entire cortex but EEG and MEG are limited to the activations near the surface. In an effort to make a comparison between the data from the present investigation and EEG and MEG data in the literature, the separations from the patient and control groups have been recalculated using only those activations which are near to the surface of the brain. The centre of mass was calculated using the SI activations whose x axis value was within the BA1 region defined in blue and yellow in the graphs (Figures 69 to Figures 76). The new separations for the patients and control subjects are shown in Table 28. The results from the initial patient scans show a separation for the healthy hand in the expected range in 3 out of 4 patients. Additionally, the separations for the CRPS digits are smaller than the healthy hand in all patients, as seen in the previous EEG/MEG data. Disappointingly, this trend does not continue in the results from the second patient scans. Although the separations for the CRPS digits have either remained the same or increased, the separations for the healthy digits have decreased dramatically in all patients. The control subjects demonstrate separations in the range 1.9 to 11.4 mm. Although the values for each patient and subject have changed from the previous calculations, the variability and smaller-than-expected distances remain.

Comparison of the results from the first and second patient scans showed no significant changes to the T-scores, cortical digit separations or the direction of movement between the digits that could be correlated with changes in the patients' symptoms. The maximum SI cluster sizes did show some correlation with the improvement or non-improvement of the disease for one patient. Patient 2 demonstrated smaller cluster sizes compared to the healthy hand in the first scans; at the time of the second scans, her symptoms in D5 had improved, the D5

Table 28: The Euclidean separations for the left and right hands for the patients and control subjects in study 5 were recalculated using the centre of mass (estimated error ± 2 mm) of the SI activations that were close to the surface of the brain to simulate MEG and EEG data. The centre of mass was weighted to the T-score. The CRPS digits are underlined.

Subject	LD1-D5 mm	RD1-D5 mm
P1a	15.5	2.5
P2a	5.1	15.9
P3a	8.7	3.9
P4a	13.8	3.6
P1b	2.3	4.7
P2b	13.9	9.9
P3b	2.9	10.6
P4b	3.4	3.2
C1	7.4	4.0
C2	11.5	10.4
C3	3.3	1.9
C4	2.7	8.0

cluster size increased to the lower limit of the healthy range. However, the patient reported continued pain in D1 at the time of the second scans and this cluster size remained small. These results are in agreement with the findings of other CRPS imaging studies [28, 37], i.e., that cortical changes are linked with the disease and that as symptoms improve the changes reverse to the healthy range.

Pleger et al. [29, 36, 37], Maihofner et al. [28, 38] and Juottonen et al. [26] have found correlations between the amount of cortical reorganisation and the amount of pain experienced by patients. Here, a link with pain is suggested by the results of patients 2 and 3 (patient 3 did not experience hyperalgesia or allodynia and demonstrated cluster sizes in the healthy range in both measurements). However, patients 1 and 4 experienced a reduction in the amount of pain (assessed via the patients giving their overall pain level a number between 1 - 10) experienced between the scans but the results do not reflect this. More information about the sustained pain levels between the scans and a larger sample size is needed to positively correlate the pain levels with changes in the maximum SI cluster sizes.

9.7 Conclusions

In studies 1 to 4 it has been shown that it is possible for a vibrotactile stimulus to produce SI activations in healthy subjects that are detectable with fMRI. A stronger stimulus and a longer scanning time were found to be important factors to enable the activations to be detected frequently and with a high statistical significance.

Multiple SI activations were found for stimulation to each digit (LD1, LD5, RD1 and RD5). The location and number of foci detected were not constant for each digit, even within subjects for repeat measurements. Examining the RD1 and RD5 non-patient data for all 5 studies together revealed a centre of activity for RD1 and another for RD5 close to the BA1/BA3 border. The activations were distributed throughout the SI area resulting in an overlap between the representations of the digits for each hand. This led to large variations in the separations between the digit representations, when calculated on the basis of a centre of mass.

The number of foci, location and separation of the activations in the CRPS patient group did not reveal any differences that correlate with the presence or extent of the disease. The validity of the observed differences in the T-scores of the most activated voxel in SI between the CRPS digits and the healthy digits is questionable due to an upgrade of the MRI scanner during the study. Changes in cluster sizes were detected in two of the four patients and some of the changes that were observed in the repeat scans appeared to correlate with the levels of pain that the patients experienced. In three out of the four patients, the digits of the unaffected hand demonstrated smaller cluster sizes compared to the CRPS digits (and smaller than the corresponding cluster sizes in the control group).

9.8 Future work

As mentioned in section 9.3, there is some suggestion that focusing on activations in BA3, rather than in BA1, might reveal more consistent information about the digit representations. (However, some previous studies on BA3 activations have observed activations which exhibit no somatotopic mapping). If a more consistent fMRI measurement could be established (see also next paragraph), a study with larger patient and control groups would be warranted as further work is needed to confirm the trends observed in the patient study. The T-scores and cluster sizes should be analysed for both the affected and healthy digits. It would also be useful to have more information about the level of pain experienced by the patients on a daily basis to allow better correlation of cortical changes with pain levels. Perhaps asking the patient to assess their overall pain levels by assigning a number and recording it on a daily chart would be suitable.

For future studies, it is essential that an imager with a higher field strength than 1.5 T should be used, improving the signal to noise ratio and allowing a higher voxel resolution. It would also reduce the draining vein contributions and allow the experiments to be of shorter duration reducing attentional effects in the data. Additionally, a different technique of 'phase-locking' might be used to obtain the tactile data. This involves changing how the stimulus is presented and how the data is processed. Currently, a block paradigm is used where stimulation delivered to a single site is interspersed with periods of no stimulation. In phase-locking, stimulation is presented sequentially over a number of sites with the stimulus sequence repeated many times. Different sites are periodically stimulated at the same frequency but with different phase. The processing technique used in the present studies involves specifying every stimulation event and creating a model of the expected haemodynamic response. In phase-locking, the data is analysed by comparing the haemodynamic response to a sinusoidual wave function where the period of the wave is described by the time for one repetition of the regular stimulus sequence. The resulting haemodynamic response will have a certain

Figure 90: Five finger vibrotactile stimulator units, designed based on the current two finger system.

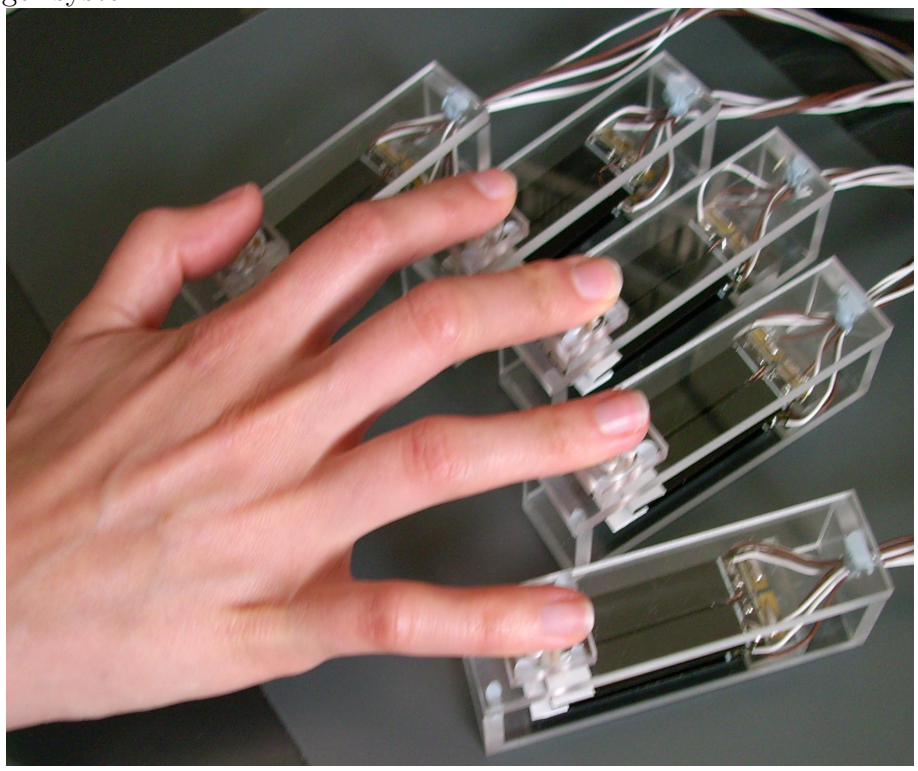

phase lag for each stimulation site allowing the activated voxels relating to each stimulus location to be determined. This technique has already been used in a few tactile imaging studies with good effect [9, 115, 117, 118].

In the context of phase-locking, but also for future studies in general, it would be useful to extend the stimulation protocol to deliver vibrotactile stimulation to all five digits. Although a degree of overlapping would be expected, the data may reveal a more subtle somatotopic mapping in the brain. Work has already begun with the construction of a stimulator that is capable of delivering a vibrotactile stimulus to all five digits, shown in Figure 90. This design was based on the current two-finger device. The design of the unit casings were too bulky to allow all five fingertips to rest comfortably on the contactors so the surrounding cases have been slim-lined in the new equipment. The stimulation is generated in the same way using piezoelectric cantilevers driven by a sinusoidal wave. Use was made of some similar 5 channel hardware (similar to the 2 channel hardware used

in the studies reported in previous chapters) already available in the laboratory. Each channel has two operational amplifiers in a bridge configuration and opto-isolators have been added creating an identical circuit to the 2 channel system constructed previously. The computer software has also been adapted to allow the logic '1' signal to be sent along the 5 channels instead of only 2. A fMRI protocol is currently being designed and tested using a phase-locking paradigm for the digit stimulation.

Bibliography

[1] Francis, S. T., E. F. Kelly, et al. (2000). 'fMRI of the Responses to Vibratory Stimulation of Digit Tips.' NeuroImage 11(3): 188-202.

[2] Gelnar, P., B. R. Krauss, N. M. Szeverenyi, A. V. Apkarian. (1998). 'Fingertip Representation in the Human Somatosensory cortex: An fMRI Study.' Neuroimage 7: 261-283.

[3] Kurth, R., K. Villringer, et al. (2000). 'fMRI shows multiple somatotopic digit representations in human primary somatosensory cortex.' Neuroreport 11(7): 1487-1491.

[4] Trulsson, M., S. T. Francis, et al. (2001). 'Cortical responses to single mechanoreceptive afferent microstimulation revealed with fMRI.' Neuroimage 13(4): 613-622.

[5] McGlone, F., E. F. Kelly, et al. (2002). 'Functional neuroimaging studies of human somatosensory cortex.' Behavioural Brain Research 135(1-2): 147-158.

[6] van Westen, D., P. Fransson, et al. (2004). 'Fingersomatotopy in area 3b: an fMRI-study.' BMC Neuroscience 5.

[7] Maldjian, J. A., A. Gottschalk, et al. (1999). 'The Sensory Somatotopic Map of the Human Hand Demonstrated at 4 Tesla.' NeuroImage 10(1): 55-62.

[8] Maldjian, J. A., A. Gottschalk, et al. (1999). 'Mapping of secondary somatosensory cortex activation induced by vibrational stimulation:an fMRI study.' Brain Research 824: 291-295.

[9] Overduin, S. A. and P. Servos (2004). 'Distributed digit somatotopy in primary somatosensory cortex.' NeuroImage 23(2): 462-472.

[10] Kurth, R., K. Villringer, et al. (1998). 'fMRI assessment of somatotopy in human Brodmann area 3b by electrical finger stimulation.' Neuroreport 9(2): 207-212.

[11] Ruben, J., J. Schwiemann, et al. (2001). 'Somatotopic organization of human secondary somatosensory cortex.' Cerebral Cortex 11(5): 463-473.

[12] Kaas, J. H., R. J. Nelson, M. Sur, C. S. Lin, M. M. Merzenich. (1978). 'Multiple Representations of The Body Within the Primary Somatosensory Cortex of Primates.' Science 204: 521-523.

[13] Talbot, W. H., Dariansm.I, et al. (1968). 'Sense of flutter-vibration - comparison of human capacity with response patterns of mechanoreceptive afferents from monkey hand.' Journal of Neurophysiology 31(2): 301-334.

[14] Tommerdalh, M., Whitsel B., et al. (1999). 'Responses of contralateral SI and SII in cat to same-site cutaneous flutter versus vibration.' Journal of Neurophysiology 82:1982-1992

[15] Harrington, G. S., J. H. Downs (2001). 'FMRI mapping of the somatosensory cortex with vibratory stimuli. Is there a dependency on stimulus frequency?' Brain Research 897: 188-192.

[16] Nelson, A. J., W. R. Staines, et al. (2004). 'Activation in SI and SII; the influence of vibrotactile amplitude during passive and task-relevant stimulation.' Cognitive Brain Research 19(2): 174-184.

[17] Arthurs, O. J., H. Johansen-Berg, et al. (2004). 'Attention differentially modulates the coupling of fMRI BOLD and evoked potential signal amplitudes in the human somatosensory cortex.' Experimental Brain Research 157(3): 269-274.

[18] Hamalainen, H., J. Hiltunen, I. Titievskaja. (2002). 'Activation of somatosensory cortical areas varies with attentional state: an fMRI study.' Behavioural Brain Research 135: 159-165.

[19] Johansen-Berg, H., V. Christensen, et al. (2000). 'Attention to touch modulates activity in both primary and secondary somatosensory areas.' Neuroreport 11(6): 1237-1241.

[20] Pleger, B., A. N. Foerster, et al. (2003). 'Functional Imaging of Perceptual Learning in Human Primary and Secondary Cortex.' Neuron 40: 643-653.

[21] Hodzic A., R. Veit, et al. (2004). 'Improvement and Decline in Tactile Discrimination Behavior after Cortical Plasticity Induced by Passive Tactile Coactivation.' J of Neuroscience 24(2): 442-446.

[22] Schaefer M., H. Flor, et al. (2007). 'Morphing the body: Illusory feeling of an elongated arm affects somatosensory homunculus.' NeuroImage 36: 700-705.

[23] Butterworth, S., S. Francis, et al. (2003). 'Abnormal cortical sensory activation in dystonia: an fMRI study.' Movement Disorders 18(6): 673-682.

[24] Sanger, T. D., A. Pascual-Leone, et al. (2002). 'Nonlinear sensory cortex response to simultaneous tactile stimuli in writer's cramp.' Movement Disorders 17(1): 105-111.

[25] Peller, M., K. E. Zeuner, et al. (2006). 'The basal ganglia are hyperactive during the discrimination of tactile stimuli in writer's cramp.' Brain 129:2697-2708.

[26] Juottonen, K., M. Gockel, et al. (2002). 'Altered central sensorimotor processing in patients with complex regional pain syndrome.' Pain 98(3): 315-323.

[27] Maihofner, C., C. Forster, et al. (2005). 'Brain processing during mechanical hyperalgesia in complex regional pain syndrome: a functional MRI study.' Pain 114(1-2): 93-103.

[28] Maihofner, C., H. O. Handwerker, et al. (2004). 'Cortical reorganization during recovery from complex regional pain syndrome.' Neurology 63(4):693-701.

[29] Pleger, B., P. Ragert, et al. (2006). 'Patterns of cortical reorganization parallel impaired tactile discrimination and pain intensity in complex regional pain syndrome.' NeuroImage 32: 503-510.

[30] Maihofner, C., R. Baron, et al. (2007). 'The motor system shows adaptive changes in complex regional pain syndrome.' Brain 130: 2671-2687.

[31] Flor, H., E. Thomas, et al. (1998). 'Cortical reorganization and phantom phenomena in congenital and traumatic upper-extremity amputees.' Experimental Brain Research 119(2): 205-212.

[32] Halligan, P.W., J. C. Marshall, D. T. Wade, J. Davey, D. Morrison. (1993). 'Thumb in cheek sensory reorganisation and perceptual plasticity after limb amputation.' NeuroReport 3: 233-236.

[33] Ramachandran, V. S., M. Stewart, D. C. Rogers-Ramachandran. (1992). 'Perceptual correlates of massive cortical reorganization.' NeuroReport 7: 583-586.

[34] Janig, W. and R. Baron. (2004). 'Experimental approach to CRPS.' Pain 108(1-2): 3-7.

[35] Janig, W. and R. Baron (2003). 'Complex regional pain syndrome: mystery explained?' Lancet Neurology 2(11): 687-697.

[36] Pleger, B., M. Tegenthoff, et al. (2004). 'Mean sustained pain levels are linked to hemispherical side-to-side differences of primary somatosensory cortex in the complex regional pain syndrome I.' Experimental Brain Research 155(1): 115-119.

[37] Pleger, B., M. Tegenthoff, et al. (2005). 'Sensorimotor Returning in Complex Regional Pain Syndrome Parallels Pain Reduction.' Ann Neurol 57: 425-429.

[38] Maihofner, C., H. O. Handwerker, et al. (2003). 'Patterns of cortical reorganisation in complex regional pain syndrome.' Neurology 61: 1707-1715

[39] *http://stemcells.nih.gov/info/scireport/chapter8.asp*

[40] Purves, D., G.J. Augustine, D. Fitzpatrick, W.C. Hall, A.S. LaMantia, J.O. McNamara, L.E. White. (2008). 'Neuroscience.' 4th Ed, Sinauer Associates Inc.

[41] Kamal, S. M. (2005) 'Brain Activation Due to a Vibrotactile Stimulator Array on the Fingertip: An fMRI Study.' PhD Thesis, University of Exeter.

[42] Kandel, E., J. Schwartz, T. Jessel. (2000). 'Principles of neural science.' 4th Edition, McGraw-Hill.

[43] Thornbury, J., C. M. Mistretta. (1981). 'Tactile sensitivity as a function of age.' Journals of Gerontology 36(1): 34-39.

[44] Winwood, R. S. and J. L. Smith (1992). 'Sear's anatomy and physiology for nurses.', Edward.

[45] Geyer S., A. Schleicher, K. Zilles. (1999). 'Areas 3s, 3b and 1 of Human Primary Somatosensory Cortex: 1. Microstructural Organisation and Interindividual Variability.' NeuroImage 10: 63-83.

[46] Kass J. H., R. J. Nelson, M. Sur, C. S. Lin, M. M. Merzenich (1979). 'Multiple representations of the body within the primary somatosensory cortex of primates.' Science 2004: 521-523.

[47] Talairach, J., P. Tournoux. (1993). 'Referentially Orientated Cerebral MRI Anatomy.' Thieme Medical Publishers Inc.

[48] *http://www.nature.com/nrn/journal/v3/n3/box/nrn756_BX1.html*

[49] *http://imaging.mrc-cbu.cam.ac.uk/imaging/CbuImaging*

[50] International Consortium for Brain Mapping:

http://www.loni.ucla.edu/ICBM/

[51] Marshall, A. T. and A. J. Crisp. (2000). 'Reflex sympathetic dystrophy.' Rheumatology 39(7): 692-695.

[52] Kurvers, H. A. J. M. (1998). 'Reflex sympathetic dystrophy: facts and hypostheses.' Vascular Medicine 3: 207-214.

[53] Kurvers, H. A. J. M. (1997). 'Reflex sympathetic dystrophy: a clinical and experimental study.' Book ISBN 90-9010533-6

[54] Baron, R. and W. Janig. (2004). 'Complex regional pain syndromes - how do we escape the diagnostic trap?' Lancet 364(9447): 1739-1741.

[55] De Vlieger, P., G. Crombez, et al. (2006). 'Worrying about chronic pain. An examination of worry and problem solving in adults who identify as chronic pain sufferers.' Pain 120(1-2): 138-144.

[56] Guo, T. Z., S. C. Offley, et al. (2004). 'Substance P signaling contributes to the vascular and nociceptive abnormalities observed in a tibial fracture rat model of complex regional pain syndrome type I.' Pain 108(1-2): 95-107.

[57] *http://www.uni-tuebingen.de/medizinischepsychologie/links/crps1.htm*

[58] Ribbers, G. M., A. C. Geurts, et al. (2003). 'Pharmacologic treatment of complex regional pain syndrome I: A conceptual framework.' Archives of Physical Medicine and Rehabilitation 84(1): 141-146.

[59] Schott, G. D. (2001). 'Reflex sympathetic dystrophy.' Journal of Neurology Neurosurgery and Psychiatry 71(3): 291-295.

[60] Wasner, G., J. Schattschneider, et al. (2002). 'Skin temperature side differences - a diagnostic tool for CRPS?' Pain 98(1-2): 19-26.

[61] *http://www.medical-acupuncture.co.uk/journal/1998nov/six.shtml*

[62] Weber, M., F. Birklein, et al. (2001). 'Facilitated neurogenic inflammation in complex regional pain syndrome.' Pain 91(3): 251-257.

[63] Coderre, T. J., D. N. Xanthos, et al. (2004). 'Chronic post-ischemia pain (CPIP): a novel animal model of complex regional pain syndrome-Type I (CRPS-I; reflex sympathetic dystrophy) produced by prolonged hindpaw ischemia and reperfusion in the rat.' Pain 112(1-2): 94-105.

[64] McCabe, C. S., R. C. Haigh, et al. (2003). 'A controlled pilot study of the utility of mirror visual feedback in the treatment of complex regional pain syndrome (type 1).' Rheumatology 42(1): 97-101.

[65] Moseley, G. L. (2004). 'Graded motor imagery is effective for long-standing complex regional pain syndrome: a randomised controlled trial.' Pain 108(1-2): 192-198.

[66] Ramachandran, V. S. and S. Blakeslee. (1998). 'Phantoms in the brain: human nature and the architecture of the mind,' Fourth Estate Ltd.

[67] Ramachandran, V. S. and D. Rogers-Ramachandran. (2000). 'Phantom limbs and neural plasticity.' Archives of Neurology 57(3): 317-320.

[68] Houghton, A. D., G. Nicholls, et al. (1994). 'Phantom Pain - Natural-History and Association with Rehabilitation.' Annals of the Royal College of Surgeons of England 76(1): 22-25.

[69] Halligan, P. W., A. Zeman, et al. (1999). 'Phantoms in the brain - Question the assumption that the adult brain is 'hard wired'.' British Medical Journal 319(7210): 587-588.

[70] Haigh, R. C., C. S. McCabe, et al. (2003). 'Joint stiffness in a phantom limb: evidence of central nervous system involvement in rheumatoid arthritis.' Rheumatology 42(7): 888-892.

[71] Moseley, G. L. and S. C. Gandevia. (2005). 'Sensory-motor incongruence and reports of 'pain'.' Rheumatology 44(9): 1083-1085.

[72] Mansfield, P. (1977). 'Multi-Planar Image-Formation Using NMR Spin Echoes.' Journal of Physics C-Solid State Physics 10(3): L55-L58.

[73] Ogawa, S., T. M. Lee, et al. (1990). 'Brain magnetic-resonance-imaging with contrast dependent on blood oxygenation.' Proceedings of the National Academy of Sciences of the United States of America 87(24): 9868-9872.

[74] Ogawa, S., T. M. Lee, et al. (1990). 'Oxygenation-sensitive contrast in magnetic-resonance image of rodent brain at high magnetic-fields.' Magnetic Resonance in Medicine 14(1): 68-78.

[75] Ogawa, S., R. S. Menon, et al. (1993). 'Functional brain mapping by blood oxygenation level-dependent contrast magnetic-resonance-imaging - a comparison of signal characteristics with a biophysical model.' Biophysical Journal 64(3): 803-812.

[76] Ogawa, S., D. W. Tank, et al. (1992). 'Intrinsic signal changes accompanying sensory stimulation - functional brain mapping with magnetic-resonance-imaging.' Proceedings of the National Academy of Sciences of the United States of America 89(13): 5951-5955.

[77] Belliveau, J. W., D. N. Kennedy, et al. (1991). 'Functional mapping of the human visual-cortex by magnetic-resonance-imaging.' Science 254(5032): 716-719.

[78] Belliveau, J. W., B. R. Rosen, et al. (1990). 'Functional cerebral imaging by susceptibility-contrast NMR.' Magnetic Resonance in Medicine 14(3): 538-546.

[79] *http://scien.stanford.edu/class/psych221/projects/06/cukur/mri.html*

[80] *http://www.revisemri.com/questions/pulse_sequences/se_ge_differences*

[81] *http://www.revisemri.com/questions/pulse_sequences/epi*

[82] McRobbie, D., E. Moore, et al. (2003). 'MRI from picture to proton.' Cambridge University Press.

[83] Buxton, R. (2002). 'Introduction to Functional Magnetic Resonance Imaging.' Cambridge University Press.

[84] Buxton, R. (2001). 'The elusive initial dip'. Neuroimage 13: 953-958.

[85] van der Zwaag, W., S. Francis, et al. (2009). 'fMRI at 1.5, 3 and 7 T: Characterising BOLD signal changes'. Neuroimage 47(4):1425-1434.

[86] Boxerman, J., P. Bandettini, et al. (1995). 'The intravascular contribution to fMRI signal change: MonteCarlo modeling and diffusion-weighted studies in vivo'. Magnetic Resonance in Medicine 34:4-10.

[87] *http://www.fmrib.ox.ac.uk/education/fmri/introduction-to-fmri/what-does-fmri-measure*

[88] Gowland, P., S. Francis, P. Morris R. Bowtell. (2002). 'Watching the brain at work.' Physics World 15(12): 31-35.

[89] Mayhew, J., Y. Zheng, Y. Hou, B. Vuksanovic, J. Berwick, S. Askew, P. Coffey (1999). 'Spectroscopic Analysis of Changes in Remitted Illumination:

The Response to Increased Neural Activity in Brain.' NeuroImage 10: 304-326.

[90] Henson, R. (2008). 'SPM Minicourse' at the University of Exeter.

[91] Glover, G., T. Li, et al. (2000). 'Image-based method for retrospective correction of physiological motion effects in fMRI: RETROICOR'. Magnetic Resonance in Medicine 44:162-167.

[92] *http://www.revisemri.com/questions/artefacts/motion_phase*

[93] *http://users.fmrib.ox.ac.uk/˜ stuart/thesis/chapter4/chapter_4.html*

[94] Hornak, J. P. (2004). 'The Basics of MRI.'

http://www.cis.rit.edu/htbooks/mri/inside.htm

[95] Peninsula Magnetic Resonance Research Centre

http://www.centres.ex.ac.uk/pmrrc/index.shtml

[96] MRIcro software:

http://www.sph.sc.edu/comd/rorden/mricro.html

[97] Statistical Parametric Mapping software and manual:

http://www.fil.ion.ucl.ac.uk/spm/

[98] Matlab software:

http://www.mathworks.co.uk/

[99] Ashburner, J., K. Friston, W. Penny. (2004). 'Human Brain Function.' 2nd Ed,

http://www.fil.ion.ucl.ac.uk/spm/doc/books/hbf2/

[100] Schulz, M., W. Chau, et al. (2004). 'An integrative MEG-fMRI study of the primary somatosensory cortex using cross-modal correspondence analysis.' NeuroImage 22(1): 120-133.

[101] Sleigh, A., S. Francis, et al. (2001). 'Effect of frequency of vibrotactile stimulation on the Brain Response measured using fMRI.' Neuroimage 13(6): S1254-S1254.

[102] Blatow, M., E. Nennig, et al. (2007). 'fMRI reflects functional connectivity of human somatosensory cortex.' Neuroimage 37(3): 927-936.

[103] Bingel U., J. Lorenz, et al. (2004). 'Somatotopic organization of human somatosensory cortices for pain: a single trial fMRI study.' Neuroimage 23: 224-232.

[104] Chanter C.M., (1999). 'Design and Development of Vibrotactile Stimulator Array for the Fingertip.' PhD thesis, University of Exeter.

[105] Maldjian, J, P. Laurienti, et al. (2003). 'An Automated Method for Neuroanatomic and Cytoarchitectonic Atlas-based Interrogation of fMRI Data Sets.' NeuroImage 19: 1233-1239.

[106] Maldjian J, P. Laurienti, et al. (2004). 'Precentral Gyrus Discrepancy in Electronic Versions of the Talairach Atlas.' Neuroimage 21(1): 450-455.

[107] Lancaster J,, et al. (2000). 'WFU Pickatlas User Manual v2.4.' Wake Forest University School of Medicine.

[108] Lancaster J, P. Kochunov, et al. (2000). 'Automatic Talairach Labels for Functional Activation Sites.' NeuroImage 5: S483.

[109] *http://www.talairach.org/client.html*

[110] Ribbers, G. M., Mulder, T., A. C. Geurts, et al. (2002). 'Reflex Sympathetic Dystrophy of the Left Hand and Motor Impairments of the Unaffected Right Hand: Impaired Central Motor Processing?' Archives of Physical Medicine and Rehabilitation 83: 81-85.

[111] Gieteling, E., Rijn, M., et al. (2008). 'Cerebral activaiton during motor imagery in complex regional pain syndrome type 1 with dystonia.' Pain 134: 302-309.

[112] Krauss, T., Kurth, R., et al. (2001). 'Representational overlap of adjacent fingers in multiple areas of human primary somatosensory cortex depends on electrical stimulus intensity: an fMRI study.' Brain Research 899: 36-46

[113] Nencka, A., D. Rowe. (2007). 'Reducing the unwanted draining vein BOLD contribution in fMRI with statistical post-processing methods.' Neuroimage 37(1):177-188.

[114] Hernandez-Garcia, L., A. Vazquez, D. Rowe. (2009). 'Complex-Valued Analysis of Arterial Spin Labeling-Based Functional Magnetic Resonance Imaging Signals.' Magnetic Resonance in Medicine 62(6):1597-1608.

[115] Panchuelo, R., Francis, S., et al. (2008). 'Mapping somatosensory cortex with fMRI at 1mm isoptropic resolution.' Poster, International Society for Magnetic Resonance in Medicine.

[116] Kim, S., T. Suh. (2007). 'fMRI Visualization Software: Segmentation, Inflation, and Flattening.' World Congress on Med. Phys. and Biomed. Eng. 14:2370-2372.

[117] Duncan, R., Boynton, G. (2007). 'Tactile Hyperacuity Thresholds Correlate with Finger Maps in Primary Somatosensory Cortex.' Cerebral Cortex 17: 2878-2891.

[118] Huang, R., Sereno, M. (2007). 'Dodecapus: An MR-compatible system for somatosensory stimulation.' Neuroimage 34: 1060-1073.

Appendix A

Experimental Procedure

A.1 Healthy Participant Information

A.1.1 MRI Information Sheet

Information sheet for volunteers - Magnetic resonance imaging

Magnetic resonance imaging (MRI) is a system for producing pictures of the human body. It does not usually involve any injections (non-invasive) and does not use x-rays or other ionising radiation. It is a very safe technique and may be used on the majority of subjects.

The technique relies on a powerful magnet which you will lie inside of. The strong magnetic field allows the system to detect the amount and the location of water within the body. Using this information, pictures of the soft tissues within the body are produced. If you suffer from claustrophobia you might find the

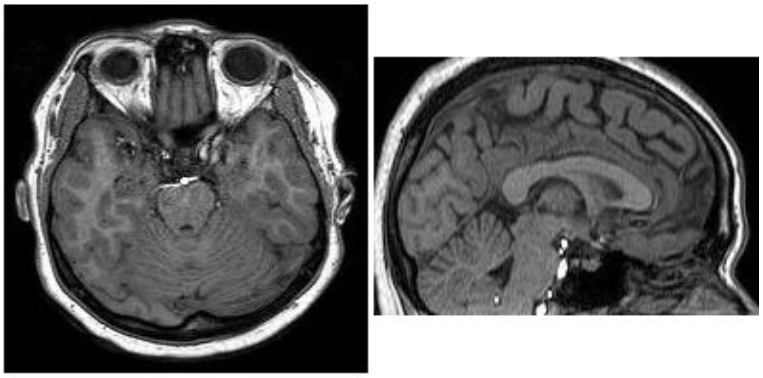

environment uncomfortable please discuss this with the operator before entering the scanner suite.

During the scan, the system makes a lot of noise and you will be provided with headphones. The magnetic field will strongly attract metal objects. As a result no metal objects may be taken in to the scanning room itself, this includes coins, keys, pens, etc. All jewellery should be also be removed. Also, as we are imaging the head, we would ask you not to wear makeup as some of the pigments used contain iron and will prevent a good image being taken.

You will be asked to fill in 3 forms before you are scanned. The first is a safety checklist and registration form. We will treat all information as confidential. We will use any imaging data acquired anonymously and this form will be archived separately from your data. The second is a data consent form. Your imaging data can form part of a substantial resource which we would like to draw on in the future for further studies and teaching purposes. This consent is entirely optional.

You will also have to sign a consent form for the study which you are taking part in which will outline any extra information and confirm that you have had everything explained to you before you start.

Once you are in the system, the operators will be in constant contact with you. If at any time you feel uncomfortable or wish to end the scanning process you will be able to do so by squeezing a device that will stop the scan and alert

the operator. Someone will then come and help you.

If you have any questions, or wish to see the scanner before signing the consent forms please ask.

A.1.2 Study Protocol

Information sheet for volunteers: study protocol

STUDY TITLE

Tactile fMRI Study

PURPOSE OF STUDY

The purpose of this study is to locate the somatosensory areas of the brain which activate when the fingertips are stimulated. This will provide a standard template which will then be used to determine if there are differences in the location of the activity in patients with certain diseases. This information will improve our understanding of these diseases and possibly allow treatments to be made more effective.

PROCEDURES

Participating in the study will require you to lye in the scanner for 2 sessions lasting approximately 30 mins each. During imaging a cage like device will be placed around the head to help the scanner produce clearer pictures. Two of your fingertips will be resting lightly over the holes on two small plastic devices which are attached to a board that will rest across your abdomen. The holes contain wooden cylinders which will vibrate up and down quickly touching the fingertip. They are non-invasive and are not intended to cause pain. The vibrations will take place periodically during imaging. The scanning procedure will be carried out twice, once with stimulation on the left hand and once on the right hand. You will be able to rest outside of the scanner room between sessions.

POTENTIAL RISKS

Some discomfort from lying in the scanner is possible for those who may be claustrophobic. There are also hazards due to the strong magnetic field. Volunteers

are required to complete a safety checklist prior to entering the scanner room and to remove all loose metal objects. Please note, the checklist allows us to assess if it is safe for you to enter the strong magnetic field by asking questions about your health. Sometimes people are not able to participate due to their previous medical history. We will advise you if this is the case.

There is some evidence that the strong magnetic field may have adverse effects on the unborn baby during the first 3 months of pregnancy. If you are less than 3 months pregnant or believe you may be less than 3 months pregnant then you will not be able to participate in the study.

WITHDRAWAL/PREMATURE COMPLETION

Your participation in this study is voluntary, and you may discontinue at any time, without prejudice.

INVITATION TO ASK FURTHER QUESTIONS

You should ask any questions you have concerning this study before you sign the consent form.

A.1.3 Consent Form

CONSENT

Have you read the information sheet? Yes/No

Have you had an opportunity to ask questions and discuss this study? Yes/No

Have you received satisfactory answers to your questions? Yes/No

Are you satisfied with the amount of information that you have been given? Yes/No

The study has been explained to you by whom? Yes/No

Do you understand that you are free to withdraw from the study:

- at any time
- without having to give a reason for withdrawing
- without prejudice? Yes/No

Do you agree to take part in the study? Yes/No

Volunteers signature

Investigators signature

Date

A.1.4 MRI Safety Checklist

Participant Safety Checklist

Name:

Date of Birth:

Weight:

Name of Study/Volunteer Number:

Please check the following list carefully, answering all appropriate questions. Please do not hesitate to ask staff, if you have any queries regarding these questions.

1.Do you have a pacemaker, artificial heart valve or coronary stent? Yes/No
2.Have you ever had major surgery? Yes/No
If yes, please give brief details.

3.Do you have any aneurysm clips (clips put around blood vessels during surgery)? Yes/No
4.Do you have any implants in your body?
Joint replacements, pins or wires? Yes/No
Implanted cardioverter defibrillator (ICD)? Yes/No
Electronic implant or device? Yes/No
Magnetically-activated implant or device? Yes/No
Neurostimulation system? Yes/No
Spinal cord stimulator? Yes/No
Insulin or infusion pump? Yes/No
Implanted drug infusion pump? Yes/No
Internal electrodes or wires? Yes/No
Bone growth/bone fusion stimulator? Yes/No
Any type of prosthesis? Yes/No

Heart valve prosthesis? Yes/No

Eyelid spring or wire? Yes/No

Metallic stent, filter or coil? Yes/No

Shunt (spinal or intraventricular)? Yes/No

Vascular access port and/or catheter? Yes/No

Wire mesh implant? Yes/No

Bone/joint pin, screw, nail, wire, plate etc.? Yes/No

Other Implant.....

5.Do you have an artificial limb, calliper or surgical corset? Yes/No

6.Do you have any shrapnel or metal fragments, for example from working in a machine tool shop? Yes/No

7.Do you have a cochlear implant? Yes/No

8.Do you wear dentures, plate or a hearing aid? Yes/No

9.Are you wearing a skin patch (e.g. anti-smoking medication), have any tattoos, body piercing, permanent makeup or coloured contact lenses? Yes/No

10.Are you aware of any metal objects present within or about your body, other than those described above? Yes/No

11.Are you susceptible to claustrophobia? Yes/No

12.Do you suffer from blackout, diabetes, epilepsy or fits? Yes/No

For women:

13.Are you pregnant or experiencing a late menstrual period? Yes/No

14.Do you have an intra-uterine contraceptive device fitted? Yes/No

15.Are you taking any type of fertility medication or having fertility treatment? Yes/No

Important Instructions

Remove all metallic objects before entering the scanner room including hearing aids, mobile phones, keys, glasses, hair pins, jewellery, watches, safety pins,

paperclips, credit cards, magnetic strip cards, coins, pens, pocket knives, nail clippers, steel-toed boots/shoes and all tools. Loose metallic objects are especially prohibited within the MR environment.

I have understood the above questions and have marked the answers correctly.

Signature

Date

MR Centre Staff Signature

A.2 Patient Information

A.2.1 Study Protocol and Information Sheet

Study: Cortical Reorganisation and Complex Regional Pain Syndrome

We would like to invite you to take part in a research study. Before you decide you need to understand why the research is being done and what it would involve for you. Please take time to read the following information carefully. Talk to others about the study if you wish. Ask us if there is anything that is not clear or if you would like more information. Take time to decide whether or not you wish to take part.

What is the purpose of the study?

In patients with CRPS, we are investigating how the brain processes nerve signals from the fingertips and also how the brain processes 3D images. Changes in sensation message pathways may play a part in the development of painful conditions.

Why have I been invited to take part?

We have invited you to take part in this research as you have been diagnosed with complex regional pain syndrome by a qualified physician, the disease is present in your hand and you have had it for less than 6 months.

Do I have to take part?

It is up to you to decide. We will describe the study and go through this information sheet, which we will then give to you. We will then ask you to sign a consent form to show you have agreed to take part. You are free to withdraw at any time, without giving a reason. This would not affect the future care you receive. If you withdraw from the study, we will ask for your consent in order to use the research data.

What will happen to me if I take part?

This study uses magnetic resonance imaging (MRI) which is a system for producing pictures of the human body. The study will require you to make 2 visits, three months apart, to the Magnetic Resonance Imaging Centre at the University of Exeter, Heavitree Road, Exeter. During each visit you will need to lie in the magnetic resonance scanner for 2 sessions lasting approximately 40 minutes each.

On arrival at the MRI Centre you will need to fill out a safety checklist to ensure it is safe for you to enter the scanner room. Sometimes, people are not able to have a MRI scan due to their previous medical history or pregnancy. We will provide a pregnancy test if appropriate.

During imaging a helmet-like device will be placed over your head to help the scanner produce clearer pictures. Two of your fingertips will be resting lightly over some equipment which will periodically vibrate in a non-painful and non-invasive way. The scanning procedure will be carried out twice, once with stimulation on the left hand and once on the right hand. You will be able to rest outside of the scanner room between sessions. During the second session, we will periodically project an image of a 3D cube onto a screen for you to look at. If you are claustrophobic, we will be happy for you to try out lying in the scanner to see what it is like.

During the study you can continue your treatments as normal. This study will not interfere with them. However, we would like to see whether the brain processing changes before and after treatment. You will come back to the scanner 3 months into your treatment for further scanning sessions.

Expenses and payments

Reasonable traveling expenses will be reimbursed by the Rheumatology Department at the Royal Devon and Exeter Hospital.

What are the possible disadvantages and risks of taking part?

Magnetic resonance imaging is a very safe technique and may be used on the majority of people. It does not involve any injections and does not use x-rays.. If you are claustrophobic you might find the scanner environment uncomfortable as you will need to lie in a small space.

Due to the strong magnetic field you will need to remove all loose metal objects before entering the scanner room, e.g. glasses, jewellery, coins, etc. Attached metal zips, buttons, etc on clothes are fine.

You will also need to remove any makeup as some brands can contain metal particles which can reduce the quality of the images.

What will happen if other conditions are found in the images?

The images we obtain show blood flow in the brain and they are not of a high enough quality to diagnose medical conditions. Additionally, our researchers are not qualified radiologists and therefore are not trained in MRI diagnosis. However, in the unlikely event that something unusual is seen on the scans we would refer the images anonymously to a qualified radiologist at the Royal Devon and Exeter Hospital for a professional opinion. You will then be contacted by us if the radiologist believes further investigation or treatment is required.

Women: Harm to the unborn child

There is some evidence that the strong magnetic field may have adverse effects on the unborn baby during the first 3 months of pregnancy. If you are less than 3 months pregnant or believe you may be less than 3 months pregnant then you will not be able to participate in the study. We will provide a pregnancy test if appropriate.

What are the possible benefits of taking part?

We cannot promise the study will help you but the information we gain from this study may help improve the treatments for people with Complex Regional Pain Syndrome.

What if there is a problem?

If you have a concern about any aspect of this study, you should ask to speak to the researchers who will do their best to answer your questions (01392 403705). If you remain unhappy and wish to complain formally, you can do this through the NHS Complaints Procedure. Details can be obtained from your hospital.

What if relevant new information becomes available?

Sometimes we get new information about the condition and the treatment being studied. If this happens, your research doctor will tell you and discuss whether you should continue in the study. If you decide to continue in the study he may ask you to sign an updated consent form.

If the study is stopped for any other reason, we will tell you immediately.

What will happen if I dont want to carry on with the study?

If you withdraw from the study, we will need to use the data collected up to your withdrawal.

Harm

In the event that something does go wrong and you are harmed during the research and this is due to someones negligence then you may have grounds for legal action for compensation against the Royal Devon and Exeter Hospital or the Bath National Hospital for Rheumatic Diseases NHS Trusts but you may have to pay your legal costs. The normal National Health Service complaints mechanisms will still be available to you.

Will my taking part in the study be kept confidential?

Yes. We will follow ethical and legal practice and all information about you will be handled in confidence. All information which is collected about you during the course of the research will be kept strictly confidential, and any information about you which leaves the hospital will have your name and address removed so that you cannot be recognised.

Involvement of the General Practitioner/Family doctor (GP)

With your consent, we would like to inform your GP that you are participating in this research. They will be informed that the research does not interfere with any treatments you might receive and that you will not be offered additional treatments by the research team..

What will happen to the results of the research study?

The results from this study will be published in the form of papers submitted to scientific journals and also presentations at relevant scientific conferences. You will be sent a summary of the findings of the study. You will not be identified in any report or publication.

Who is organising and funding the research?

This research is a collaboration between the Royal Devon and Exeter Foundation Trust, Bath Royal National Hospital for Rheumatic Diseases and the University of Exeter. The research is kindly supported by a grant from the Devon Arthritis and Allied Research Trust (DAART).

Who has reviewed the study?

All research in the NHS is looked at by an independent group of people, called a Research Ethics Committee to protect your safety, rights, wellbeing and dignity.

This study has been reviewed and given favourable opinion by Devon and Torbay Research Ethics Committee.

Further information and contact details

For general information about Complex Regional Pain Syndrome contact your GP, hospital clinic or visit the RSDUK website - www.rsd-crps.co.uk

If you have questions about the research please contact Dr Haigh on 01392 403705. If you are unsure about taking part and wish to discuss this with someone you can contact the research team, speak to one of your health care practitioners or your GP.

If you are unhappy with the study please contact Dr Haigh on 01392 403705.

A.2.2 Sample GP Letter

Royal Devon and Exeter
Hospital (Wonford)
Barrack Road
Exeter
EX2 5DW
Tel: 01392 411611
PRINCESS ELIZABETH ORTHOPAEDIC CENTRE
Direct Dial: 01392 403705
Direct Fax: 01392 403505

Dear Dr

I am writing to inform you that your patient, ... of..... has agreed to take part in an fMRI research study to investigate pain pathways in Complex Regional Pain Syndrome (previously Reflex Sympathetic Dystrophy). Your patient will have a series of MRI scan images taken whilst they are (1) moving their hand, (2) having their hand stimulated and (3) being shown pictures of 3D cubes. We are looking at cortical reorganisation in this condition. A copy of the research proposal is available on request.

Management of the condition should continue as normal. The research will not affect any treatments and no additional treatments are offered to the participant in this observational study.

The study is being jointly undertaken by the Royal Devon and Exeter Foundation Trust, Bath Royal National Hospital for Rheumatic Diseases and the University of Exeter and is kindly supported by a grant from the Devon Arthritis and Allied Research Trust (DAART).

If you would like further information about this research then please do not hesitate to contact me on 01392 403705.

Yours sincerely

Dr Richard C Haigh

Consultant Rheumatologist and Hon. Senior Clinical Lecturer

Appendix B

Results

B.1 Study 1

Table 29: Statistics of the SI activations for study 1. All values shown above an uncorrected p value threshold of ≤ 0.001.

Subject	Stimulation	x	y	z	Cluster size (2 mm^3 voxels)	T-score
1	LD1	44	-38	66	4	3.84
		56	-24	56	4	3.75
		40	-8	42	2	3.29
		46	-16	50	1	3.25
		46	-8	48	4	3.23
		48	-14	46	1	3.23
		42	-6	60	1	3.2
	LD5	32	-44	52	7	4.38
		62	-16	46	5	4.36
		46	-26	58	5	4.19
		54	-30	58	11	4.13
		66	-40	40	9	3.73
		56	-26	40	2	3.71
		64	-22	42	2	3.46
		44	-22	66	6	3.27
		62	-10	40	2	3.26
		58	-34	38	1	3.1
	RD1	-46	-42	60	20	5.05
		-58	-18	46	18	4.97
		-54	-20	36	25	4.68
		-60	-32	44	8	4.25
		-56	-8	46	18	4.03
		-56	-30	40	3	3.91
		-32	-26	48	6	3.77
		-56	-8	42	2	3.66
		-52	-34	56	3	3.41
		-58	-26	50	18	3.39
		-30	-24	40	1	3.34
		-62	-36	42	5	3.32
	RD5	-56	-20	48	26	6.41
		-52	-22	36	20	5.29
		-46	-22	48	7	3.89
		-62	-20	36	6	3.83
		-40	-26	40	1	3.36
		-40	-36	42	1	3.27
		-40	-42	54	1	3.26
		-32	-38	54	2	3.17

Table 30: Statistics of the SI activations for study 1. All values shown above an uncorrected p value threshold of ≤ 0.001.

Subject	Stimulation	x	y	z	Cluster size (2 mm^3 voxels)	T-score
2	LD1	46	-30	66	17	6.27
		58	-16	54	14	5.52
		54	-20	38	14	5.49
		56	-30	56	22	5.44
		48	-40	60	33	5.23
		50	-26	50	22	5.01
		62	-26	50	22	4.69
		42	-26	36	17	4.45
		56	-12	42	5	4
		38	-30	50	17	3.83
		60	-18	46	14	3.64
		52	-42	46	3	3.36
		38	-6	64	1	3.27
		52	-42	54	1	3.21
		54	-44	52	3	3.18
		54	-10	40	1	3.11
	LD5	40	-28	60	40	4.42
		38	-36	50	3	3.75
		38	-44	42	4	3.70
		56	-16	36	7	3.60
		62	-38	44	2	3.54
		36	-12	54	2	3.47
		54	-22	56	2	3.29
		64	-18	38	1	3.26
		44	-14	36	1	3.26
		34	-6	36	1	3.12
	RD1	-58	-12	46	135	8.20
		-56	-26	50	121	7.51
		-52	-32	56	121	6.63
		-42	-38	64	121	6.58
		-34	-18	48	5	4.03
		-32	-34	66	1	3.19
	RD5	-58	-12	46	63	6.92
		-52	-30	52	86	5.99
		-46	-36	42	86	5.71
		-56	-40	48	22	4.97
		-34	-38	56	7	3.88
		-32	-30	58	2	3.7
		-58	-44	38	2	3.62
		-36	-36	52	1	3.57
		-42	-42	40	3	3.48
		-54	-6	42	1	3.23

Table 31: Statistics of the SI activations for study 1. All values shown above an uncorrected p value threshold of ≤ 0.001.

Subject	Stimulation	x	y	z	Cluster size (2 mm^3 voxels)	T-score
3	LD1	48	-22	40	563	8.19
		62	-36	48	29	4.37
		44	-6	58	11	4.06
		36	-42	48	11	3.73
		68	-28	38	1	3.72
		46	-34	42	6	3.63
		36	-38	42	3	3.63
		52	-44	46	2	3.49
	LD5	44	-26	58	103	6.10
		44	-20	44	103	5.50
		40	-22	66	103	5.19
		48	-42	60	25	3.95
		54	-36	54	25	3.90
		56	-10	38	3	3.81
		48	-38	42	5	3.77
		34	-30	48	4	3.66
		60	-40	46	6	3.58
		64	-34	44	3	3.33
		34	-26	36	2	3.17
		48	-6	54	1	3.15
	RD1	-48	-26	48	26	6.42
		-52	-40	44	13	4.65
		-52	-38	54	11	4.27
		-54	-6	48	6	4.12
		-44	-10	60	23	3.96
		-42	-40	60	11	3.87
		-42	-28	40	26	3.80
		-56	-20	46	22	3.76
		-52	-20	38	22	3.61
		-50	-26	56	26	3.46
		-42	-40	56	3	3.43
		-40	-10	60	2	3.41
		-56	-30	36	5	3.35
		-40	-12	52	1	3.11

Table 32: Statistics of the SI activations for study 1. All values shown above an uncorrected p value threshold of ≤ 0.001.

Subject	Stimulation	x	y	z	Cluster size (2 mm^3 voxels)	T-score
3	RD5	-54	-34	38	306	6.72
		-32	-42	40	96	5.73
		-34	-32	44	5	3.87
		-42	-42	46	3	3.48
		-34	-30	40	2	3.43
		-36	-20	66	1	3.37
		-54	-6	48	2	3.34
		-32	-14	40	1	3.33
		-38	-40	58	1	3.24
		-32	-44	50	1	3.13
4	LD1	58	-8	46	19	5.09
		52	-18	46	13	4.55
		50	-12	38	6	3.93
		50	-38	52	8	4.03
		40	-12	48	3	3.62
		52	-28	52	2	3.59
		38	-28	60	2	3.91
		32	-36	46	1	3.24
		44	-44	48	2	3.18
		34	-12	40	1	3.15
	LD5	54	-22	52	7	5.04
		48	-20	64	7	4.2
		58	-8	44	6	3.66
		50	-30	52	3	3.25

Table 33: Statistics of the SI activations for study 1. All values shown above an uncorrected p value threshold of ≤ 0.001.

Subject	Stimulation	x	y	z	Cluster size (2 mm^3 voxels)	T-score
4	RD1	-54	-6	50	25	5.61
		-34	-6	36	4	4.21
		-52	-18	52	4	3.94
		-48	-28	52	8	3.79
		-42	-22	38	5	3.69
		-32	-8	60	9	3.63
		-46	-44	42	3	3.56
		-34	-6	50	2	3.55
		-42	-26	46	2	3.51
		-32	-32	66	2	3.51
		-40	-8	52	6	3.45
		-48	-16	36	2	3.44
		-38	-40	44	2	3.37
		-42	-44	60	4	3.34
		-32	-6	66	1	3.33
		-44	-14	60	1	3.31
		-50	-14	58	3	3.26
		-42	-32	62	1	3.24
		-36	-32	46	1	3.24
		-50	-26	42	2	3.19
		-32	-12	54	1	3.11
		-50	-42	58	1	3.11

Table 34: Statistics of the SI activations for study 1. All values shown above an uncorrected p value threshold of ≤ 0.001.

Subject	Stimulation	x	y	z	Cluster size (2 mm^3 voxels)	T-score
4	RD5	-50	-20	50	16	5.84
		-58	-6	42	19	5.8
		-30	-20	58	8	5.38
		-40	-40	64	44	4.85
		-50	-16	58	15	4.82
		-46	-20	40	15	4.6
		-36	-20	42	40	4.25
		-30	-30	38	4	3.96
		-30	-30	62	14	3.92
		-58	-38	48	3	3.88
		-44	-22	64	3	3.75
		-36	-22	66	5	3.75
		-42	-18	64	13	3.73
		-30	-8	54	5	3.62
		-46	-28	44	2	3.3
		-48	-34	42	2	3.26
		-56	-36	50	1	3.25
		-36	-22	52	1	3.24
		-30	-18	36	1	3.19
		-40	-34	58	1	3.17
		-30	-8	66	1	3.13
		-56	-26	44	1	3.12
		-60	-34	44	1	3.11
5	LD1	60	-16	48	66	8.48
		52	-16	56	66	5.49
		50	-30	52	8	4.81
		56	-16	38	66	4.73
		44	-8	50	9	4.21
		38	-36	52	10	3.87
		30	-26	64	2	3.59
		46	-32	42	8	3.56
		40	-26	50	1	3.28
		36	-36	44	2	3.28
	LD5	62	-16	48	201	9.01
		56	-18	42	201	7.87
		48	-32	60	201	6.19
		36	-28	62	23	4.64
		62	-32	36	22	4.44
		44	-44	36	25	3.77
		30	-28	54	11	3.35

Table 35: Statistics of the SI activations for study 1. All values shown above an uncorrected p value threshold of ≤ 0.001.

Subject	Stimulation	x	y	z	Cluster size (2 mm^3 voxels)	T-score
5	RD1	-46	-12	52	162	7.08
		-60	-20	42	26	4.35
		-48	-36	38	9	4.22
		-58	-38	42	20	4.09
		-60	-28	46	3	3.78
		-30	-10	58	1	3.63
		-58	-36	50	4	3.45
		-50	-44	46	1	3.26
		-44	-26	40	3	3.23
		-52	-30	48	2	3.22
		-30	-10	66	2	3.2
		-38	-32	64	2	3.18
	RD5	-54	12	48	194	9.04
		-48	-30	60	154	7.62
		-40	-16	64	154	6.9
		-32	-14	60	154	6
		-36	-32	62	27	4.59
		-54	-32	50	6	3.95
		-38	-44	36	6	3.73
		-48	-42	54	3	3.69
		-44	-40	42	2	3.47
		-58	-42	44	5	3.36
		-36	-34	52	1	3.27
		-38	-36	44	1	3.26
		-50	-34	54	2	3.21
		-34	-14	48	1	3.12
6	LD1	52	-12	54	14	4.71
		46	-14	60	13	4.66
		60	-16	48	21	4.16
		40	-44	62	3	3.83
		64	-36	42	2	3.72
		52	-26	46	2	3.69
		56	-22	56	20	3.54
		56	-18	38	1	3.44
		44	-24	40	2	3.22
		56	-32	38	1	3.15
		48	-44	48	1	3.14

Table 36: Statistics of the SI activations for study 1. All values shown above an uncorrected p value threshold of ≤ 0.001.

Subject	Stimulation	x	y	z	Cluster size (2 mm^3 voxels)	T-score
6	LD5	54	-16	44	2	3.66
		58	-22	54	3	3.32
		48	-10	48	1	3.14
		42	-10	58	1	3.14
		50	-42	50	1	3.12
	RD1	-50	-10	54	230	7.02
		-52	-10	36	230	6.53
		-60	-38	48	27	5.28
		-48	-36	58	26	4.49
		-54	-38	38	12	4.48
		-40	-42	58	12	4.44
		-56	-32	52	27	4.44
		-58	-28	46	9	4.22
		-50	-28	54	2	4.11
		-46	-26	50	8	4.02
		-40	-12	44	6	3.72
		-38	-28	52	15	3.72
		-30	-22	50	3	3.5
		-48	-42	62	1	3.47
		-34	-30	66	1	3.37
		-44	-22	38	4	3.29
		-40	-16	66	1	3.23
	RD5	-46	-24	62	277	6.09
		-34	-42	42	11	4.76
		-38	-42	64	33	3.79
		-32	-42	58	33	3.72
		-42	-40	48	8	3.64
		-30	-20	60	6	3.63
		-54	-38	52	1	3.59
		-36	-12	42	2	3.42
		-32	-18	52	5	3.36
		-64	-38	36	2	3.33
		-36	-36	38	1	3.27

B.2 Study 2

Table 37: Statistics of the SI activations for study 2. All values shown above an uncorrected p value threshold of ≤ 0.001.

Subject	Stimulation	x	y	z	Cluster size (2 mm^3 voxels)	T-score
1	LD1	58	-10	48	2	3.78
		44	-12	64	2	3.77
		48	-44	58	2	3.71
		56	-6	42	4	3.7
		58	-38	44	5	3.69
		56	-22	56	3	3.63
		48	-36	48	3	3.5
		64	-38	40	1	3.41
		38	-42	60	2	3.33
		56	-42	56	1	3.27
	LD5					
	RD1	-58	-18	50	2	4.11
	RD5	-56	-20	50	13	4.49
		-38	-32	54	14	4.44
		-50	-20	40	24	4.32
		-36	-22	36	15	4.2
		-38	-20	44	15	3.95
		-58	-38	46	4	3.56
		-54	-12	54	1	3.37
		-46	-36	62	1	3.36
		-58	-44	42	1	3.23
		-46	-30	64	1	3.14
2	LD1	48	-40	62	148	8.4
		66	-16	36	148	7.16
		62	-6	42	27	4.9
		50	-14	60	13	4.84
		44	-20	66	6	4.43
		56	-22	38	2	3.54
		46	-28	54	1	3.45
		40	-8	64	2	3.34
		36	-12	58	1	3.29
		42	-28	54	2	3.28
		40	-30	36	1	3.24
	LD5	50	-36	60	8	3.73
		46	-42	64	2	3.34
		44	-20	64	2	3.27
		60	-16	38	1	3.22
		50	-24	40	1	3.19

Table 38: Statistics of the SI activations for study 2. All values shown above an uncorrected p value threshold of ≤ 0.001.

Subject	Stimulation	x	y	z	Cluster size (2 mm^3 voxels)	T-score
2	RD1	-60	-10	42	12	5.15
		-48	-26	56	18	4.56
		-52	-16	50	5	3.99
		-50	-10	58	4	3.75
	RD5	-30	-32	52	1	3.48
		-32	-28	54	2	3.33
		-58	-22	48	1	3.29
		-50	-32	36	2	3.24
		-46	-34	56	1	3.14
		-60	-40	44	1	3.13
3	LD1	62	-12	44	39	6.87
		56	-20	58	39	5
		60	-20	48	39	4.78
		50	-8	56	7	3.75
		46	-6	38	1	3.2
		56	-6	52	1	3.15
	LD5	56	-24	56	81	7.04
		50	-26	62	81	6.95
		44	-30	38	5	3.45
		40	-34	52	1	3.39
	RD1	-58	-20	48	26	6.23
		-54	-16	56	26	3.5
		-48	-16	62	7	4.8
		-56	-30	54	8	4.47
		-54	-32	48	3	3.92
		-46	-22	42	3	3.87
	RD5	-48	-32	52	1	3.17
		-56	-16	50	6	4.57
		-58	-22	44	11	4.55
		-48	-36	42	8	4.34
		-44	-20	64	16	4.23
		-52	-28	58	5	4.13
		-48	-32	62	6	3.75
		-34	-24	62	6	3.55
		-34	-22	54	2	3.55
		-46	-42	44	1	3.27

Table 39: Statistics of the SI activations for study 2. All values shown above an uncorrected p value threshold of ≤ 0.001.

Subject	Stimulation	x	y	z	Cluster size (2 mm^3 voxels)	T-score
4	LD1	58	-10	46	21	5
		54	-10	52	13	4.51
		54	-22	48	9	4.35
		30	-38	46	1	3.22
		36	-24	64	1	3.18
	LD5	36	-12	42	8	4.29
		48	-26	60	2	3.76
		44	-6	58	1	3.21
	RD1	-44	-44	64	2	3.35
		-48	-36	40	2	3.68
		-34	-42	62	1	3.46
		-56	-38	50	3	3.42
		-56	-36	46	2	3.3
	RD5	-50	-24	54	2	3.55
		-40	-42	38	1	3.34
5	LD1	62	-16	48	35	7.12
		52	-18	56	26	6.29
		56	-16	40	8	4.24
		48	-20	62	3	3.71
		36	-34	50	2	3.37
		56	-30	50	3	3.35
		48	-42	42	6	3.84
		56	-30	46	1	3.38
	LD5	58	-16	44	13	4.16
		42	-28	58	2	3.56
		38	-36	38	1	3.75
		66	-22	38	1	3.18
	RD1	-50	-22	56	53	5.59
		-42	-14	60	53	5.35
		-54	-14	50	19	5.16
		-42	-18	52	53	4.56
		-48	-32	62	9	4.34
		-54	-16	54	1	3.96
		-34	-26	62	1	3.76
		-54	-26	52	1	3.56
		-34	-22	52	1	3.5
		-40	-22	58	5	3.43
		-58	-24	46	2	3.25
		-34	-12	54	1	3.2
		-36	-32	66	1	3.18
		-48	-20	38	1	3.17
		-38	-36	62	2	3.16

Table 40: Statistics of the SI activations for study 2. All values shown above an uncorrected p value threshold of ≤ 0.001.

Subject	Stimulation	x	y	z	Cluster size (2 mm^3 voxels)	T-score
5	RD5	-48	-26	62	3	3.82
		-54	-10	52	5	3.59
		-54	-20	56	1	3.49
		-38	-24	64	6	3.48
		-56	-16	46	1	3.46
		-50	-18	40	3	3.37
		-52	-22	58	1	3.33
		-40	-18	66	4	3.3
6	LD1	58	-24	54	30	5.67
		60	-14	46	30	5.61
		54	-38	40	7	4.52
		48	-18	52	30	4.21
		54	-12	56	5	4.19
		36	-28	62	7	3.89
		46	-10	56	4	3.87
		54	-14	36	4	3.72
		54	-18	42	5	3.59
		30	-6	62	3	3.45
		50	-12	38	1	3.3
		34	-38	66	3	3.28
		46	-26	40	1	3.16
		66	-14	40	1	3.15
	LD5					
	RD1	-64	-16	40	30	5.21
		-56	-18	50	30	5.09
		-54	-10	52	6	4.4
		-52	-26	42	2	3.2
	RD5	-60	-34	48	2	3.37
		-44	-36	54	1	3.29
7	LD1	56	-28	42	28	5.05
		58	-18	52	19	4.66
		62	-26	36	28	4.25
		62	-18	42	17	4.17
		58	-34	56	8	4.05
		36	-14	42	1	3.22
		38	-26	44	1	3.21
		52	-12	56	1	3.19
		50	-34	46	1	3.16
	LD5					

Table 41: Statistics of the SI activations for study 2. All values shown above an uncorrected p value threshold of ≤ 0.001.

Subject	Stimulation	x	y	z	Cluster size (2 mm^3 voxels)	T-score
7	RD1	-62	-22	44	15	4.38
		-52	-26	58	13	4.08
		-54	-22	56	3	3.85
	RD5	-54	-30	44	6	4.23
		-58	-24	42	10	4.08
		-56	-22	48	2	3.64
		-42	-34	48	4	3.53

B.3 Study 3

B.3.1 12 minutes

Table 42: Statistics of the SI activations for study 3 after 12 minutes of scanning. All values shown above an uncorrected p value threshold of ≤ 0.001.

Subject	Stimulation	x	y	z	Cluster size (2 mm^3 voxels)	T-score
1	RD1	-58	-18	48	135	12.71
		-48	-16	60	135	8.96
		-42	-10	62	135	8.28
		-56	-8	50	8	5.87
		-62	-40	40	18	4.80
		-60	-34	38	10	4.36
		-32	-42	60	3	3.33
		-32	-32	46	2	3.27
		-60	-6	44	1	3.24
		-38	-36	58	1	3.24
		-30	-16	46	1	3.19
		-38	-34	54	1	3.17
	RD5	-58	-20	48	32	8.15
		-50	-26	36	6	4.47
		-42	-12	60	4	4.14
		-44	-30	60	8	3.96
		-36	-10	64	4	3.86
		-52	-26	58	7	3.78
		-40	-32	36	1	3.76
		-36	-32	62	4	3.52
		-48	-18	60	3	3.49
		-58	-10	46	1	3.46
		-44	-30	44	3	3.44
		-32	-34	46	3	3.36
		-56	-12	50	1	3.28
2	RD1	-58	-10	42	82	9.63
		-50	-24	56	82	7.69
		-50	-8	56	82	7.02
		-40	-24	66	52	5.47
		-42	-14	36	11	4.57
		-48	-16	40	4	4.00
		-36	-18	60	1	3.27
		-52	-14	36	2	3.22
		-44	-22	48	2	3.21
		-52	-22	38	2	3.20
		-38	-24	56	1	3.17
		-42	-24	38	1	3.14

Table 43: Statistics of the SI activations for study 3 after 12 minutes of scanning. All values shown above an uncorrected p value threshold of ≤ 0.001.

Subject	Stimulation	x	y	z	Cluster size (2 mm^3 voxels)	T-score
2	RD5	-58	-8	44	43	8.53
		-50	-24	60	43	6.88
		-56	-20	50	43	5.36
		-48	-38	58	17	4.53
		-38	-24	52	8	4.36
		-36	-14	44	5	3.96
		-48	-8	58	1	3.69
		-40	-14	58	1	3.50
		-46	-10	60	1	3.25
		-44	-12	62	1	3.24
		-48	-38	52	1	3.23
		-44	-38	52	1	3.21
		-34	-32	66	1	3.18
3	RD1	-62	-24	46	42	6.86
		-60	-14	44	42	5.58
		-48	-6	38	24	4.23
		-50	-20	48	2	3.46
		-54	-30	54	1	3.41
		-50	-6	54	4	3.39
		-54	-6	50	1	3.38
		-30	-22	38	1	3.14
	RD5	-56	-20	42	16	5.95
		-50	-22	62	6	4.53
		-62	-40	38	5	4.21
		-54	-20	36	16	4.21
		-50	-38	40	6	4.02
		-36	-12	56	1	3.93
		-50	-40	54	10	3.90
		-52	-24	58	4	3.87
		-54	-40	42	1	3.54
		-40	-22	62	2	3.34
		-56	-44	42	2	3.27

Table 44: Statistics of the SI activations for study 3 after 12 minutes of scanning. All values shown above an uncorrected p value threshold of ≤ 0.001.

Subject	Stimulation	x	y	z	Cluster size (2 mm^3 voxels)	T-score
4	RD1	-52	-8	54	26	8.51
		-54	-16	54	26	7.54
		-48	-18	40	5	4.01
		-50	-14	44	2	3.73
		-44	-42	66	2	3.51
		-48	-32	62	1	3.25
		-58	-26	40	1	3.19
	RD5	-56	-18	52	24	7.20
		-54	-12	54	8	4.81
		-38	-22	62	3	4.18
		-52	-16	36	2	3.66
		-64	-34	42	2	3.59
		-58	-14	42	1	3.32
5	RD1	-48	-32	62	67	9.91
		-54	20	44	67	8.97
		-60	-30	50	67	7.93
		-48	-16	60	15	6.07
		-40	-34	44	29	5.53
		-56	-38	48	9	4.27
		-42	-6	62	5	4.14
		-52	-6	54	7	3.91
		-32	-8	42	1	3.77
		-32	-28	36	5	3.63
		-46	-6	38	4	3.48
		-34	-18	44	4	3.42
		-32	-6	60	1	3.31
		-40	-30	38	2	3.27
		-38	-40	66	1	3.22
		-38	-8	46	1	3.18
		-52	-30	48	1	3.17
	RD5	-56	-22	42	11	5.17
		-50	-22	46	5	3.86
		-50	-20	56	3	3.81
		-58	-40	36	1	3.36
		-58	-32	52	3	3.34
		-50	-30	60	1	3.2

Table 45: Statistics of the SI activations for study 3 after 12 minutes of scanning. All values shown above an uncorrected p value threshold of ≤ 0.001.

Subject	Stimulation	x	y	z	Cluster size (2 mm^3 voxels)	T-score
6	RD1	-58	-22	50	37	6.73
		-50	-16	48	37	4.67
		-54	-42	52	2	3.93
		-36	-16	38	4	3.85
		-46	-26	44	1	3.35
		-40	-12	56	1	3.35
		-38	-30	44	1	3.23
		-60	-36	40	1	3.19
	RD5	-56	-26	50	44	5.84
		-44	-38	54	32	5.07
		-36	-6	66	8	4.6
		-38	-44	64	8	4.5
		-52	-22	44	3	4.34
		-52	-40	56	3	4.25
		-50	-30	36	9	4.19
		-44	-18	60	3	3.92
		-40	-34	42	4	3.76
		-42	-22	60	4	3.74
		-56	-32	42	4	3.74
		-36	-38	40	5	3.69
		-36	-20	66	2	3.64
		-48	-34	48	2	3.4
		-58	-42	50	3	3.39
		-40	-24	66	1	3.36
		-52	-22	40	1	3.34
		-52	-40	36	3	3.29
		-50	-24	58	1	3.28
		-56	-24	42	1	3.24
		-58	-36	50	2	3.2
		-42	-34	48	1	3.2

Table 46: Statistics of the SI activations for study 3 after 12 minutes of scanning. All values shown above an uncorrected p value threshold of ≤ 0.001.

Subject	Stimulation	x	y	z	Cluster size (2 mm^3 voxels)	T-score
7	RD1	-54	-16	44	23	5.36
		-40	-24	56	1	3.82
		-48	-22	48	2	3.73
		-44	-20	56	1	3.47
		-54	-14	54	1	3.44
		-44	-22	40	1	3.34
	RD5	-40	-44	48	50	4.63
		-54	-44	38	23	4.59
		-46	-42	60	50	4.32
		-56	-16	42	5	4
		-58	-30	48	11	3.98
		-54	-22	48	4	3.61
		-32	-44	40	2	3.49
		-56	-12	48	3	3.45
		-58	-44	48	3	3.3
		-52	-28	56	10	3.28
		-46	-10	42	1	3.25
8	RD1	-56	-10	40	3	4.02
		-60	-22	48	1	3.84
		-62	-22	44	2	3.83
		-58	-26	52	3	3.69
		-44	-44	64	1	3.17
	RD5	-60	-28	46	17	5.63
		-48	-26	44	1	3.95
		-54	-22	48	1	3.73
		-46	-40	56	1	3.51
		-44	-8	48	1	3.16

B.3.2 20 minutes

Table 47: Statistics of the SI activations for study 3 after 20 minutes of scanning. All values shown above an uncorrected p value threshold of ≤ 0.001.

Subject	Stimulation	x	y	z	Cluster size (2 mm^3 voxels)	T-score
1	RD1	-58	-18	48	326	16.69
		-56	-8	50	8	5.5
		-60	-42	42	25	4.52
		-44	-36	58	15	4.44
		-42	-30	52	12	4.42
		-46	-32	60	11	4.27
		-30	-42	58	3	3.78
		-32	-34	46	2	3.41
		-48	-12	50	1	3.4
		-60	-6	44	1	3.19
		-54	-32	52	1	3.14
	RD5	-58	-20	48	44	9.81
		-42	-14	62	38	6.45
		-46	-30	60	13	4.87
		-44	-30	44	4	4.25
		-34	-34	46	10	4.05
		-36	-32	62	6	3.86
		-32	-22	40	1	3.37
2	RD1	-58	-10	42	120	11.9
		-50	-24	56	120	9.06
		-40	-14	66	12	5.3
		-42	-14	38	9	4.82
		-36	-6	64	13	4.59
		-52	-22	38	2	3.8
		-42	-24	38	1	3.32
		-38	-8	40	1	3.18
		-46	-16	40	1	3.15
	RD5	-58	-10	44	60	10.16
		-48	-24	58	60	8.41
		-54	-26	52	60	6.52
		-48	-36	58	11	4.33
		-48	-8	58	3	3.9
		-44	-38	52	7	3.81
		-44	-12	62	1	3.42
		-34	-6	64	2	3.41
		-52	-6	54	2	3.26
		-40	-24	54	1	3.26
		-40	-14	58	1	3.17
		-36	-16	42	1	3.16
		-40	-16	52	1	3.13

Table 48: Statistics of the SI activations for study 3 after 20 minutes of scanning. All values shown above an uncorrected p value threshold of ≤ 0.001.

Subject	Stimulation	x	y	z	Cluster size (2 mm^3 voxels)	T-score
3	RD1	-58	-20	40	41	6.11
		-58	-24	50	41	5.67
		-50	-6	54	23	5.6
		-60	-14	46	8	4.79
		-52	-44	50	4	3.69
		-48	-44	46	1	3.42
		-54	-30	54	1	3.19
	RD5	-56	-20	40	21	6.87
		-48	-20	60	12	4.62
		-62	-42	40	6	4.53
		-36	-32	62	2	3.86
		-50	-40	52	3	3.73
		-40	-22	62	2	3.67
		-30	-42	66	1	3.27
		-46	-30	62	1	3.21
		-54	-42	52	1	3.13
4	RD1	-52	-8	54	26	9.99
		-54	-16	52	26	9.37
		-50	-18	40	26	4.36
		-44	-44	64	3	4.01
		-54	-14	38	4	3.63
		-54	-32	58	2	3.55
		-48	-12	50	3	3.51
		-60	-6	38	1	3.44
		-44	-16	46	1	3.44
		-40	-22	40	1	3.44
		-44	-24	48	2	3.38
		-38	-36	64	1	3.27
		-40	-22	36	1	3.17
	RD5	-56	-18	52	38	7.74
		-52	-16	38	2	4.41
		-36	-26	36	2	3.79
		-60	-36	42	4	3.71
		-58	-30	44	1	3.34
		-64	-34	42	1	3.26
		-52	-16	42	1	3.14

Table 49: Statistics of the SI activations for study 3 after 20 minutes of scanning. All values shown above an uncorrected p value threshold of ≤ 0.001.

Subject	Stimulation	x	y	z	Cluster size (2 mm^3 voxels)	T-score
5	RD1	-48	-32	62	119	11.76
		-56	-16	50	119	11.51
		-60	-30	50	119	9.33
		-42	-6	62	12	5.28
		-52	-6	52	11	4.79
		-46	-6	38	10	4.55
		-40	-36	46	13	4.5
		-38	-8	46	5	4.44
		-56	-38	48	8	4.12
		-30	-30	36	9	3.86
		-38	-30	38	1	3.73
		-32	-6	60	1	3.57
		-40	-18	44	1	3.3
		-32	-40	52	2	3.3
		-44	-12	44	2	3.25
		-34	-16	38	1	3.24
		-50	-36	42	1	3.15
	RD5	-56	-22	42	12	4.35
		-50	-20	56	8	4.35
		-52	-30	58	5	4.11
		-56	-38	44	12	4.07
		-40	-32	42	7	3.97
		-56	-14	48	6	3.7
		-58	-38	50	1	3.49
		-40	-18	38	3	3.39
		-52	-6	52	1	3.35
		-62	-42	38	1	3.35
		-52	-30	40	2	3.31
		-56	-16	36	1	3.29
		-50	-36	58	1	3.14

Table 50: Statistics of the SI activations for study 3 after 20 minutes of scanning. All values shown above an uncorrected p value threshold of ≤ 0.001.

Subject	Stimulation	x	y	z	Cluster size (2 mm^3 voxels)	T-score
6	RD1	-56	-26	52	38	9.09
		-56	-14	52	38	6.95
		-54	-22	44	38	5.1
		-54	-32	46	9	4.28
		-46	-26	42	4	3.98
		-58	-44	50	5	3.65
		-58	-36	50	15	3.51
		-34	-14	50	2	3.39
		-44	-36	38	1	3.19
		-56	-40	42	1	3.18
		-56	-40	36	1	3.17
	RD5	-56	-26	50	56	6.18
		-44	-38	54	12	5.69
		-40	-22	58	8	4.69
		-36	-40	42	11	4.67
		-46	-30	64	6	4.65
		-54	-32	44	10	4.36
		-38	-40	48	12	4.09
		-44	-18	60	5	3.9
		-58	-36	50	2	3.56
		-36	-20	66	1	3.48
		-40	-24	66	5	3.47
		-30	-16	46	3	3.42
		-52	-40	38	2	3.42
		-56	-26	40	1	3.39
7	RD1	-54	-16	44	8	4.49
		-46	-34	64	1	3.53
		-58	-34	36	3	3.34
		-52	-38	58	1	3.14
	RD5	-56	-12	48	20	5.26
		-54	-20	46	20	4.6
		-58	-30	52	15	4.56
		-54	-44	38	23	4.39
		-40	-44	48	9	4.26
		-50	-16	56	2	4.25
		-32	-44	38	2	3.38
		-48	-42	60	5	3.35
		-52	-24	52	1	3.27

Table 51: Statistics of the SI activations for study 3 after 20 minutes of scanning. All values shown above an uncorrected p value threshold of ≤ 0.001.

Subject	Stimulation	x	y	z	Cluster size (2 mm^3 voxels)	T-score
8	RD1	-58	-26	52	5	4.34
		-60	-22	48	1	3.37
		-60	-32	46	1	3.37
		-62	-22	44	1	3.27
		-44	-6	46	3	3.26
		-58	-40	44	2	3.24
		-56	-8	38	1	3.22
	RD5	-60	-28	48	11	5.41
		-46	-6	48	3	4.24
		-60	-22	40	2	3.54
		-56	-24	46	1	3.42

B.4 Study 4

Table 52: Statistics of the SI activations for study 4. All values shown above an uncorrected p value threshold of ≤ 0.001.

Subject	Stimulation	x	y	z	Cluster size (2 mm^3 voxels)	T-score
1	RD1	-58	-22	46	82	12.65
		-48	-24	42	82	7.17
		-52	-30	52	82	6.81
		-38	-24	58	3	3.91
		-42	-16	62	4	3.9
	RD5	-60	-22	46	42	11.04
		-42	-26	64	25	6.99
		-48	-32	60	25	6.08
		-58	-16	38	42	5.45
		-36	-34	42	31	4.91
		-44	-16	60	7	4.58
		-56	-44	48	5	4.47
		-42	-36	66	4	4.19
		-54	-30	46	25	4.14
		-42	-32	42	2	3.73
		-42	-30	38	2	3.66
		-32	-18	62	5	3.65
		-30	-42	46	4	3.56
		-52	-36	54	1	3.19
		-44	-6	44	1	3.16
2	RD1	-52	-24	54	104	11.6
		-58	-10	42	104	11.12
		-58	-18	46	104	6.58
		-42	-24	66	18	6.12
		-34	-6	64	21	5.46
		-34	-16	58	6	5.12
		-46	-16	36	12	4.34
		-46	-32	54	22	4.21
		-34	-32	64	14	4.01
		-44	-32	46	4	3.62
		-36	-30	40	1	3.57
		-42	-36	44	4	3.57
		-40	-30	52	1	3.35

Table 53: Statistics of the SI activations for study 4. All values shown above an uncorrected p value threshold of ≤ 0.001.

Subject	Stimulation	x	y	z	Cluster size (2 mm^3 voxels)	T-score
2	RD5	-48	-24	58	61	8.97
		-60	-12	44	61	8.56
		-56	-26	46	61	4.9
		-40	-14	54	12	4.42
		-48	-32	56	7	4.23
		-36	-32	44	9	4.1
		-36	-32	66	5	3.53
		-42	-28	46	2	3.28
		-42	-30	40	1	3.21
		-46	-10	58	2	3.21
		-42	-40	60	1	3.16
		-42	-38	56	1	3.15
3	RD1	-60	-44	46	13	4.87
		-58	-24	50	2	3.86
		-50	-38	50	1	3.83
		-44	-16	42	5	3.82
		-56	-40	42	1	3.65
	RD5	-58	-22	40	40	6.69
		-52	-24	58	32	6.66
		-44	-32	66	20	5.68
		-42	-22	60	12	5.35
		-48	-32	62	32	4.05
		-40	-14	52	1	3.45
		-38	-22	50	1	3.2
4	RD1	-54	-18	52	50	10.94
		-50	-20	40	50	7.26
		-44	-22	46	21	5.21
		-48	-14	48	50	4.6
		-56	-16	40	4	3.5
		-34	-20	54	2	3.48
		-38	-42	66	3	3.35
		-40	-30	36	5	3.32
	RD5	-56	-18	52	17	8.11
		-40	-6	62	9	5.04
		-50	-18	38	17	4.59
		-58	-14	44	17	3.88
		-62	-36	36	2	3.43
		-46	-26	56	1	3.31
		-36	-34	46	1	3.18
		-58	-28	52	1	3.17
		-50	-18	60	1	3.14

Table 54: Statistics of the SI activations for study 4. All values shown above an uncorrected p value threshold of ≤ 0.001.

Subject	Stimulation	x	y	z	Cluster size (2 mm^3 voxels)	T-score
5	RD1	-52	-28	58	263	15.47
		-56	-16	48	263	14.53
		-60	-28	48	263	12.92
		-42	-38	48	27	5.87
		-38	-32	44	27	5.47
		-38	-32	58	2	4
		-44	-6	60	1	3.15
		-40	-10	62	1	3.14
		-30	-44	64	1	3.14
		-44	-42	38	1	3.13
		-62	-14	36	1	3.13
	RD5	-56	-20	44	65	9.06
		-60	-28	48	65	8.69
		-52	-28	58	65	7.71
		-42	-28	56	5	4
		-40	-6	54	1	3.87
		-44	-32	48	2	3.61
		-50	-16	58	4	3.48
		-52	-28	48	1	3.23
		-48	-10	40	2	3.17
		-38	-44	64	1	3.13
6	RD1	-56	-26	52	319	13.36
		-58	-12	48	319	10.51
		-42	-18	66	1	3.82
		-44	-16	64	1	3.27
		-42	-42	64	1	3.7
		-54	-32	38	34	4.72
		-44	-44	50	10	3.43
		-38	-42	52	6	3.71
		-56	-42	46	6	3.51
		-54	-38	36	1	3.3
		-32	-22	52	1	3.21

Table 55: Statistics of the SI activations for study 4. All values shown above an uncorrected p value threshold of ≤ 0.001.

Subject	Stimulation	x	y	z	Cluster size (2 mm^3 voxels)	T-score
6	RD5	-54	-24	50	44	7.68
		-42	-20	58	21	6.72
		-48	-28	62	17	5.15
		-44	-12	62	3	4.2
		-50	-18	60	6	4.14
		-62	-26	46	1	3.19
		-34	-20	60	21	3.41
		-52	-44	56	31	4.95
		-32	-18	50	6	4.34
		-52	-34	42	6	3.87
		-62	-30	42	2	3.46
		-34	-28	62	1	3.16
7	RD1	-56	-12	46	27	6.1
		-50	-22	48	4	4.72
		-52	-38	38	6	3.73
		-54	-42	56	1	3.62
		-56	-32	54	2	3.13
	RD5	-56	-12	50	10	4.91
		-54	-42	36	25	4.56
		-50	-14	52	8	4.18
		-52	-20	56	9	3.87
		-42	-10	54	3	3.77
		-30	-14	54	1	3.75
		-42	-30	48	6	3.7
		-58	-14	40	10	3.58
		-34	-44	38	2	3.4
		-52	-22	48	3	3.37
		-32	-30	40	1	3.16
8	RD1	-62	-22	42	26	8.86
		-58	-28	50	27	6.98
		-58	-40	48	5	4.32
		-56	-28	42	2	4.17
		-62	-42	40	4	4.06
		-44	-44	64	1	3.77
		-52	-30	58	1	3.46
		-38	-28	62	1	3.41
		-52	-44	58	2	3.4
		-48	-6	58	2	3.22
		-50	-40	48	1	3.13

Table 56: Statistics of the SI activations for study 4. All values shown above an uncorrected p value threshold of ≤ 0.001.

Subject	Stimulation	x	y	z	Cluster size (2 mm^3 voxels)	T-score
8	RD5	-58	-22	48	17	5.48
		-62	-18	40	17	5.23
		-52	-26	56	8	4.31
		-44	-10	56	5	3.83
		-52	-34	56	3	3.82
		-50	-20	46	3	3.81
		-54	-16	36	3	3.72
		-40	-24	46	3	3.65
		-58	-6	38	1	3.54
		-46	-20	42	1	3.21
		-42	-12	48	1	3.14

B.5 Study 5

B.5.1 CRPS Patients

First Patient Scans

Table 57: Statistics of the SI activations for study 5. All values shown above an uncorrected p value threshold of ≤ 0.001.

Subject	Stimulation	x	y	z	Cluster size (2 mm^3 voxels)	T-score
P1a	LD1	46	-12	56	186	13.88
		38	-16	66	186	11.77
		52	-16	52	186	10.80
		64	-14	40	50	7.78
		32	-26	66	4	5.00
		52	-28	54	7	4.18
		38	-44	44	3	3.73
		56	-22	46	4	3.70
		32	-26	56	7	3.69
		32	-36	56	1	3.33
		62	-32	46	1	3.29
	LD5	38	-18	58	1067	13.61
		34	-44	50	21	4.98
		50	-36	50	3	4.45
		56	-16	38	10	4.42
		44	-40	64	3	4
		54	-44	44	5	3.84
		38	-10	50	10	3.75
		54	-32	56	2	3.52
		56	-22	44	2	3.15
	RD1	-48	-34	62	922	13.84
		-54	-24	52	922	12.73
		-50	-38	42	3	3.53
		-40	-14	40	1	3.46
		-42	-36	50	1	3.34
		-42	-38	36	1	3.20
		-40	-34	44	1	3.13
	RD5	-50	-30	60	838	12.54
		-34	-18	62	838	12.48
		-48	-40	44	2	3.49
		-44	-38	36	1	3.45
		-38	-34	48	1	3.28
		-42	-34	36	1	3.22
		-40	-32	46	1	3.14
		-36	-6	42	1	3.13

Table 58: Statistics of the SI activations for study 5. All values shown above an uncorrected p value threshold of ≤ 0.001.

Subject	Stimulation	x	y	z	Cluster size (2 mm^3 voxels)	T-score
P2a	LD1	60	-24	44	69	9.82
		58	-14	48	69	8.78
		52	-30	48	43	6.47
		52	-38	54	43	6.47
		46	-40	60	43	5.59
		38	-16	66	9	4.84
		64	-22	36	69	4.68
		44	-20	66	13	4.51
		46	-42	46	7	4.50
		56	-34	38	4	4.06
		44	-18	42	2	3.96
		62	-44	44	17	3.95
		38	-36	48	6	3.74
		44	-26	40	2	3.68
		64	-34	44	2	3.42
		42	-30	62	4	3.41
		56	-30	54	2	3.40
		36	-28	60	1	3.27
		64	-32	38	2	3.25
		30	-18	52	1	3.21
		54	-24	56	1	3.18
		34	-38	66	1	3.11

Table 59: Statistics of the SI activations for study 5. All values shown above an uncorrected p value threshold of ≤ 0.001.

Subject	Stimulation	x	y	z	Cluster size (2 mm^3 voxels)	T-score
P2a	LD5	54	-22	42	18	6.12
		44	-38	52	23	5.25
		46	-38	58	22	5.24
		52	-30	48	23	5.22
		54	-36	54	22	4.8
		54	-44	42	10	4.73
		50	-28	58	23	4.7
		58	-44	48	7	4.6
		42	-40	40	19	4.46
		64	-32	42	12	4.38
		58	-30	40	18	4.32
		64	-22	40	18	4.28
		66	-22	36	13	4.23
		30	-34	60	4	4.14
		34	-10	38	5	3.97
		56	-8	50	4	3.95
		56	-38	36	6	3.92
		52	-34	38	2	3.89
		40	-30	42	3	3.54
		30	-10	50	2	3.49
		60	-30	50	1	3.41
		50	-24	36	1	3.35
		64	-34	36	9	3.32
		34	-12	48	3	3.31
		38	-26	60	1	3.29
		48	-16	52	1	3.27
		52	-20	52	1	3.17
		36	-32	46	1	3.15
	RD1	-54	-16	50	348	8.83
		-46	-32	62	348	8.77
		-42	-8	62	25	6.82
		-30	-34	66	19	5.36
		-38	-32	64	10	5.11
		-60	-32	50	13	4.37
		-36	-14	56	25	3.97
		-34	-24	58	3	3.92
		-32	-42	44	21	3.90
		-50	-6	42	3	3.85
		-50	-10	50	1	3.79
		-34	-24	54	1	3.65
		-42	-8	44	1	3.17
		-34	-16	36	1	3.17

Table 60: Statistics of the SI activations for study 5. All values shown above an uncorrected p value threshold of ≤ 0.001.

Subject	Stimulation	x	y	z	Cluster size (2 mm^3 voxels)	T-score
P2a	RD5	-38	-20	66	49	7.89
		-40	-42	66	115	6.75
		-46	-28	60	115	6.14
		-34	-28	42	8	4.12
		-44	-30	44	1	3.61
		-54	-24	54	5	3.54
		-62	-32	46	2	3.38
		-60	-44	46	4	3.35
		-36	-40	38	1	3.28
		-38	-20	58	1	3.20
P3a	LD1	54	-26	54	34	6.42
		50	-14	48	13	5.15
		46	-34	62	13	5.07
		38	-32	58	13	4.63
		38	-12	44	14	4.50
		52	-12	56	12	4.47
		44	-10	60	8	4.23
		62	-16	44	9	4.12
		44	-10	50	7	4.03
		32	-30	48	12	4.02
		48	-20	40	13	3.91
		38	-12	54	4	3.48
		46	-42	36	1	3.44
		44	-38	58	1	3.33
		56	-34	48	1	3.31
		30	-30	64	3	3.26
	LD5	46	-34	62	132	8.86
		52	-22	48	132	8.85
		56	-14	50	7	4.68
		52	-44	46	28	4.15
		66	-20	40	6	3.96
		60	-30	36	2	3.47
		30	-6	40	5	3.39
		60	-42	38	6	3.38
		32	-44	38	2	3.31
		36	-32	62	1	3.27
		34	-42	40	1	3.16

Table 61: Statistics of the SI activations for study 5. All values shown above an uncorrected p value threshold of ≤ 0.001.

Subject	Stimulation	x	y	z	Cluster size (2 mm^3 voxels)	T-score
P3a	RD1	-52	-24	56	178	10.19
		-48	-30	60	178	8.03
		-56	-24	48	178	7.38
		-38	-14	66	13	4.32
		-42	-12	60	8	4.27
		-64	-28	36	10	4.14
		-30	-30	38	1	3.49
		-52	-42	50	3	3.47
		-34	-30	64	1	3.16
		-46	-16	44	1	3.11
	RD5	-46	-30	60	129	10.15
		-42	-36	64	129	7.48
		-54	-24	56	129	7.27
		-48	-38	38	12	4.37
		-50	-12	48	3	3.79
		-62	-30	38	5	3.77
		-32	-26	38	2	3.52
		-34	-44	58	4	3.49
		-34	-24	48	1	3.21
P4a	LD1	50	-6	38	13	4.88
		46	-42	52	3	3.81
		58	-8	40	14	3.81
		34	-26	38	2	3.79
		42	-20	64	3	3.55
		46	-8	40	2	3.53
		46	-8	56	2	3.50
		40	-14	36	4	3.49
		50	-36	54	1	3.47
		44	-22	42	1	3.31
		36	-42	50	2	3.26
		54	-28	56	1	3.22
		46	-40	44	1	3.19
	LD5	58	-20	44	2	3.63
		58	-38	54	3	3.48
		52	-18	38	1	3.41
		64	-22	36	1	3.25
		54	-40	44	1	3.23
		60	-6	42	1	3.12

Table 62: Statistics of the SI activations for study 5. All values shown above an uncorrected p value threshold of ≤ 0.001.

Subject	Stimulation	x	y	z	Cluster size (2 mm^3 voxels)	T-score
P4a	RD1	-54	-10	50	45	8.07
		-44	-18	50	45	6.34
		-46	-12	58	45	4.46
		-44	-36	64	70	7.78
		-50	-32	46	7	4.10
		-52	-22	42	4	3.57
		-40	-26	62	1	3.54
		-64	-26	40	2	3.41
		-32	-38	38	20	4.61
		-40	-38	38	17	4.43
		-38	-14	62	7	4.18
		-32	-16	52	5	4.06
		-42	-38	48	9	3.91
		-34	-24	48	1	3.32
		-52	-44	38	3	3.26
		-44	-38	36	1	3.20
		-32	-32	50	1	3.16
		-50	-38	48	1	3.15
		-54	-12	38	1	3.12
		-30	-32	54	1	3.20
	RD5	-54	-32	56	15	7.49
		-40	-36	66	18	5.80
		-52	-32	44	13	4.48
		-36	-22	62	6	4.27
		-40	-14	66	10	4.25
		-44	-16	58	5	4.12
		-48	-18	62	10	4.10
		-52	-24	58	15	4.08
		-58	-18	46	4	3.91
		-48	-22	60	5	3.86
		-56	-6	46	4	3.80
		-40	-22	54	3	3.71
		-40	-24	50	7	3.60
		-48	-18	38	1	3.54
		-50	-40	50	2	3.52
		-40	-22	58	1	3.25
		-42	-30	64	1	3.22
		-32	-36	66	1	3.17
		-50	-8	40	1	3.14
		-56	-28	48	15	3.13
		-60	-40	36	1	3.11

Second Patient Scans

Table 63: Statistics of the SI activations for study 5. All values shown above an uncorrected p value threshold of ≤ 0.001.

Subject	Stimulation	x	y	z	Cluster size (2 mm^3 voxels)	T-score
P1b	LD1	46	-14	58	101	10.42
		54	-12	46	101	9.44
		38	-16	42	100	7.43
		38	-12	62	4	4.18
		36	-34	62	5	4.02
		44	-24	42	5	3.85
		64	-38	44	3	3.76
		62	-14	38	1	3.62
		54	-38	52	9	3.5
		54	-6	52	2	3.33
		58	-26	46	1	3.33
		48	-24	44	1	3.29
		44	-42	60	1	3.16
		30	-12	38	2	3.17
	LD5	36	-20	58	67	8.37
		30	-24	48	67	6.52
		30	-40	60	7	4.7
		52	-20	56	14	4.53
		54	-12	46	5	4.37
		30	-38	40	4	3.98
		58	-36	42	7	3.68
		38	-12	48	1	3.51
		42	-26	52	1	3.24
		48	-14	56	1	3.23
		46	-26	44	1	3.21
		50	-16	58	1	3.16
		52	-40	48	1	3.15
		44	-26	40	1	3.11
	RD1	-48	-34	60	1268	15.4
		-48	-26	50	1268	13.18
		-34	-8	66	1268	12.86
		-44	-38	38	7	4.89
		-36	-44	36	2	3.26
		-36	-36	40	1	3.15

Table 64: Statistics of the SI activations for study 5. All values shown above an uncorrected p value threshold of ≤ 0.001.

Subject	Stimulation	x	y	z	Cluster size (2 mm^3 voxels)	T-score
P1b	RD5	-32	-18	60	970	13.79
		-34	-8	66	970	12.38
		-48	-32	60	970	11.11
		-50	-18	50	11	4.1
		-44	-36	40	6	4.05
		-38	-42	58	4	3.98
		-42	-10	38	5	3.62
		-58	-44	46	1	3.28
		-32	-44	48	2	3.26
		-30	-42	50	1	3.22
		-30	-44	54	1	3.16
		-48	-8	44	1	3.12
P2b	LD1	56	-12	50	39	6.76
		58	-24	46	39	6.28
		60	-14	42	39	4.92
		42	-18	62	4	3.67
		46	-28	36	1	3.28
		32	-16	58	1	3.23
		44	-22	42	1	3.2
		46	-8	58	1	3.13
	LD5	58	-24	46	35	6.06
		66	-30	40	20	5.5
		50	-38	60	17	5.18
		62	-42	46	22	4.91
		56	-32	56	17	4.83
		62	-34	46	20	4.55
		48	-26	62	8	4.09
		66	-22	42	35	4.05
		50	-34	38	10	3.73
		42	-34	46	3	3.65
		34	-6	36	1	3.62
		46	-36	52	17	3.42
		44	-22	56	1	3.33
		50	-42	36	1	3.28
		42	-8	64	1	3.2
		34	-20	36	1	3.16
		30	-36	46	2	3.18

Table 65: Statistics of the SI activations for study 5. All values shown above an uncorrected p value threshold of ≤ 0.001.

Subject	Stimulation	x	y	z	Cluster size (2 mm^3 voxels)	T-score
P2b	RD1	-38	-44	64	288	7.46
		-64	-34	36	9	4.32
		-30	-10	56	9	4.22
		-34	-28	42	17	4.08
		-54	-24	44	5	3.98
		-34	-24	52	2	3.76
		-42	-20	40	6	3.72
		-54	-34	50	2	3.65
		-48	-26	42	3	3.46
		-34	-44	40	5	3.42
		-50	-32	46	1	3.3
		-32	-34	60	1	3.3
		-30	-36	62	1	3.28
		-38	-20	42	1	3.2
		-40	-28	64	1	3.11
	RD5	-40	-18	62	312	9.10
		-46	-30	64	312	7.84
		-40	-38	66	312	7.82
		-34	-28	42	19	5.68
		-60	-16	44	18	4.94
		-44	-6	60	9	4.83
		-48	-22	40	4	3.86
		-64	-40	38	1	3.84
		-58	-30	42	1	3.78
		-34	-38	40	12	3.71
		-52	-24	42	1	3.64
		-38	-12	54	3	3.62
		-58	-24	48	2	3.60
		-34	-28	52	3	3.57
		-48	-8	50	1	3.48
		-48	-34	40	2	3.40
		-52	-32	42	1	3.37
		-32	-38	52	2	3.37
		-40	-42	38	1	3.22
		-42	-30	52	1	3.21
		-52	-26	50	1	3.14
		-36	-20	46	1	3.11

Table 66: Statistics of the SI activations for study 5. All values shown above an uncorrected p value threshold of ≤ 0.001.

Subject	Stimulation	x	y	z	Cluster size (2 mm^3 voxels)	T-score
P3b	LD1	54	-22	52	96	11.00
		46	-34	64	96	9.56
		44	-6	62	28	6.62
		38	-14	48	28	6.62
		64	-42	38	13	5.72
		44	-26	66	5	4.66
		40	-36	54	5	4.31
		52	-10	58	7	4.27
		54	-40	46	11	4.18
		48	-26	46	8	4.03
		68	-20	40	15	3.76
		36	-26	56	2	3.22
		44	-26	52	1.0	3.19
	LD5	30	-40	64	2	3.50
		32	-10	60	2	3.56
		34	-24	52	35	5.26
		38	-32	56	1	3.20
		38	-32	52	1	3.16
		44	-12	64	3	3.96
		46	-34	64	44	7.35
		46	-22	60	35	5.16
		48	-18	42	6	3.99
		50	-18	58	1	3.37
		54	-22	54	92	8.00
		54	-40	46	17	5.21
		54	-40	58	1	3.30
		62	-12	44	3	3.33

Table 67: Statistics of the SI activations for study 5. All values shown above an uncorrected p value threshold of ≤ 0.001.

Subject	Stimulation	x	y	z	Cluster size (2 mm^3 voxels)	T-score
P3b	RD1	-52	-20	58	215	12.54
		-48	-28	60	215	8.92
		-44	-36	42	25	5.84
		-34	-16	46	15	5.02
		-36	-22	56	15	4.43
		-32	-44	40	6	3.66
		-52	-24	40	1	3.61
		-36	-28	38	2	3.59
		-42	-42	40	3	3.54
		-56	-30	42	2	3.40
		-52	-20	36	1	3.30
		-48	-32	48	1	3.23
		-58	-32	50	1	3.13
		-38	-34	54	1	3.13
		-54	-40	50	1	3.11
		-30	-32	44	1	3.29
		-30	-40	66	1	3.11
P3b	RD5	-58	-20	46	421	10.6
		-56	-26	52	421	9.79
		-32	-44	36	23	4.08
		-54	-40	40	6	4.08
		-38	-14	56	5	3.92
		-60	-36	46	1	3.91
		-32	-6	44	2	3.76
		-58	-10	42	3	3.49
		-40	-42	38	2	3.42
P4b	LD1	64	-44	40	97	7.97
		60	-28	50	96	6.63
		50	-38	60	21	6.07
		42	-36	52	48	5.57
		58	-8	36	37	5.20
		44	-10	52	17	5.13
		60	-18	44	18	4.75
		64	-26	36	17	3.83
		50	-22	44	4	3.76
		32	-38	42	5	3.63
		38	-42	40	5	3.59
		56	-42	52	1	3.58
		52	-28	38	1	3.19
		52	-30	58	22	3.18
		54	-36	42	1	3.15
		54	-36	46	2	3.15

Table 68: Statistics of the SI activations for study 5. All values shown above an uncorrected p value threshold of ≤ 0.001.

Subject	Stimulation	x	y	z	Cluster size (2 mm^3 voxels)	T-score
P4b	LD5	56	-42	50	21	5.33
		50	-16	44	3	3.7
		48	-32	46	2	3.64
		62	-42	44	5	3.3
	RD1	-54	-8	46	228	11.61
		-56	-30	52	228	9.94
		-42	-38	62	60	8.76
		-36	-42	48	65	7.14
		-46	-36	50	65	5.87
		-32	-32	64	25	5.48
		-42	-26	36	12	4.03
		-60	-28	40	3	3.76
		-38	-20	52	7	3.74
		-30	-40	36	7	3.69
		-44	-44	50	1	3.14
	RD5	-54	-30	56	22	6.78
		-60	-18	44	57	6.42
		-52	-10	38	57	6.39
		-30	-14	58	21	5.45
		-54	-42	44	21	5.25
		-42	-20	56	30	5.23
		-46	-36	62	6	4.70
		-32	-18	48	10	4.70
		-44	-38	52	33	4.66
		-46	-28	38	33	4.58
		-40	-24	48	31	4.50
		-50	-32	44	33	4.29
		-32	-34	64	11	3.94
		-46	-14	48	3	3.61
		-38	-40	62	6	3.39
		-30	-34	54	1	3.31

B.5.2 Patient Controls

Table 69: Statistics of the SI activations for study 5. All values shown above an uncorrected p value threshold of ≤ 0.001.

Subject	Stimulation	x	y	z	Cluster size (2 mm^3 voxels)	T-score
Control 1	LD1	54	-28	48	594	12.77
		56	-34	56	594	11.8
		48	-40	62	594	10.46
		30	-8	64	81	6.1
		42	-12	66	5	4.33
		34	-40	60	8	4.1
		36	-6	44	5	4.09
		36	-38	56	1	3.53
		42	-42	48	6	3.46
		42	-22	66	1	3.38
	LD5	56	-28	48	258	11.19
		48	-38	62	258	9.48
		38	-46	50	7	3.98
		64	-8	40	6	3.83
		52	-34	44	7	3.79
		64	-32	48	1	3.35
	RD1	-50	-32	58	416	11.14
		-58	-28	50	416	10.3
		-44	-36	62	416	9.19
		-36	-14	60	53	4.68
		-38	-40	52	27	4.44
		-32	-32	40	5	4.2
		-36	-44	38	2	3.39
		-30	-6	44	3	3.33
		-44	-24	60	1	3.25
		-54	-8	46	2	3.19
		-38	-18	46	1	3.13
	RD5	-58	-30	48	61	6.04
		-50	-32	58	61	5.97
		-44	-36	64	61	5.81
		-64	-22	36	1	3.49
		-46	-32	36	1	3.32
		-40	-30	56	1	3.11

Table 70: Statistics of the SI activations for study 5. All values shown above an uncorrected p value threshold of ≤ 0.001.

Subject	Stimulation	x	y	z	Cluster size (2 mm^3 voxels)	T-score
Control 2	LD1	42	-12	56	411	12.18
		38	-44	50	11	4.67
		52	-16	58	8	4.39
		54	-36	50	17	4.38
		54	-28	44	2	4.18
		44	-8	38	2	4.11
		56	-34	56	5	3.77
		48	-30	56	3	3.68
		62	-28	42	7	3.61
		66	-28	42	7	3.61
		66	-38	38	7	3.6
		64	-40	42	7	3.59
		42	-36	58	1	3.4
	LD5	50	-20	58	133	9.9
		40	-26	50	133	8.22
		32	-32	56	20	3.94
		60	-26	52	1	3.21
		58	-28	54	1	3.18
		52	-32	58	1	3.12
	RD1	-58	-14	44	236	9.29
		-52	-10	52	236	7.37
		-40	-8	62	36	6.72
		-56	-34	52	16	5.78
		-34	-14	54	38	5.22
		-60	-26	44	6	4.45
		-54	-44	54	5	3.65
		-44	-32	46	2	3.47
		-38	-38	46	1	3.23

Table 71: Statistics of the SI activations for study 5. All values shown above an uncorrected p value threshold of ≤ 0.001.

Subject	Stimulation	x	y	z	Cluster size (2 mm^3 voxels)	T-score
Control 2	RD5	-40	-30	56	42	6.33
		-36	-36	66	42	5.43
		-58	-16	44	47	4.98
		-48	-22	56	14	4.9
		-32	-10	54	8	4.69
		-46	-14	58	14	4.66
		-36	-18	66	10	4.42
		-36	-20	60	11	4.24
		-48	-28	40	2	3.79
		-50	-14	36	8	3.7
		-60	-36	46	5	3.6
		-44	-22	48	3	3.53
		-48	-44	56	4	3.45
		-56	-38	52	1	3.45
		-52	-32	56	2	3.39
		-30	-32	46	1	3.38
		-38	-34	46	1	3.18
		-30	-42	50	1	3.13
Control 3	LD1	56	-16	54	424	11.37
		46	-18	64	424	8.17
		46	-38	64	424	8.03
		38	-14	40	11	5.84
		32	-26	46	8	5.08
		54	-24	42	1	3.24
		30	-24	54	7	3.34
	LD5	62	-44	36	37	3.52
		58	-18	52	14	5.37
		62	-14	46	13	4.01
		44	-36	50	33	5.32
		40	-22	54	20	4.49
		40	-22	66	20	4.01
		52	-28	56	8	4.48
		54	-16	56	9	4.21
		46	-20	62	8	4.19
		46	-34	66	2	3.58
		48	-20	56	4	3.37
		44	-30	46	1	3.2

Table 72: Statistics of the SI activations for study 5. All values shown above an uncorrected p value threshold of ≤ 0.001.

Subject	Stimulation	x	y	z	Cluster size (2 mm^3 voxels)	T-score
Control 3	RD1	-50	-24	52	132	9.22
		-54	-12	48	132	7.24
		-54	-30	42	132	6.31
		-30	-44	50	39	5.18
		-40	-12	64	12	4.7
		-42	-40	60	13	4.6
		-34	-36	56	8	4.26
		-42	-44	66	1	3.94
		-40	-38	50	13	3.93
		-36	-38	38	2	3.92
		-42	-22	54	5	3.78
		-46	-34	50	1	3.54
		-44	-10	60	1	3.48
		-34	-22	44	1	3.39
		-34	-26	44	1	3.39
		-38	-36	40	1	3.36
		-42	-10	52	1	3.3
		-34	-44	60	2	3.28
		-42	-16	58	1	3.27
		-30	-36	46	1	3.11
	RD5	-46	-20	60	25	6.17
		-50	-20	46	37	6.03
		-54	-32	40	28	5.98
		-46	-34	56	37	5.01
		-40	-28	60	6	4.44
		-54	-22	56	1	4.22
		-56	-32	52	36	4.21
		-40	-10	66	2	4.19
		-30	-42	46	5	3.98
		-44	-26	66	2	3.65
		-42	-20	50	2	3.59
		-32	-32	58	1	3.56
		-44	-16	56	2	3.5
		-36	-6	52	2	3.29
		-44	-34	66	1	3.19

Table 73: Statistics of the SI activations for study 5. All values shown above an uncorrected p value threshold of ≤ 0.001.

Subject	Stimulation	x	y	z	Cluster size (2 mm^3 voxels)	T-score
Control 4	LD1	40	-20	60	337	10
		46	-30	66	337	9.07
		52	-22	56	337	8.37
		32	-28	56	17	4.15
		36	-38	56	2	3.69
		30	-24	64	17	3.24
	LD5	44	-30	66	466	11.35
		32	-26	60	466	9.98
		62	-34	36	8	3.76
		50	-14	56	6	3.59
		40	-14	56	2	3.48
		36	-10	48	2	3.22
		30	-10	44	1	3.18
		46	-14	62	1	3.14
	RD1	-58	-14	44	385	10.71
		-48	-16	60	385	8
		-34	-12	66	32	7.71
		-40	-20	64	32	5.72
		-40	-24	46	29	6.71
		-44	-34	44	16	4.5
		-34	-28	56	9	4.42
		-36	-14	40	7	4.28
		-50	-40	44	16	4.28
		-44	-44	48	16	4
		-32	-14	58	32	3.83
		-62	-38	44	2	3.81
		-44	-6	38	2	3.42
	RD5	-64	-22	38	212	9.81
		-46	-34	64	212	8.51
		-48	-12	58	55	5.83
		-34	-12	58	16	4.32
		-58	-20	52	4	3.82
		-50	-44	58	1	3.3
		-32	-42	52	1	3.2